UNIVERSIDAD DE CASTILLA – LA MANCHA
FACULTAD DE CIENCIAS Y TECNOLOGÍAS QUÍMICAS
DEPARTAMENTO DE INGENIERÍA QUÍMICA

HIDROGENACIÓN ELECTROCATALÍTICA DE CINAMALDEHÍDO

Memoria que para optar al grado de Doctor en Ingeniería Química presenta:

MARÍA JOSÉ TORRES GÓMEZ - CALCERRADA

Directores:
Dr. Paula Sánchez Paredes
Dr. Ana Raquel de la Osa Puebla

Composición del tribunal:
Dr. Fernando Dorado Fernández
Dr. José María Gómez Martín
Dr. Carmen Belén Molina Caballero

Profesores que han emitido informes favorables de la tesis:
Dr. Amaya Romero Izquierdo
Dr. María Jesús Ramos Marcos

Ciudad Real, 28 octubre 2019

Dña. Paula Sánchez Paredes, Catedrática de Ingeniería Química de la Universidad de Castilla – La Mancha y **Dña. Ana Raquel de la Osa Puebla**, Profesora Contratada Doctora Interina de Ingeniería Química de la Universidad de Castilla – La Mancha,

CERTIFICAN: Que el presente trabajo de investigación titulado "Hidrogenación electrocatalítica de cinamaldehído" constituye la memoria que presenta **Dña. María José Torres Gómez – Calcerrada** para aspirar al grado de Doctor en Ingeniería Química y que ha sido realizada en los laboratorios del Departamento de Ingeniería Química bajo su supervisión.

Y para que conste a efectos oportunos, firman el presente certificado.

En Ciudad Real, a 28 de octubre de 2019

Dña. Paula Sánchez Paredes Dña. Ana Raquel de la Osa Puebla

Índice

ÍNDICE

RESUMEN 1

DESCRIPCIÓN DEL TRABAJO REALIZADO

A. INTRODUCCIÓN 14

A.1. Hidrogenación catalítica

A.2. Hidrogenación catalítica de cinamaldehído 18

A.3. Procesos electroquímicos

A.3.1. El hidrógeno como combustible alternativo y su producción vía electroquímica 26

A.3.2. Producción de hidrógeno mediante electrólisis de agua en celdas de membrana polimérica. 30

A.3.3. Procesos de hidrogenación electrocatalítica de moléculas orgánicas 35

A.4. Objetivo y alcance de la tesis 39

B. MÉTODOS E INSTALACIONES EXPERIMENTALES 42

B.1. Reactivos empleados

B.2. Preparación de catalizadores 43

B.2.1. Método de impregnación y reducción con borohidruro

B.2.2. Método de impregnación y reducción con ácido fórmico 45

B.2.3. Método de impregnación y reducción del poliol modificado 46

B.3. Preparación de electrodos y MEAs 47

B.4. Técnicas de caracterización físico–químicas

B.4.1. Análisis de difracción de rayos X

B.4.2. Espectroscopía de emisión de plasma por inducción (ICP–AES) 49

B.4.3. Adsorción / desorción de N_2

B.4.4. Quimisorción de hidrógeno 50

B.4.5. Titraciones ácido/base 52

B.4.6. Reducción a temperatura programada (TPR)

B.5. Técnicas de caracterización electroquímica 53

B.5.1. Voltametría cíclica

B.5.2. Reacción de Reducción/Evolución de Hidrógeno 55

B.5.3. Estudios de impedancia electroquímica 56

B.6. Hidrogenación electroquímica de cinamaldehído 57

B.7. Instalaciones experimentales electrocatalíticas empleadas 58

B.7.1. Sistema de disco rotatorio
B.7.2. Celda electroquímica tipo PEM 59
C. RESULTADOS Y DISCUSIÓN 62
D. CONCLUSIONES Y RECOMENDACIONES 70
E. BIBLIOGRAFÍA 74

SECTION I: ELECTROCATALYTIC HYDROGENATION OF CINNAMALDEHYDE: STUDY OF REACTION CONDITIONS

CHAPTER 1: ELECTROCATALYTIC HYDROGENATION OF CINNAMALDEHYDE IN A POLIMERIC ELECTROLYTE MEMBRANE REACTOR: STUDY OF OPERATIONAL CONDITIONS

ABSTRACT 85
1. INTRODUCTION 87
2. EXPERIMENTAL 88
2.1. Membrane electrode assembly (MEA) preparation
2.2. Electrocatalytic hydrogenation in a proton exchange membrane reactor 89
3. RESULTS AND DISCUSSION 90
4. CONCLUSIONS 98

SECTION II: CATALYSTS SYNTHESIS FOR THE ELECTROCHEMICAL HYDROGENATION OF CINNAMALDEHYDE

CHAPTER 2: ELECTROCATALYTIC HYDROGENATION OF CINNAMALDEHYDE BY PT/C CATALYSTS PREPARED BY ONE-POT IMPREGNATION-REDUCTION METHOD

ABSTRACT 107
1. INTRODUCTION 109
2. EXPERIMENTAL 111
2.1. Catalysts
2.2. Physicochemical characterization 113
2.3. Electrochemical characterization
2.4. Membrane electrode assembly (MEA) preparation
2.5. Electrocatalytic hydrogenation tests 114
3. RESULTS AND DISCUSSION
3.1. Physicochemical characterization 114
3.2. Electrochemical characterization 120
3.3. Electrocatalytic tests 125

4. CONCLUSIONS 129

CHAPTER 3: PT/C CATALYSTS FOR THE ELECTROCATALYTIC HYDROGENATION OF CINNAMALDEHYDE: INFLUENCE OF THE REDUCING AGENT

ABSTRACT 137

1. INTRODUCTION 139

2. EXPERIMENTAL

2.1. Syntesis of Pt/C-R cathodic catalysts 141

2.2. Physicochemical characterization 142

2.3. Electrochemical characterization

2.4. Membrane electrode assembly (MEA) preparation 143

2.5. Electrocatalytic Hydrogenation tests

3. RESULTS AND DISCUSSION 144

3.1. Physicochemical characterization

3.2. Electrochemical characterization 151

3.3. Electrocatalytic hydrogenation of CMA in a PEM cell 155

4. CONCLUSIONS 157

CHAPTER 4: ELECTROCATALYTIC HYDROGENATION OF CINNAMALDEHYDE IN A PEM CELL. THE ROLE OF SODIUM HYDROXIDE AND PLATINUM LOADING

ABSTRACT 166

1. INTRODUCTION 167

2. EXPERIMENTAL

2.1. Catalysts synthesis 169

2.2. Physicochemical characterization

2.3. Electrochemical characterization

2.4. Membrane electrode assembly (MEA) preparation 170

2.5. Electrocatalytic hydrogenation of CMA in a proton exchange membrane reactor

3. RESULTS AND DISCUSSION 171

3.1. Influence of platinum loading

3.1.1. Physicochemical characterization of Pt-m/C-0.2 cathodes 171

3.1.2. Electrochemical characterization of Pt-m/C-0.2 cathodes 176

3.1.3. Electrochemical hydrogenation of cinnamaldehyde in PEM cell on Pt-m/C-0.2 cathodes 178

3.2. Influence of the pH in the synthesis procedure 180
3.2.1. Physicochemical characterization of Pt-15/C-X cathodes 180
3.2.2. Electrochemical characterization of Pt-15/C-X cathodes 184
3.2.3. Electrochemical hydrogenation of cinnamaldehyde in PEM cell on Pt-15C-X cathodes 186
4. CONCLUSIONS 189

SECTION III: ELECTROCATALYTIC HYDROGENATION OF CINNAMALDEHYDE: INFLUENCE OF ACTIVE METALS AND ADDITIVES

CHAPTER 5: BIMETALLIC CATALYST FOR THE ELECTROCATALYTIC HYDROGENATION OF CINNAMALDEHYDE IN A PEM CELL

ABSTRACT 199
1. INTRODUCTION 201
2. EXPERIMENTAL 203
2.1. Catalysts
2.2. Physicochemical characterization 204
2.3. Electrochemical characterization
2.4. Membrane electrode assembly (MEA) preparation 205
2.5. Electrocatalytic hydrogenation tests
3. RESULTS AND DISCUSSION 206
3.1. Physicochemical characterization
3.2. Electrochemical characterization 214
3.3. Electrocatalytic hydrogenation tests in PEM cell 221
4. CONCLUSIONS 224

CHAPTER 6: BIMETALLIC PTNI/C AND PTCO/C CATHODES FOR THE SELECTIVE HYDROGENATION OF CINNAMALDEHYDE IN A PEM CELL: INFLUENCE OF THE PT/M RATIO AND CATHODIC MEDIA ADDITIVES

ABSTRACT 235
1. INTRODUCTION 237
2. EXPERIMENTAL 239
2.1. Cathode – Catalysts synthesis
2.2. Physicochemical characterization 240
2.3. Electrochemical characterization
2.4. Membrane electrode assembly (MEA) preparation 241

2.5. Electrocatalytic hydrogenation tests
3. RESULTS AND DISCUSSION
3.1. Physicochemical characterization Pt_yM_{1-y}/C cathodic catalysts
3.2. Electrochemical characterization of Pt_yM_{1-y}/C cathodic catalysts 248
3.3. Electrochemical hydrogenation of CMA in PEM cell 252
4. CONCLUSIONS

SECTION IV: SUPPORTS AND GDL MATERIALS FOR THE ELECTROCATALYTIC HYDROGENATION OF CINNAMALDEHYDE

CHAPTER 7: ELECTROCATALYTIC HYDROGENATION OF CINNAMALDEHYDE IN A POLIMERIC ELECTROLYTE MEMBRANE REACTOR: INFLUENCE OF THE CATHODIC SUPPORT AND GDL.

ABSTRACT 271
1. INTRODUCTION 273
2. EXPERIMENTAL
2.1. Catalysts Synthesis 278
2.2. Physicochemical characterization
2.3. Electrochemical characterization 279
2.4. Membrane electrode assembly (MEA) preparation
2.5. Electrocatalytic hydrogenation tests
3. RESULTS AND DISCUSSION 280
3.1. Characterization of PtCo-based electrocatalysts
3.1.1. Physicochemical characterization
3.1.2. Electrochemical characterization 286
3.1.3. Influence of the support on the electrochemical hydrogenation of cinnamaldehyde 290
3.2. Influence of the gas diffusion layer on the electrochemical hydrogenation of cinnamaldehyde 293
4. CONCLUSIONS 296

PRODUCCIÓN CIENTÍFICA

Artículos 307
Congresos 308

Resumen

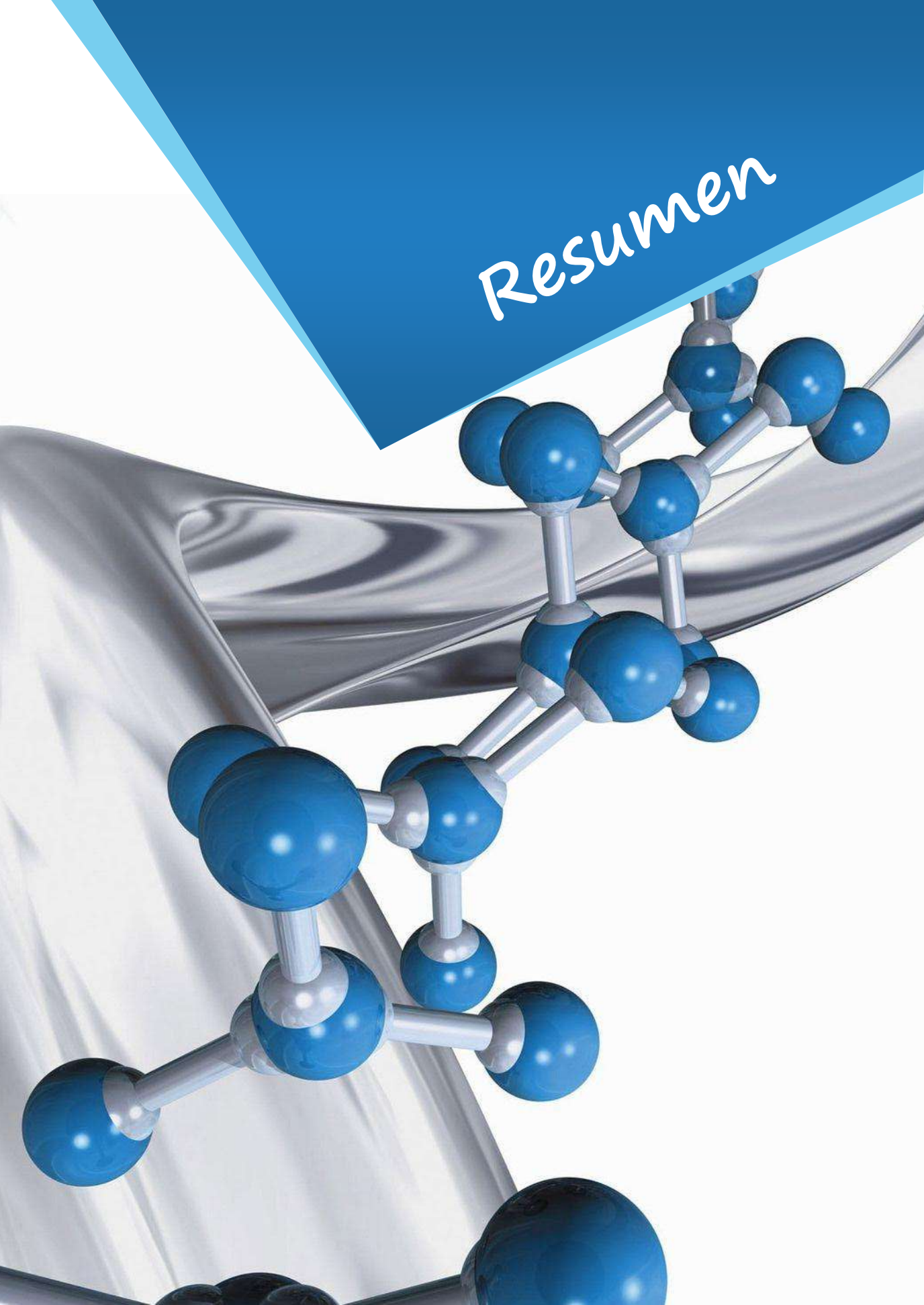

El presente trabajo forma parte de un amplio programa de investigación sobre Producción de hidrógeno en reactores electroquímicos de membrana polimérica y su posterior uso en la síntesis de productos de alto valor añadido, desarrollado por el Departamento de Ingeniería Química de la Universidad de Castilla – La Mancha. Este programa iniciado en el año 2013 ha sido financiado por el Programa Estatal de Investigación, Desarrollo e Innovación orientada a los retos de la sociedad, mediante los proyectos CTQ2013 – 45030 – R y CTQ2016 – 75491 – R, convocados por el Ministerio de Economía y Competitividad del gobierno de España.

La problemática energética actual se centra en dos aspectos fundamentales: la dependencia casi exclusiva de los combustibles fósiles, y su efecto negativo para el medio ambiente. El petróleo es una fuente de energía muy eficiente y fácil de explotar, pero es un bien escaso que viene siendo explotado por países con situaciones políticas muy inestables que causan constantes fluctuaciones en su precio y hacen muy difícil prever su disponibilidad a largo y corto plazo. Esta problemática creciente y la demanda de recursos naturales han provocado un enorme interés en la energía verde sostenible.

La economía del hidrógeno es una alternativa que, a largo plazo, tiene como objetivo desplazar el actual escenario energético hacia otro que combinaría la "limpieza" del hidrógeno, obtenido a partir de procesos que no generarían CO_2, con la eficiencia de las celdas de combustible para producir electricidad y calor, o los electrolizadores PEM en los que sería posible su utilización en procesos de hidrogenación de moléculas de alto valor añadido.

Diversos autores han demostrado la posibilidad de emplear los reactores electroquímicos de membrana polimérica tipo PEM como reactores de hidrogenación de moléculas como el o-xileno, acetileno o

acetona. Sin embargo, todos ellos alimentan el hidrógeno al ánodo en lugar de transferirlo a través de la membrana polimérica. La posibilidad de acoplar un proceso de electrolisis a este tipo de sistemas permitiría producir hidrógeno in-situ para llevar a cabo el proceso de hidrogenación, evitando su transporte y almacenaje.

Por otro lado, la hidrogenación selectiva de los aldehídos α,β-insaturados a sus correspondientes alcoholes insaturados sigue siendo un obstáculo en la producción de ciertos productos químicos. Ello es debido a que la hidrogenación selectiva del doble enlace C=C se ve termodinámicamente favorecida frente a la hidrogenación de C=O. Un ejemplo de este tipo de aldehídos α,β-insaturados es el cinamaldehído (CMA). Este compuesto tiene como principales productos de la hidrogenación de sus dobles enlaces el hidrocinamaldehído (HCMA, hidrogenación del enlace C=C) que se utiliza en la industria farmacéutica por ser un importante intermediario en la preparación de productos farmacéuticos utilizados en el tratamiento del VIH, y el alcohol cinámico (CMO, hidrogenación del enlace C=O) que se utiliza principalmente en perfumería debido a su olor y a sus propiedades de fijación. Normalmente, estos procesos de hidrogenación se realizan a escala industrial en condiciones de presión y temperatura elevadas mediante catálisis convencional. Estas operaciones llevan costes asociados a la eliminación tanto del catalizador como de los disolventes, que pueden ser perjudiciales para el medio ambiente.

Por tanto, se planteó una investigación encaminada al desarrollo de un proceso de hidrogenación selectiva de un aldehído α-β insaturado (CMA) en una celda de intercambio protónico tipo PEM en condiciones suaves, produciendo el hidrogeno in-situ a partir de electrólisis de agua. Para tal fin, el programa de investigación se centró en los siguientes objetivos:

- Revisión bibliográfica, estado de arte.
- Puesta a punto de las instalaciones en las que llevar a cabo ensayos de hidrogenación electrocatalítica.
- Desarrollo y puesta a punto de las técnicas analíticas necesarias, para la caracterización e identificación cualitativa y cuantitativa de los productos de reacción obtenidos.
- Demostración de la viabilidad del sistema planteado utilizando catalizadores comerciales.
- Optimización de las condiciones de operación (temperatura, intensidad de corriente aplicada, concentración y caudal de reactivo suministrado a la celda PEM).
- Estudio de optimización de las etapas necesarias y el agente reductor más adecuado para la síntesis de catalizadores de Pt utilizados en el compartimento catódico. En estos métodos de preparación la fase activa se reduce in situ con un agente químico reductor.
- Optimización de la carga de fase activa requerida para obtener los mejores resultados de hidrogenación electrocatalítica.
- Estudio de la influencia de la adición de un segundo metal y del ratio Pt/M.
- Estudio de la influencia de una base débil a la disolución de reactivo (catolito) en la producción de compuestos no deseados.
- Estudio de la influencia del soporte electrocatalítico en catalizadores bimetálicos de platino/cobalto.
- Estudio de la influencia del material utilizado como capa de difusión de gases en los resultados de hidrogenación.

En el Capítulo 1, tras la puesta en marcha de la instalación se estudió el efecto de las condiciones de operación en la hidrogenación electrocatalítica de cinamaldehído, usando catalizadores comerciales. En el caso del ánodo se utilizó un catalizador comercial de IrO_2 al 99 % de pureza, típico de electrolisis de agua y que se mantendrá en estudios posteriores. Como cátodo se utilizó un catalizador comercial de platino soportado sobre carbón activo al 20 % en peso. En primer lugar, se estudió la producción de hidrógeno comparando el valor experimental con el teórico. Tras comprobar que estos valores eran muy semejantes siguiendo la ley de Faraday. Se realizaron experimentos utilizando como disolución anódica agua milli-Q y como disolución catódica 100 ppm de cinamaldehído disueltos en 2 – propanol. Alternando fases en circuito abierto y fases en las cuales se aplicaba una intensidad de corriente de 0,1 A se comprueba que la hidrogenación sucedía por vía electroquímica. Los resultados de estos experimentos demostraron que, efectivamente, en ausencia de intensidad eléctrica, no se produce la hidrogenación del cinamaldehído. A continuación, se estudió la influencia de las condiciones de operación realizando experimentos a diferentes temperaturas (55, 65, 70 y 75 ºC), caudales (1, 2 y 3 $ml \cdot min^{-1}$) e intensidades diferentes (0,05 y 0.1 A). En estos experimentos se concluyó que el proceso de hidrogenación presenta resultados más satisfactorios cuando se trabaja con un caudal de 1 $ml \cdot min^{-1}$, 70 ºC de temperatura de trabajo y una intensidad de corriente aplicada de 0,05 A. Obteniéndose valores de conversión de un 11 % y selectividades hacia alcohol cinámico en torno a un 45 %.

Seguidamente, en el Capítulo 2 se analizó la influencia del método de preparación del catalizador catódico basado en platino soportado sobre carbón Vulcan XC-72, estableciendo diferentes modificaciones a partir de un método simple en el cual el catalizador se reduce in – situ mediante una reacción con $NaBH_4$. Estas modificaciones consistieron en

la adición de las etapas de evaporación de disolvente en rotavapor, lavado final del filtrado hasta pH = 7 y adición de la sal precursora de la fase activa en forma de gota a gota. Los resultados demuestran que la incorporación de las diferentes etapas mejora los resultados de la hidrogenación obteniéndose valores ligeramente superiores de selectividad hacia alcohol cinámico.

A continuación, en el Capítulo 3 se evaluó el uso de diferentes agentes de reducción in – situ del catalizador catódico. Se realizaron síntesis de catalizadores de Pt soportados sobre Vulcan XC-72 mediante el método optimizado anteriormente, utilizando como agente reductor $NaBH_4$, KBH_4, HCOOH, H_2 y etilenglicol. Pudo observarse que el catalizador reducido con KBH_4 demuestra los valores más altos de conversión, pero la selectividad más baja hacia los productos de interés. El catalizador reducido con etilenglicol por el método del poliol modificado resulta ser el más interesante ya que permite llegar a un compromiso entre conversión y selectividad. Además, se eligió este método para futuras síntesis ya que permite controlar el tamaño de partícula de los catalizadores obtenidos a partir del control de pH.

Posteriormente, en el Capítulo 4 se llevó a cabo la optimización de la carga de fase activa del catalizador catódico sintetizando catalizadores basados en Pt (10 – 20 % en peso) soportados sobre Vulcan XC–72 mediante el método del poliol modificado. Asimismo, se estudió la influencia de la variación del pH durante la síntesis modificando la concentración de NaOH entre 0,05 – 0,2 M. a partir de los resultados de caracterización y los ensayos electrocatalíticos se llegó a la conclusión de que la cantidad optima de Pt en el catalizador es de un 15 %, sintetizado con una concentración de NaOH de 0,2 M, debido a que los valores de conversión son superiores en este caso y se llegó a la conclusión de que, aunque los valores de selectividad hacia los productos de interés eran

menores, mediante etapas futuras (con posible adición de un segundo metal), podría mejorarse dicha selectividad.

En el Capítulo 5 se analizó la influencia de la incorporación de un segundo metal de carácter menos noble a la estructura del catalizador con el fin de modificar la selectividad hacia los productos de interés y disminuir costes asociados al catalizador. Se realizaron síntesis utilizando el método del poliol modificado con una carga máxima del 15 % incorporando Fe, Cu, Sn, Co y Ni a la estructura del catalizador. Los resultados demuestran que la adición de un segundo metal tiene un efecto negativo en la conversión; en cambio, los catalizadores que incorporan en su estructura Ni y Co presentan la selectividad más baja a compuestos indeseados y la mayor selectividad hacia los compuestos de interés

Seguidamente, en el Capítulo 6, basándose en la bibliografía existente hasta el momento, se abordaron diferentes puntos de interés. El primero de ellos consistió en el estudio de la influencia en el proceso de hidrogenación de la adición de una base débil en el medio de reacción. Se realizaron estudios añadiendo $NaHCO_3$ y NH_4OH en la disolución catódica en diferentes cantidades equivalentes. Estos estudios demostraron que en el caso del NH_4OH la formación de compuestos indeseados puede ser eliminado casi por completo. Paralelamente a este estudio, se realizaron síntesis de catalizadores de PtCo con diferentes proporciones Pt/Co para ver su efecto sobre el proceso de hidrogenación. Estos experimentos demostraron un incremento en la selectividad hacia el compuesto de interés cuando se combinan la adición de NH_4OH con el incremento de la cantidad de cobalto en la estructura del catalizador.

Posteriormente, en el Capítulo 7 se han llevado a cabo estudios con diferentes soportes y capas de difusión de gases. Primeramente, se han sintetizado catalizadores bimetálicos de platino cobalto soportados

sobre diferentes materiales, Vulcan XC–72 comercial, nanofibras de carbono funcionalizadas de baja densidad (CNF LS) y nanofibras de carbono funcionalizadas de baja densidad sometidas a un tratamiento de limpieza con el objetivo de eliminar las posibles trazas de níquel y silicio (CNF LS D) presentes en el soporte. Los resultados de este estudio demuestran que el catalizador de platino/cobalto soportado sobre Vulcan XC–72 ofrece mejores resultados en cuanto a selectividad a los compuestos deseados posiblemente debido a su elevada área superficial y a la orientación de los planos cristalinos, más adecuada para la reacción de estudio. Por último, se han realizado experimentos comparando el titanio poros (utilizado a lo largo de todos los experimentos descritos anteriormente), con papel de carbono, obteniéndose mayores selectividades hacia los compuestos de interés en el caso de la utilización de titanio poroso como material para la capa de difusión de gases debido a que posee una mayor resistencia mecánica y una resistencia eléctrica menor.

Descripción del Trabajo Realizado

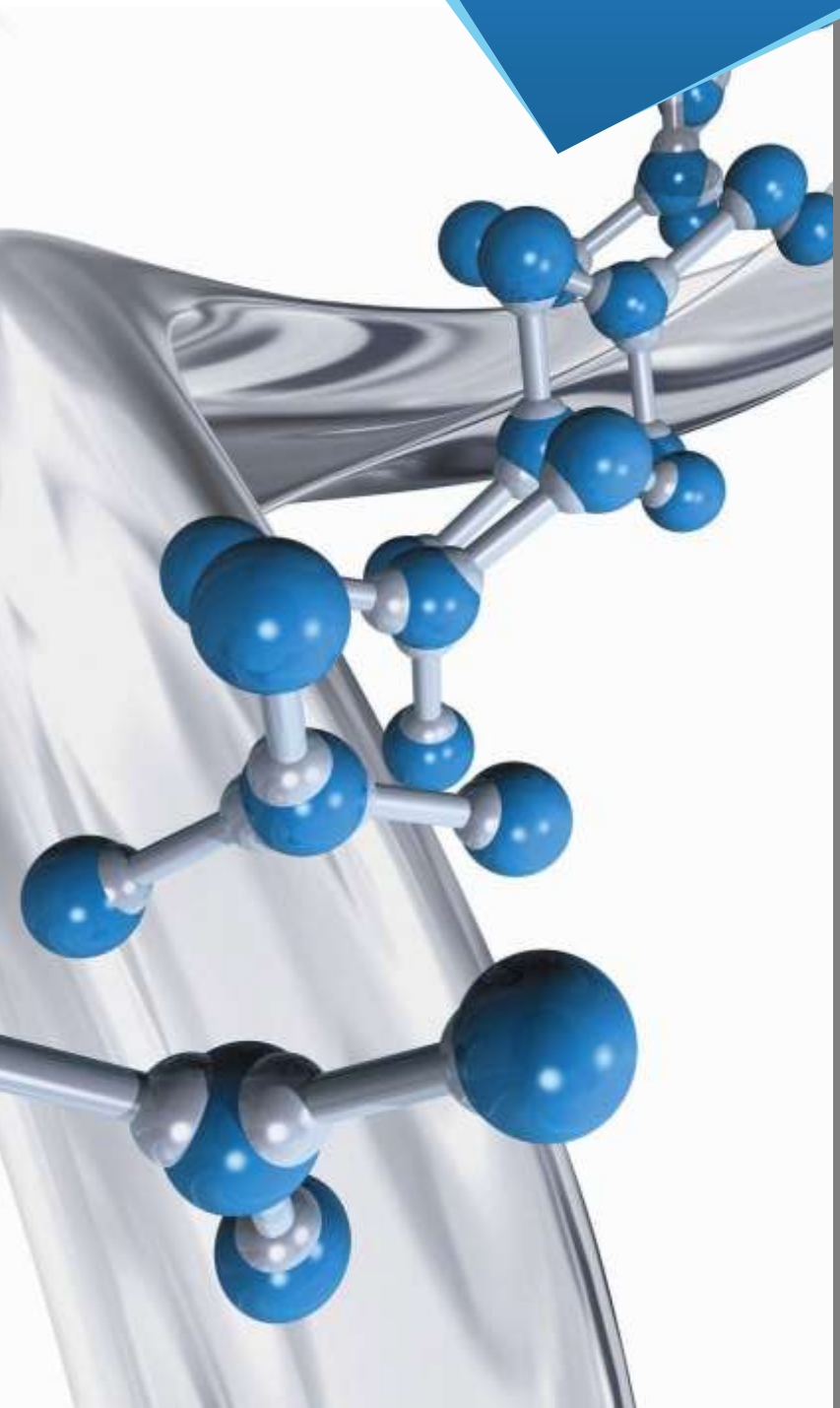

A. INTRODUCCIÓN
- A.1. Hidrogenación electrocatalítica
- A.2. Hidrogenación catalítica de cinamaldehído
- A.3. Procesos electroquímicos
- A.4. Objetivo y alcance de la tesis

B. MÉTODOS E INSATALACIONES EXPERIMENTALES
- B.1. Reactivos empleados
- B.2. Preparación de catalizadores
- B.3. Preparación de electrodos y MEAs
- B.4. Técnicas de caracterización físico – químicas
- B.5. Tecnicas de caracterización electroquímica
- B.6. Hidrogenación electroquímica de cinamaldehído
- B.7. Instalaciones Experimentales Electrocatalíticas empleadas

C. RESULTADOS Y DISCUSIÓN

D. CONCLUSIONES Y RECOMENDACIONES

E. BIBLIOGRAFÍA

Este trabajo forma parte de un amplio programa de investigación sobre aplicación de sistemas electrocatalíticos en procesos de interés energético y medioambiental que se viene desarrollando, durante los últimos años en el Departamento de Ingeniería Química de la Universidad de Castilla – La Mancha.

En particular, esta Tesis Doctoral tiene como objetivo la hidrogenación electrocatalítica de cinamaldehído en una celda de intercambio protónico tipo PEM, produciendo el hidrógeno in - situ a partir de electrólisis de agua. Este trabajo ha sido financiado mediante una beca predoctoral para la formación de personal investigador del Ministerio de Economía y Competitividad de España.

A. INTRODUCCIÓN

A.1. HIDROGENACIÓN CATALÍTICA

Los procesos de hidrogenación son habituales en la industria química, petroquímica y de química fina. A diferencia de la industria petroquímica, que se caracteriza por producciones en grandes volúmenes, la química fina involucra la producción en pequeñas cantidades de sustancias conteniendo moléculas con funciones específicas a partir de productos naturales o sintéticos. Los productos generalmente, responden a especificaciones muy estrictas y son comercializados a precios altos [1].

Los denominados químicos finos y especialidades químicas encuentran su campo de aplicación en la energía nuclear, la electrónica, la industria agroalimenticia, la industria farmacéutica, etc. Estas actividades industriales se caracterizan por un alto valor agregado en los productos que elaboran, haciendo que se justifiquen importantes inversiones en investigación y desarrollo, lo cual permite incorporar innovaciones tecnológicas en los procesos asociados. La mayor parte de las veces se trata de procesos que implican la transformación de moléculas orgánicas complejas, las cuales pueden incluir heteroátomos como oxígeno, fósforo, nitrógeno, azufre y halógenos.

La química fina ha sido durante años un campo exclusivo de la síntesis orgánica y de la catálisis homogénea. Recientemente, debido al avance logrado en el conocimiento de los mecanismos fundamentales que rigen la catálisis heterogénea, se registra un notable incremento de las investigaciones básicas y aplicadas que utilizan catalizadores sólidos en reacciones de interés en el campo de la química fina. La mayor ventaja de la catálisis homogénea radica en la posibilidad de caracterizar intermediarios y a través de estos determinar mecanismos de reacción.

Sin embargo, su principal dificultad es la separación de los productos y la recuperación del catalizador. Este último aspecto resulta la principal ventaja que promueve el desarrollo de la catálisis heterogénea, cuyos costes son menores, tiene más fácil manejo y una separación efectiva del catalizador.

En cualquier proceso catalítico heterogéneo, se pueden considerar varias etapas consecutivas, desde que el reactivo llega a la superficie del catalizador hasta que se obtiene el producto final. Estas etapas en un catalizador poroso son:

a) Difusión del reactivo (o reactivos) a través de los poros del catalizador.
b) Adsorción del reactivo sobre la superficie del catalizador.
c) Reacción química propiamente dicha con formación del producto adsorbido.
d) Desorción del producto.
e) Difusión del producto a través de los poros del catalizador.

La hidrogenación es una forma particular de reducción en la que el hidrógeno se añade a compuestos orgánicos insaturados, en unas condiciones de presión y temperatura adecuadas y en presencia de un catalizador. En 1912 Paul Sabatier recibió el Premio Nobel de Química por sus investigaciones en el uso de metales finamente divididos en reacciones de hidrogenación [2]. Desde entonces la catálisis heterogénea en química orgánica se ha desarrollado enormemente. Se ha reconocido que el rol más importante del catalizador metálico es generar hidrógeno atómico adsorbido, el que, en contraste con la molécula de hidrógeno relativamente inerte, puede adicionarse fácilmente a varias uniones insaturadas: C=C, C=O, C≡N, etc. El proceso de hidrogenación se hace más complejo cuando la molécula a hidrogenar posee dos o más grupos funcionales de reactividad comparable. Esta situación se da en moléculas

que poseen grupos C=C y C=O conjugados, tales como aldehídos o cetonas α,β-insaturados.

La evolución de la hidrogenación catalítica depende de varios factores incluyendo el tipo de catalizador, la concentración del reactivo, el disolvente, la temperatura y la presión. Por ello, la optimización de un proceso de hidrogenación requiere la selección de múltiples parámetros de operación tales como la síntesis del catalizador, la temperatura, la presión, el disolvente, la presencia de otros compuestos y la relación sustrato-catalizador, entre otras.

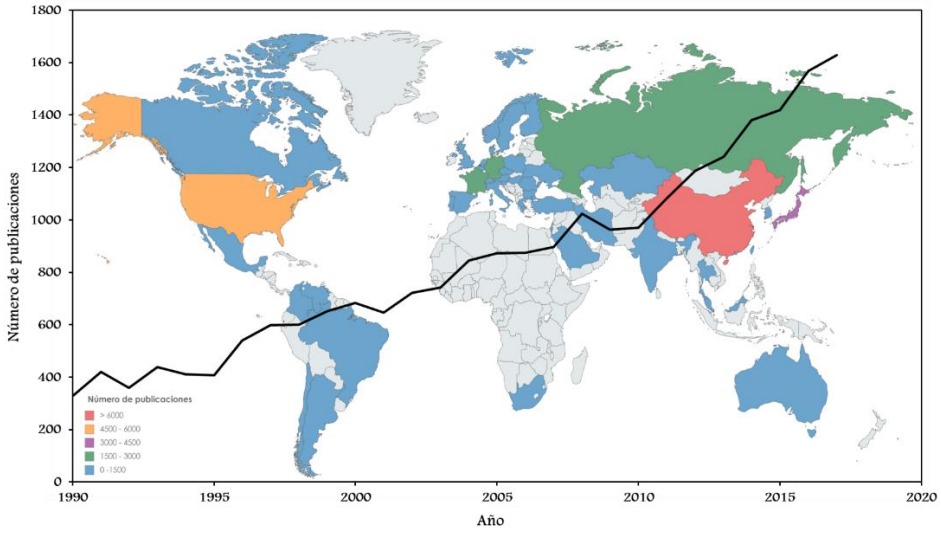

Figura A.1. Publicaciones relacionadas con la hidrogenación de aldehídos α,β - insaturados y su distribución por países. Fuente: www.scopus.com

En particular, la hidrogenación catalítica de compuestos orgánicos α,β-insaturados es un proceso maduro de gran relevancia científica debido a su gran potencial práctico. No obstante, es un proceso en ocasiones complejo, especialmente cuando se desean condiciones para mantener un sistema de flujo continuo. Por ello, en las últimas décadas se han llevado a cabo numerosas investigaciones al respecto, como queda

recogido en la Figura A.1, donde se presenta la distribución por países y el número de publicaciones en la materia desde los años 90 [3]. Como puede apreciarse, son las grandes potencias mundiales como China las que aportan un mayor número de contribuciones, lo que reafirma la importancia de estos procesos a nivel industrial.

Los catalizadores que se emplean normalmente para llevar a cabo las reacciones de hidrogenación, contienen metales nobles soportados como componentes activos, como por ejemplo Ir, Pt, Ru, Rh y Pd, siendo el platino el metal más utilizado como catalizador para la hidrogenación, en particular, de aldehídos α,β-insaturados.

A continuación, se muestra la Tabla A.1 en la que se recogen algunos de los compuestos más estudiados en las reacciones de hidrogenación catalítica, así como los catalizadores empleados, las condiciones de operación y los principales productos de reacción que se originan [4-12].

Tabla A.1. Compuestos estudiados en reacciones de hidrogenación

Molécula a hidrogenar	Catalizador		Condiciones de operación		Productos
	Fase activa	Soporte	P (atm)	T (ºC)	
Nitroareno	Au, Pt, Ni, Ru	Sn-TiO_2	2-13	45-127	Anilina
CO	Ni, Rh	SiO_2, TiO_2, Al_2O_3	1	25-100	Metano
1,3-Butadieno	Pt, Pd, Au	Al_2O_3	4-5	40-450	1-Buteno n-Butano
Acetileno	Pd, Au	SiO_2, TiO_2	1	50-180	Etileno
Cinamaldehído	Au, Ir, Rh, Ru, Au, Cu, Pt, Pd	ZrO_2, SiO_2, Al_2O_3, ZnO, MgO	1-10	50-130	Alcohol cinámico Hidrocinamaldehído 3-Fenilpropanol

Finalmente destacar que, en las últimas décadas ha habido un aumento progresivo en el número de investigaciones destinadas a encontrar sistemas catalíticos que permitan llevar a cabo estos procesos en continuo, en condiciones de operación suaves, con bajo impacto ambiental, facilitando la eliminación de disolventes, etc. y encaminando la reacción hacia la hidrogenación selectiva al producto de interés, en definitiva, en lo que se ha venido a llamar química verde.

A.2. HIDROGENACIÓN CATALÍTICA DE CINAMALDEHÍDO

La hidrogenación selectiva de aldehídos α,β-insaturados, asistida por catalizadores metálicos, en su mayoría metales nobles como el Pt, Ru, Pd, es una etapa clave en la obtención de productos farmacéuticos, saborizantes y fragancias. Termodinámicamente, la hidrogenación de ambos enlaces (C=C y C=O) en un aldehído α,β-insaturado es viable, no obstante, la hidrogenación del enlace C=C se ve favorecida termodinámicamente frente a la hidrogenación del enlace C=O ya que existe una diferencia de entalpía libre de reacción de unos 35 KJ mol^{-1} que favorece la hidrogenación del doble enlace, dejando intacto el grupo funcional carbonilo. De esta forma, cuando el producto de interés deriva de la hidrogenación del doble enlace C=O, resulta vital encontrar un catalizador que sea selectivo hacia la producción del alcohol insaturado.

El cinamaldehído (Figura A.2.), de fórmula molecular C_9H_8O y masa molecular 136,2 g/mol, se encuentra presente en la naturaleza como trans-cinamaldehído, y está compuesto por un aldehído insaturado unido a un grupo fenilo, que le confiere aromaticidad. Tiene color amarillo pálido, y presenta una baja solubilidad en agua, siendo muy soluble en aceites.

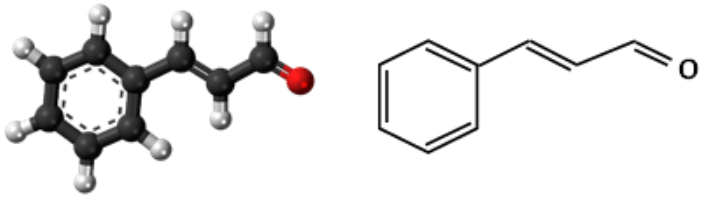

Figura A.2. Molécula de cinamaldehído.

El cinamaldehído, es el componente mayoritario de la canela, una de las especias más comunes en la cocina de prácticamente cualquier cultura y cuyo uso se remonta siglos atrás, especialmente en India. Este aldehído α,β- insaturado también es el responsable de la mayor parte de las propiedades terapéuticas de esta especia como antioxidante, antiinflamatorio y como remedio contra los resfriados [13]. No obstante, éstas no son las únicas propiedades del cinamaldehído, sino que esta molécula presenta otras muchas propiedades beneficiosas para el ser humano, recogidas a continuación en la Figura A.3.:

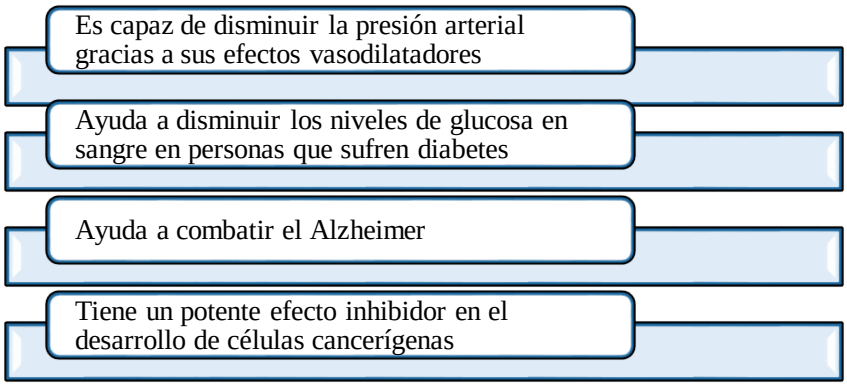

Figura A.3. Resumen de las propiedades terapéuticas del cinamaldehído

Por otro lado, si bien es cierto que el cinamaldehído tiene numerosas e interesantes aplicaciones, los productos que se obtienen de la hidrogenación catalítica de esta molécula no son menos interesantes. La hidrogenación selectiva del cinamaldehído (CMA, Figura A.4.) es un

buen ejemplo de este tipo de reacciones de gran importancia comercial, permitiendo la obtención de alcohol cinámico (CMO), hidrocinamaldehído (HCMA) y del alcohol hidrocinámico (HCMO).

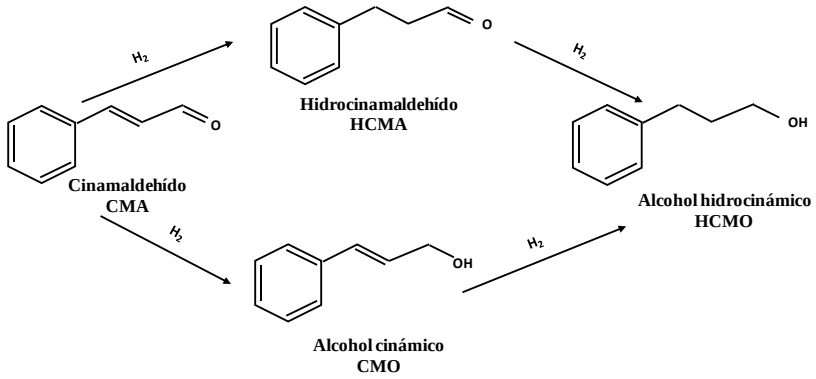

Figura A.4. Moléculas derivadas de la hidrogenación del cinamaldehído.

El alcohol cinámico, producto obtenido de la hidrogenación del enlace C=O, es un producto de gran interés en la química fina, particularmente en la industria de la perfumería por su valor como fijador de mezclas que contienen fragancias del tipo jazmín, lila y rosa [14]. También se emplea en la industria farmacéutica en la síntesis del antibiótico cloromicetina [1].

Otro producto de interés es el hidrocinamaldehído (HCMA), obtenido de la hidrogenación en paralelo del doble enlace C=C, importante intermedio de reacción en la preparación de fármacos usados en el tratamiento del VIH [15]. También se emplea como material de partida para sintetizar otros medicamentos [16].

Por otro lado, la hidrogenación de cualquiera de los productos anteriores conduce a la formación del alcohol hidrocinámico (HCMO), compuesto usado como conservante en cosmética debido a sus propiedades antimicrobianas contra bacterias y mohos.

A pesar de los numerosos trabajos publicados en la literatura relacionados con la obtención de catalizadores para la hidrogenación selectiva de cinamaldehído hacia alcohol cinámico o hidrocinamaldehído, el origen de la selectividad es aún hoy materia de debate [17-19]. La hidrogenación selectiva de cinamaldehído a alcohol cinámico es un reto ya que implica la hidrogenación competitiva del doble enlace carbonilo frente a la hidrogenación termodinámicamente favorable del doble enlace olefínico. Factores como la naturaleza del metal activo, su estructura superficial y planos cristalinos, el método de preparación del catalizador, las características del soporte, el disolvente (polaridad y solubilidad de hidrógeno), las condiciones de reacción y los aditivos/promotores utilizados son clave para abordar dicho objetivo.

De acuerdo con *Josep A. y col.* se ha observado que, utilizando catalizadores de Co/Al_2O_3, variar las condiciones a las cuales se lleva a cabo la reacción de hidrogenación modifica obviamente el desarrollo de la misma. Aumentos en la presión o la temperatura favorecen la cinética de la reacción pero desfavorecen la hidrogenación del enlace C=O, disminuyendo de esta manera la selectividad hacia el alcohol cinámico [20]. Un catalizador utilizado para un proceso de hidrogenación debe tener un área superficial suficiente, adsorber tanto el hidrogeno como el grupo funcional a hidrogenar en sus formas reactivas, orientación espacial de los reactantes adsorbidos para formar los productos deseados, debe ser suficientemente estable, no contener compuestos susceptibles a envenenamiento, a menos que estos compuestos se hayan añadido intencionadamente para controlar conversión o selectividad, y por último permitir una rápida desorción de los productos de la superficie del catalizador.

La mayoría de los catalizadores heterogéneos empleados para hidrogenación se engloban en dos subcategorías. La primera de ellas está

compuesta por metales nobles como Platino, Paladio, Rutenio, Rodio, Osmio, Iridio, Plata y Oro. La segunda categoría la componen metales menos nobles como Niquel, Cobalto, Cobre y Hierro. No obstante, se utiliza Pt en aquellos casos en los que se desee dirigir la selectividad hacia la producción del alcohol insaturado, ya que es el metal más activo para este fin. Sin embargo, desde el punto de vista de la economía del proceso, siempre es deseable desarrollar catalizadores basados en metales no nobles como Fe, Co, Ni y Cu, así como catalizadores bimetálicos. En general, Os, Ir, Ru, Pt, Co y Cu son selectivos a la formación de CMO, mientras que Rh, Pd y Ni lo son para la formación de hidrocinnamaldehído y alcohol hidrocinámico [21]. Factores tanto electrónicos como geométricos, relacionados con la naturaleza del metal activo, a través de los diferentes planos cristalinos expuestos, influyen en los diferentes modos de adsorción de CMA y, por tanto, en la selectividad. Además, los catalizadores basados en Co, Ni y Cu se caracterizan por presentar interacciones metal-soporte relativamente fuertes que influyen en el grado de reducción, dispersión de metal y evolución de la fase activa. Sin embargo, dichas interacciones metal-soporte, relacionadas a su vez con el tamaño de partícula se pueden moderar mediante la adopción de métodos adecuados de preparación.

En particular, la selectividad a alcohol cinámico es altamente dependiente de la composición y estructura del catalizador. El tamaño de partícula influye en la selectividad obtenida hacia el alcohol cinámico debido a un efecto estérico entre el grupo fenilo y la superficie metálica. En caso de superficies planas se impide la adsorción preferencial del doble enlace C=C y se favorece la adsorción del grupo C=O [15]. Diversos estudios determinan que la selectividad hacia alcohol cinámico se ve favorecida con el incremento del tamaño de partícula metálica en catálisis convencional [22-30]. No obstante, es preciso estudiar otros

factores como el tipo de soporte o la presencia de un segundo metal, ya que pueden modificar la selectividad hacia el producto de interés.

Con respecto al soporte donde dispersar el metal activo, son esenciales sus características electrónicas y geométricas [31, 32]. Los soportes convencionales suelen ser óxidos metálicos con carácter ácido o básico y algunos tipos de carbones. La hidrogenación de la molécula de cinamaldehído requiere soportes de una elevada porosidad y alta área superficial, para que la relación de área activa por unidad de volumen sea elevada y la difusión de reactivos y productos a través de su estructura resulte favorecida, facilitando la llegada de los mismos a los centros activos. Por otro lado, deben poseer centros deficientes de electrones y sitios ácidos de Lewis en la superficie del catalizador para promover la formación del alcohol cinámico debido a que proporciona sitios adecuados de adsorción para el grupo carbonilo (C=O). Un aumento en la densidad electrónica de los centros activos del metal disminuye la probabilidad de activación del doble enlace C=C y por consiguiente disminuye la selectividad en la hidrogenación de enlaces olefínicos. Así, soportes tales como Al_2O_3, SiO_2 ó C presentan una alta selectividad hacia el alcohol cinámico, tal y como describen *Bhogeswararao*, S. y col [33, 34].

En comparación con los catalizadores monometálicos, los catalizadores bimetálicos tienen una superficie estructural compleja, donde el segundo metal está expuesto en la superficie, en la región cercana a la superficie o dentro del cuerpo de soporte. Se ha demostrado que la estructura superficial del catalizador bimetálico es fundamental para sus propiedades catalíticas. El segundo metal puede influenciar al primero a través de interacciones electrónicas o modificando la arquitectura del sitio activo. A menudo, las interacciones entre los dos metales son complejas y en gran parte desconocidas, en consecuencia, el

procedimiento de preparación de estos influye de forma crítica en la naturaleza del sistema catalítico obtenido.

El efecto de la adición de un segundo metal puede clasificarse en tres categorías principales: aumentar la actividad catalítica, modificar la selectividad, y mejorar la estabilidad del catalizador. La presencia del segundo metal puede tener un efecto simple como la reducción del primer metal por transferencia de hidrógeno, o puede causar más interacciones las cuales se pueden dividir en cinco fenómenos diferentes:

- **Efectos geométricos**, la adición de un metal promotor altera la geometría de los sitios activos que contiene el metal catalíticamente activo.
- **Efectos electrónicos**, por la modificación de las propiedades electrónicas de los sitios activos por transferencia de electrones entre los dos metales.
- **Efectos de estabilización**, permitiendo una mejora de la estabilidad del metal catalíticamente activo.
- **Efectos sinérgicos**, ambas especies metálicas participan en la unión química de intermedios de reacción y estados de transición.
- **Efectos bifuncionales**, cada especie de metal proporciona una función diferente en el mecanismo de reacción.

Los efectos geométricos y electrónicos afectan a la actividad catalítica y a la selectividad, mientras que los efectos sinérgicos y bifuncionales, normalmente, mejoran la velocidad de reacción, pero también pueden conducir a la creación de nuevas vías de reacción [35]. No obstante, y teniendo en cuenta lo descrito anteriormente, conseguir catalizadores basados en metales no nobles con máxima actividad y selectividad sigue siendo un desafío.

Por otro lado, se sabe que los disolventes tienen un efecto significativo sobre la velocidad de hidrogenación catalítica, atribuido a varios factores, que incluyen la solubilidad del hidrógeno, la interacción termodinámica del disolvente con los reactivos y los productos, la adsorción competitiva del disolvente, etc. La reacción de hidrogenación de cinamaldehído se puede describir como una reacción paralela consecutiva en la que se pueden reducir uno o ambos grupos funcionales insaturados, cuyo esquema de reacción puede variar fuertemente en función de la polaridad de los disolventes usados.

Para disolventes apolares el esquema de reacción es el descrito en la Figura A.4., en la que los productos principales son HCMA, CMO y HCMO. Además, puede formarse β-metil estireno a través de reacciones consecutivas del alcohol cinámico [36]. Cuando se usan disolventes polares, como por ejemplo alcoholes, además de los productos obtenidos en presencia de disolventes apolares, se forman diacetales de cinamaldehído e hidrocinamaldehído debido posiblemente a la reacción entre el cinamaldehído y el disolvente. Se cree que una molécula de aldehído reacciona con una molécula de alcohol para formar un producto de adición moderadamente estable (hemiacetal), que luego se combina con una segunda molécula del alcohol y produce derivados estables (diacetales) [37, 38]. La formación de estos compuestos es reversible y el grado de equilibrio depende de la polaridad del disolvente. Si bien, se ha de destacar que, aunque en presencia de disolventes apolares no se producen compuestos acetales indeseados, la velocidad de reacción es significativamente inferior. Por ello, a menudo se opta por el uso de disolventes polares como metanol, etanol o isopropanol y, con el objetivo de mejorar la selectividad del sistema, se añaden compuestos para modular la acidez superficial y prevenir la formación de dichos acetales [39].

En general, la adición de una base en la mezcla de reacción mejora significativamente la selectividad hacia CMO [40] debido a un bloqueo estérico de los sitios que dan lugar a la hidrogenación del enlace C=C y/o a un efecto electrónico. Se puede suponer que estas bases interactúan con la superficie del metal a través de su único par de electrones, lo que puede reducir la hidrogenación del enlace C=C. La mejora de la selectividad hacia la hidrogenación del enlace C=O en presencia de hidróxidos alcalinos se atribuye a la polarización de este enlace a través de la interacción entre el catión metálico, que actúa como un sitio ácido de Lewis, y el único par de electrones del átomo de oxígeno en el grupo C=O [41].

A.3. PROCESOS ELECTROQUÍMICOS

A.3.1. El hidrógeno como combustible alternativo y su producción vía electroquímica.

Según el informe emitido por la Agencia Internacional de Energía (AIE), la demanda global de energía aumentará más de un 25 % hasta 2040. Por otro lado, se prevé una grave escasez de petróleo y gas en un futuro cercano [42, 43]. Con el aumento de la demanda mundial de energía y el cambio climático generado a partir de la emisión de CO_2 originada por los combustibles fosiles, existe una necesidad inminente de encontrar una alternativa química para producir energía que sirva de alternativa a los combustibles fósiles.

El hidrógeno (del griego "formador de agua") es uno de los productos químicos más prometedores en cuanto a la generación de energía [43-46] debido a que puede generar energía produciendo únicamente agua como subproducto y a que la energía producida por unidad de masa del hidrógeno (142 MJ/kg) es al menos tres veces mayor que la de otros combustibles químicos comunes (a modo de ejemplo, el

valor equivalente para los hidrocarburos líquidos es de aproximadamente 47 MJ/kg). El hidrógeno se produjo artificialmente por primera vez a principios del siglo XVI mezclando metales con ácidos. Es un elemento abundante, equitativamente distribuido a lo largo del mundo y que también puede servir como materia prima para sintetizar combustible líquido fácilmente transportable como el metano [47]. Sin embargo, el hidrógeno no se encuentra de forma aislada en la naturaleza sino formando moléculas con otros elementos, como el agua o los hidrocarburos. Esto hace que no se pueda aprovechar directamente, sino que es necesario producirlo a partir de diferentes métodos, y dicha producción resulta un factor crítico para la llamada "economía del hidrógeno". Debido a su importancia como vector energético, en la actualidad hay numerosas investigaciones relacionadas con su producción y almacenamiento. Existen diferentes fuentes a partir de las cuales se puede obtener H_2, como son el agua, la biomasa, el gas natural, el petróleo o el carbón. Lamentablemente, alrededor del 95% de la producción de H_2 se basa en el uso de combustibles fósiles (reformado con vapor de gas natural) y el H_2 producido a partir de electrólisis de agua y biomasa ha irrumpido más tarde suponiendo únicamente el 4 y 1% respectivamente [48]. El lastre del alto consumo eléctrico que llevan consigo los procesos electroquímicos son los responsables de esta cifra.

La mayoría del hidrógeno que se produce (en torno a 70 millones de toneladas al año según la Agencia Internacional de la Energía) se consume como materia prima de otros procesos químicos, en lugar de destinarse a la producción de energía eléctrica. Debido a esto, tanto la Unión Europea como Estados Unidos y Japón apuestan directamente por la utilización de hidrógeno como materia prima para la producción de energía por las siguientes razones [6-8].

- Eficiencia energética: la energía química del H_2 puede ser convertida directamente en energía eléctrica sin subproductos ni pasos intermedios.
- Reducción de la dependencia energética hacia los combustibles fósiles: estos combustibles son reservas finitas y sus yacimientos están muy concentrados geográficamente, lo que da lugar a presiones políticas por parte de los países productores.
- Ventajas medioambientales: la producción de electricidad a partir de hidrógeno está libre de emisiones contaminantes.

Se han hecho grandes esfuerzos en favor de la economía del hidrógeno, un ejemplo de ello es los automóviles con pila de combustible de hidrógeno distribuido por Toyota desde 2014. Sin embargo, actualmente existen todavía serios problemas de seguridad, transporte y menor densidad energética del hidrógeno en los países en desarrollo en comparación con los combustibles líquidos basados en carbono que hacen difícil la implementación más amplia del hidrógeno como vector energético.

En este sentido y gracias a la creciente tendencia a la descarbonización del sistema energético. Debido a esto, numerosas tecnologías alternativas para la obtención de hidrogeno están ganado importancia, especialmente las técnicas de producción de hidrógeno vía electroquímica.

El proceso de electrólisis de agua consiste en la ruptura de la molécula de H_2O en oxigeno (O_2) e hidrógeno (H_2). La entalpía estándar de formación del agua a 25 ^{o}C y 1 atm es ΔH^0_f = -285,8 KJ/mol, un aporte energético, que puede ser en forma de energía calorífica o eléctrica.

El proceso de electrolisis fue descubierto por Troostwijk and Diemann in 1789 [49]. Unos años después, 1800 Alessandro Volta invento la pila eléctrica, y unas semanas después William Nicholson y Anthony Carlisle la utilizaron para realizar la electrólisis de agua. Este proceso consiste en hacer pasar corriente eléctrica continua a través de dos electrodos sumergidos en agua, de forma que el flujo de electrones provenientes del polo positivo (ánodo) al negativo (cátodo) permiten una reacción de oxidación – reducción sobre la superficie de los electrodos. El hidrógeno se distribuye en el cátodo, y por el contrario el oxígeno se forma en torno al ánodo, obteniéndose un hidrógeno de elevada pureza que puede utilizarse en la industria electrónica, farmacéutica o alimenticia además de otras aplicaciones.

En los últimos años el proceso de electrólisis de agua ha generado un gran interés ya que permite la producción de H_2 de elevada pureza a partir de agua, la cual está distribuida abundantemente por toda la superficie terrestre, lo que suscita un elevado interés en este tipo de proceso, especialmente si la electricidad requerida procede de fuentes renovables (eólica o solar).

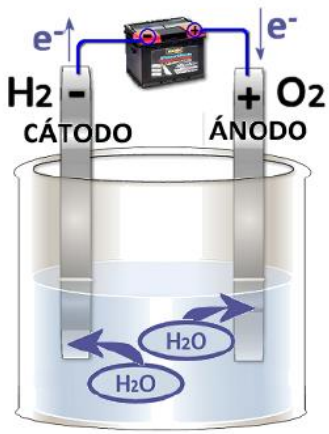

Figura A.5. Descomposición electroquímica del agua.

A.3.2. Producción de hidrógeno mediante electrólisis de agua en celdas de membrana polimérica.

La electrólisis de agua en medio ácido, basada en membranas de electrolito polimérico (PEM) es una tecnología moderna. El proceso inicialmente desarrollado por General Electric en la década de los 70, ofrecía diversas ventajas, pero a pesar de ello, y debido al elevado coste de los materiales necesarios para su desarrollo, la tecnología PEM quedó durante mucho tiempo relegada a las aplicaciones militares y aeroespaciales.

Para la reacción general de electrólisis de agua, hay tres principales tecnologías que se presentarán a continuación en la Tabla A.2.

- Alcalina, con un electrodo líquido (usualmente potasa).
- Polimérica, con un ionómero ácido.
- De alta temperatura, con un óxido sólido como electrolito.

Tabla A.2. Reacciones, intervalos y portadores de carga en diferentes tipos de electrólisis (fuente: STOLDEN, D(2010)).

Tecnología	Temperatura (ºC)	Cátodo (HER)	Portador de carga	Ánodo (OER)
Alcalina	40-90	$2H_2O + 2e^- \rightarrow H_2 + 2OH^-$	OH^-	$2OH^- \rightarrow \frac{1}{2}O_2 + H_2O + 2e^-$
Polimérica	20-100	$2H^+ + 2e^- \rightarrow H_2$	$2H^+$	$H_2O \rightarrow \frac{1}{2}O_2 + 2H^+ + 2e^-$
Alta Temp.	700-1000	$H_2O + 2e^- \rightarrow H_2 + 2O^{2-}$	O^{2-}	$O^{2-} \rightarrow \frac{1}{2}O_2 + 2e^-$

La Tabla A.2. muestra un resumen de las diferentes ecuaciones para la evolución de la reacción del hidrógeno (hydrogen evolution reaction, HER) y la del oxígeno (oxygen evolution reaction OER), el intervalo de temperaturas convencional y el protagonismo de los iones como portadores de carga a través de la membrana.

Actualmente, los electrolizadores han cobrado interés por sus aplicaciones de pilas de combustible o como sistemas de almacenamiento de energía. Las principales ventajas de los electrolizadores PEM son las siguientes (Figura A.6.):

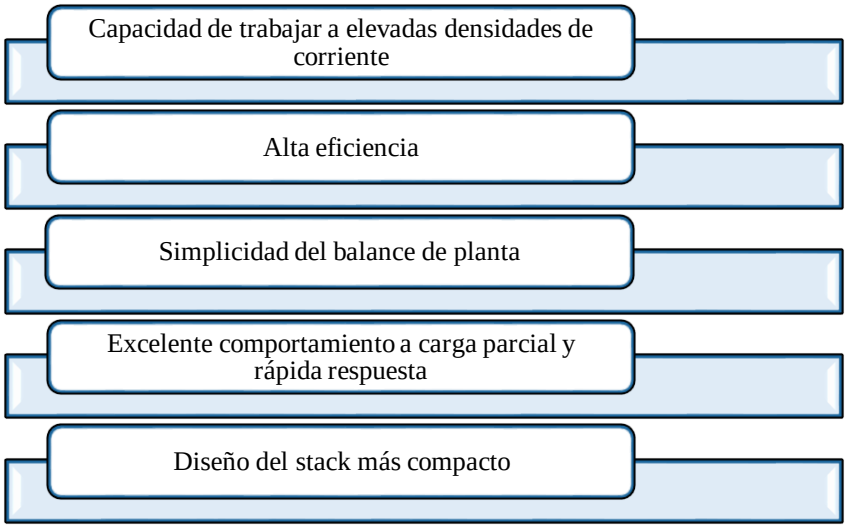

Figura A.6. Principales características de los electrolizadores PEM.

El elemento principal de una celda de electrólisis es la membrana polimérica, que es una estructura semipermeable, generalmente compuesta por ionómeros, diseñada para conducir protones o aniones hidroxilo. Su función esencial, una vez que se encuentra ensamblada con los electrodos formando una MEA (Membrane Electrode Assembly) en una celda de combustible o electrolizador tipo PEM (Proton Exchage Membrane), consiste en separar los reactivos y transportar los iones.

Los requisitos fundamentales que ha de satisfacer la membrana son:

- Alta conductividad iónica.
- Alta estabilidad mecánica.
- Estabilidad química a largo plazo.
- Bajo coste

- Proceso de producción respetuoso con el medio ambiente.

Los electrolizadores de intercambio protónico (PEM) pueden fabricarse a partir de membranas poliméricas puras o compuestas. En este sentido, una de las membranas poliméricas más utilizadas son las perfluorosulfonadas [50]. Estas se pueden adquirir comercialmente a través de compañías como Nafion®, Dow® (Dow Chemicals), Flemion® (asashi Glass), Aciplex® (Asashi Chemicals) y Sterion® (Hydrogen Works). Presentan ventajas como una alta resistencia a los ambientes oxidantes y reductores que hay en las celdas de combustible y han demostrado su estabilidad y fiabilidad en ensayos de larga duración. Además, cuando las membranas están hidratadas completamente, la conductividad llega a ser de 0,2 $S \cdot cm^{-1}$, que supone una mínima pérdida óhmica en operación [51]. Hay que reseñar que estas membranas deben estar hidratadas para permitir el paso de especies iónicas a su través, debido a la interconexión producida entre las regiones hidrófilas del polímero [52, 53].

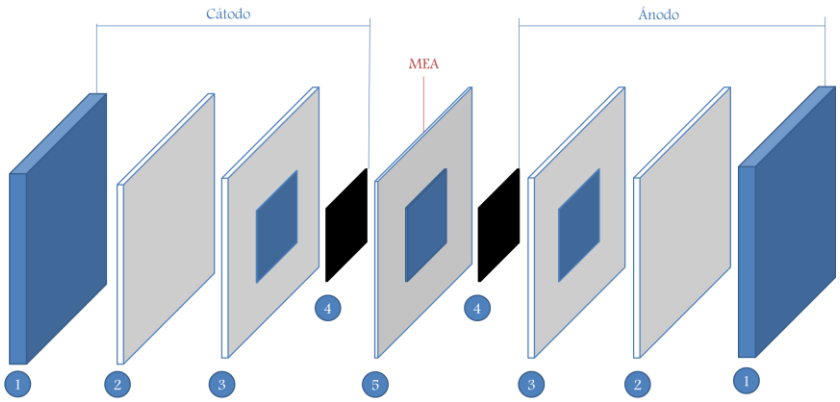

Figura A.7.Esquema celda PEM. (1. Placas bipolares, 2. Juntas, 3. Protectores de las capas difusoras de gases, 4. Capas difusoras de gases, 5. MEA.

Los electrolizadores PEM ofrecen la posibilidad de generar hidrógeno y oxígeno "in-situ" en pequeñas, pero altamente eficientes unidades que son capaces de trabajar de forma autónoma.

Los componentes fundamentales de una celda de electrólisis tipo PEM son: membrana de intercambio iónica, capa de difusión de gases, capa catalítica (que forma la MEA junto con la membrana) y las placas bipolares.

- **Capa catalítica:** zona en la que se producen las reacciones electroquímicas que tienen lugar en el reactor. Se sitúa entre el electrolito polimérico y la capa de difusión de gases, en contacto íntimo con ambas. Su presencia permite acelerar tanto las reacciones de oxidación como las de reducción, ya que en caso contrario, éstas serían demasiado lentas [54]. El otro componente de la capa catalítica es el soporte, que actúa como conductor electroquímico y permite la dispersión del catalizador para incrementar su área activa. En el caso de su empleo en reacciones de hidrogenación de hidrocarburos insaturados los catalizadores más empleados son Pt, Pd y Ru. Estos metales nobles tienen el inconveniente de su elevado precio y limitada disponibilidad, lo que hace necesaria la búsqueda de otros con metales de transición (Cu, Ni, Sn, Fe, etc) más económicos. La presencia del segundo metal conseguiría reducir la carga metálica, así como producir algún otro efecto beneficioso como aumentar la selectividad hacia otros compuestos que pueden resultar de interés.
- **Capa de difusión de gases:** (gas diffusion layer, GDL), se sitúa entre la capa catalítica y las placas bipolares. Para fabricar la capa de difusión se usan materiales carbonosos, como papeles y telas de carbón. Últimamente, se deposita sobre la capa de difusión de gases otra capa formada por carbón y Teflón, para proporcionar un

carácter hidrófobo, de tal manera que se ayude a mantener el balance de agua en el sistema y así reducir las resistencias de contacto entre la capa catalítica y el soporte [55]. En ocasiones, pueden utilizarse para la capa de difusión de gases materiales metálicos de gran resistencia química, como puede ser el titanio poroso [56].

- **Placas bipolares:** son el soporte del resto de elementos, facilitando el tránsito de electrones a través del circuito externo. A escala de laboratorio, estas placas suelen ser de grafito, debido a su estabilidad y alta conductividad química y térmica. Sin embargo, a escala real el grafito tiene una viabilidad limitada debido a sus costes, fragilidad y difícil mecanización por lo que se han propuesto materiales como el acero inoxidable o el titanio como alternativa [54].

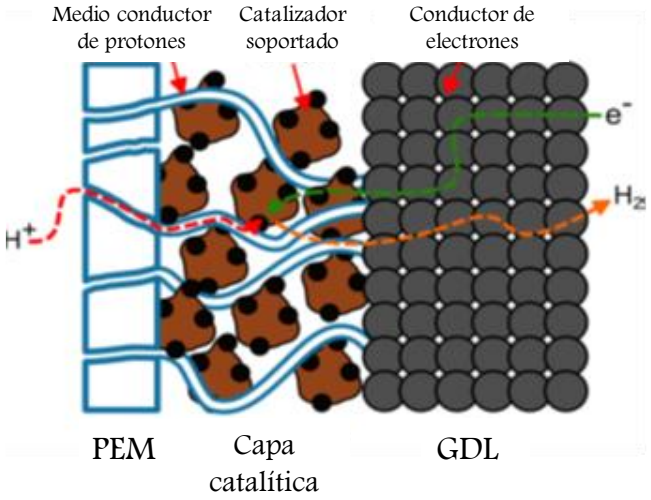

Figura A.8. Transporte de gases, protones y electrones en electrodo catódico de celda PEM.

El diseño de una celda polimérica se muestra de manera sencilla en la Figura A.7. Las partes anódica y catódica de la celda están separadas por la membrana polimérica. En algunos casos, los electrodos van

directamente depositados sobre la membrana, el conjunto membrana-electrodos junto con la capa de difusión de gases recibe el nombre de MEA (del inglés, membrane electrode assembly). Esta MEA se sitúa entre los colectores de corriente, que se encargan de distribuir la corriente a través de la celda electroquímica dando lugar al proceso electrolítico.

Un electrodo efectivo es aquel que equilibra correctamente los distintos medios de transporte de los procesos necesarios para el funcionamiento del sistema PEM (Figura A.8.). Se requieren tres procesos de transporte:

- Transporte de los protones desde la membrana al catalizador.
- Electrones desde los colectores de corriente al catalizador a través de la capa de difusión de gases.
- Transporte del reactante y de los productos desde la superficie del catalizador hacia los canales difusores y viceversa.

A.3.3. Procesos de hidrogenación electrocatalítica de moléculas orgánicas.

En los procesos de hidrogenación de compuestos orgánicos tradicionales resulta imperativo el control de las condiciones de operación, debido a que se requiere alta presión y temperatura y una fuente de hidrógeno de alta pureza. Por ello, la electrosíntesis supone un proceso alternativo y seguro para sintetizar reactivos como cetonas, aldehídos, compuestos nitrogenados, nitrilos, hidrocarburos aromáticos y olefinas.

La hidrogenación electroquímica, por tanto, es una alternativa a la hidrogenación catalítica convencional, ya que este tipo de procesos se llevan a cabo bajo condiciones moderadas de presión (atmosférica) y temperatura (<80^{o}C). Sin embargo, cabe destacar que, a pesar de las

distintas configuraciones electroquímicas disponibles, apenas se encuentran estudios sobre procesos de hidrogenación en celda PEM. No obstante, ha ganado importancia en las últimas dos décadas debido a su interés tanto industrial como medioambiental. En la Tabla A.3 se muestran algunas moléculas hidrogenadas electroquímicamente y que han sido publicadas recientemente:

Tabla A.3. Moléculas orgánicas hidrogenadas electrocatalíticamente. Presión atmosférica y temperatura ambiente.

Moléculas	Catalizadores		Productos	Configuración	Ref.
	Fase activa	Soporte			
Etileno	Pt		Etano		[40]
Benceno	Pt, Rh		Ciclohexano		[57]
Acetofenona	Pd		1-Feniletanol		[58]
			Etilbenceno		[59]
Tolueno	Pt, Rh, Ru	Carbón	Metilciclohexano	Celda PEM Celda H	[60]
Ácido mucónico	Cu, Fe Pd, Ni, Sn, Pb		Poliamidas y poliésteres (nylon) de base biológica		[61]

Por otro lado, los avances realizados en la fabricación de materiales nanoestructurados soportados sobre materiales conductores, junto con el uso de membranas poliméricas sólidas de intercambio que pueden ser utilizadas para la fabricación de MEAs, han dado lugar a numerosos avances en el campo de las celdas de membrana polimérica PEM. Actualmente hay una gran cantidad de celdas de membrana polimérica en el mercado que podrían ser empleadas para la síntesis electroquímica a escala industrial de productos farmacéuticos y de química fina [58].

De acuerdo con lo publicado en literatura disponible [62-64], el mecanismo de hidrogenación electroquímica de una molécula orgánica

insaturada se divide en tres pasos. El mecanismo se describe por las reacciones (Ec. A.1 – A.3) donde M representa la superficie metálica, (H)M representa el hidrogeno quimisorbido, y (Y=Z)M el sustrato orgánico absorbido. El primer paso es la electroducción de agua (a iones hidrónio) con la formación de hidrogeno adsorbido en la superficie del electrodo (Reacción de Volmer, Ec. A.1), seguido por la reacción del sustrato adsorbido (Y=Z) con el hidrogeno quimisorbido (Ec. A.3.). En el sistema tiene lugar una reacción competitiva entre la reacción de hidrogenación (Ec. A.3) y la desorción de hidrogeno por un sentido electroquímico (Ec. A.5, reacción de Heyrovsky) y/o químico (Ec. A.6, reacción de Tafel)

$$H_3O^+ + 2e^- + M \rightleftarrows 2(H)M + 2(OH^-)H_2O \quad \text{[Ec. A.1]}$$

$$Y{=}Z + M \rightleftarrows (Y{=}Z)M \quad \text{[Ec. A.2]}$$

$$(Y{=}Z)M + 2(H)M \rightleftarrows (YH\text{-}ZH)M \quad \text{[Ec. A.3]}$$

$$(YH\text{-}ZH)M \rightleftarrows YH\text{-}ZH + M \quad \text{[Ec. A.4]}$$

$$H_2O + (H)M + e^- \rightleftarrows M + H_2 + OH^- \quad \text{[Ec. A.5]}$$

$$2(H)M \rightleftarrows 2M + H_2 \quad \text{[Ec. A.6]}$$

Sin embargo, en procesos de hidrogenación electroquímica de sustancias orgánicas, los únicos procesos que tienen lugar son los de hidrogenación y evolución de hidrógeno [65], estableciéndose la eficiencia de corriente como una medida de la competitividad de estas dos reacciones. La eficiencia de la hidrogenación electroquímica está relacionada con cada una de estas reacciones, las cuales dependen de la naturaleza del electrodo, el reactivo empleado o las condiciones de reacción. Para los compuestos orgánicos es importante tener un buen equilibrio adsorción/desorción, ya que la adsorción/desorción demasiado baja o demasiado fuerte resulta perjudicial. Cabe destacar que

también se producen reacciones competitivas tales como la producción de hidrógeno molecular.

Las celdas PEM de membrana polimérica pueden resultar excelentes reactores para la hidrogenación selectiva de dichas moléculas orgánicas insaturadas de acuerdo con el mecanismo de reacción que ocurre en el compartimento catódico detallado anteriormente. El tipo y composición de los productos vendrá determinado por numerosos factores, como el tipo de soporte, la utilización de un disolvente prótico o aprótico, pH, la naturaleza y morfología que conforma el catalizador y el electrodo [66].

Tabla A.4. Comparación entre hidrogenación por via electrocatalítica e hidrogenación catalitica convencional.

	HIDROGENACIÓN POR VÍA ELECTROCATALÍTICA	HIDROGENACIÓN CATALITICA CONVENCIONAL
VENTAJAS	- Condiciones más suaves de trabajo (P y T). - Posibilidad de producir el hidrógeno in-situ de alta pureza - Control fácil y rápido del caudal de producción de H_2. - Unidad compacta que combina la producción de H_2 con la reacción de hidrogenación catalítica - Reducción del impacto medioambiental - Posibilidad de operar en modo continuo	- Tecnología madura - Experiencia práctica en plantas - Selectividades y conversiones muy altas.
INCONVENIENTES	- Tecnología poco desarrollada - Experiencia práctica limitada - Necesidad de catalizadores muy específicos.	- Altas presiones de reacción (1 – 10 atm) - Posible dificultad a la hora de extraer el catalizador. - Uso de recursos no renovables

Como se expone anteriormente, el interés de esta configuración viene motivado por el hecho de que en este caso no se requiere de una fuente de hidrógeno externa, sino que se produce hidrógeno in-situ. Además, es posible operar en modo continuo en la cámara catódica. Por

todo ello la hidrogenación electroquímica es considerada como una alternativa interesante, más económica y segura que los precedentes convencionales.

A.4. OBJETIVO Y ALCANCE DE LA TESIS

Hasta la fecha, no se han abordado estudios sobre hidrogenación electroquímica de cinamaldehído. Por esta razón y dado el gran valor añadido de los productos obtenidos de la hidrogenación de dicha molécula, el objetivo de esta Tesis Doctoral está orientado al estudio de la reacción de hidrogenación del cinamaldehído por vía electroquímica, la reacción se llevó a cabo en un electrolizador tipo PEM en el que se producía H^+ mediante electrólisis de agua en el compartimento anódico, que atravesaba la membrana de intercambio protónico para recombinarse en el cátodo.

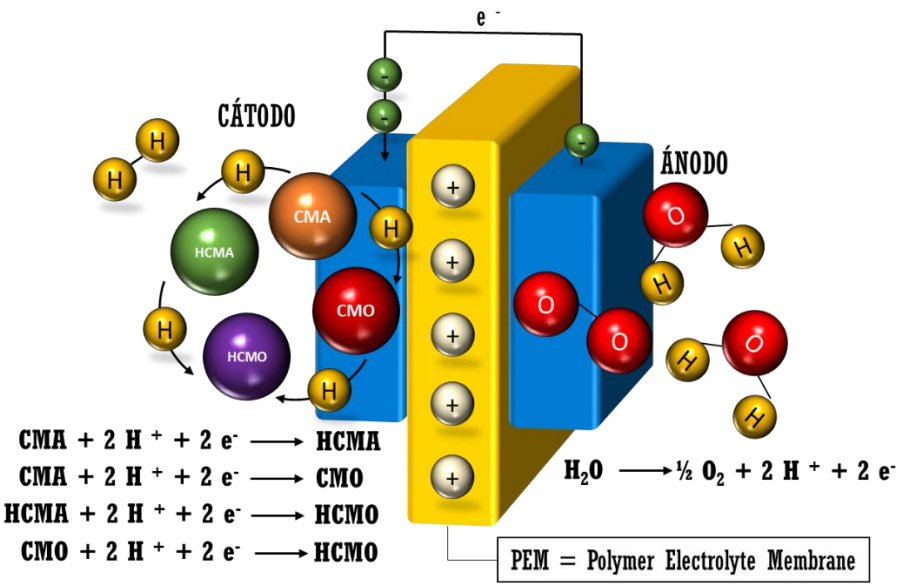

Figura A.9. Esquema de la hidrogenación electroquímica de cinamaldehído.

La presente Tesis Doctoral se centró especialmente en estudio de la composición del cátodo (manteniendo en todos los casos la composición del ánodo, IrO_2 comercial al 99 %).

Con el fin de alcanzar el objetivo general se ha desarrollado un programa de trabajo que se puede dividir en los siguientes objetivos parciales:

- Revisión bibliográfica de los estudios publicados para orientar y explicar adecuadamente la experimentación.
- Optimización de las condiciones de operación: temperatura, intensidad de corriente aplicada, modo de operación y caudal de reactivo suministrado a la celda PEM.
- Estudio de los diferentes métodos de preparación del catalizador de Pt utilizado en el compartimento catódico reduciendo la fase activa in-situ con un agente químico reductor.
- Estudiar los agentes reductores de la fase activa presente en el catalizador que dieran como resultado los valores más altos de conversión y selectividad.
- Estudio de la influencia de la carga de metal activo y la concentración de NaOH en el proceso de síntesis.
- Estudiar de la influencia de la adición de un segundo metal de carácter menos noble que el Pt.
- Estudio de la influencia de la modificación de cargas de metal activo en catalizadores bimetálicos de PtNi y PtCo.
- Estudiar la influencia de la adición de una base débil a la disolución de reactivo para estudiar su posible influencia en la producción de compuestos no deseados.
- Estudio de la influencia del material utilizado para la capa de difusión de gases.

- Estudiar diferentes soportes catalíticos y su influencia en la conversión y selectividad hacia los productos deseados.

En la siguiente Figura se muestra a modo de resumen los diferentes objetivos y etapas que se han seguido en la presente Tesis Doctoral.

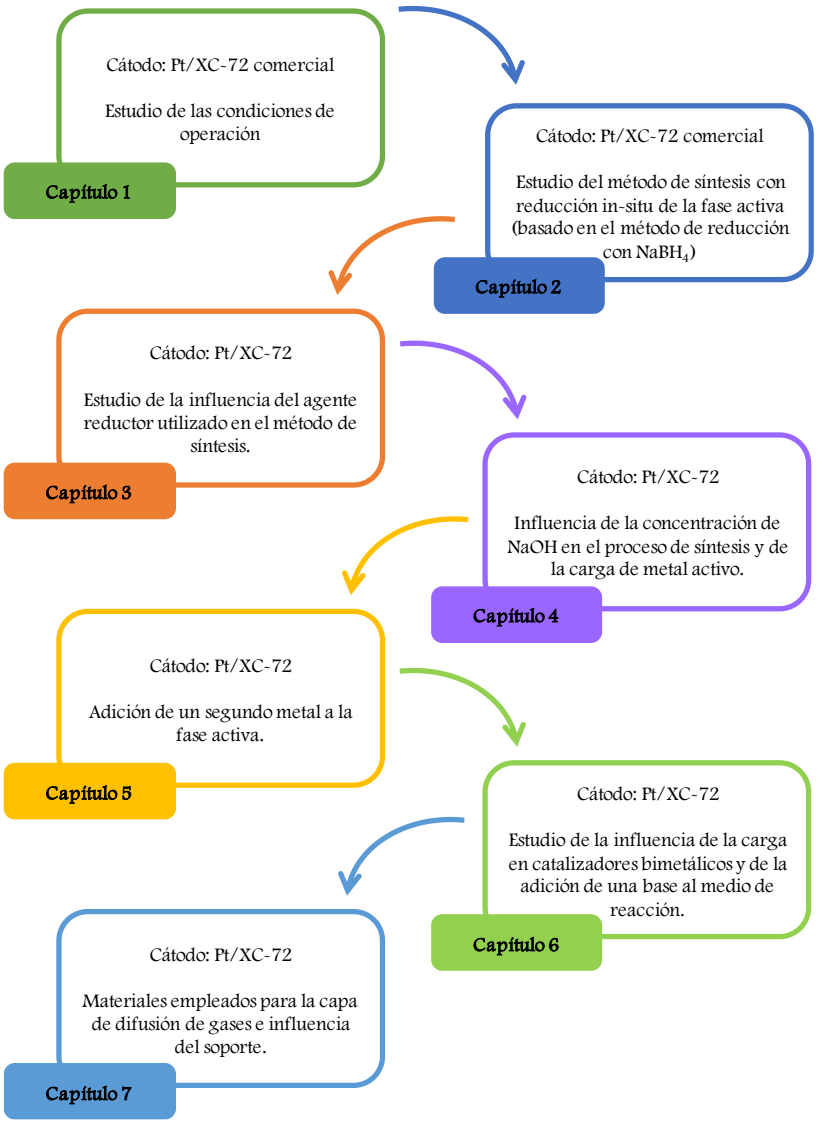

Figura 1.10. Esquema resumen de los distintos objetivos de la tesis doctoral.

B. MÉTODOS E INSTALACIONES EXPERIMENTALES

B.1. REACTIVOS EMPLEADOS

En las tablas B.1, B.2 y B.3 se muestran los reactivos comerciales empleados para la síntesis y caracterización de los distintos catalizadores que dan lugar a los electrodos (ánodo y cátodo), preparación de tintas, tratamiento de membranas y experimentos de hidrogenación electrocatalítica de cinamaldehído.

Tabla B.1. *Gases empleados*

Gases	Envase	Suministrador	Pureza (%)
Aire	Botella de acero a 200 bar	PRAXAIR	99,99
Nitrógeno			
Hidrógeno			
Oxígeno			
Argón			
H_2 (5 % vol)/Ar			5
H_2 (20 % vol)/Ar			20

Tabla B.2. Reactivos líquidos empleados

Reactivo	Pureza (%)	Suministrador
Agua Milli-Q	----------	----------
Nitrógeno líquido	----------	----------
Agua oxigenada (H_2O_2)	33	PANREAC
Ácido sulfúrico (H_2SO_4)	95 – 97	SIGMA ALDRICH
Nafion (5 %wt)	5	ALDRICH CHEMISTRY
2-propanol (preparación tintas)	99,9	SIGMA ALDRICH
Ácido perclórico ($HClO_4$)	70	PANREAC
2-propanol (disolvente)	HPLC	VWR CHEMICALS
Amoniaco (NH_4OH)	32	PANREAC APPLICHEM
Cinamaldehído	99	ALDRICH CHEMISTRY
Ácido Clorhídrico (HCl)	37	PANREAC
Etilenglicol ($C_2H_6O_2$)	99,8	SIGMA ALDRICH
Ácido fórmico (HCOOH)	85	PANREAC

Tabla B.3. Reactivos sólidos empleados

Reactivo	Pureza (%)	Suministrador
Carbón Vulcan XC-72	----------	FUEL CELL STORE
Ácido Hexacloroplatínico Hexahidratado ($H_2PtCl_6 \cdot H_2O$)	99,9	CYMIT QUÍMICA
Óxido de Iridio (IrO_2)	99	ALFA AESAR LOT: 61400797
Cloruro Sódico (NaCl)	99	PANREAC APPLICHEM
Hidruro sódico (NaOH)	98	PANREAC APPLICHEM
Cloruro de cobre ($CuCl_2$)	99,9	SIGMA ALDRICH
Cloruro de niquel hexahidratado ($NiCl_2 \cdot 6H_2O$)	98	PANREAC
Cloruro de hierro (III) ($FeCl_3$)	97	PANREAC
Cloruro de cobalto hexahidratado ($CoCl_2 \cdot 6H_2O$)	97	SIGMA ALDRICH
Cloruro de estaño dihidratado ($SnCl_2 \cdot 2H_2O$)	99,9	SIGMA ALDRICH
Borohidruro de sodio ($NaBH_4$)	99,9	ALDRICH CHEMISTRY
Borohidruro de potasio (KBH_4)	99,9	ALDRICH CHEMISTRY
Membrana de Nafion	----------	HIDROGENA

B.2. PREPARACIÓN DE CATALIZADORES

B.2.1. Método de impregnación y reducción con borohidruro

La síntesis de algunos de los catalizadores empleados como cátodo (capítulos 2 y 3) se lleva a cabo mediante el método de impregnación y reducción in-situ con borohidruro, cuyo procedimiento es el siguiente:

- 400 ml de agua mili-Q se calientan a 70 ºC y se agitan mediante una placa calefactora marca AGIMATIC-N.
- A continuación, se adiciona la cantidad requerida de soporte en polvo y se agita durante 6 horas.
- Seguidamente, se incorpora la sal precursora de Pt, en la cantidad requerida, y se agita durante 12 horas con el fin de obtener una mezcla homogénea para conseguir una mejor deposición de ambos metales.
- La disolución se calienta de nuevo a 80ºC y se agrega a la mezcla el agente reductor ($NaBH_4$) en disolución al 5% en peso,

utilizando como base de cálculo 20 ml de disolución por cada gramo de metal total a reducir [67].

- El sistema se deja enfriar en agitación con el fin de completar el proceso de impregnación
- La disolución se filtra y se lava con 400 ml de agua desionizada en un Kitasato marca SIMAX mediante una bomba modelo ABM 4EKF63CX-4.
- Finalmente, el polvo resultante se deja secar durante 12 horas a 80 ºC en una estufa marca SELECTA.

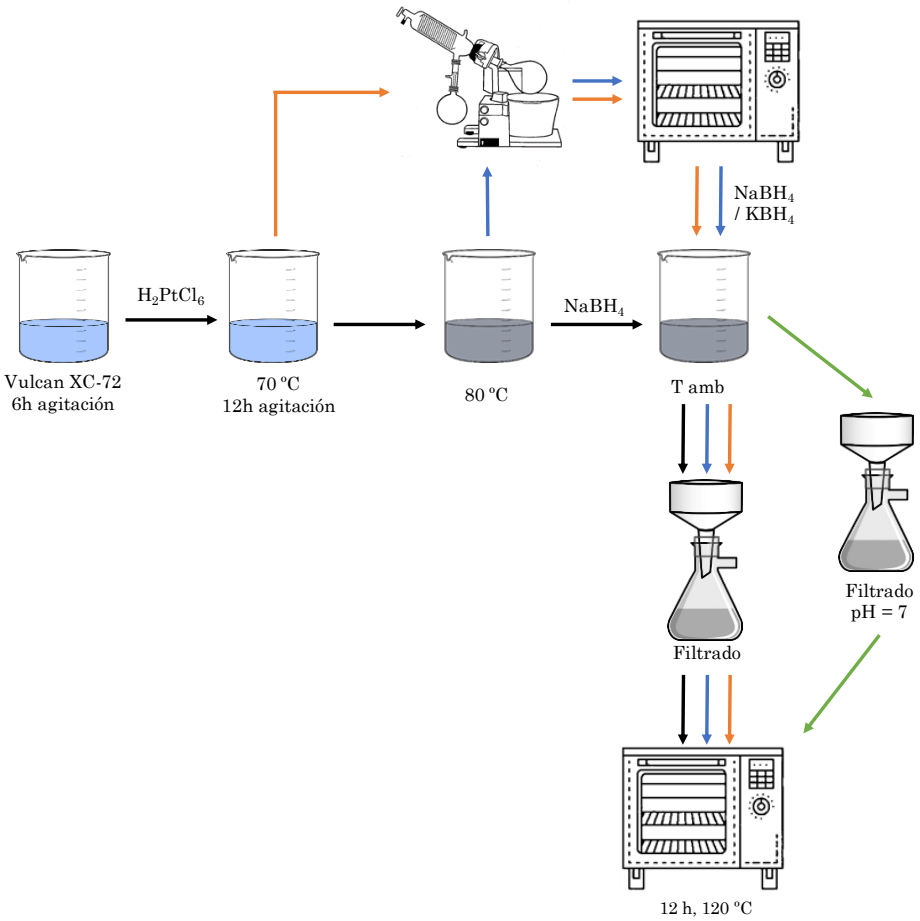

Figura B.1. Esquema del método de impregnación y reducción con borohidruro.

No obstante, este método se modificó con el objetivo de obtener mejores resultados electrocatalíticos. Para ello, se añadieron diferentes modificaciones al método original para los estudios realizados en el Capítulo 2:

- Evaporación del disolvente a vacío previamente a la adición del agente reductor.
- Lavado durante la filtración con la cantidad de disolvente necesaria para conseguir un pH = 7.
- Incorporación de la sal precursora de platino gota a gota.

Mediante el procedimiento experimental anteriormente descrito, en el Capítulo 3 de la presente tesis doctoral se sintetizaron catalizadores catódicos cambiando el agente reductor por KBH_4. La figura B.1. muestra un esquema del proceso de síntesis con las modificaciones realizadas.

B.2.2. Método de impregnación y reducción con ácido fórmico

Este método consiste en utilizar ácido fórmico como agente reductor de las sales precursoras de Pt. Con esta técnica se sintetizó el catalizador Pt/C-FA utilizado en el Capítulo 3. El procedimiento es el siguiente:

- 500 ml de disolución acuosa de ácido fórmico 0,1 M a los cuales se incorpora el soporte, se calientan hasta una temperatura de 70 ºC bajo agitación constante con una placa AGIMATIC-N.
- Seguidamente, se añade la sal de metal precursor gota a gota y se aumenta la temperatura hasta 80 ºC.
- Cuando se alcanza la temperatura de 80 ºC, se deja enfriar la disolución a temperatura ambiente bajo agitación constante.

- La disolución se filtra y se lava tres veces con 300 ml de agua desionizada en un Kitasato marca SIMAX mediante una bomba modelo ABM 4EKF63CX-4.
- Finalmente, se seca en estufa (SELECTA) durante 12 horas.

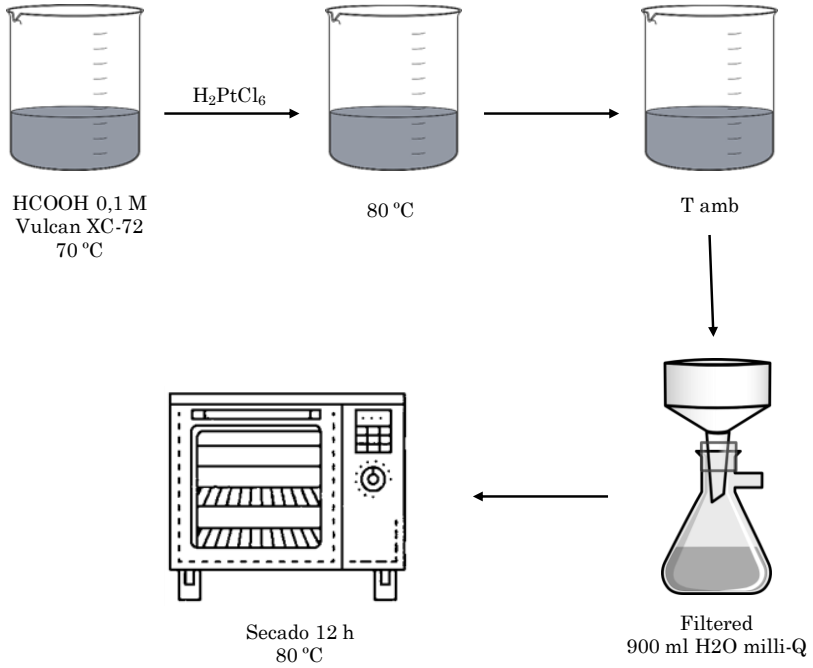

Figura B.2. Esquema del método de impregnación y reducción con ácido fórmico.

B.2.3. Método de impregnación y reducción del poliol modificado

Este método emplea etilenglicol como estabilizante y agente reductor, además de actuar como surfactante para prevenir la formación de aglomerados antes de formar partículas coloidales de catalizador. Además, se emplea también hidróxido sódico, que tiene como objetivo el control del pH durante la síntesis. Las condiciones de síntesis varían respecto a los anteriores métodos según se describe en la Figura B.3. Mediante este método se sintetizaron los catalizadores estudiados en los Capítulos 3 – 7 de la presente memoria. La carga de los catalizadores

sintetizados por el método descrito varía en función de los requerimientos de la investigación.

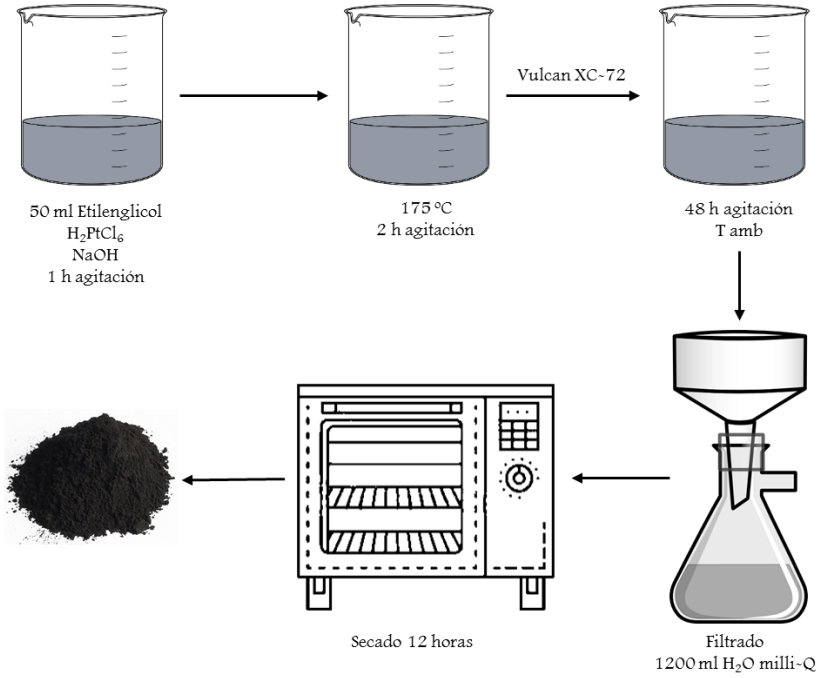

Figura B.3. Método de reducción del poliol modificado

B.2.4. Método de impregnación humeda incipiente

Este método consiste en utilizar una corriente de H_2 gaseoso como agente reductor de forma posterior a la síntesis del catalizador. Con esta técnica se sintetizó el catalizador Pt/C-IM utilizado en el Capítulo 3. El procedimiento es el siguiente:

- Primeramente, el soporte se mantiene a vacio a temperatura ambiente durante 2 horas con el objetivo de eliminar el agua y otras impurezas.
- Posteriormente, una cierta cantidad de disolución acuosa que contiene la sal precursora de Pt se añade gota a gota en el

soporte lo que permite que la disolución acusa penetre en los poros del soporte, donde se deposita el metal precursor.

- Seguidamente, se elimina el disolvente sometiendo la muestra a condiciones de vacio durante 2 horas a una temperatura de 90 ^{o}C.
- El polvo resultante se seca en una estufa (SELECTA) durante 12 horas.
- Finalmente, el catalizador se reduce a su estado metálico mediante una corriente de H_2 (100 ml/min) a 250 ^{o}C durante dos horas.

B.3. PREPARACIÓN DE ELECTRODOS Y MEAs.

Para llevar a cabo reacciones de hidrogenación electrocatalítica en celda PEM es necesario por un lado acondicionar la membrana (Hidrogena Desarrollos Energéticos) de intercambio protónico y por otro preparar las tintas de catalizador que dan lugar a los electrodos. El proceso de pretratamiento de la membrana consiste en:

- 1 hora en una disolución de H_2O_2 al 3 % para eliminar posibles compuestos orgánicos.
- 1 hora en agua mili-Q a ebullición con el objetivo de eliminar residuos del proceso anterior.
- 1 hora en una disolución de H_2SO_4 0,5 mol·L^{-1} necesaria para activar la membrana.
- 1 hora en agua mili-Q a ebullición para eliminar los compuestos impregnados en la membrana.

Respecto a la preparación de tintas, la tinta empleada se prepara a partir de óxido de iridio (IrO_2) comercial para dar lugar a un electrodo anódico (2 mg·cm^{-2}). Para ello, se disuelve el catalizador en una

proporción adecuada de agua y Nafión (15,4% en peso). Y se agita mediante ultrasonidos durante dos horas.

La tinta que da lugar al cátodo se prepara a partir de la disolución de los catalizadores empleados en los Capítulos 1 – 7 de la presente tesis doctoral disueltos en 2 – propanol y Nafion® (5 %wt) con una carga de 0,5 $mg \cdot cm^{-2}$ de carga metálica total. Posteriormente se agita de forma análoga a las tintas anódicas.

A continuación, se deposita directamente y de forma uniforme a ambos lados de la membrana la tienta preparada anteriormente mediante aerografía (impregnación por spray). Así se da lugar al conjunto membrana – electrodo que se encuentra situado entre capas de difusión de gases conductoras (Ti poroso) en el caso de los estudios realizados en los Capítulos 1 – 6 y parte del Capítulo 7. En el Capítulo 7 la MEA está constituida por IrO_2 (ánodo), el catalizador catódico objeto de estudio y una capa de difusión de gases de papel de carbón (Fuel Cell Earth) conformando la superficie del electrodo de trabajo de 4 cm^2 (2 cm x 2 cm). Utilizando esta configuración se evita la etapa de ensamblaje presión y temperatura convencional.

B.4. TÉCNICAS DE CARACTERIZACIÓN FÍSICO - QUÍMICAS

B.4.1. Análisis de difracción de rayos X

Esta técnica permite analizar la estructura cristalina del catalizador y obtener un tamaño de partícula aproximado mediante la ecuación de Scherrer [68]. Esta técnica se empleó en los Capítulos 1 – 7 de la presente Tesis Doctoral.

Las medidas de DRX se llevaron a cabo en un difractómetro Philips PW-1700, que utiliza radiación Kα de Cu (λ = 1,5418 Å). Todas

las muestras han sido escaneadas a una velocidad de $0{,}02^{o}\cdot paso^{-1}$ en el intervalo $5^{o} < 2\theta < 90^{o}$ (tiempo de escaneo = $2\ s\cdot paso^{-1}$).

B.4.2. Espectroscopía de emisión de plasma por inducción (ICP-AES)

A partir de la espectrometría de masa se midió el contenido de Pt y del segundo metal M en el caso de los catalizadores bimetálicos (Capítulos 2 – 7). El objetivo del ICP-AES es hacer que los elementos emitan su onda de luz específica, la cual puede ser medida permitiendo determinar la cantidad de dicho elemento. El quipo utilizado para realizar los análisis es un Varian Liberty RL sequential ICP-AES de análisis multielemental. Las muestras se diluyen previamente utilizando una disolución equimolecular $HF/HCl/H_2O_2$ con el objetivo de asegurar la disolución total del metal.

B.4.3. Adsorción/desorción de N_2

El principio de medida del área superficial total de un sólido por fisisorción de un gas consiste en determinar el número de moléculas de gas requeridas para cubrir la superficie del mismo con una monocapa de adsorbato. Conocida el área ocupada por una molécula, parámetros como el área superficial del sólido, tamaño medio de poro y volumen total de poro pueden determinarse a partir del número de moléculas de gas adsorbidas, medidas voluméricas o gravimétricamente. Esta técnica se ha empleado para caraterizar cada uno de los catalizadores sintetizados de esta Tesis Doctoral.

El área superficial de los catalizadores ha sido analizada en un equipo de la marca Micromeritics ASAP 2010, que utiliza N_2 a – 196 ^{o}C como adsorbato. Previamente al análisis todas las muestras fueron desgasificadas a vacio a 180 ^{o}C ($1\cdot10^{-2}$ torr) durante 8 horas. El área

específica total ha sido determinada mediante el método de BET multipunto con un error relativo de menos del 5 %.

El volumen total de poro se determinó mediante la cantidad de vapor adsorbida a una presión relativa P/P_0 = 0,99, asumiendo que los poros son posteriormente llenados con adsorbato líquido. Por otro lado, el tamaño medio de poro se estimó a partir del valor de volumen total de poro y el área superficial, asumiendo que los poros que no se llenaban a presiones relativas inferiores a 1 no contribuían al volumen y área superficial de la muestra y una geometría cilíndrica de poro.

Las distribuciones de diametros de mesoporo y microporo, se determinarion mediante los métodos propuestos por Barret, Joyner y Halenda (BJH) y Horvath – Kawazoe, respectivamente.

B.4.4. Quimisorción de hidrógeno

La quimisorción se empleó para la determinación del área metálica activa de los catalizadores sintetizados en los Capítulos 2 – 4, utilizando H_2 como molécula sonda. Los experimentos de quimisorción se realizaron en un equipo de la marca AutoChem 2950 HP. Para ello se cargaron las muestras (0,05 g) en un reactor en U de cuarzo para posteriormente ser gasificadas en atmosfera de He. Tras enfriamiento a 40 ^{o}C y se realizaron adiciones de H_2 mediante pulsos bajo atmosfera de He hasta que el consumo de H_2 deja de ser detectado por el TCD. La dispersión metálica se calcula según la ecuación siguiente:

$$D\ (\%) = 100\left(\frac{V_S \cdot SF_{calc}}{SW \cdot 22414}\right) \cdot GMW_{calc} \qquad \text{[Ec. B.1]}$$

donde Vs es el volumen quimisorbido (cm^3 STP), SF_{calc} es el factor estequeometrico, SW corresponde con el peso de muestra (g) y GMW_{calc} es el peso molecular ($g \cdot g\text{-}mol^{-1}$)).

Por otro lado, el tamaño de partícula activo se ha calculado con la siguiente ecuación:

$$APS = \frac{6}{(D_{calc}) \cdot \left(\frac{W_s}{GMW_{calc}}\right) \cdot (6{,}023 \cdot 10^{23}) \cdot (SA_{calc})} \qquad \text{[Ec. B.2]}$$

donde D_{calc} es la densidad del metal ($g \cdot cm^3$) y SA_{calc} es el área superficial específica (por gramo de metal).

Por último, el área metálica superficial de las partículas (CSA), se calcula mediante la siguiente ecuación:

$$CSA = \left(\frac{V_s}{W_S \cdot 22414}\right) \cdot (SF_{calc}) \cdot (6{,}023 \cdot 10^{23}) \cdot (SA_{calc}) \qquad \text{[Ec. B.3]}$$

B.4.5. Titraciones ácido/base

Se llevaron a cabo titraciones con el objetivo de determinar el carácter ácido o básico de los catalizadores sintetizados. Las distintas titraciones se llevaron a cabo en el equipo SCHOTT Titroline (Titroline SCHOTT). Dicha técnica consiste en la disolución de 25 mg de muestra con 25 mL de una disolución de NaCl 0,1 $mol \cdot L^{-1}$, que se llevó a pH 11 con NaOH 0,1 $mol \cdot L^{-1}$. A continuación, se añade 0,01 mL de HCl 0,1 $mol \cdot L^{-1}$ hasta llegar a un valor de pH de 3. La basicidad de la muestra se calcula dividiendo el volumen de HCl gastado entre la cantidad de

muestra inicial y se expresa en $cm^3 \cdot g^{-1}$. En los catalizadores empleados en los Capítulos 2 – 7 se realizaron titraciones ácido base.

B.4.6. Reducción a temperatura programada (TPR)

Este tipo de análisis se ha realizado en cada uno de los catalizadores sintetizados a lo largo de esta Tesis Doctoral. La reducción a temperatura programada es una técnica que permite, en función de la temperatura de reducción de los óxidos metálicos, conocer qué óxidos y en qué cantidad relativa se encuentran presentes en la superficie de nuestro catalizador, de acuerdo al área bajo la curva de consumo de H_2. Los distintos ensayos se llevaron a cabo en un equipo Micromerits AutoChem 2950 HP equipado con un detector TCD. Las muestras (0,15 g) se cargaron en un reactor en U de cuarzo y fueron calentadas a 900 ^oC (con una rampa de calentamiento de 5 $^oC \cdot min^{-1}$), bajo atmosfera de reducción (20% v/v H_2/Ar, 60 $NmL \cdot min^{-1}$).

B.5. TÉCNICAS DE CARACTERIZACIÓN ELECTROQUÍMICA

Las técnicas de caracterización electroquímicas proporcionan información sobre la relación entre la intensidad de corriente y el potencial. Para realizar las medidas de polarización se utilizó un Potenciostato-Galvanostato, (Autolab, PGSTAT128N, Ecochemie, The Netherlands).

La semicelda electroquímica acoplada al electrodo de disco rotatorio consta de una celda de vidrio, de 200 ml, en la que se acopla una tapa que permite la instalación de tres electrodos (electrodo de trabajo, electrodo de referencia y contraelectrodo) y una tubería de entrada y salida para inertizar la disolución de trabajo mediante el burbujeo de nitrógeno dentro de la celda. El electrodo de referencia es

Ag/AgCl Metrohm® (KCl 3 mol·L^{-1}) y el contra-electrodo una hoja de platino (1 cm^2, Metrohm). El electrodo de trabajo (de área geométrica de 0,53 cm^2) es donde se deposita el catalizador objeto de estudio.

En el caso particular de la caracterización electroquímica, se depositan 10 µl de catalizador sobre la punta del carbón vítreo. En este caso, la tinta se prepara con 2 mg de catalizador; 0,75 ml de 2-propanol; 0,25 ml de agua milli-Q y 8 µl de Nafion.

B.5.1. Voltametría cíclica

La voltametría cíclica o voltamperometría, es una técnica de análisis cuantitativo ampliamente empleada para caracterizar un sistema electroquímico. Esta técnica permite observar el comportamiento de óxido-reducción es un intervalo amplio de potencial. De ella se puede extraer información tan interesante como electrones transferidos en la reacción, potenciales formales, mecanismos de reacción o coeficientes. Además, mediante este ensayo se puede determinar la estabilidad frente a la corrosión electroquímica de los electrodos. Para este test electroquímico se ha utilizado una semicelda de tres electrodos. Como electrodo de trabajo se ha utilizado un electrodo de carbón vítreo de 5 mm de diámetro (Metrohm, Autolab), un contraelectrodo de Pt (Metrohm), y un electrodo de referencia de Ag/AgCl (Metrohm). Como electrolito se ha utilizado una disolución de $HClO_4$ 0,1 M (Scharlab). Previamente a todos los experimentos de caracterización el electrodo de trabajo ha sido limpiado mediante pulido con pasta de alumina (0,3 µm).

Antes de cada voltametría, la celda fue sometida a una desoxigenación mediante burbujeo de N_2 durante 20 minutos para conseguir la atmosfera inerte necesaria. Tras la purga, se realizó una limpieza electroquímica del catalizador ciclando el potencial varias veces desde 0,0 a 1,3 V vs RHE. Todos los potenciales referidos en esta tesis

doctoral están referidos al electrodo estándar de hidrógeno (RHE) de acuerdo con la ecuación de Nernst:

$$E_{RHE}=E_{Ag/AgCl}+0{,}059\cdot pH+E^{0}_{Ag/AgCl} \qquad \text{[Eq. 2.5]}$$

donde E_{RHE} es el potencial corregido vs RHE, $E^{o}_{Ag/AgCl}$ = 0,1976 a 25 ^{o}C, y $E_{Ag/AgCl}$ es el potencial medido experimentalmente con respecto al electrodo Ag/AgCl.

Para conocer la actividad electrocatalítica de los catalizadores estudiados se realizaron 500 voltametrías cíclicas (0,0 – 1,3 V vs RHE) at 50 mV·s^{-1}. Esta actividad electrocatalítica se determina a partir del cálculo del área superficial electroquímica activa (ECSA), que hace referencia a la dispersión del catalizador sobre la superficie del electrodo, y ha sido calculada mediante la siguiente ecuación:

$$ECSA = \frac{A_{Pt}}{v \cdot C} \cdot \frac{1}{L_e} \qquad \text{[Ec. B.4]}$$

donde A_{Pt} es el área de desorción de H_2 (A·V·cm^{-2}), v es la velocidad de escaneo (V·s^{-1}), C es la carga requerida para reducir un protón en la monocapa de platino active (0,21 mC·cm^{-2}) and Le es la carga de Platino en la capa catalítica.

Del mismo modo, se puede calcular el grado de degradación que sufre el electrodo durante un determinado tiempo de trabajo. Esta desactivación se calcularía como el porcentaje de perdida de carga de los catalizadores estudiados. Esta técnica ha sido empleada para conocer tanto la actividad electroquímica como la degradación del catalizador en cada uno de los catalizadores empleados a lo largo de esta Tesis Doctoral.

B.5.2. Reacción de Reducción/Evolución de Hidrógeno

El estudio de la reacción de reducción/evolución de hidrógeno se llevó a cabo a cabo por medio de una técnica de voltametría de barrido lineal la cual permite conocer la actividad catalítica del catalizador.

Para estos experimentos de caracterización electroquímica el electrodo fue primeramente saturado con hidrogeno puro (99,9999%). Después, se realizaron curvas de polarización desde 500 hasta 3000 rpm, aplicando un intervalo de potencial de 0,2 hasta 0,7 vs RHE, con una velocidad de barrido de 5 $mV \cdot s^{-1}$. Tanto la constante cinética como el orden de reacción se calculan mediante la siguiente ecuación:

$$\frac{1}{i} = \frac{1}{i_K} + \frac{1}{i_L} \qquad \text{[Ec. B.5]}$$

$$\frac{1}{i} = \frac{1}{i_K} + \frac{1}{B_L \cdot \omega^{1/2}} \qquad \text{[Ec. B.6]}$$

donde i representa la intensidad experimental, ik la corriente cinética en ausencia de limitaciones de transferencia de masa, id la corriente difusional y B_L la constante de Levich. Estos términos se pueden calcular con las siguientes ecuaciones:

$$i_K = k \cdot n \cdot A \cdot F \cdot C_{H_2} \qquad \text{[Ec. B.7]}$$

$$i_L = 0{,}62 \cdot n \cdot F \cdot A \cdot D^{2/3} \cdot \omega^{1/2} \cdot \upsilon^{-1/6} \cdot C_{O2} \qquad \text{[Ec. B.8]}$$

donde n es el número de electrones transferidos, F es la constante de Faraday (96485 $C \cdot mol^{-1}$), D es el coeficiente de difusión del H_2 en el electrolito. La corriente cinética y los electrones transferidos se

determinan gráficamente mediante la representación de Koutecky – Levich ($1/i$ vs $1/\omega^{1/2}$).

De este método de caracterización electroquímica se obtiene una curva de densidad de corriente frente al potencial a partir de cuyos datos cinéticos obtenidos de las reacciones de reducción/evolución fue realizado un análisis de Koutecky-Levich.

B.5.3. Estudios de impedancia electroquímica.

Con el objetivo de conocer la influencia de la capa de difusión de gases en la resistencia de la celda electroquímica, en el Capítulo 7 se han realizado estudios de impedancia electroquímica. Esta técnica permite cuantificar las diferentes resistencias que existen en el proceso: i) resistencia eléctrica correspondiente a la membrana o el ensamblaje, ii) resistencia del transporte de materia a través del ánodo y del cátodo. Los experimentos de impedancia electroquímica se han realizado a 70 ^{o}C, 1 atm y 0,5 ml·min^{-1} variando la frecuencia de 1000 a 0,1 Hz en un intervalo de potencial de 1,4 to 1,8 V. Para la cuantificación de estas resistencias se han realizado diagramas de Nyquist en los cuales se ha representado la resistencia real (Z') frente a la resistencia imaginaría (Z").

B.6. HIDROGENACIÓN ELECTROQUÍMICA DE CINAMALDEHÍDO

Los experimentos de hidrogenación electrocatalítica se han llevado a cabo en una celda tipo PEM. El cálculo de la producción de hidrógeno en el cátodo se ha realizado mediante la Ley de Faraday:

$$r_{H2} = \frac{I}{n \cdot F} \qquad \text{[Ec. B.9]}$$

donde r_{H2} es la velocidad de producción de hidrógeno ($mol \cdot s^{-1}$), n es el número de electrones intercambiados y F es la constante de Faraday (96485 $C \cdot mol^{-1}$).

Por otro lado, la conversión de CMA, selectividad hacia los diferentes compuestos, frecuencia de conversiones (TOF) y rendimiento a los productos deseados, se ha calculado de la siguiente manera:

$$\text{CMA conversion (\%)} = \left(\frac{m_{CMA}}{m_{CMAo} - m_{CMA}}\right) \qquad \text{[Ec. B.10]}$$

$$\text{Selectivity}_i\ (\%) = \frac{m_i}{m_{CMAo} - m_{CMA}} \times 100 \qquad \text{[Ec. B.11]}$$

$$\text{Yield}_{CMO} = \frac{\text{CMA conversion (\%)} \cdot \text{Selectivity}_{CMO}(\%)}{100} \qquad \text{[Ec. B.12]}$$

$$\text{TOF} = \frac{\text{CMA converted } (^{mol}/_{s})}{\text{mols surface Pt determined by } H_2 \text{ chemisorption}} \qquad \text{[Ec. B.13]}$$

B.7. INSTALACIONES EXPERIMENTALES ELECTROCATALÍTICAS EMPLEADAS

B.7.1. Sistema de disco rotatorio

El electrodo de disco rotatorio (EDR) es un sistema hidrodinámico ampliamente utilizado en estudios cinéticos ya que permite variar la velocidad de transporte de masa en un intervalo muy amplio. Un EDR consta de un disco con un material electrocatalítico rodeado por un tubo de un material no conductor (polietileno, teflón, etc.) construido de manera que sólo la superficie del electrodo en forma de disco está en contacto con la solución electrolítica. El electrodo gira en dirección perpendicular al eje de la cara del disco, de tal forma que se establecen

patrones de flujo bien definidos. Un esquema de la configuración experimental se muestra en la Figura B.4.

Figura 4. Representación esquemática de la instalación de semicelda

B.7.2. Celda electroquímica tipo PEM

Los experimentos de hidrogenación electrocatalítica de cinamaldehído se han llevado a cabo en una instalación como la que se describe a continuación, la cual está dotada de cuatro secciones: sistema de alimentación, sistema de reacción, sistema de polarización y sistema de análisis.

En la Figura B.5. se muestra una descripción de las partes que componen la instalación experimental en la que se han realizado los experimentos electrocatalíticos:

- Sistema de alimentación: constituido por una bomba peristáltica multicanal de la marca Heidolph (1 – 60 ml·min^{-1}), que permite la alimentación a los compartimentos anódico y catódico. Estas disoluciones se almacenan en matraces de 1 litro de capacidad (ALAMO) donde son calentados a la temperatura de trabajo mediante unas mantas calefactoras (SELECTA).

- Sistema de reacción: constituido por en un electrolizador tipo PEM cuyos componentes se esquematizan en la Figura B.5. La membrana sobre la cual se depositan los catalizadores/electrodos se sitúa entre dos placas difusoras de gases de 4 cm^2 (2 cm x 2 cm), protegidas por dos planchas de Teflón, cuya finalidad es asegurar un buen sellado entre los compartimentos anódico y catódico, y evitar de esta manera que tenga lugar un cortocircuito en la celda. A ambos lados de la MEA se sitúan dos placas bipolares de titanio con una serie de ranuras paralelas que sirven para dirigir el caudal, y cuya función es distribuir los productos y los reactivos y actuar como colectores de corriente. Todos los elementos citados anteriormente se encuentran situados entre dos placas de Teflón, cubiertas por dos capas de acero inoxidable, de 1 cm de espesor. El conjunto de la celda se sujeta con tornillos y tuercas empleando una llave dinamométrica (Gdore, 547 – 379) aplicando un par de torsión de 3,5 N·m, para asegurar una correcta estabilidad mecánica. Asimismo, tanto la celda, como las correspondientes entradas y salidas de los respectivos productos está dotada con un sistema de calentamiento y control de temperatura.
- Sistema de polarización: constituido por un potenciostato–galvanostato Autolab (PGSTAT128N), que permite la aplicación de la diferencia de potencial deseada entre los electrodos de la celda.
- Sistema de análisis: Los productos de la reacción de electrohidrogenación de cinamaldehído se analizan offline, cada 15 minutos, en un cromatógrafo de gases (modelo 7820A, AGILENT TECHNOLOGIES), equipado con una columna capilar DB-624 (30 m x 0,25 mm x 1,4 μm) y un detector ionizador de llama (FID). Este cromatógrafo fue calibrado previamente con patrones comerciales.

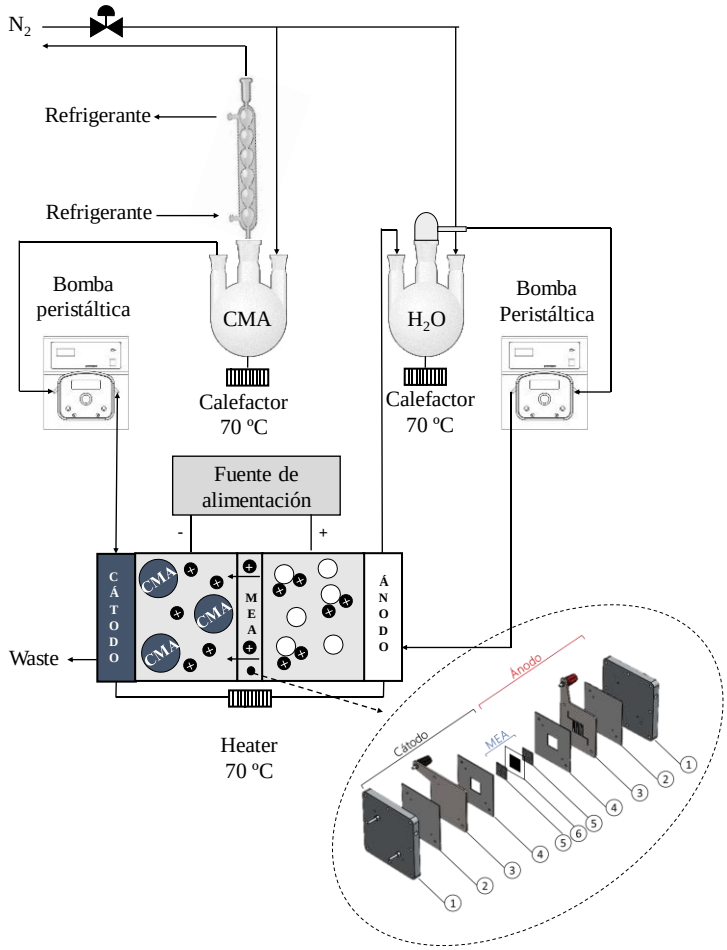

Figura B.5. Esquema instalación experimental y celda PEM. 1. Placas bipolares, 2. Juntas, 3. Colectores de corriente, 4. Protectores de las capas difusoras de gases, 5. Capas difusoras de gases, 6. Membrana con electrodo (MEA).

C. RESULTADOS Y DISCUSIÓN

La presente Tesis Doctoral está dirigida al estudio de la hidrogenación electroquímica de cinamaldehído en una celda electrocatalítica tipo PEM, ahondando en el estudio de diferentes catalizadores y componentes de la cámara catódica, donde tiene lugar la hidrogenación, manteniendo en todos los casos como catalizador anódico IrO_2 comercial. Para ello, en primer lugar, se ha corroborado la viabilidad técnica del sistema planteado en el que se produce hidrógeno in-situ mediante electrólisis de agua. A partir de ahí se han realizado estudios para determinar las mejores condiciones de operación, utilizando un catalizador Pt/C comercial al 20 % conformando la **Sección I**. El objetivo de la **Sección II** ha sido la optimización de un método de síntesis y reducción in situ que dé lugar a un catalizador catódico cuyas características mejoren los resultados de hidrogenación electrocatalítica de cinamaldehído. Para ello se ha realizado la optimización del método de síntesis convencional basado en borohidruro sódico y a continuación se ha estudiado la influencia del agente reductor. Finalmente, una vez seleccionado un método de síntesis óptimo, se llevó a cabo una optimización tanto de la carga de metal como del pH establecido durante el método de síntesis ([NaOH]). En la **Sección III**, se ha llevado a cabo estudios acerca de la influencia de la incorporación de un segundo metal al tradicional Pt/C, atendiendo tanto a la proporción Pt-M/C, donde M es el segundo metal (M = Sn, Cu, Ni, Co, Fe), la influencia de la adición de una base en el medio catódico de reacción. Por último, en la **Sección IV** se ha estudiado la influencia del soporte y se ha realizado un estudio de la influencia del material utilizado para la capa de difusión de gases.

En el **Capítulo 1** se realizaron estudios de optimización de las condiciones de operación empleadas, utilizando en todos los

experimentos catalizadores comerciales (IrO_2 al 99,9 % para el ánodo y Pt/C al 20 % en peso para el cátodo). En primer lugar, tras comprobar que la cantidad de hidrógeno generada en el proceso se ajustaba a la teórica predicha por la ecuación de Faraday, se realizaron experimentos con el objetivo de comprobar la viabilidad del proceso de hidrogenación electrocatalítica alternando intervalos en circuito abierto (en los cuales no era aplicada intensidad de corriente alguna), con intervalos en los cuales se aplicaban 0,1 A. Efectivamente, pudo comprobarse que el proceso de hidrogenación ocurría vía electrocatalítica y que el sistema planteado era viable ya que los valores de conversión y selectividad por paso son comparables a los obtenidos en bibliografía.

Tras comprobarse la viabilidad del proceso de electrohidrogenación, se realizaron experimentos variando el modo de operación en la cámara catódica. Tras estos experimentos se concluyó que el mejor modo de operación era recirculación para la cámara anódica y continuo para la cámara catódica, ya que la recirculación de los productos generados provoca una mayor conversión, pero a su vez una sobrehidrogenación de los productos deseados hacia compuestos que no resultan de interés. Posteriormente, se llevó a cabo un estudio a diferentes caudales de alimentación (1–3 $ml \cdot min^{-1}$), comprobándose que para un caudal aplicado de 1 $ml \cdot min^{-1}$ la conversión y selectividad hacia los productos deseados era mayor, debido a que se aumenta el tiempo de residencia del reactivo y esto provoca una mayor selectividad hacia los productos de interés (la hidrogenación del enlace C=C es 30 veces más rápida que la del enlace C=O). Seguidamente, se realizaron experimentos a diferentes intensidades (OCP, 0,05 A y 0,1 A), con el objetivo de conocer la dependencia del proceso de hidrogenación de la corriente aplicada a la celda. Los resultados demuestran que operar a intensidades de corriente de 0,1 A no favorece el proceso de

hidrogenación debido a que se genera un gran exceso de hidrógeno en la cámara catódica y, al ser la reacción de evolución de hidrógeno competitiva con la reacción de hidrogenación, un aumento de la cantidad de protones deriva en una mayor producción de H_2 y en una mayor producción de acetales. Por tanto, se demostró que una intensidad de 0,05 A resulta más interesante para el proceso de electrohidrogenación. Por último, se realizaron experimentos a diferentes temperaturas de trabajo (55 a 75 ºC) en las condiciones anteriormente seleccionadas. Se comprobó que la conversión aumenta con la temperatura debido a que se favorece la cinética del sistema. Sin embargo, temperaturas más altas se acercan mucho a la temperatura de ebullición del disolvente utilizado, donde la solubilidad del hidrógeno disminuye. Por lo tanto, resulta más interesante utilizar una temperatura de trabajo de 70 ºC donde se llega a valores de conversión del 16 %.

En el **Capítulo 2** se realizó un estudio de optimización del método de síntesis del catalizador empleado como cátodo en el proceso de investigación (conservándose en el caso del ánodo el IrO_2). Para ello se sintetizaron cuatro catalizadores de platino al 20 % soportados sobre Vulcan XC–72 utilizando un método de impregnación y reducción in–situ del metal activo con $NaBH_4$ y estableciendo tres modificaciones a dicho método (ver Sección B.2.1.). i) Una etapa de evaporación del disolvente en rotavapor, ii) lavado con agua hasta pH neutro y iii) adición del precursor metálico gota a gota para mejorar la dispersión del catalizador. Los resultados de caracterización demostraron que las modificaciones añadidas al proceso de síntesis afectaban notablemente a factores como el tamaño de partícula, la dispersión, el carácter básico del catalizador y el área electroquímica activa de los catalizadores.

Comparado con el catalizador Pt/C comercial, el catalizador sintetizado siguiendo dichas modificaciones en el método de preparación

presenta una mayor selectividad hacia CMO, con independencia de la etapa de adición de la sal metálica gota a gota.

En el **Capítulo 3** se realizó un estudio sobre la influencia del agente reductor en los catalizadores utilizados en el proceso de hidrogenación. Para ello se sintetizaron diferentes catalizadores de Pt/XC–72 al 20 % de carga metálica utilizando diferentes agentes reductores como $NaBH_4$, KBH_4, etilenglicol, HCOOH. Además, se sintetizó un catalizador que fue reducido de la forma convencional, mediante flujo de hidrógeno (los métodos de preparación de cada uno de los catalizadores se encuentran detallados en la sección B.2). A partir de la caracterización fisicoquímica y electroquímica se observa la gran influencia que supone el agente reductor en parámetros como el tamaño de partícula, dispersión y basicidad.

Los experimentos de hidrogenación en celda PEM demuestran que, si bien el catalizador reducido con $NaBH_4$ mejora en gran medida la selectividad hacia alcohol cinámico, es el catalizador reducido con etilenglicol el que ofrece unos resultados más equilibrados en términos de conversión y selectividad. Por este motivo, y por la posibilidad que ofrece este método de variar el tamaño de partícula a partir de la concentración de NaOH en el proceso de síntesis, se selecciona este catalizador como el más idóneo para continuar con los estudios de electrohidrogenación.

En el **Capítulo 4** se realizó un estudio de optimización de la carga de Pt y el pH durante la síntesis para catalizadores sintetizados mediante el método del poliol modificado (cuyo procedimiento detallado se encuentra en la Sección B.2.3.). Para ello se sintetizaron catalizadores de Pt/XC–72 tanto con diferentes cargas (10, 15 y 20 % en peso) como utilizando diferentes concentraciones de NaOH durante la síntesis (0,05,

0,125 y 0,2 M). Los resultados de caracterización demuestran que tanto la variación de la carga de metal activo como la concentración de NaOH tiene un efecto significativo sobre el tamaño de partícula y el área electroquímica activa.

Tras la caracterización de los catalizadores se realizaron experimentos de hidrogenación de cinamaldehído en celda PEM. Los resultados demuestran que, si bien en catálisis convencional el tamaño de partícula tiene una gran influencia sobre los resultados de hidrogenación de cinamaldehído, no es así en el caso de la hidrogenación electrocatálitica. El catalizador Pt/XC-72 al 15 % en peso ofrece un mayor compromiso entre conversión y selectividad a CMO, lo cual puede ser debido a que mayores cargas de Pt cuando se fija una carga constante en el electrodo (0,5 $mg \cdot cm^{-2}$) reduce la homogeneidad de la distribución de Pt afectando a los resultados de hidrogenación. Por otro lado, los mejores resultados en el estudio de la influencia del tamaño de partícula se obtienen para el catalizador de Pt/XC - 72 sintetizado con una concentración de NaOH 0,2 M, el cual demuestra una mayor conversión y rendimiento a CMO.

En el **Capítulo 5** se ha llevado a cabo un estudio acerca de las ventajas que podría tener en el proceso de hidrogenación la incorporación de un segundo metal. Para este estudio se seleccionaron Sn, Cu, Ni, Co y Fe que, según la bibliografía existente, producen buenos resultados en cuanto a hidrogenación de cinamaldehído cuando se combinan con el platino en catálisis convencional. Los catalizadores catódicos bimetálicos se sintetizaron mediante el método del poliol modificado, con una carga total del 15 % (siguiendo las condiciones estudiadas en el Capítulo 1 y según el método optimizado en los Capítulos

3 y 4). Todos los catalizadores sintetizados fueron caracterizados siguiendo todas las técnicas descritas para los capítulos anteriores.

Los resultados demuestran que la adición de un segundo metal, si bien no mejora los valores de conversión, sí que tiene una gran influencia en la selectividad hacia los productos deseados. De este estudio pueden destacarse dos catalizadores. En primer lugar, el PtNi/C, ya que la producción de compuestos no deseados se ve reducida, debido a que el niquel muestra preferencia para la hidrogenación del enlace C=C para la producción de hidrocinamaldehído y su posterior hidrogenación hacia alcohol hidrocinámico, siendo por tanto este catalizador el más interesante para la hidrogenación selectiva de cinamaldehído hacia hidrocinamaldehído. En segundo lugar, se selecciona el catalizador PtCo/C, que da lugar a una mayor selectividad hacia alcohol cinámico de acuerdo con la bibliografía disponible relativa a catálisis convencional. Por ello, ambos catalizadores se seleccionan con el objetivo de mejorar en estudios posteriores los valores tanto de conversión como de selectividad hacia los compuestos deseados.

En el **Capítulo 6** se ha estudiado la influencia de la adición de diferentes bases al medio de reacción (cámara catódica) trabajando con catalizadores bimetálicos PtCo/C y PtNi/C con diferentes cargas y los soportes catalíticos empleados. En primer lugar, se ha estudiado la influencia de la proporción Pt/Co y Pt/Ni en catalizadores sintetizados por el método del poliol modificado (según esta descrito en la Sección B.2.3.) en los que se va variando la proporción Pt/Co y Pt/Ni. Posteriormente, utilizando como cátodo el catalizador $Pt_{55}Co_{45}$/XC-72, se han realizado experimentos añadiendo diferentes equivalentes de $NaHCO_3$ y NH_4OH al medio de reacción, con el objetivo de minimizar la producción de compuestos no deseados. Seguidamente, seleccionando NH_4OH como mejor opción, se realizó un estudio en el que se evaluaba

la influencia de la misma en las distintas cargas de catalizador. Finalmente, se estudió la influencia de diferentes soportes carbonosos.

A partir de los resultados de caracterización y de los ensayos electrocatalíticos, se ha demostrado que, tanto en el caso del cobalto como en el del níquel, el empleo de cargas elevadas del metal menos noble no favorece los resultados de hidrogenación teniendo en cuenta la selectividad hacia compuestos no deseados (Co) o la conversión (Ni). Esto puede deberse a la presencia de óxidos de estos metales, que en el caso de estar presentes en un porcentaje muy elevado recubren las nanopartículas de Pt dificultando su intervención en el proceso catalítico. La adición de bicarbonato de sodio no resulta de interés en el proceso de hidrogenación electrocatalítica, al no observarse mejoras de ningún tipo cuando interviene en el proceso. Sin embargo, la adición de 0,75 equivalentes al medio de reacción, consigue eliminar casi por completo la producción de compuestos no deseados (aprox = 0,5 %). Este comportamiento puede deberse a la combinación de los iones OH^- con el doble enlace C=C, dificultando su hidrogenación y favoreciendo la selectividad hacia alcohol cinámico. Este efecto es diferente en función del contenido del segundo metal, y la adición de 0,75 equivalentes de amoniaco a las diferentes cargas de catalizador ofrece mejores resultados de hidrogenación con el catalizador $Pt_{55}Co_{45}$/XC-72.

Por último, en el **Capítulo 7** una vez seleccionanda la fase activa y el medio de reacción, se evaluó la influencia del soporte empleado. Se llevaron a cabo síntesis de catalizadores PtCo (55 % Pt, 45 % Co) utilizando tres soportes diferentes. Estos soportes fueron Vulcan XC-72, nanofibras de carbono funcionalizadas de baja densidad (CNF LS) y nanofibras de carbono funcionalizadas de baja densidad sometidas a un tratamiento de limpieza para eliminar posibles trazas de Si y Ni (CNF LS D). Estos catalizadores fueron caracterizados tanto fisicoquímica como

electroquímicamente por las técnicas descritas anteriormente. Finalmente, se realizaron estudios de hidrogenación empleando estos catalizadores junto con las condiciones anteriormente estudiadas. El catalizador soportado sobre carbón activado Vulcan XC-72 es el que ofrece los mejores resultados de hidrogenación debido tanto a su elevada área superficial como a la relación que existe entre la orientación de los planos cristalinos (determinada mediante voltametrías cíclica) y selectividad hacia los dobles enlaces presentes en el cinamaldehído.

Finalmente, se ha evaluado la influencia del material empleado para la capa de difusión de gases. Para ello, se han realizado experimentos de hidrogenación con las condiciones anteriormente empleadas empleando dos materiales diferentes como capa de difusión de gases, titanio poroso y papel de carbono. A partir de los ensayos de hidrogenación electrocatalítica y de la caracterización electroquímica (ensayos de impedancia) se ha demostrado que los mejores resultados se obtienen con la capa de difusión de gases de titanio poroso, ya que muestra una mejor estabilidad mecánica y ofrece menor resistencia, impidiendo la acumulación de reactivos y productos en los canales de la celda y su posterior hidrogenación a compuestos no deseados.

D. CONCLUSIONES Y RECOMENDACIONES

De los resultados obtenidos en la presente Tesis Doctoral, se derivan las siguientes conclusiones:

- La hidrogenación electroquímica de cinamaldehído en una celda de intercambio protónico tipo PEM, produciendo el hidrógeno in–situ a partir de electrólisis de agua, resulta técnicamente viable.
- Las mejores condiciones de trabajo para la hidrogenación de cinamaldehído en una celda de intercambio protónico tipo PEM se consiguen cuando se trabaja con un modo de operación en recirculación en la cámara anódica y continuo en la cámara catódica, aplicando una intensidad de 0,5 A, 70 ^{o}C de temperatura y un caudal de alimentación de 1 ml·min^{-1}.
- Del estudio desarrollado en el Capítulo 2 puede concluirse que el catalizador de Pt soportado sobre Vulcan XC-72, sintetizado con un proceso de reducción in situ con $NaBH_4$ y etapas intermedias de evaporación del disolvente a vacío y lavado hasta pH neutro, ofrece unos resultados muy parecidos al catalizador en el cual se incorpora la etapa de adición de la sal precursora gota a gota. Ambos catalizadores ofrecen los mejores en cuanto a selectividad a alcohol cinámico.
- En el estudio realizado en el Capítulo 3 acerca de los agentes reductores empleados en el proceso de síntesis de catalizadores de Pt/XC-72, el etilenglicol ofrece valores de conversión más elevados en comparación con los otros catalizadores empleados.
- El catalizador de 15Pt/C preparado con una carga metálica del 15 % en peso, ofrece mejores resultados de hidrogenación debido a una distribución más homogénea de las partículas y una adecuada basicidad relativa.

- En la síntesis mediante el método del poliol modificado, la concentración de NaOH empleada tiene una influencia significativa en el tamaño de partícula activa. Se ha demostrado que el empleo de una concentración de NaOH de 0,2 M disminuye el diámetro de partícula, aumentando la dispersión y el área electroquímica activa sin perjudicar la degradación del catalizador. Todo ello se traduce en una mejora de los resultados de hidrogenación electrocatalítica y rendimiento en particular a CMO.
- La adición de un segundo metal a la estructura del platino tiene una gran influencia en los resultados de hidrogenación electroquímica de cinamaldehído. En particular, la incorporación del níquel a la estructura catalítica mejora la selectividad hacia hidrocinamaldehído, mientras que la adición de cobalto mejora la selectividad hacia alcohol cinámico.
- Respecto al ratio Pt/Ni o Pt/Co, según el estudio realizado en el Capítulo 6, pequeños porcentajes de Ni y Co incorporados a la estructura del catalizador mejoran la selectividad hacia los compuestos deseados reduciendo la producción de las reacciones secundarias.
- La incorporación de pequeñas cantidades de una base débil como es el NH_4OH eliminan casi por completo la producción de compuestos no deseados debido a la posible interacción del ion hidroxilo con el doble enlace C=C, que aumenta la selectividad hacia el alcohol cinámico. Se ha demostrado así que, la combinación del catalizador PtCo/XC-72 (55 % Pt, 45 % Co) con 0,75 equivalentes de NH_4OH ofrece los mejores resultados de hidrogenación electrocatalítica de CMA en términos de selectividad hacia alcohol cinámico y producción de compuestos no deseados.

- En el estudio realizado utilizando diferentes soportes, las mejores características electrocatalíticas para la hidrogenación electroquímica de cinamaldehído se obtienen cuando se emplea el catalizador soportado sobre Vulcan XC-72 debido a que posee un área electroquímica superior y una orientación cristalina más apropiada para el proceso de electrohidrogenación.
- Por último, se ha demostrado que el empleo de titanio poroso como capa de difusión de gases ofrece mejores resultados de hidrogenación que el papel de carbono debido a que presenta una mayor resistencia mecánica que facilita la circulación de los reactivos y productos a través de los canales de la celda.

Con la finalidad de completar en un futuro los resultados obtenidos en la presente Tesis Doctoral, se recomienda:

- Emplear moléculas de origen biomásico como fuente de electrones en sustitución del agua como bioetanol, furfural, etilenglicol, celulosa, etc. que permitan la revalorización de dichas moléculas.
- Estudiar el empleo de otros compuestos como metales activos o soportes como pueden ser las perovskitas.
- Realizar un estudio más amplio acerca de los soportes utilizados con el objetivo de mejorar la conversión del proceso electrocatalítico.
- Estudiar el empleo de energías alternativas como fuente de electricidad para hacer el proceso más competitivo.
- Realizar un estudio exergético que permita seleccionar las condiciones óptimas de operación para el proceso de hidrogenación electrocatalítica de cinamaldehído.

- Estudiar la posibilidad de un escalado del proceso que permita tanto trabajar con concentraciones más elevadas, como aumentar la conversión del proceso.

E. BIBLIOGRAFÍA

1. Bertolini, G.R., *Síntesis y caracterización de nuevos catalizadores heterogéneos basados en heteropolimolibdatos para la hidrogenación selectiva de cinamaldehído.* 2013, Universidad Nacional de La Plata.
2. Sabatier, P., *Hydrogénations et déshydrogénations par catalyse.* Berichte der deutschen chemischen Gesellschaft, 1911. **44**(3): p. 1984-2001.
3. Alvarado, J.A.S., *Hidrogenación selectiva de isoforona sobre catalizadores de Pt/ZW modificados con Fe y Mn.* 2013, Escuela Superior de Ingeniería Química e Industrias Extractivas, Mexico.
4. Solymosi, F., I. Tombácz, and M. Kocsis, *Hydrogenation of CO on supported Rh catalysts.* Journal of Catalysis, 1982. **75**(1): p. 78-93.
5. Goodman, D.W., et al., *Kinetics of the hydrogenation of CO over a single crystal nickel catalyst.* Journal of Catalysis, 1980. **63**(1): p. 226-234.
6. Sárkány, A., A. Horváth, and A. Beck, *Hydrogenation of acetylene over low loaded Pd and Pd-Au/SiO2 catalysts.* Applied Catalysis A: General, 2002. **229**(1): p. 117-125.
7. Sarkany, A., G. Stefler, and J.W. Hightower, *Participation of support sites in hydrogenation of 1,3-butadiene over Pt/Al2O3 catalysts.* Applied Catalysis A: General, 1995. **127**(1): p. 77-92.
8. Sarkany, A., et al., *Promoter Effect of Pd in Hydrogenation of 1,3-Butadiene over Co-Pd Catalysts.* Journal of Catalysis, 1995. **157**(1): p. 179-189.
9. Choudhary, T.V., et al., *Acetylene Hydrogenation on Au-Based Catalysts.* Catalysis Letters, 2003. **86**(1): p. 1-8.
10. Liao, X.-M., et al., *Hydrogenation of cinnamaldehyde over bimetallic Au–Cu/CeO2 catalyst under a mild condition.* Chinese Chemical Letters, 2017. **28**(2): p. 293-296.
11. Zhang, Y., et al., *Selective Hydrogenation of Cinnamaldehyde to Cinnamyl Alcohol over Au Catalysts: Influence of the Oxide-Supports.* Catalysis Letters, 2017. **147**(1): p. 102-109.
12. Wang, L., et al., *Single-site catalyst promoters accelerate metal-catalyzed nitroarene hydrogenation.* Nature Communications, 2018. **9**(1): p. 1362.
13. Balmont, C.C., *Cinamaldehído: no solo un dulce aroma.* 2014.
14. Hugo Alfonso Rojas Sarmiento, C.P.C.M., José Jobanny Martínez Zambrano, *Hidrogenación de Cinamaldehído y Benzalcetona sobre catalizadores de Au, Ir y Au-Ir soportadoes en SiO_2.* Bistua, 2011. **9**(73-77).

15. Rojas Sarmiento, H.A., J.J. Martínez Zambrano, and P.A. Reyes, *Estudio cinético de la hidrogenación de trans-cinamaldehído sobre catalizadores de Ir/Nb2O5.* Revista Facultad de Ingeniería Universidad de Antioquia, 2010(55): p. 9-17.
16. Reddy, B.M., et al., *Vapour phase hydrogenation of cinnamaldehyde over silica supported transition metal-based bimetallic catalysts.* Journal of Molecular Catalysis A: Chemical, 2006. **247**(1): p. 80-87.
17. Santori, G.F., M.L. Casella, and O.A. Ferretti, *Hydrogenation of carbonyl compounds using tin-modified platinum-based catalysts prepared via surface organometallic chemistry on metals (SOMC/M).* Journal of Molecular Catalysis A: Chemical, 2002. **186**(1-2): p. 223-239.
18. Lashdaf, M., et al., *Behaviour of palladium and ruthenium catalysts on alumina and silica prepared by gas and liquid phase deposition in cinnamaldehyde hydrogenation.* Applied Catalysis A: General, 2003. **241**(1-2): p. 65-75.
19. Breen, J.P., et al., *Steric effects in the selective hydrogenation of cinnamaldehyde to cinnamyl alcohol using an Ir/C catalyst.* Applied Catalysis A: General, 2004. **268**(1–2): p. 267-274.
20. Joseph Antony Raj, K., et al., *Selective Hydrogenation of Cinnamaldehyde over Cobalt Supported on Alumina, Silica and Titania.* Catalysis Letters, 2012. **142**(1): p. 87-94.
21. Rylander, P.N., *Hydrogenation Methods*, ed. A. Press. 1990, New York.
22. Galvagno, S., et al., *Hydrogenation of cinnamaldehyde over Ru/C catalysts: effect of Ru particle size.* Journal of Molecular Catalysis, 1991. **64**(2): p. 237-246.
23. Gallezot, P., Richard, D., and Bergeret, G., *"New Catalytic Materials"*, in *ACS Symposium Series*, E.T.K. Baker, Editor. 1991, American Chemical Society: Whashington, DC.
24. Giroir-Fendler, A., D. Richard, and P. Gallezot, *Selectivity in Cinnamaldehyde Hydrogenation of Group-VIII Metals Supported on Graphite and Carbon*, in *Studies in Surface Science and Catalysis*, M. Guisnet, et al., Editors. 1988, Elsevier. p. 171-178.
25. Nitta, Y., K. Ueno, and T. Imanaka, *Selective hydrogenation of αβ-unsaturated aldehydes on cobaltsilica catalysts obtained from cobalt chrysotile.* Applied Catalysis, 1989. **56**(1): p. 9-22.
26. Nitta, Y., Y. Hiramatsu, and T. Imanaka, *Effects of preparation variables of supported-cobalt catalysts on the selective hydrogenation of α,β-unsaturated aldehydes.* Journal of Catalysis, 1990. **126**(1): p. 235-245.

27. Richard, D., et al., *Characterization and selectivity in cinnamaldehyde hydrogenation of graphite-supported platinum catalysts prepared from a zero-valent platinum complex.* Catalysis Today, 1989. **6**(1-2): p. 171-179.
28. Gallezot, P., A. Giroir-Fendler, and D. Richard, *Chemioselectivity in cinnamaldehyde hydrogenation induced by shape selectivity effects in Pt-Y zeolite catalysts.* Catalysis Letters, 1990. **5**(2): p. 169-174.
29. Fouilloux, P., *Selective hydrogenation of cinnamaldehyde to cinnamyl alcohol on Pt-Co and Pt-Ru/C catalysts*, in *Studies in Surface Science and Catalysis*. 1988. p. 123-129.
30. Poltarzewski, Z., et al., *Hydrogenation of α,β-unsaturated aldehydes over PtSn/Nylon.* Journal of Catalysis, 1986. **102**(1): p. 190-198.
31. Isaeva, V., A. Derouault, and J. Barrault, *Synthesis of Ru, Rh and Pd complexes immobilized on modified supports. Investigation of the hydrogenation of cinnamaldehyde.* Bulletin de la Societe Chimique de France, 1996. **133**(4): p. 351-357.
32. Blackmond, D.G., et al., *Geometric and electronic effects in the selective hydrogenation of α, β-unsaturated aldehydes over zeolite-supported metals.* Journal of Catalysis, 1991. **131**(2): p. 401-411.
33. Prakash, M.G., et al., *Studies on Ni–M (M=Cu, Ag, Au) bimetallic catalysts for selective hydrogenation of cinnamaldehyde.* Catalysis Today, 2016. **263**: p. 105-111.
34. Espro, C., et al., *On the formation of cinnamyl alcohol during the hydrogenation of cinnamaldehyde under mild conditions on supported palladium catalysts.* Reaction Kinetics, Mechanisms and Catalysis, 2016. **118**(1): p. 223-233.
35. Dimas Rivera, G.L., *Síntesis y aplicación de catalizadores bimetálicos Pt y Pd con Fe sobre alúmina en la desorción del furfural y la hidrogenación del 2-metilfurano.* 2015, Universidad Autónoma de Nuevo León: México.
36. Asedegbega Nieto, E., et al., *Modification of catalytic properties over carbon supported Ru–Cu and Ni–Cu bimetallics.* Vol. 300. 2006. 120–129.
37. Hájek, J., et al., *Ruthenium-modified MCM-41 mesoporous molecular sieve and Y zeolite catalysts for selective hydrogenation of cinnamaldehyde.* Applied Catalysis A: General, 2003. **251**(2): p. 385-396.
38. Yepez, A., et al., *Mechanistic insights into the hydroconversion of cinnamaldehyde using mechanochemically-synthesized Pd/Al-SBA-15 catalysts.* Green Chemistry, 2015. **17**(1): p. 565-572.

39. Liu, H., Z. Li, and Y. Li, *Chemoselective Hydrogenation of Cinnamaldehyde over a Pt-Lewis Acid Collaborative Catalyst under Ambient Conditions.* Industrial & Engineering Chemistry Research, 2015. **54**(5): p. 1487-1497.
40. Sedighi, S. and C.L. Gardner, *A kinetic study of the electrochemical hydrogenation of ethylene.* Electrochimica Acta, 2010. **55**(5): p. 1701-1708.
41. Leng, F., et al., *Selectivity shifts in hydrogenation of cinnamaldehyde on electron-deficient ruthenium nanoparticles.* Comptes Rendus Chimie, 2018. **21**(3): p. 346-353.
42. Weisz, P.B., *Basic Choices and Constraints on Long-Term Energy Supplies.* Physics Today, 2004. **57**(7): p. 47.
43. Crabtree, G.W., M.S. Dresselhaus, and M.V. Buchanan, *The hydrogen economy.* Physics Today, 2004. **57**(12): p. 39-44.
44. Barreto, L., A. Makihira, and K. Riahi, *The hydrogen economy in the 21st century: A sustainable development scenario.* International Journal of Hydrogen Energy, 2003. **28**(3): p. 267-284.
45. Penner, S.S., *Steps toward the hydrogen economy.* Energy, 2006. **31**(1): p. 33-43.
46. Rifkin, J., *The Hydrogen Economy: The Creation of the Worldwide Energy Web and the Redistribution of Power on Earth*, ed. P.P. Inc. 2002.
47. Olah, G.A., A. Goeppert, and G.K.S. Prakash, *Beyond Oil and Gas: The Methanol Economy: Second Edition*. Beyond Oil and Gas: The Methanol Economy: Second Edition. 2009. 1-334.
48. da Silva Veras, T., et al., *Hydrogen: Trends, production and characterization of the main process worldwide.* International Journal of Hydrogen Energy, 2017. **42**(4): p. 2018-2033.
49. Trasatti, S., *Water electrolysis: who first?* Journal of Electroanalytical Chemistry, 1999. **476**(1): p. 90-91.
50. Muthumeenal, A., S.S. Pethaiah, and A. Nagendran, *Investigation of SPES as PEM for hydrogen production through electrochemical reforming of aqueous methanol.* Renewable Energy, 2016. **91**: p. 75-82.
51. Higashihara, T., K. Matsumoto, and M. Ueda, *Sulfonated aromatic hydrocarbon polymers as proton exchange membranes for fuel cells.* Polymer, 2009. **50**(23): p. 5341-5357.
52. Verma, A. and R. Pitchumani, *Influence of membrane properties on the transient behavior of polymer electrolyte fuel cells.* Journal of Power Sources, 2014. **268**: p. 733-743.

53. Carrette, L., K.A. Friedrich, and U. Stimming, *Fuel cells: Principles, types, fuels, and applications.* ChemPhysChem, 2000. **1**(4): p. 163-193.
54. Woodman, A.S., et al., *Development of corrosion-resistant coatings for fuel cell bipolar plates.* Proceedings of the AESF Annual Technical Conference, 1999: p. 717-725.
55. Lim, C. and C.Y. Wang, *Effects of hydrophobic polymer content in GDL on power performance of a PEM fuel cell.* Electrochimica Acta, 2004. **49**(24): p. 4149-4156.
56. Corrales-Sánchez, T., J. Ampurdanés, and A. Urakawa, *MoS2-based materials as alternative cathode catalyst for PEM electrolysis.* International Journal of Hydrogen Energy, 2014. **39**(35): p. 20837-20843.
57. Huang, H., Y. Yu, and K.H. Chung, *Performance of Au/Nafion/Pt electrodes in benzene–water electrochemical hydrogenation.* International Journal of Hydrogen Energy, 2014. **39**(25): p. 13832-13837.
58. Sáez, A., et al., *Electrocatalytic hydrogenation of acetophenone using a Polymer Electrolyte Membrane Electrochemical Reactor.* Electrochimica Acta, 2013. **91**: p. 69-74.
59. Villalba, M., M. del Pozo, and E.J. Calvo, *Electrocatalytic hydrogenation of acetophenone and benzophenone using palladium electrodes.* Electrochimica Acta, 2015. **164**: p. 125-131.
60. Takano, K., et al., *Electrocatalytic Hydrogenation of Toluene Using a Proton Exchange Membrane Reactor.* Bulletin of the Chemical Society of Japan, 2016. **89**(10): p. 1178-1183.
61. Matthiesen, J.E., et al., *Electrochemical Conversion of Muconic Acid to Biobased Diacid Monomers.* ACS Sustainable Chemistry & Engineering, 2016. **4**(6): p. 3575-3585.
62. Yoshida, J.-i., et al., *Modern Strategies in Electroorganic Synthesis.* Chemical Reviews, 2008. **108**(7): p. 2265-2299.
63. Vielstich, W., *Electrochemical energy conversion: methanol fuel cell as example.* Journal of the Brazilian Chemical Society, 2003. **14**: p. 503-509.
64. Montiel, V., et al., *Use of MEA technology in the synthesis of pharmaceutical compounds: The electrosynthesis of N-acetyl-l-cysteine.* Electrochemistry Communications, 2010. **12**(1): p. 118-121.
65. Mahdavi, B., et al., *Electrocatalytic hydrogenation of conjugated enones on nickel boride, nickel, and Raney nickel electrodes.* Vol. 73. 2011. 846-852.

66. Yuan, X.-Z., et al., *Electro-generative hydrogenation of allyl alcohol applying PEM fuel cell reactor.* Electrochemistry Communications, 2003. **5**(2): p. 189-193.

67. Lobato, J., et al., *Study of different bimetallic anodic catalysts supported on carbon for a high temperature polybenzimidazole-based direct ethanol fuel cell.* Applied Catalysis B: Environmental, 2009. **91**(1): p. 269-274.

68. Hargreaves, J.S.J., *Some considerations related to the use of the Scherrer equation in powder X-ray diffraction as applied to heterogeneous catalysts.* Catalysis, Structure & Reactivity, 2016. **2**(1-4): p. 33-37.

Section I: Electrocatalytic Hydrogenation of Cinnamaldehyde: Study of reaction conditions

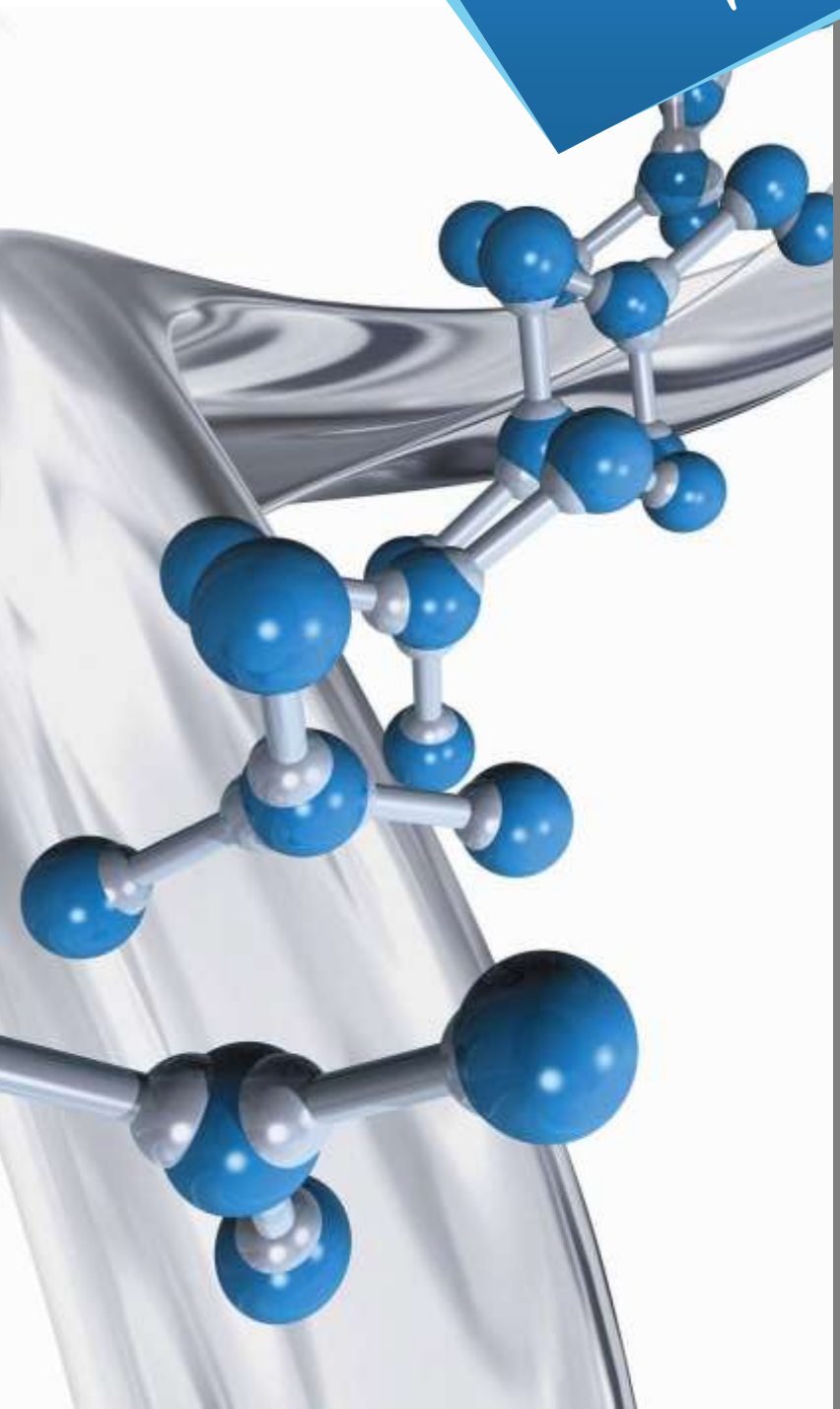

Chapter 1: Electrocatalytic hydrogenation of cinnamaldehyde in a polymeric electrolyte membrane reactor: Study of operational conditions

Chapter 1: Electrocatalytic hydrogenation of cinnamaldehyde in a polymeric electrolyte membrane reactor. Study of operational conditions

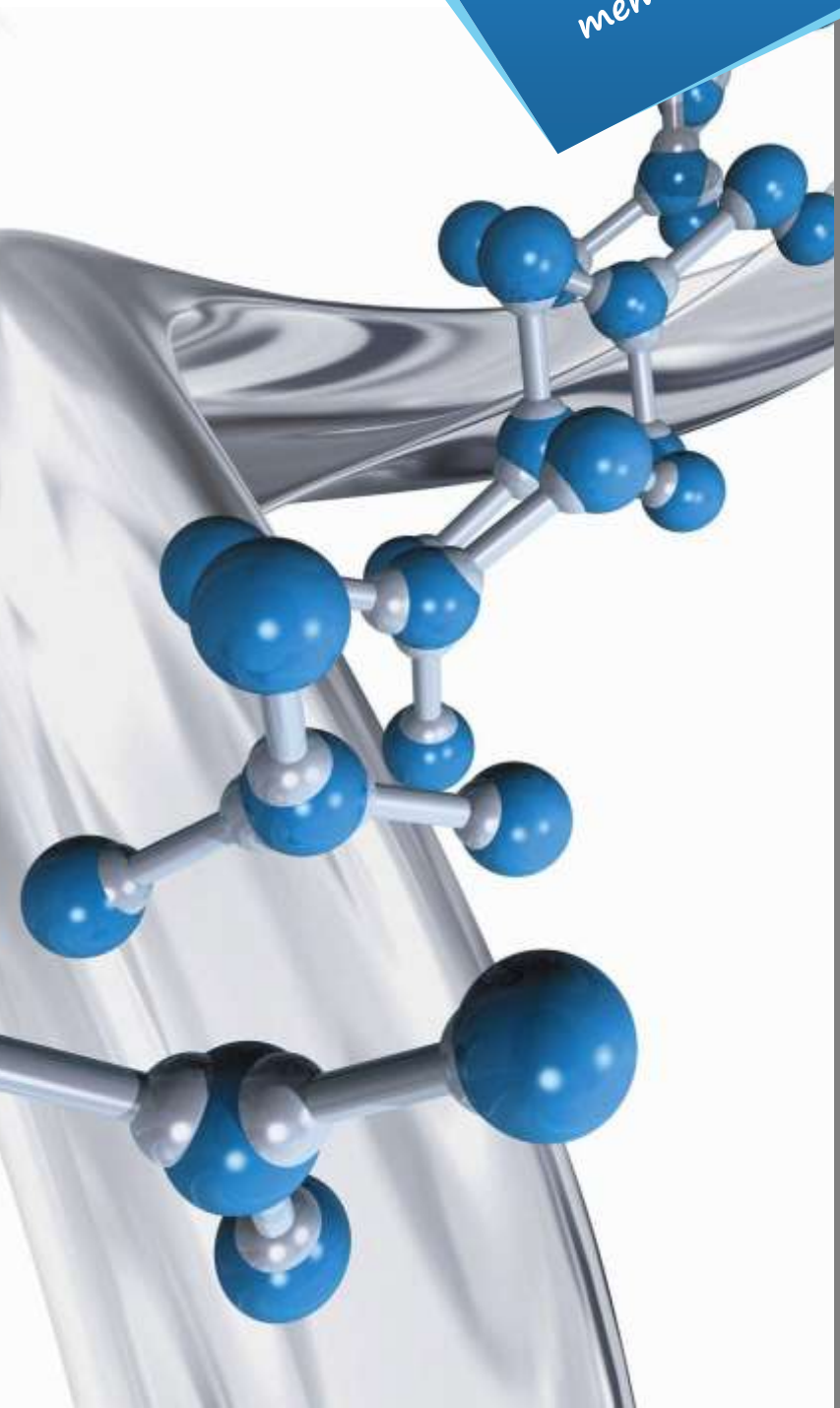

1. INTRODUCTION

2. EXPERIMENTAL
   2.1. Membrane electrode assembly
   2.2. Electrocatalític hydrogenation in a proton Exchange membrane reactor

3. RESULTS AND DISCUSSION

4. CONCLUSIONS

Abstract

This chapter reports for the first time the electrocatalytic hydrogenation of cinnamaldehyde to valuable products in a Polymer Electrolyte Membrane reactor under mild conditions (atmospheric pressure and mild temperature). The proposed concept addresses an initial approach to the integration of hydrogen generation from water electrolysis, where protons are generated in the anodic chamber of the cell, with the electrochemical hydrogenation of cinnamaldehyde at the cathode chamber. The production of fine chemical using this technology is demonstrated to be feasible and provides a suitable alternative to remedy the limitations related to the conventional catalytic hydrogenation process since there is no need of an external hydrogen source and the use of electrical energy may come from renewable energy sources. Moreover, in order to optimize the system, a study of the most important reaction conditions (flow rate, applied current and temperature) is conducted. The choice of suitable reaction and polarization conditions as well as working in continuous mode in the cathode chamber resulted to play a key role shifting selectivity to the synthesis of fine chemicals or pharmaceuticals against undesired products.

Figure 1.1 shows a schematic representation about the most important aspect about this chapter.

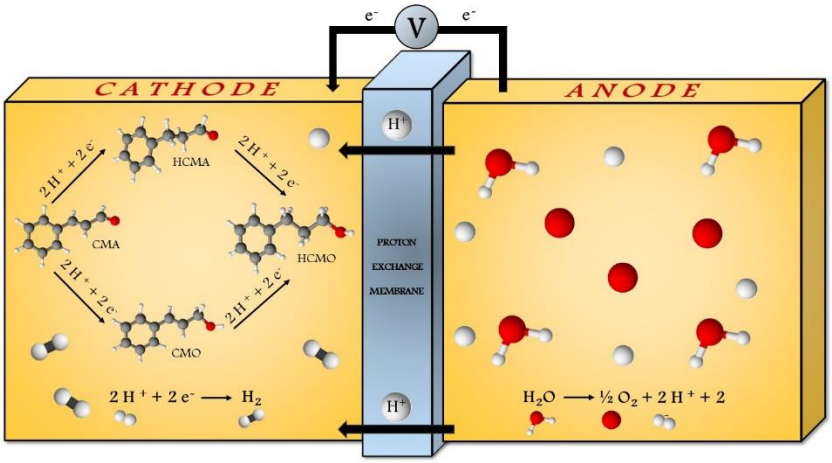

Figure 1.1. *Graphical Abstract Chapter 1.*

1. INTRODUCTION

Catalytic hydrogenation of α,β-unsaturated aldehydes is a reaction of industrial relevance, which finds application in the production of a large number of fine chemicals and is often used as a sensitive test reaction. A typical example is the hydrogenation of cinnamaldehyde (CMA) to its unsaturated alcohol, cinnamyl alcohol (CMO), which is a key material in the synthesis of flavourings, pharmaceuticals and perfumes. However, selective production of this unsaturated alcohol is still a challenge since the hydrogenation of the C=C double bond is thermodynamically favoured rather than the C=O double bond, resulting in the formation of mainly hydrocinnalmaldehyde (HCMA) and low yields of the desired product [1, 2]. Therefore, catalysts based on noble metals such as Pt, Ru or Pd have been developed to accomplish selective liquid phase hydrogenation of the C=O double bond while keeping the other intact [3]. Among them, platinum catalysts seem to be active and selective when the desired product is CMO [4-6].

Conventionally, catalytic hydrogenation of CMA is implemented in a batch autoclave reactor (limiting the scale-up), working at high temperature and pressure conditions due to the low H_2 solubility in the reactants. Other critical issues of this process are the corrosive nature of solvents and disposal of the reaction wastes, the large amount of catalyst used, its lack of reusability and separation, and the need of an external source of hydrogen gas, which typically comes from reforming reactions from hydrocarbon fuels. By contrast, electrocatalytic hydrogenation (ECH) offers a sustainable alternative for the production of fine chemicals at mild reaction conditions (low temperature and room pressure), especially when combined with renewable energy sources since high purity atomic hydrogen can be generated in-situ in a

polymeric proton exchange membrane reactor (PEMR). Another advantage of electrochemical membrane reactors is that the reaction performance on the electrocatalyst can be controlled by modifying the polarization conditions, which may allow to regulate activity and selectivity. Different inorganic (CO_2) [7] and organic molecules have been hydrogenated (o-xylene, benzene, acetophenone, benzophenone, toluene or muconic acid) in different electrocatalytic configurations [8-14]. However, to our knowledge there are no previous works concerning the electrochemical hydrogenation of cinnamaldehyde. Therefore, as an initial step in this direction, results from the first experimental studies of ECH of CMA in a PEMR are presented in this chapter. Moreover, in order to enhance CMO production, the influence of reaction conditions is also reported.

2. EXPERIMENTAL

2.1. Membrane electrode assembly (MEA) preparation

Anode and cathode were prepared using commercial IrO_2 (99 wt. %) and Pt/C (20 wt. %), purchased from Alfa Aesar, with a catalyst loading of 2 and 0.5 mg/cm^2, respectively. Coating inks contained proper amounts of each electrocatalyst dispersed in a solution of Nafion ionomer (5 wt. %, Sigma-Aldrich) and water (anode) or 2-propanol (cathode). Ink solutions were sonicated for 2 h using an ultrasonic bath (110 W/50-60 Hz, Selecta) before deposition. Nafion® 115 (180 μm Hidrogena) was used as the polymer electrolyte membrane and pretreated as previously described [15, 16]. Membrane electrode assembly (MEA) was then prepared by spraying the catalyst inks directly on the pretreated membrane (2 x 2 cm^2 active area).

2.2. Electrocatalytic hydrogenation in a proton exchange membrane reactor

Electrocatalytic hydrogenation tests were performed in a PEMR detailed elsewhere [16]. It consists of the MEA (Nafion membrane coated with commercial electrocatalysts), two current collectors of 2 mm thickness (made of Titanium Grade 1) equipped with a machined serpentine flow field of 0.25 cm^3, which served as flow channels, and two porous titanium plates used as gas diffusion layers (2 x 2 cm^2, 1 mm thickness, $Ø_{pore}$ = 50 μm, XinliFilters). This composition was sandwiched between two PTFE (Polytetrafluoroethylene) gaskets, designed to prevent sealing between the anodic and cathodic compartments and avoid short-circuiting of the cell. These components were finally placed between two external PTFE plates covered by a cell housing made of aluminum. The cell had provisions for heating and temperature control.

Deionized water was supplied to the anode compartment while a 100 ppm cinnamaldehyde solution in 2-propanol was fed to the cathode chamber using a peristatic multi pump (1-3 ml/min flow rate, HEIDOLPH). Both feeding solutions were preheated at a temperature between 55 and 75 °C under N_2 purge. In order to avoid the evaporation of the cathodic solution, a cooling condensation column was installed (-4 °C). The anode chamber operated in recycle mode, recirculating this stream to the feed reservoir, while the cathode chamber operated in continuous. Constant current densities were applied to the cell via a potentiostat-galvanostat Autolab PGSTAT128N, which was also used for monitoring the potential flowing through the cell. Hydrogen production flow rate was followed by a high-precision flowmeter (Mervilab) and verified via Faraday´s Law. ECH products were analyzed offline in an Agilent Technologies 7820A gas chromatograph equipped with a FID

detector and a capillary column (Agilent DB-624, 30 m x 0.25 mm x 0.5 μm) using helium as a carrier gas.

3. RESULTS AND DISCUSSION

A series of preliminary experiments was carried out to determine the feasibility of electrocatalytic hydrogenation of cinnamaldehyde in a PEMR with in situ hydrogen production. Firstly, hydrogen flow rate resulting from water electrolysis was tested at atmospheric pressure and 75ºC.

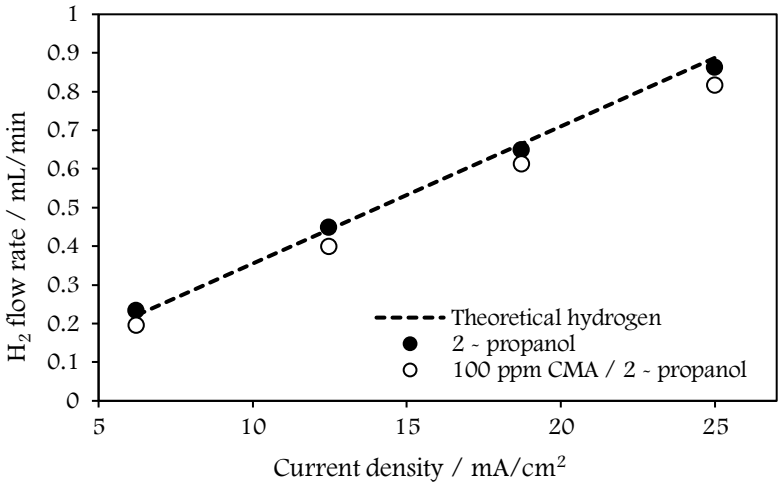

Figure 1.2. *Experimental/theoretical H_2 production rates vs current density. Conditions: atmospheric pressure, 60 min TOS, 75 ºC, 1 mL/min feeding flow rate. Anode chamber: H_2O.*

Results depicted in Figure 1.2 show that, in absence of cinnamaldehyde at the cathode chamber (blank experiment), an increase in the applied current density supplied by the electrolytic cell generated a higher amount of highly pure H_2, which was cross-checked at the exit of the cathode of the PEMR. It can be observed that experimentally measured H_2 production rate perfectly fitted theoretical data predicted by Faraday's Law, demonstrating that the applied electrical energy was used for H_2 production [17]. The same experiment was then performed

by feeding a 100 ppm of cinnamaldehyde solution to the cathode chamber. Data shifted to lower values of H_2 production rate, which was attributed to the reaction of part of the hydrogen atoms electrogenerated at the cathode with the double bonds in the CMA.

In addition, a third experiment of three step changes was accomplished (at the same reaction conditions by feeding CMA to the cathode) to demonstrate the possible ECH of CMA: i) open circuit potential (OCP), ii) galvanostatic imposition of 25 mA/cm^2 current density, iii) OCP. From Figure 1.3 the system was verified to conduct ECH exclusively under polarization conditions (0.1 A) where 11.5% of cinnamaldehyde was converted. Note that no activity was observed by feeding pure H_2 (Carburos Metálicos, 99.9999%), in OCP at the same operation conditions, to the cathodic chamber of the PEMR (as tested in a separate experiment, not shown here), confirming the electrochemical nature of the process by the reaction of CMA with protons and electrons and not by the catalytic reaction with the H_2 evolved to the gas phase.

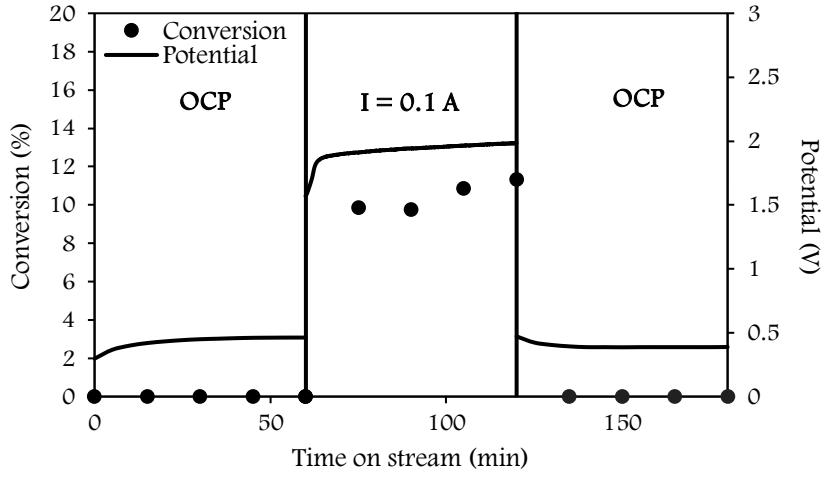

Figure 1.3. *Viability of electrocatalytic hydrogenation of CMA in PEMR. Conditions: atmospheric pressure, 60 min TOS, 75 °C, 1 mL/min feeding flow rate. Anode chamber: H_2O; Cathode chamber: 100 ppm CMA/2-propanol.*

Therefore, for the first time in the available literature, the electrochemical hydrogenation of CMA has been demonstrated to be feasible under PEM cell configuration and mild reaction conditions, using the protons diffused at the cathode from water electrolysis that occurs in the anode chamber and electricity as the driving force.

Over the last two decades, fine chemical industry has been trying to change the operation in batch mode to a continuous production in order to intensify the process and facilitate scale-up [18]. In this sense, taking advance of the easiness of PEMRs to be scaled-up and considering potential possibilities of electrocatalytic hydrogenation process, working in continuous was selected as the most suitable mode of operation to approach this work.

Even more, the first parameter of study was the operation mode in order to achieve better hydrogenations results. In order to check this parameter two experiments were carried out in different conditions. First, one experiment of 24 hours with the aim of accumulate products resulting of the continuous hydrogenation in discontinuous mode, and a second experiment in continuous mode of one hour of duration. Both experiments were carried out at 75 ^{o}C and 1 ml/min of flow rate. Note from Figure 1.4 that recycle mode of operation resulted in the null formation of CMO in favour of its further hydrogenation to undesired higher molecular weight products, due to the accumulation effect as time on stream went by [19, 20]. In contrast, operating under continuous mode was seemed to provide both HCMA and CMO, apart from phenylpropanol (HCMO) and side products, whose proportion is found to depend on the applied reaction conditions as detailed along this work.

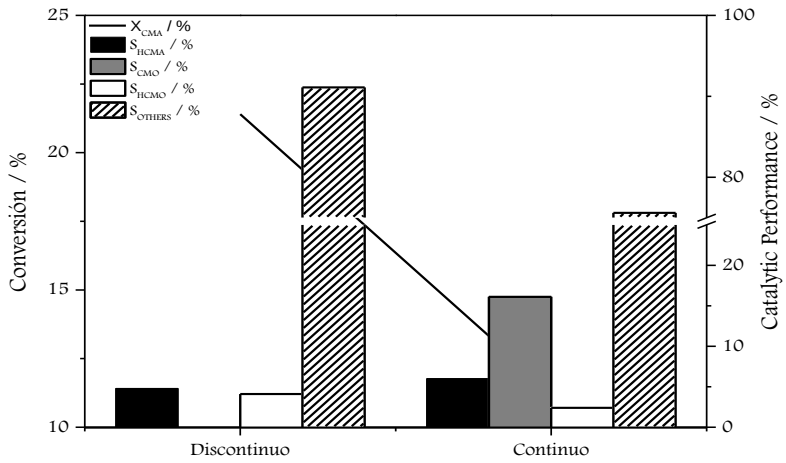

Figure 1.4. *Influence of the operation mode on the hydrogenation of cinnamaldhyde. Conditions: atmospheric pressure, 1440 min TOS (discontinuous mode), 60 min TOS (continuous mode), 75 °C, 1 mL/min feeding flow rate. Anode chamber: H_2O; Cathode chamber: 100 ppm CMA/2-propanol.*

Once ECH process was demonstrated to be viable, the next step was to optimize the main operation parameters. To that end, a series of experiments was carried out at different conditions, i.e. feeding flow rate, applied current and reaction temperature.

Secondly, the next parameter of study was the feeding flow rate in both compartments of the electrochemical cell. In order to check its effect on CMA conversion and products distribution, three experiments were run for 1 h, at 75°C, under constant current density (25 mA/cm^2, 0.1 A) by varying the flow rate between 1-3 mL/min. Note that cinnamaldehyde can be converted to HCMA, CMO, HCMO and species derived from further hydrogenation (side products denoted as 'others'). The first two compounds are formed through parallel reduction of different functional groups present in starting substrate, while HCMO derives from consecutive hydrogenation of both. Note that although relative selectivity, only referred to the fine chemical of interest, is usually reported along the literature, the formation of side products should not

be dismissed since, above 60ºC, high amounts of products such as methylstyrene, phenylpropane and especially acetals are often obtained when polar solvents are used [21-23]. Hence, selectivity values shown in this work were calculated considering all products derived from the ECH reaction.

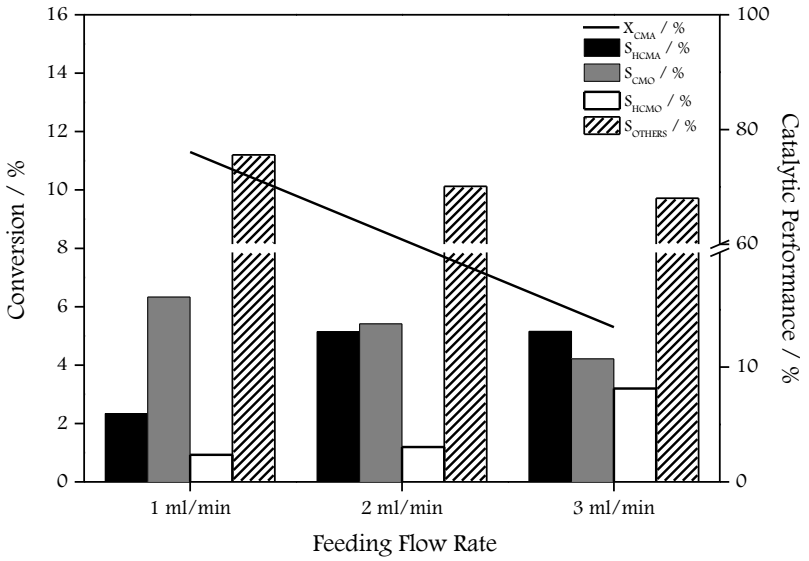

Figure 1.5.*Influence of the flow rate on the electrochemial hydrogenation of cinnamaldehyde. Conditions: atmospheric pressure, 60 min TOS (continuous mode), 75 ºC, 0.1 A. Anode chamber: H_2O; Cathode chamber: 100 ppm CMA/2-propanol.*

As displayed in Figure 1.5, in all the cases a considerable amount of side products was generated, mainly favored by the activity of cinnamaldehyde and the alcohol solvent [23, 24]. It is known that solvents have a significant effect on the catalytic hydrogenation performance, attributed to several factors such as hydrogen solubility, the thermodynamic interaction of the solvent with reactants and products or the competitive adsorption of the solvent. Particularly, the hydrogenation scheme of cinnamaldehyde seems to depend on the polarity of the solvent. In the presence of apolar solvents the reaction mainly results in HCMA, CMO and HCMO. In addition, β-methyl styrene can be formed through consecutive reactions of CMO. On the other

hand, when polar solvents (such as alcohols) are used, apart from the main products, cinnamaldehyde diacetals and hydrocinnamaldehyde can be reversible formed possibly due to the reaction between the aldehyde and the solvent molecules. However, it should be noted that although undesirable acetal compounds are not produced in the presence of apolar solvents, the reaction rate is significantly lower. Therefore, polar solvents such as methanol, ethanol or isopropanol are commonly used to carry out this reaction. In this sense, it should be mention that electrocatalytic hydrogenation selectivity results shown in this work agree with those reported on conventional hydrogenation of cinnamaldehyde, where from 20 up to 70-90% acetals can be obtained in analogous conditions (polar solvents and certain acidity) despite working at high pressure [21-24]. Regarding the production of the main fine chemicals, a negative effect on both ECH conversion and selectivity to the unsaturated alcohol was observed when increasing flow rate from 1 to 3 mL/min. As the residence time of reagents was shortened and considering that hydrogenation of the C=C bond is 30 times faster than that of the C=O bond, hydrogenation to HCMA and HCMO was promoted instead of CMO formation. Therefore, 1 mL/min feeding flow rate was selected as the optimal value for an adequate electrochemical hydrogenation of CMA in the PEMR.

Next step was to check the influence of the applied current on the electrochemical hydrogenation of cinnamaldehyde by modifying its value from OCP up to 0.1 A, then returning to OCP. Cell reaction temperature and inlet flow rate were set at 75 ^{o}C and 1 mL/min, respectively. Figure 1.6 depicts CMA conversion and products selectivity. As commented above, it can be observed that ECH of cinnamaldehyde is a reversible process that only takes place under polarization conditions. CMA conversion was observed not to depend on the applied current at the explored range. It is related to the fact that, at high current densities,

the rate of H^+ generation is already in excess in comparison with its consumption by reaction with CMA, so that hydrogen evolution reaction competes with CMA hydrogenation, involving the recombination of excessive protons and electrons to produce H_2 [10, 11]. However, selectivity can be shifted towards the main valuable chemicals by controlling the applied polarization conditions. In this sense, as the applied current rises to 0.1 A, selectivity to the undesired products experienced a marked increase at the expense of HCMA, HCMO and especially CMO, which dropped sharply. This could be explained by the fact that at 0.1 A, a high rate of protons supply occurs leading to further hydrogenation reactions to acetals or ethers. According to the results, it can be concluded that the most suitable applied current for CMA hydrogenation was 0.05 A. This value of applied current was not only more favorable in terms of energy consumption but also improved selectivity towards the main valuable chemicals by reducing the generation of undesired side products to the half, leading to a higher CMO yield.

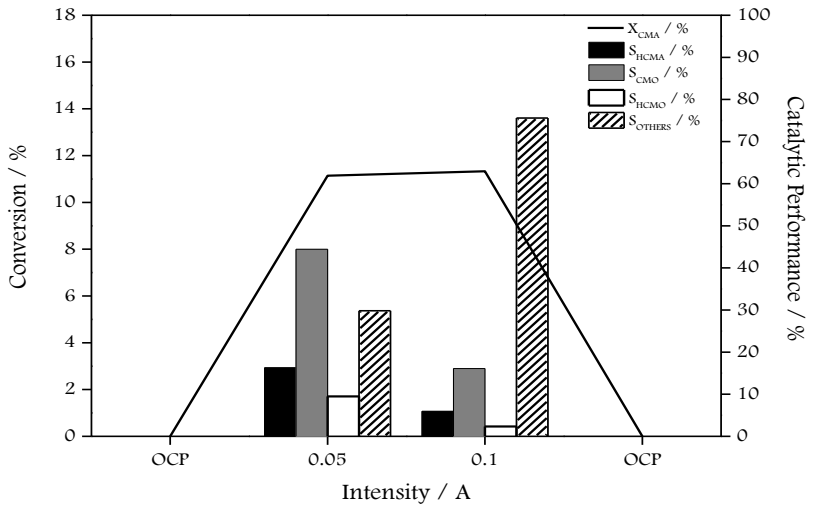

Figure 1.6. *Influence of the applied current on the electrochemial hydrogenation of cinnamaldehyde. Conditions: atmospheric pressure, 60 min TOS (continuous mode), 75 ºC, 1 ml·min^{-1}. Anode chamber: H_2O; Cathode chamber: 100 ppm CMA/2-propanol.*

Last step in this work was to study the influence of the temperature cell on CMA electrochemical hydrogenation performance.

To this end, ECH experiments were performed at four different temperatures ranging from 55 to 75°C under the conditions selected above. Results are presented in Figure 1.7. As expected, conversion of CMA linearly increased with reaction temperature up to 16% at 70°C. However, above this temperature, the hydrogenation conversion was limited due to the lower solubility of hydrogen at the closeness of the boiling point of the solvent, so that 75°C should be dismiss. It can be also seen that selectivity to CMO was slightly modified under the range of study. However, in agreement with the available literature, lower temperatures facilitate the production of CMO, while higher ones decrease the selectivity to this product. It is due to the fact that temperature may favor both the competitive adsorption between CMA and CMO on the active catalytic sites and the consecutive hydrogenation of the latter one, leading to HCMA, HCMO or even side products such as those obtained from aldol condensation [5, 25]. Therefore, in order to enhance the CMO yield 70°C was selected as the optimum temperature for future experiments.

It should be also mentioned that electrochemical hydrogenation of CMA was found to proceed with an apparent activation energy of 16 kJ/mol (from the slope of the corresponding Arrhenius plot, not shown here), which was in good agreement to those reported in conventional pressurized catalytic hydrogenation (15.4-21 kJ/mol) over commercial Pt/G [26] or Pt/SBA-15 or fumed silica [27].

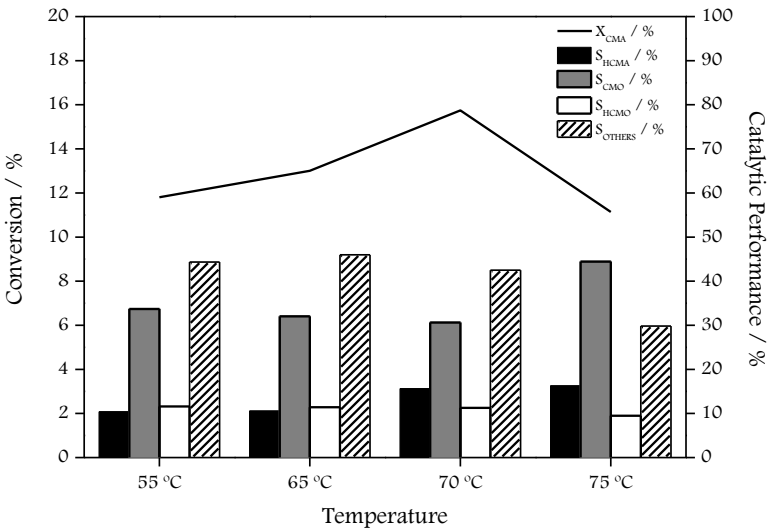

Figure 1.7. *Influence of the temperature on the electrochemial hydrogenation of cinnamaldehyde. Conditions: atmospheric pressure, 60 min TOS (continuous mode), 0.05 A, 1 ml·min $^{-1}$. Anode chamber: H_2O; Cathode chamber: 100 ppm CMA/2-propanol.*

Results presented above point out that the electrocatalytic hydrogenation process of cinnamaldehyde can be correctly performed under mild conditions in a PEMR, working without any external H_2 source by using electricity as the driving force.

4. CONCLUSIONS

The electrocatalytic hydrogenation of cinnamaldehyde is demonstrated to be feasible at a commercial Pt/C cathode in a polymeric exchange membrane reactor under mild conditions. This process is an alternative route to produce cinnamyl alcohol, hydrocinnamaldehyde and phenylpropanol in a lesser extent, and even further hydrogenation products, which does not require a supply of hydrogen since protons are generated in situ by water electrolysis. Working under continuous mode and proper reaction conditions (flow rate, temperature and applied current temperature) greatly influenced product yields, promoting the

formation of cinnamyl alcohol and controlling the production of extra H_2 and side products. Despite the promising initial attempt of the proposed system, a suitable catalyst design is being conducted to improve CMO yield to a further extent.

REFERENCES

1. Bachiller-Baeza, B., I. Rodríguez-Ramos, and A. Guerrero-Ruiz, *Influence of Mg and Ce addition to ruthenium based catalysts used in the selective hydrogenation of α,β-unsaturated aldehydes.* Applied Catalysis A: General, 2001. **205**(1): p. 227-237.
2. Claus, P., *Selective hydrogenation of ά,β-unsaturated aldehydes and other C=O and C=C bonds containing compounds.* Topics in Catalysis, 1998. **5**(1): p. 51-62.
3. Gallezot, P. and D. Richard, *Selective Hydrogenation of α,β-Unsaturated Aldehydes.* Catalysis Reviews, 1998. **40**(1-2): p. 81-126.
4. Giroir-Fendler, A., D. Richard, and P. Gallezot, *Selectivity in Cinnamaldehyde Hydrogenation of Group-VIII Metals Supported on Graphite and Carbon.* Studies in Surface Science and Catalysis, 1988. **41**: p. 171-178.
5. Manikandan, D., D. Divakar, and T. Sivakumar, *Utilization of clay minerals for developing Pt nanoparticles and their catalytic activity in the selective hydrogenation of cinnamaldehyde.* Catalysis Communications, 2007. **8**(11): p. 1781-1786.
6. Li, Y., P.-F. Zhu, and R.-X. Zhou, *Selective hydrogenation of cinnamaldehyde to cinnamyl alcohol with carbon nanotubes supported Pt-Co catalysts.* Applied Surface Science, 2008. **254**(9): p. 2609-2614.
7. Gutiérrez-Guerra, N., et al., *Electrocatalytic conversion of CO2 to added-value chemicals in a high-temperature proton-exchange membrane reactor.* Electrochemistry Communications, 2017. **81**: p. 128-131.
8. Fonocho, R., C.L. Gardner, and M. Ternan, *A study of the electrochemical hydrogenation of o-xylene in a PEM hydrogenation reactor.* Electrochimica Acta, 2012. **75**: p. 171-178.
9. Huang, H., Y. Yu, and K.H. Chung, *Performance of Au/Nafion/Pt electrodes in benzene–water electrochemical hydrogenation.* International Journal of Hydrogen Energy, 2014. **39**(25): p. 13832-13837.
10. Sáez, A., et al., *Electrocatalytic hydrogenation of acetophenone using a Polymer Electrolyte Membrane Electrochemical Reactor.* Electrochimica Acta, 2013. **91**: p. 69-74.
11. Takano, K., et al., *Electrocatalytic hydrogenation of toluene using a proton exchange membrane reactor.* Bulletin of the Chemical Society of Japan, 2016. **89**(10): p. 1178-1183.

12. Wakisaka, M. and M. Kunitake, *Direct electrochemical hydrogenation of toluene at Pt electrodes in a microemulsion electrolyte solution.* Electrochemistry Communications, 2016. **64**: p. 5-8.
13. Matthiesen, J.E., et al., *Electrochemical Conversion of Muconic Acid to Biobased Diacid Monomers.* ACS Sustainable Chemistry & Engineering, 2016. **4**(6): p. 3575-3585.
14. Villalba, M., M. del Pozo, and E.J. Calvo, *Electrocatalytic hydrogenation of acetophenone and benzophenone using palladium electrodes.* Electrochimica Acta, 2015. **164**: p. 125-131.
15. de la Osa, A.R., et al., *Electrochemical reforming of alcohols on nanostructured platinum-tin catalyst-electrodes.* Applied Catalysis B: Environmental, 2015. **179**: p. 276-284.
16. Corrales-Sánchez, T., J. Ampurdanés, and A. Urakawa, *MoS2-based materials as alternative cathode catalyst for PEM electrolysis.* International Journal of Hydrogen Energy, 2014. **39**(35): p. 20837-20843.
17. Caravaca, A., et al., *From biomass to pure hydrogen: Electrochemical reforming of bio-ethanol in a PEM electrolyser.* Applied Catalysis B: Environmental, 2013. **134**: p. 302-309.
18. Calabrese, G.S. and S. Pissavini, *From batch to continuous flow processing in chemicals manufacturing.* AIChE Journal, 2011. **57**(4): p. 828-834.
19. Garkhedkar, A.M., et al., *Intensifying Hydrogenation of Cinnamaldehyde to Cinnamyl Alcohol: Catalyst, Solvent and Operating Conditions.* Indian Chemical Engineer, 2015. **57**(3-4): p. 219-239.
20. Durndell, L.J., K. Wilson, and A.F. Lee, *Platinum-catalysed cinnamaldehyde hydrogenation in continuous flow.* RSC Advances, 2015. **5**(97): p. 80022-80026.
21. Li, Y., et al., *Influence of Preparation Modes on Pt–Ni/CNTs Catalysts Used in the Selective Hydrogenation of Cinnamaldehyde to Hydrocinnamaldehyde.* Catalysis Letters, 2008. **126**(3): p. 280-285.
22. Wang, D. and Y. Zhu, *An Effective Pt-Cu/SiO2 Catalyst for the Selective Hydrogenation of Cinnamaldehyde.* Journal of Chemistry, 2018. **2018**: p. 7.
23. Zhang, L., *Selective hydrogenation of α,β[alpha,beta]-unsaturated aldehydes towards clean synthesis over noble metal catalysts in mass transfer efficient three phase reactors*, in *School of Chemical Engineering*. 1998, University of Birmingham. p. 409.

24. Leng, F., et al., *Selectivity shifts in hydrogenation of cinnamaldehyde on electron-deficient ruthenium nanoparticles.* Comptes Rendus Chimie, 2018. **21**(3): p. 346-353.
25. Yang, X., et al., *High-performance Pd–Au bimetallic catalyst with mesoporous silica nanoparticles as support and its catalysis of cinnamaldehyde hydrogenation.* Journal of Catalysis, 2012. **291**: p. 36-43.
26. Koo-amornpattana, W. and J.M. Winterbottom, *Pt and Pt-alloy catalysts and their properties for the liquid-phase hydrogenation of cinnamaldehyde.* Catalysis Today, 2001. **66**(2): p. 277-287.
27. Durndell, L.J., et al., *Selectivity control in Pt-catalyzed cinnamaldehyde hydrogenation.* Scientific Reports 2015. **5**: p. 9425.

Section II: Catalysts synthesis for the electrochemical hydrogenation of cinnamaldehyde

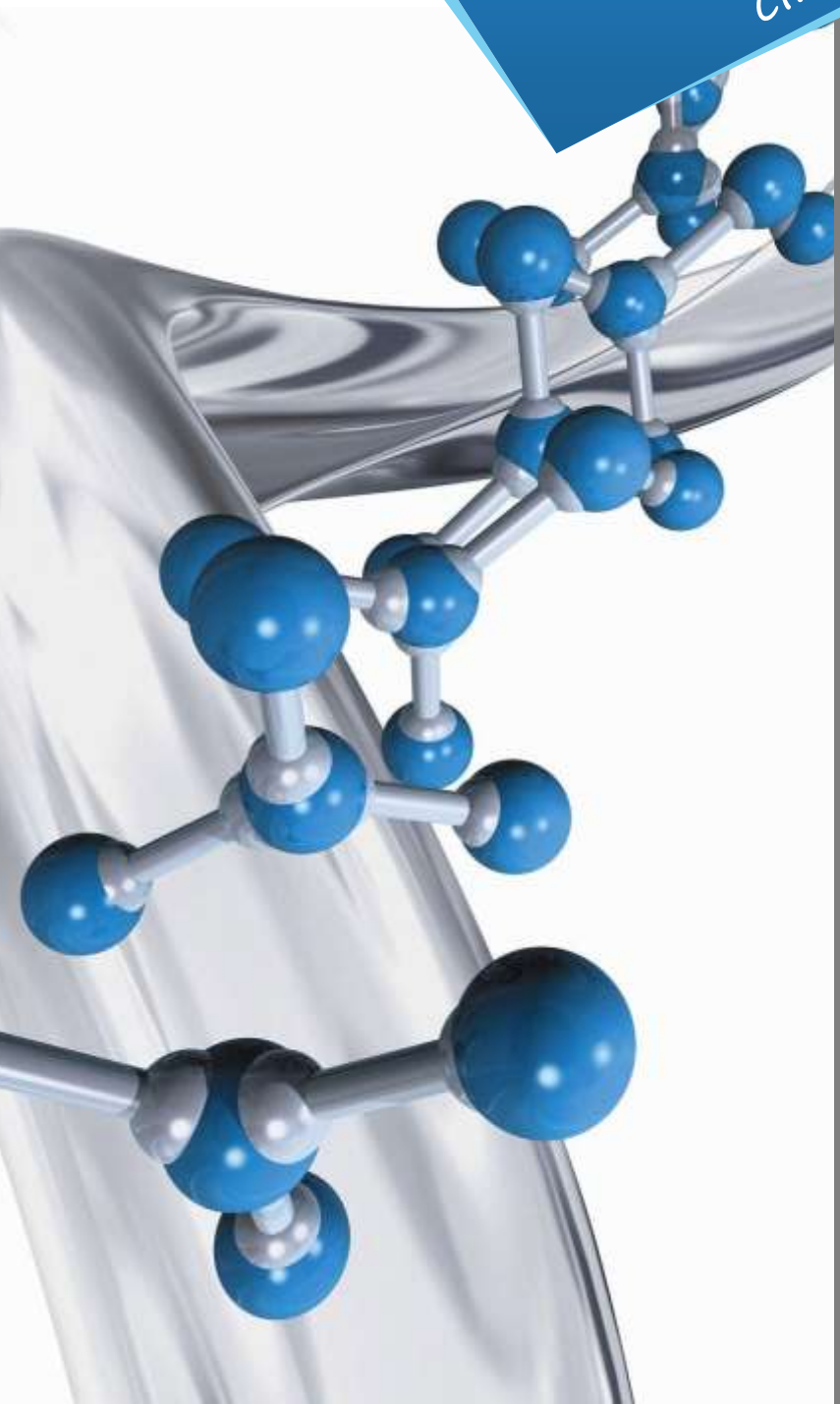

Chapter 2: Electrocatalytic Hydrogenation of cinnamaldehyde by Pt/C catalysts prepared by one-pot impregnation-reduction method

Chapter 3: Pt/C Catalysts for the electrocatalytic hydrogenation of cinnamaldehyde: Influence of the reducing agent.

Chapter 4: Electrocatalytic Hydrogenation of cinnamaldehyde in a PEM cell. The role of sodium hydroxide and platinum loading.

Chapter 2: Electrocatalytic Hydrogenation of Cinnamaldehyde by Pt/C Catalysts Prepared by One-Pot Impregnation-Reduction Method

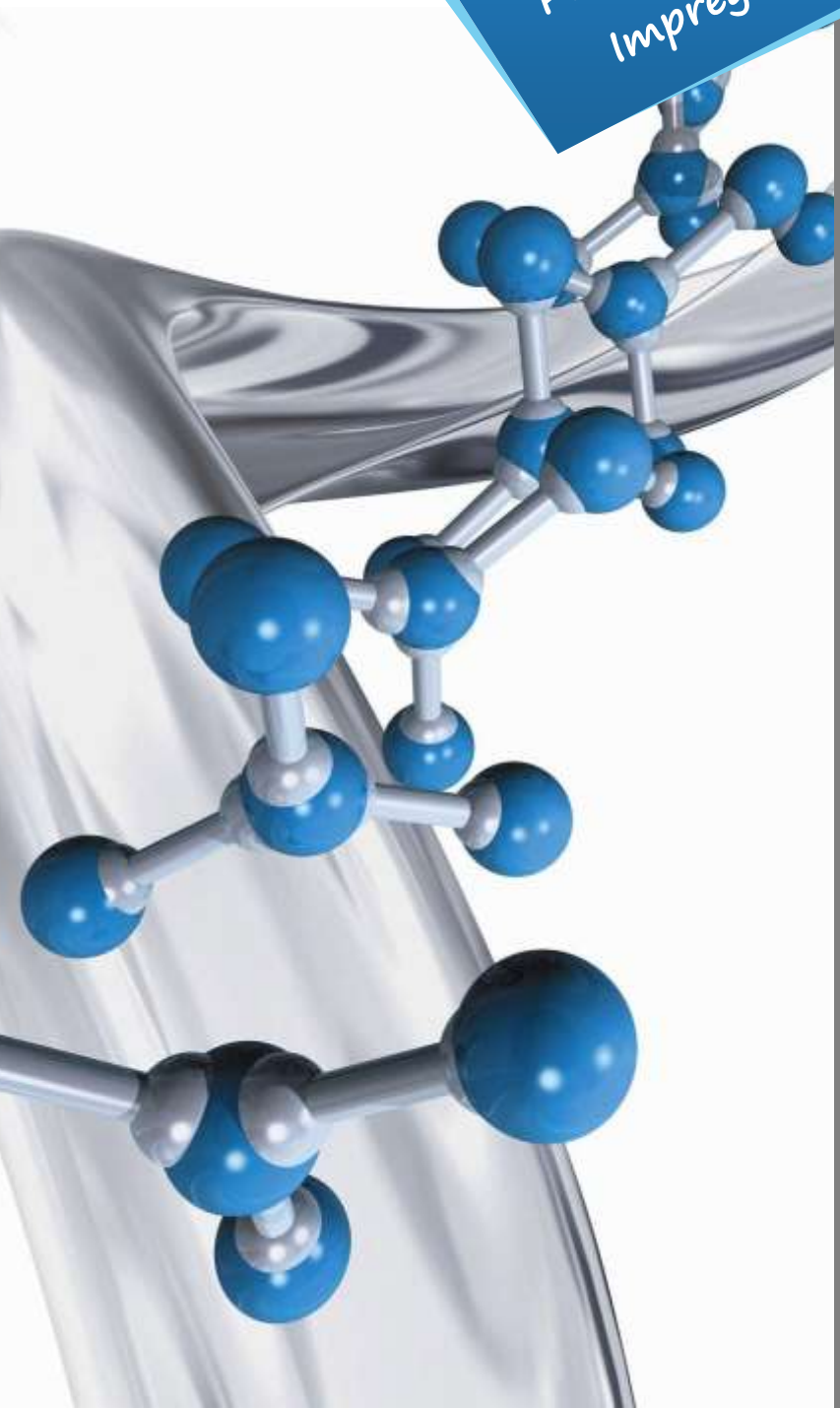

1. INTRODUCTION

2. EXPERIMENTAL
2.1. Catalysts
2.2. Physicochemical characterization
2.3. Electrochemical characterization
2.4. Membrane electrode assembly (MEA) preparation
2.5. Electrocatalytic hydrogenation tests

3. RESULTS AND DISCUSSION
3.1 Physicochemical characterization
3.2. Electrochemical characterization
3.3. Electrocatalytic tests

4. CONCLUSIONS

Abstract

In this work, carbon-supported platinum catalysts were synthesized by one-pot impregnation-reduction method and tested in the electrocatalytic hydrogenation of cinnamaldehyde (CMA) with the aim to maximize the production of cinnamyl alcohol (CMO). The method was improved sequentially (solvent evaporation under vacuum, inclusion of a washing step and addition of the metal salt precursor dropwise) in order to evaluate how these improvements affected the physicochemical and electrochemical properties of the catalysts. Physicochemical characterization was carried out by N_2 adsorption-desorption, TPR, XRD, H_2 pulse chemisorption and acid-base titrations, whereas cyclic voltammetry and kinetic studies of the hydrogen evolution reaction (HER/HOR) were performed to evaluate the electrochemical properties. Results revealed that those catalysts that showed a good compromise between Pt dispersion, basic character and high electrochemical surface area were more active in terms of CMA conversion and CMO selectivity. The catalyst prepared dropwise, under vacuum and washed showed the highest yield to CMO.

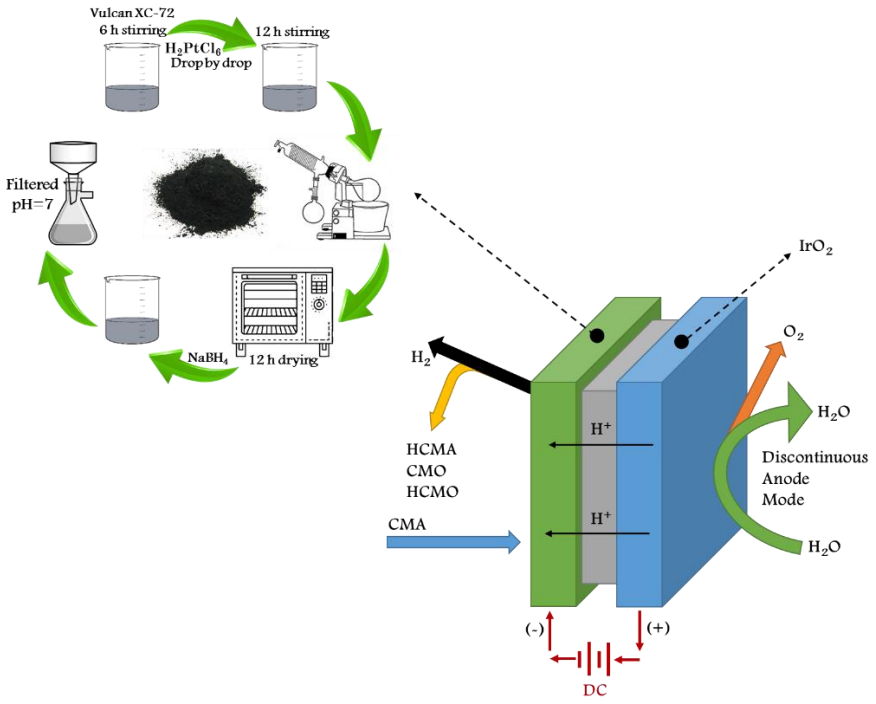

Figure 2.1. *Graphical abstract Chapter 2.*

1. INTRODUCTION

The selective hydrogenation of α-β unsaturated aldehydes to the corresponding unsaturated alcohols is a key step in the production of added-value chemicals, which are widely used in the chemical industry. In fact, the high consumer expenditure on luxurious consumer goods due to the changing lifestyle as well as the consciousness pertaining to health and safety result in a rising demand from organic food, beverages, low toxiticy perfumes, surfactants and agrochemicals that are expected to enhance cinnamaldehyde (CMA) market trend and support related technological advancements. In particular, the synthesis of cinnamyl alcohol (CMO) from the selective hydrogenation of cinnamaldehyde attracts a great interest, since this alcohol is used as an additive in the food and pharmaceutical industries [1]. This reaction requires the hydrogenation of the C=O bond of CMA, which is neither thermodynamically nor kinetically favourable respect to that of the C=C bond that lead to hydrocinnamaldehyde (HCMA) [2-4]. Therefore, it is still crucial to develop selective catalysts that hydrogenate the C=O group and maximize the production of CMO.

In this sense, numerous studies about the catalytic hydrogenation of CMA have been carried out. Among the most recent ones, Wei *et al.* [3] synthesize CeO_2 and ZrO_2-supported Pt catalysts for the hydrogenation of CMA at 10 bar and 60 °C. He *et al.* [2] used MoO_x nanorods-supported Ir nanoparticles in the reaction at 20 bar and 100 °C. Finally, Piqueras *et al.* [5] carried out the CMA hydrogenation in supercritical CO_2 media, using Cu, Pt and Au-based catalysts. The main drawbacks related to these kind of reactions are the need for an external hydrogen source and the operation under high pressure and/or temperature, which affect economical and safety concerns. Moreover, this reaction system is traditionally conducted in batch operation mode, which is associated

with long contact times and additional cleaning and catalyst/solvent (often toxic or hazardoous compounds) separation stages, raising the economy of the process [6-8].

Electrocatalytic hydrogenation has been demonstrated to be a promising alternative to catalytic hydrogenation since it can be carried out at mild conditions, *i.e.*, room temperature and pressure [9] and simplifies the scalability of the process. The electrocatalytic hydrogenation of different organic compounds such as acetylene [10, 11], acetophenone [9, 12], furfural [13] or aldehydes as benzaldehyde and pentanal [14] has been successfully performed, using electrodes based in Au, Ag, Pd and Pt. In the electrocatalytic process, the hydrogen source (H^+) is generated *in situ* in the anode through H_2O electrolysis, which avoids the use of high-cost H_2 gas and improves the economy of the process [15]. Then, H^+ migrates through a protonic exchange membrane (PEM) to the cathode, where the reduction of the organic substrate takes place by a coupled proton–electron transfer process [13]. However, despite the low toxicity of cinnamaldehyde and wide industrial application of its derivates, the electrocatalytic hydrogenation of this molecule has been barely studied and only few works report results from its electrohydrogenation for comparison purposes with respect to other aldehydes [16] or the influence of reaction conditions on a PEM cell using a Pt/C commercial catalyst.

Conventional catalytic hydrogenation of CMA has been reported to be strongly affected by the catalyst characteristics such as the adjunction of promoters, the size of the metal particles and the nature of the support [17], so that special attention should be paid to the electrocatalyst properties as well. In this regard, Zhao *et al.*[13] used Pt/ACF catalysts with different Pt concentrations in the electrocatalytic hydrogenation of furfural, and concluded that the metal-support interaction and the pore

blockage affected the catalytic activity. Regarding the active phase, Pt has been used in numerous catalytic [3, 18, 19] and electrocatalytic [20-22] hydrogenations, since it shows an ideal electronic configuration for these reactions and outstanding dispersion properties. As for support, carbon Vulcan XC-72 is widely used in the preparation of electrocatalysts due to its good compromise between electrical conductivity and high surface area [23].

In this work, Pt/C catalysts were synthesized by different one-pot impregnation-reduction methods, in which some procedure steps, such as the introduction of the Pt precursor, were modified with the aim to analyse their influence on the catalyst properties. The prepared catalysts were characterised by physicochemical and electrochemical techniques, and then tested in the electrocatalytic hydrogenation of CMA. The yield to cinnamyl alcohol (CMO) was used as the optimization criterion. Reaction results were analysed together with the physicochemical and electrochemical catalysts properties in order to identify those that influenced the most. Catalytic results of the commercial Pt/C (carbon black, i.e carbon Vulcan XC-72) were included as a reference.

2. EXPERIMENTAL

2.1. Catalysts

Pt/C electrocatalysts, used as cathode, were synthesized by one pot impregnation-reduction method, using $NaBH_4$ (supplied by Sigma-Aldrich) as reducing agent and carbon Vulcan XC-72 (provided by FuelCell Store). However, in order to optimize the catalyst properties, the parent method was modified. Pt-based catalysts were labelled Pt/C-I, where I varies from 1 to 4 respective to the preparation method.

In the first procedure (catalyst denoted as Pt/C-1 and referred to the parent preparation method), 0.4 g of the as-received carbon black

support were dispersed in 400 mL of deionized water under stirring and heated up to 70°C. 0.27 g of a 0.05 $g \cdot mL^{-1}$ solution of the platinum salt precursor ($H_2PtCl_6 \cdot 6H_2O$, Sigma-Aldrich) were then added to the support solution and heated to 80°C. After that, the reducing agent (0.05 $g \cdot mL^{-1}$) was added to the carbon-precursor solution, which was cooled down to room temperature. The mixture was then filtered and washed with deionized water at 80°C. The catalyst was subsequently dried for 24 hours at 120 °C.

Pt/C-2 was prepared using the procedure described by Zheng *et al.* [4]. Firstly, the support was added to 200 mL of deionized water under stirring for 6 h. After that, a 0.5 $mol \cdot L^{-1}$ solution of the platinum salt precursor was added to the support solution and kept under stirring for 12 h. The solvent was then removed by rotary evaporation in a water bath at 60°C. The sample was subsequently dried at 80 °C for 12 h and reduced by adding a certain amount of 0.2 M $NaBH_4$ solution, being the molar ratio $NaBH_4/H_2PtCl_6$ = 10. Finally, the catalyst was filtered and dried for 12 h at 120 °C.

Pt/C-3 was synthetized by the same procedure followed in the synthesis, reduction, drying and calcination of catalyst Pt/C-2 but in this case a washing step until pH = 7 between filtration and drying was included.

Pt/C-4 was prepared analogously to Pt/C-3 but the addition of the Pt precursor solution was carried out dropwise to achieve a better metal dispersion.

Physicochemical and electrochemical properties of Pt/C-I catalysts, as well as their catalytic performance for CMA electrocatalytic

hydrogenation were compared to those of a commercial Pt/C catalyst purchased from Alfa Aesar (denoted as Pt/C-C).

Commercial IrO_2 (99 wt. %, Alfa Aesar) was used as anode electrocatalyst in this work.

2.2. Physicochemical characterization

An inductively coupled plasma spectrometer (ICP, Model Liberty Sequential, VARIAN) was used to analyze Pt content. Surface area/porosity measurements were collected in a Micromeritics ASAP 2010 sorptometer unit, with N_2 at 77 K as the adsorbate. Acid-base properties of the catalyst and support were analyzed by HCl titrations performed on a SCHOTT Titroline apparatus. In order to check species present in the catalyst and also to calculate particle size, XRD analyses were performed on a Phillips PW-1700 diffractometer using nickel-filtered Cu Kα radiation. In addition, temperature-programmed reduction (TPR) experiments were conducted in a Micromeritics AutoChem 2950 HP unit. The same unit was used to carry out H_2 pulse chemisorption experiments to calculate Pt metal dispersion, active particle size and CSA.

2.3. Electrochemical characterization

In order to measure the electrochemical surface area (ECSA) and deactivation degree of the catalysts [24] electrochemical characterization was performed by means of cyclic voltammetry experiments carried out in a computer-controlled potentiostat Autolab PGSTAT128N (Ecochemie, The Netherlands), using a single cell of three-electrode system (see Section B.5.). Polarization curves were also conducted from 500 to 3000 rpm, by applying a potential range between 0.2 and 0.7 V (vs RHE) (5

mV·s^{-1} scan rate) in order to study the kinetics of the Hydrogen Evolution Reaction (HER/HOR).

2.4. Membrane electrode assembly (MEA) preparation

The Membrane Electrode Assembly (MEA) was prepared by spraying an ink containing a solution of the electrocatalyst and Nafion ionomer directly to the pretreated Nafion ®115 membrane. Commercial IrO_2 (diluted in water) was used as anode with a fixed loading of 2 mg ·cm^{-2} while the synthesized Pt/C-I (diluted in 2-propanol) catalysts were used as cathode in the electrochemical PEM cell with 0.5 mg·cm^{-2} loading.

2.5. Electrocatalytic hydrogenation tests

Electrocatalytic hydrogenation experiments (100 ppm of CMA in 2-propanol, 1 mL·min^{-1} feeding rate) were carried out at ambient pressure, 70^{o}C, using a Polymer Electrolyte Membrane (PEM) described in detail in Chapter 2 [25].

3. RESULTS AND DISCUSSION

3.1. Physicochemical characterization

Table 2.1 summarizes the main physicochemical properties of the support and Pt/C catalysts used in this work. The textural parameters (BET surface area, pore volume and average pore diameter) were evaluated by N_2 adsorption-desorption measurements, whereas Figure 2.2 depicts the isotherms of the support and all the samples.

Table 2.1. *Main physicochemical properties of Pt/C catalysts.*

Catalyst	XRD Particle size (nm)[1]	BET Surface Area ($m^2 \cdot g^{-1}$)	Pore Volume ($cm^3 \cdot g^{-1}$)	Average Pore Diameter (nm)[2]	Dispersion (%)[3]	Active Particle Size (nm)[3]	CSA ($m^2 \, g^{-1}$)[3]
Pt/C-C	7	183	0.679	15.3	50.8	2.2	125
Pt/C-1	16	164	0.404	10.5	9.3	12.9	23
Pt/C-2	10	149	0.301	8.4	24.3	4.7	60
Pt/C-3	12	162	0.462	11.6	21.9	5.2	54
Pt/C-4	10	159	0.486	12.4	35.4	3.2	87

[1] Calculated from the Pt (220) peak using the Debye-Scherrer equation

[2] Calculated assuming cylindrical pore geometry

[3]Calculated using Pulse Chemisorption

Vulcan XC-72 has a relatively large specific surface area (231±1 $m^2 \cdot g^{-1}$), a total pore volume of 0.403 $cm^3 \cdot g^{-1}$ and an average pore diameter of 7.7 nm. It presents a mesoporous structure but also comprises a large amount of micropores. Isotherms showed a type I adsorption-desorption profile, according to the IUPAC classification, which is associated to microporous materials. Firstly, the N_2 adsorption volume increased sharply in the micropore region, *i.e.*, at very low partial pressures ($P/P_0 < 0.005$). Then, there was a slight increase of N_2 adsorption volume at higher partial pressures, which could be attributed to the presence of some mesopores in the sample. This fact was corroborated with the hysteresis loop observed, which is ascribed to the capillary condensation that takes place on mesopores [26]. Note that the same applies to Pt/C-C catalyst, which is supported on carbon black. Regarding the textural parameters, it was observed in all cases that, once the metal precursor was introduced in the support, the BET surface area and pore volume experienced an important decrease. This fact could be attributed to the pore blockage by the metal particles, which prevent N_2 molecules to be adsorbed on them.

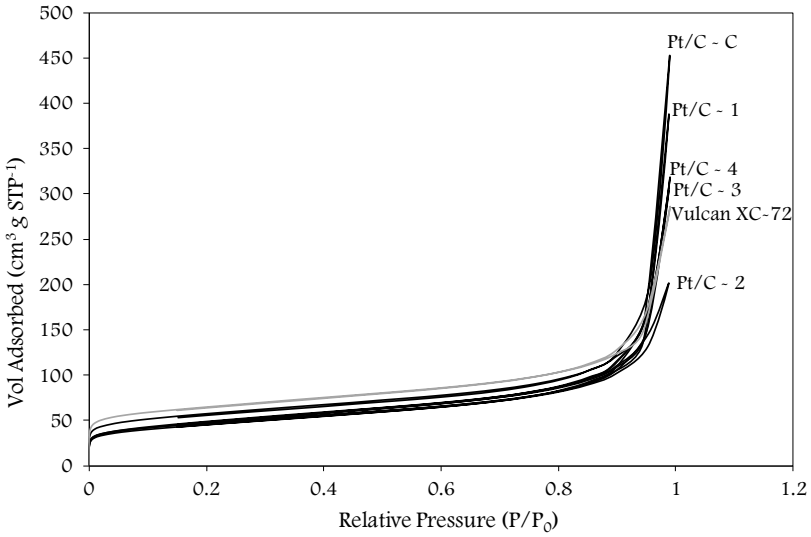

Figure 2.2. *Nitrogen adsorption desorption isotherms of the support and the studied catalysts.*

Regarding the average pore diameter, it was observed that the value of the Pt/C catalysts was higher than that of the support, which suggested that the Pt particles were mainly deposited on the micropores. However, the increase observed in Pt/C-2 was lower than that of the other catalysts. This fact, together with the decrease of pore volume, could be associated to a worse dispersion of the Pt particles.

In order to verify the proper reduction of Pt particles during the one-pot catalyst synthesis, TPR analyses were performed. Figure 2.3 showed the TPR profiles of the support and the catalysts used in this work. On the one hand, none of the catalyst showed any appreciable peak below 350 ºC. According to previous works [27], if Pt reduction was required, a measurable consumption of hydrogen would be observed in the range 130 -230 ºC [28], so it was possible to conclude that Pt was reduced during the catalyst synthesis. On the other hand, all samples showed hydrogen consumption peaks in the range 600-700 ºC, being those of the catalysts higher than that of the support. Indeed, another peak at 400 ºC was observed in Pt/C-C, Pt/C-2 and Pt/C-3. All these

peaks were ascribed to the gasification of the carbonaceous support [29], which was catalysed by the Pt particles. All things considered, the prepared catalysts were not required to be reduced prior to reaction.

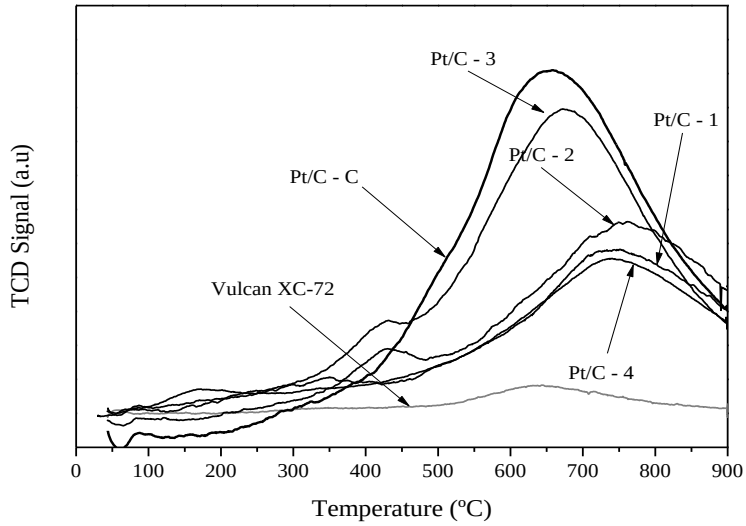

Figure 2.3. *Temperature-programmed reduction (TPR) profiles of Pt/C catalysts and the support.*

The crystalline structures of the support and the prepared catalysts were analysed by X-ray diffraction (Figure 2.4). All catalysts exhibited diffraction peaks at 40, 47, 68, 82, and 87°, which corresponded to the (1 1 1), (2 0 0), (2 2 0), (3 1 1) and (2 2 2) planes of Pt with face-centered cubic structure (JCPDS: 87-0647) and confirmed the reduction of Pt during the catalyst synthesis. The Pt average crystallite size was calculated from the Debye-Scherrer equation, using the (220) peak (see Table 2.1). Results revealed that Pt/C -1 showed the largest Pt particles, followed by Pt/C -3, Pt/C -2 and Pt/C -4, which showed similar values. On the other hand, commercial Pt/C - C was the catalyst with the smallest Pt particles. In addition, all Pt/C-I samples and the parent support exhibited one diffraction peak at 26°, which corresponded to the (0 0 2) plane of carbon. The small and broad morphology of the peak revealed the amorphous character of Vulcan XC-72.

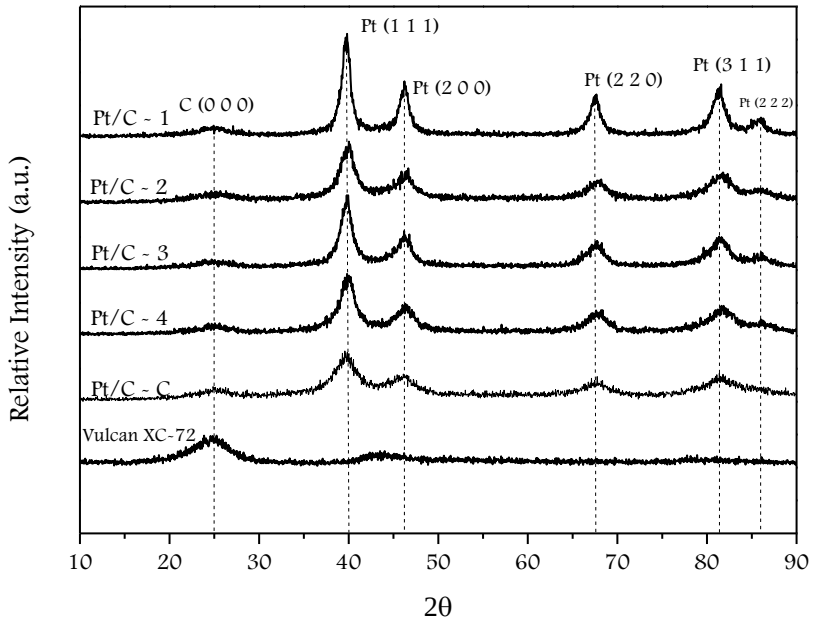

Figure 2.4. XRD patterns of Pt/C catalysts and the support.

H_2 pulse chemisorption experiments provided information about the metal dispersion, active metal particle size and chemical surface area of Pt/C-I catalysts. These variables were calculated assuming an adsorption stoichiometry of one hydrogen atom per surface Pt atom. Results are listed in Table 2.1. In agreement with results related to particle size obtained from XRD, it is observed that Pt/C-1 exhibited the lowest dispersion value, about 2.5 times lower than that of Pt/C-2, so as expected the solvent evaporation under vacuum favoured the dispersion of Pt particles (see also active particle size). However, the neutralisation procedure included in the synthesis procedure of Pt/C-3 led to a loss of metal dispersion, which can be mitigated if the metal is poured on the support dropwise, as observed in Pt/C-4. It is also important to note that dispersion values of all the prepared catalysts were much lower than that of the commercial catalyst Pt/C-C, which accordingly provided the highest CSA value.

From HCl titration profiles of the support and the cathodic catalysts, Figure 2.5 provides information about the acid-base character of the samples (ml of HCL necessaries to reach pH = 7). At first glance, it was observed that all samples exhibited basic character, since they required more volume of HCl to reach the equivalence point (compared to the blank). However, depending on the synthesis method, differences were observed. Then, the basic character increased in the following order: Pt/C-1 < Pt/C-2 < Pt/C-3 ≈ Pt/C-4. Therefore, evaporation under vacuum and washing to neutral pH prevent the catalyst from losing basic sites, whereas the addition of the salt precursor dropwise seems to influence more the particle size rather than show an appreciable effect on the basic character of the resulting catalyst.

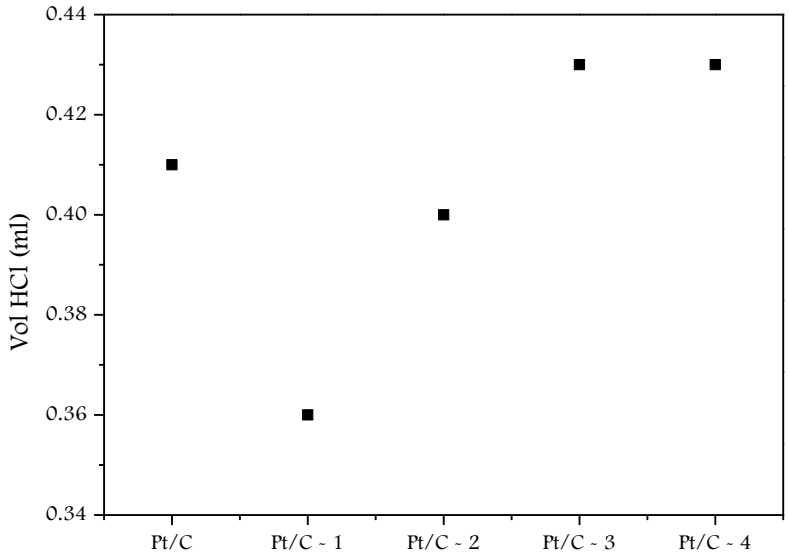

Figure 2.5. HCl titration results of all the samples used in this work (NaCl served as a blank).

3.2. Electrochemical characterization

The electrochemical resistance of the electrodes prepared with the synthesized Pt/C-I catalysts was studied by sequential cyclic voltammetry in phosphoric acid media (0.1 M). Figure 2.6 shows the cyclic voltammograms of the samples between 0.05 and 1.3 V vs RHE at a scan rate of 50 $mV \cdot s^{-1}$. On the one hand, during the cathodic scan the surface platinum oxides were reduced between 1.0 and 0.5 V (vs RHE), whereas hydrogen was desorbed at potentials below 0.4 V (vs RHE). On the other hand, samples Pt/C-2, Pt/C-3 and Pt/C-4 showed various peaks in the anodic scan (0-0.25 V vs RHE) that can be ascribed to the electro-oxidation of $Pt\text{-}H_{ads}$ to H^+. The different morphology of the peaks revealed differences in the faces of the platinum monocrystals for each catalyst [24].

As the number of cycles increased, the adsorption/desorption peaks above mentioned (see Figure 2.6) decreased, which revealed a loss of the electrochemical surface area. This loss was quantified by comparing the electrochemical surface area (ECSA) of the first cycle to that of cycle 500. Table 2.2 lists the ECSA of the samples at cycles 1 and 500, as well as the degradation degree of each sample. It can be seen that all samples experienced a decrease of ECSA values after 500 cycles, which confirmed the degradation of all the catalysts and suggested losses on the fraction of the platinum catalyst that was available to participate in electrode reactions.

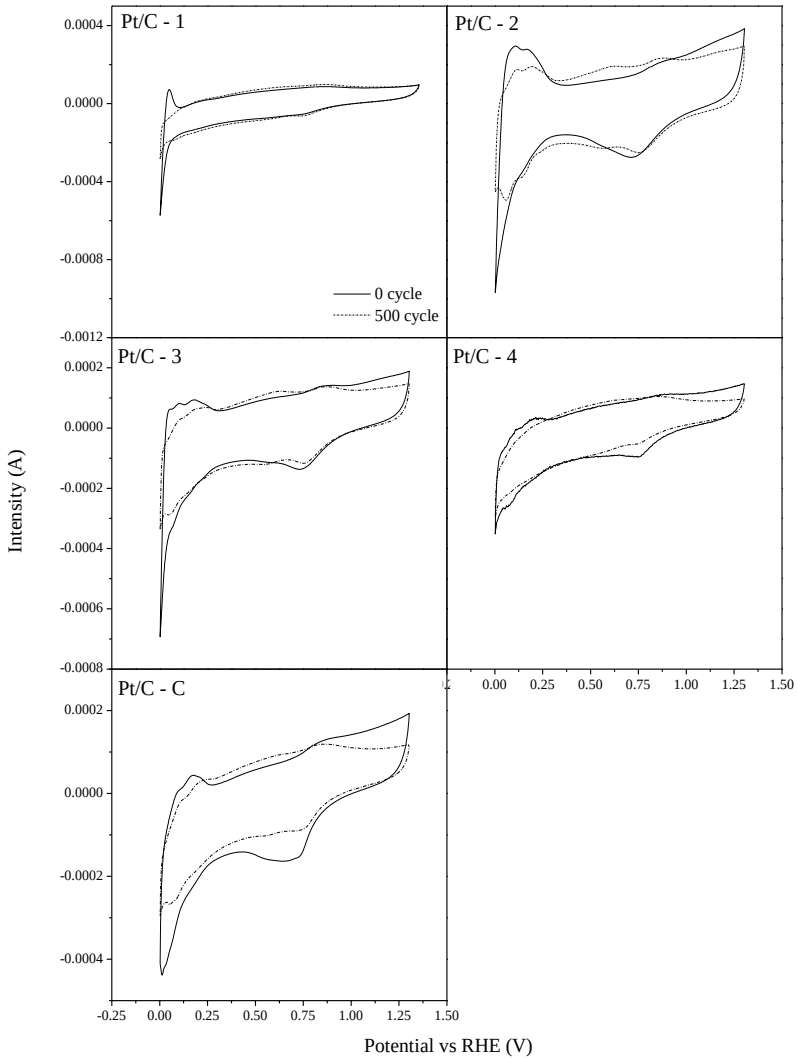

Figure 2.6. *Cyclic voltammograms of Pt/C catalysts in 0.1 M $HClO_4$, with a scan rate of 50 $mV \cdot s^{-1}$ at 25 °C.*

According to the deactivation values, despite of a lower CSA value, Pt/C-4 was the most stable catalyst, followed by Pt/C-3 and Pt/C-2. The differences between the chemical (measured by H_2 pulse chemisorption) and electrochemical surface area can be explained considering the fact that part of the Pt atoms were deposited inside the small pores of the support, being not accessible to reactants and therefore not

electrochemically active [30]. However, it is also important to note that the ECSA of these catalysts was higher than that of the commercial one, even after degradation. Taking into account these results, it can be concluded that the preparation method played an important role in the electrocatalytic properties.

Table 2.2. *ECSA values after 1 and 500 cycles and deactivation degree of Pt/C catalysts.*

Catalyst	ECSA 1st cycle	ECSA 500 th cycle	Deactivation (%)
	($m^2 \cdot g^{-1}$)		
Pt/C-C	41	19	54
Pt/C-1	35	14	60
Pt/C-2	48	29	40
Pt/C-3	49	31	37
Pt/C-4	46	30	35

According to the literature [9, 31] electrocatalytic hydrogenation of organic molecules is in competition with the hydrogen evolution reaction (HER/HOR), so that the efficiency of the electrocatalytic hydrogenation depends on this competition. Based on this theory, HER/HOR catalytic reaction studies were carried out by potential step voltammetry, using a rotating disk electrode.

The aim of these studies was to evaluate the performance of the synthesized catalysts, by analyzing in each case the kinetics of the HER/HOR reaction. Measured current was calculated as the sum of the anodic (HOR) and cathodic (HER) currents. It is important to note that HOR and HER occur simultaneously in both branches [32].

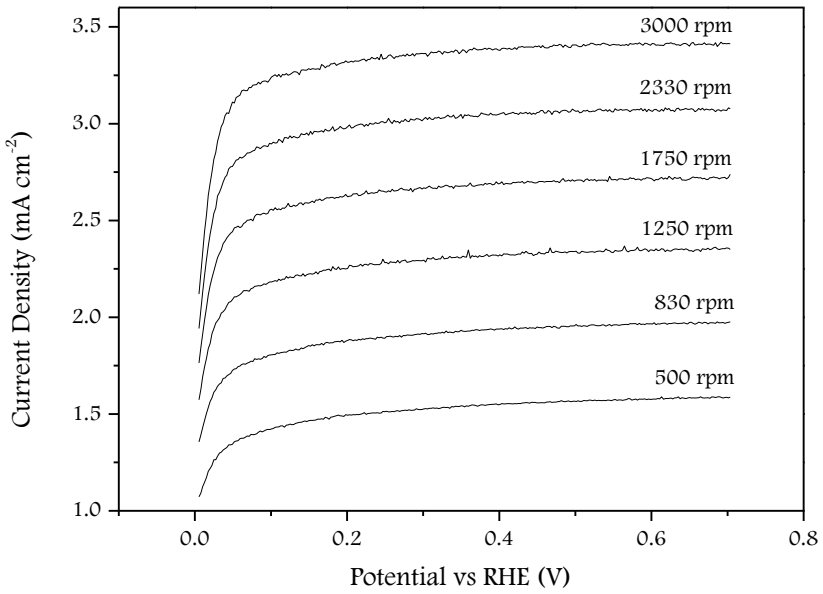

Figure 2.7. *Polarization curves of Pt/C-4 at a scan rate of 5 mV·s^{-1} in H_2 saturated $HClO_4$ 0.1 M at 25 °C (500 - 3000 rpm).*

Figure 2.7 shows the polarization curves of Pt/C-4 in $HClO_4$, at 298 K and different rotation rates. It was observed that, regardless of the applied rotating speed, the current density experienced a fast increase until ≈ 0.1 V. From this potential, the well-defined hydrogen diffusion limiting current density was reached. The data obtained in these experiments at 0.4 V was used to represent the linearized Koutecky-Levich plot, as shown in Figure 8. By doing this, the number of electrons transferred (*n*) and the kinetic rate constant (*k*) of all catalysts were obtained from the slope and intercept, respectively, and collected in Table 2.3. The kinetic rate constant is known to depend on the applied potential, temperature, electrode surface structure, composition of the catalyst, surface adsorption and reaction intermediates [33].

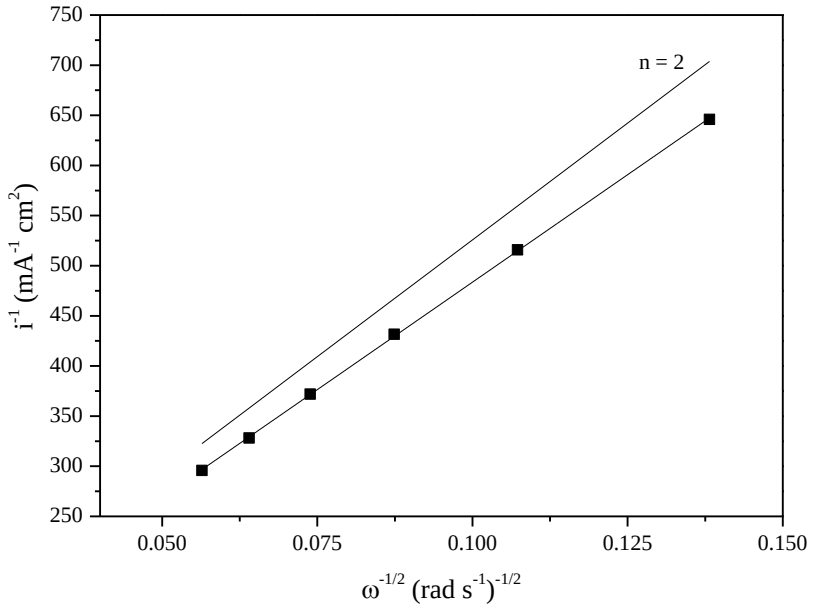

Figure 2.8. *Koutecky-Levich plot of Pt/C-4 performed in RDE at 25°C, 0.4 V (vs RHE) in $HClO_4$ 0.1 M.*

According to results from Table 2.3, it is possible to conclude that, in all cases, the HER/HOR reaction followed the two-electron mechanism. On the other hand, Pt/C-3 resulted to be the least active catalyst for this reaction, whereas Pt/C-2 showed the highest *k* value.

Table 2.3. *Number of electrons transferred in the HER/HOR reaction and kinetic rate constants determined from the Koutecky-Levich plots.*

Catalyst	n	k ($cm \cdot s^{-1}$)
Pt/C-C	2.80	0.113
Pt/C-1	2.31	0.116
Pt/C-2	2.23	0.259
Pt/C-3	2.67	0.063
Pt/C-4	2.17	0.124

3.3. Electrocatalytic tests

Figure 2.9 illustrates the main reaction pathways of the selective hydrogenation of CMA. The hydrogenation of the C=O bond lead to CMO, whereas HCMA is formed from the hydrogenation of the C=C bond. Further hydrogenation of both species results in the formation of hydrocinnamyl alcohol (HCMO) [34]. In addition, electrocatalytic hydrogenation (ECH) as well as conventional catalytic hydrogenation of aldehydes has been reported to be critically influenced by the nature of solvent, whose polarity and pH are likely to modify the interactions and rate of charge transfer between the electrode surface and the organic molecules. Therefore, when polar solvents are used as anolyte, further hydrogenation of CMA and/or HCMA to acetal-type compounds are found to occur.

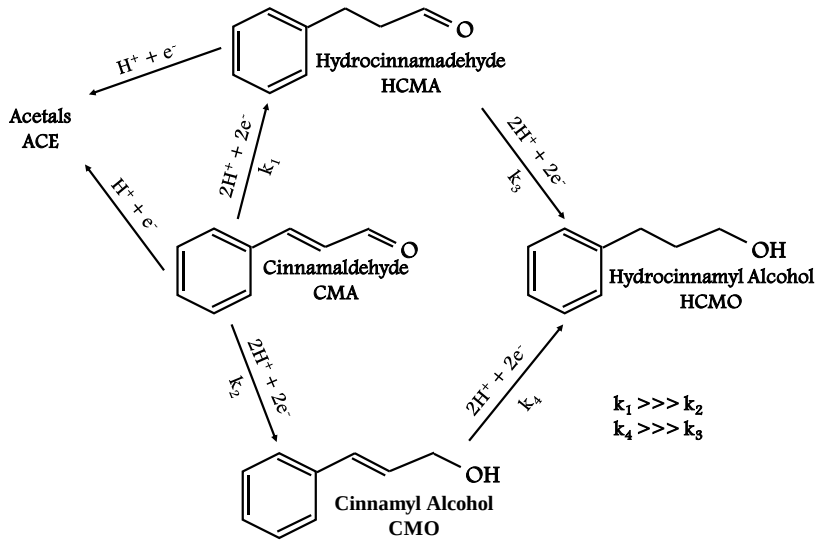

Figure 2.9. Main reaction pathways of the hydrogenation of cinnamaldehyde.

Figure 2.10 compares the CMA conversion and the selectivity to CMO, HCMA and HCMO of the studied catalysts. Moreover, the selectivity to other products (acetals or other species derived from further

hydrogenations), which was calculated as the difference between 100 % and the sum of CMO, HCMA and HCMO was included.

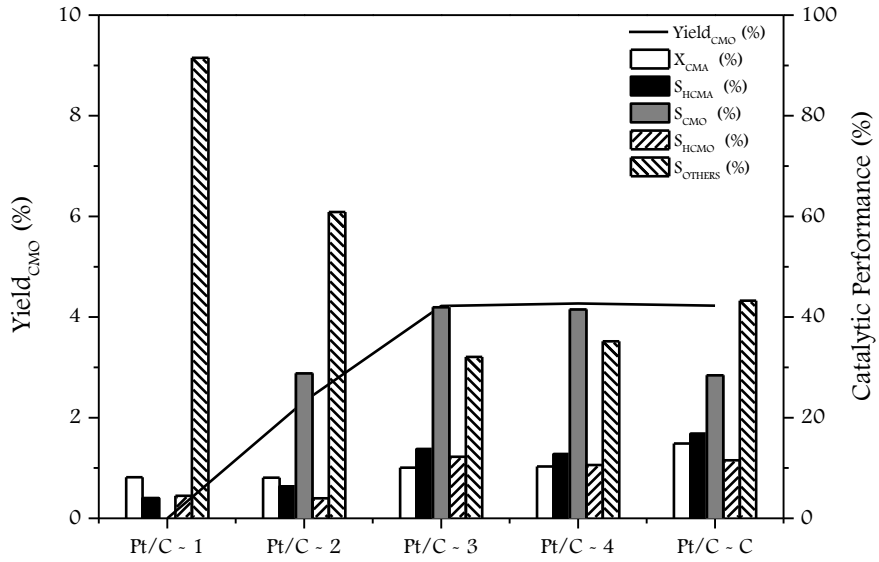

Figure 2.10. *Influence of the preparation method on the electrocatalytic hydrogenation of CMA performance. Reaction conditions: Anodic solution: H_2O, Cathodic solution: 100 ppm CMA in 2-propanol, Inlet flow: 1 NmL·min^{-1}, Intensity: 0.05 A, Temperature: 70 ^{o}C.*

The synthesis method is shown to have a great influence on the CMA conversion and products selectivity. Conversion values per single pass, working in continuous operation mode, increased as the following sequence: Pt/C-1 ≈ Pt/C-2 < Pt/C-3 ≈ Pt/C-4 < Pt/C-C. According to the characterization results, the higher the Pt dispersion, the higher the CMA conversion was. However, the Pt/C-2 conversion was not as high as expected considering its high dispersion, probably due to the high activity of this catalyst to the undesired HER/HOR reaction (see Table 2.2). In general, these results suggested that the electrocatalytic hydrogenation of CMA was not affected by the Pt structure, as reported by Durndell *et al.* [35]. To gain deeper insight about this point, Figure 2.11 shows the variation of the turnover frequency (TOF) as a function of the number of Pt active moles, which were calculated using the

dispersion values obtained by H_2 pulse chemisorption. It is observed that all catalysts except Pt/C-1 showed similar TOF values (between 1.5 and 2 h^{-1}), regardless of the number of Pt active moles, which confirmed the fact that the electrocatalytic hydrogenation of CMA was not affected by the platinum structure from 2.23 nm (Pt/C-C) to 5.17 nm (Pt/C-3). The high TOF of Pt/C-1 could be ascribed to the fact that, as the Pt particle size increased, reaction turned to be dependent on the Pt structure. However, an in-depth particle size studied, similar to that of Durndell *et al.* [35], should be carried out to give a proper conclusion.

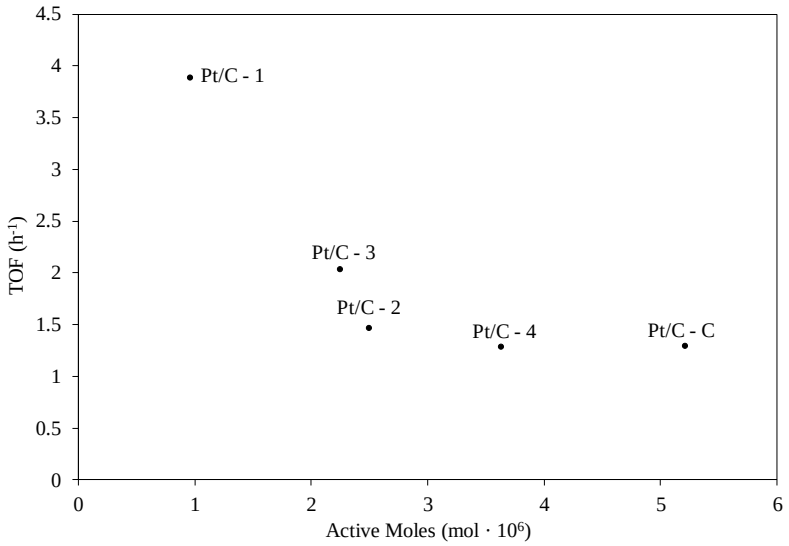

Figure 2.11. Turnover frequencies of CMA reaction (TOF CMA) related to each Pt/C catalysts.

Regarding product selectivity, it should be mentioned that selectivity of CMA ECH to non-desired compounds (i.e acetals) was found to be between 30 to 90%, which was in agreement to that obtained working on high-pressurized conventional hydrogenation, using polar solvents such as 2-propanol (20 up to 70-90% of side products) [36-38]. Note also that in case of catalysts Pt/C-3 and Pt/C-4, selectivity to side compounds was below 35%, which is three times lower that the

corresponding from conventional catalysis in a similar media. Therefore, the high basic behaviour of these two catalyst may prevent from the hydrogenation to undesired compounds.

With respect to CMO selectivity, results showed a different sequence: Pt/C-1 < Pt/C-C ≈ Pt/C-2 < Pt/C-3 ≈ Pt/C-4. In this case, there was not a straightforward explanation about the differences observed. According to the literature, Pt/C-C was not expected to be selective to CMO because of the low metal particle size. In this regard, Gallezot *et al.* [39] reported that larger faceted metal particles are more selective to CMO, because of the steric constrains experienced by the CMA molecule when it adsorbs on them, which favored the hydrogenation of the C=O bond. This fact was corroborated elsewhere [35, 40, 41]. However, Pt/C-1, which showed the biggest Pt particles, did not produce any CMO. In this case, it could be explained considering two variables: on the one hand, the low value of ECSA, which revealed the lack of available active surface and the electrical isolation of the metal particles from each other [30]. On the other hand, this catalyst showed the lowest basic character, which was also reported to affect the catalyst selectivity, as explained hereafter.

Comparison between CMO selectivity and HCl titration results revealed that, the higher the basicity of the catalyst, the higher the selectivity to this product. Handjani *et al.* [17] reported that higher selectivity to CMO has been reported on particles whose surface was enriched in electrons, most often on basic supports. In line with this explanation, Wang *et al.* [42] claimed that alkali promoters could change the adsorption mode of CMA, by reducing or suppressing the adsorption of the C=C bond by electrolytic repulsion of the phenyl ring.

Finally, the yield to CMO revealed that Pt/C-4 was the most active catalyst for the electrocatalytic hydrogenation of CMA to this product, followed by Pt/C-3 and Pt/C-C, despite of the higher conversion of the latter one. It is important to note that, despite showing better properties (higher metal dispersion and ECSA, less deactivation), Pt/C-4 electrocatalytic performance was slightly higher than that of Pt/C-3, so that the improvement related to the addition of the metal precursor dropwise did not mean a significant effect on the catalytic performance.

4. CONCLUSIONS

Considering the results above explained, the following conclusions were reached:

- Pt/C catalysts were successfully synthesized by one-pot impregnation-reduction method and used in the electrocatalytic hydrogenation of CMA.
- The improvements on the synthesis procedure (evaporation under vacuum, additional washing step and inclusion of the Pt salt precursor dropwise) noticeably affected the Pt particle size and therefore, the dispersion on the support.
- The evaporation procedure under vacuum and the inclusion of a washing step prevented the catalyst from losing of basic sites. In this sense, the addition of the salt precursor dropwise did not show a notorious effect.
- Pt/C-2 and Pt/C-4 exhibited the highest electrochemical surface area (ECSA), whereas Pt/C-C showed the lowest electrochemical deactivation degree.
- Pt/C-2 was the most active catalyst for the undesired HER/HOR reaction, whereas Pt/C-3 was the least active one.

- The metal particle size and the catalyst basicity were the properties that affected the electrocatalytic hydrogenation of CMA the most. In this regard, Pt/C-3 and Pt/C-4, which exhibited the highest basic character, were the most active catalysts for the production of CMO.
- Pt/C-4 was the most active of the synthetized catalyst for the production of CMO via electrocatalytic hydrogenation of CMA, followed by Pt/C-3 and Pt/C-C.

REFERENCES

1. Joseph Antony Raj, K., et al., *Selective Hydrogenation of Cinnamaldehyde over Cobalt Supported on Alumina, Silica and Titania.* Catalysis Letters, 2012. **142**(1): p. 87-94.
2. He, S., et al., *Chemoselective hydrogenation of α,β-unsaturated aldehydes on hydrogenated MoOx nanorods supported iridium nanoparticles.* Journal of Molecular Catalysis A: Chemical, 2016. **425**: p. 248-254.
3. Wei, S., et al., *Structure-dependent selective hydrogenation of cinnamaldehyde over high-surface-area CeO2-ZrO2 composites supported Pt nanoparticles.* Chemical Engineering Journal, 2017. **322**: p. 234-245.
4. Zheng, Q., et al., *An Effective Co-promoted Platinum of Co–Pt/SBA-15 Catalyst for Selective Hydrogenation of Cinnamaldehyde to Cinnamyl Alcohol.* Catalysis Letters, 2016. **146**(8): p. 1535-1543.
5. Piqueras, C.M., et al., *Selective hydrogenation of cinnamaldehyde in supercritical CO2 over Me–CeO2 (Me = Cu, Pt, Au): Insight of the role of Me–Ce interaction.* Applied Catalysis B: Environmental, 2016. **185**: p. 265-271.
6. Guo, Z., et al., *Pt Nanoclusters Confined within Metal–Organic Framework Cavities for Chemoselective Cinnamaldehyde Hydrogenation.* ACS Catalysis, 2014. **4**(5): p. 1340-1348.
7. Shirai, M., T. Tanaka, and M. Arai, *Selective hydrogenation of α-, β-unsaturated aldehyde to unsaturated alcohol with supported platinum catalysts at high pressures of hydrogen.* Journal of Molecular Catalysis A: Chemical, 2001. **168**(1): p. 99-103.
8. Roberge, D.M., et al., *Microreactor Technology: A Revolution for the Fine Chemical and Pharmaceutical Industries?* Chemical Engineering & Technology, 2005. **28**(3): p. 318-323.
9. Sáez, A., et al., *Electrocatalytic hydrogenation of acetophenone using a Polymer Electrolyte Membrane Electrochemical Reactor.* Electrochimica Acta, 2013. **91**: p. 69-74.
10. Huang, B., et al., *Highly selective electrochemical hydrogenation of acetylene to ethylene at Ag and Cu cathodes.* Electrochemistry Communications, 2013. **34**: p. 90-93.
11. Otsuka, K. and T. Yagi, *An Electrochemical Membrane Reactor for Selective Hydrogenation of Acetylene in Abundant Ethylene.* Journal of Catalysis, 1994. **145**(2): p. 289-294.

12. Villalba, M., M. del Pozo, and E.J. Calvo, *Electrocatalytic hydrogenation of acetophenone and benzophenone using palladium electrodes.* Electrochimica Acta, 2015. **164**: p. 125-131.
13. zhao, B., et al., *Electrocatalytic hydrogenation of furfural to furfuryl alcohol using platinum supported on activated carbon fibers.* Electrochimica Acta, 2014. **135**: p. 139-146.
14. Cantu, D.C., et al., *A Combined Experimental and Theoretical Study on the Activity and Selectivity of the Electrocatalytic Hydrogenation of Aldehydes.* ACS Catalysis, 2018. **8**(8): p. 7645-7658.
15. Kwon, Y., et al., *Electrocatalytic Conversion of Furanic Compounds.* ACS Catalysis, 2016. **6**(10): p. 6704-6717.
16. Mahdavi, B., et al., *Electrocatalytic hydrogenation of conjugated enones on nickel boride, nickel, and Raney nickel electrodes.* Canadian Journal of Chemistry, 1995. **73**(6): p. 846-852.
17. Handjani, S., et al., *Influence of the support composition and acidity on the catalytic properties of mesoporous SBA-15, Al-SBA-15, and Al2O3-supported Pt catalysts for cinnamaldehyde hydrogenation.* Journal of Catalysis, 2011. **282**(1): p. 228-236.
18. Bhanuchander, P., et al., *Direct Hydrogenolysis of Glycerol to Biopropanols over Metal Phosphate Supported Platinum Catalysts.* Catalysis Letters, 2017. **147**(4): p. 845-855.
19. Oberhauser, W., et al., *Platinum nanoparticles onto pegylated poly(lactic acid) stereocomplex for highly selective hydrogenation of aromatic nitrocompounds to anilines.* Applied Catalysis A: General, 2017. **537**: p. 50-58.
20. Kronawitter, C.X., et al., *Electrocatalytic hydrogenation of pyridinium enabled by surface proton transfer reactions.* Catalysis Science & Technology, 2017. **7**(4): p. 831-837.
21. Singh, N., et al., *Electrocatalytic Hydrogenation of Phenol over Platinum and Rhodium: Unexpected Temperature Effects Resolved.* ACS Catalysis, 2016. **6**(11): p. 7466-7470.
22. Han, X., et al., *Hydrogenated Uniform Pt Clusters Supported on Porous CaMnO3 as a Bifunctional Electrocatalyst for Enhanced Oxygen Reduction and Evolution.* Advanced Materials, 2014. **26**(13): p. 2047-2051.
23. Lázaro, M.J., et al., *Study and application of carbon black vulcan XC-72R in polymeric electrolyte fuel cells*, in *Carbon Black: Production, Properties and Uses*. 2011. p. 41-68.

24. Lobato, J., et al., *Composite Titanium Silicon Carbide as a Promising Catalyst Support for High-Temperature Proton-Exchange Membrane Fuel Cell Electrodes.* ChemCatChem, 2016. **8**(4): p. 848-854.
25. Corrales-Sánchez, T., J. Ampurdanés, and A. Urakawa, *MoS2-based materials as alternative cathode catalyst for PEM electrolysis.* International Journal of Hydrogen Energy, 2014. **39**(35): p. 20837-20843.
26. Sing, K.S.W., et al., *Reporting Physisorption Data for Gas/Solid Systems*, in *Handbook of Heterogeneous Catalysis*. 2008, Wiley-VCH Verlag GmbH & Co. KGaA.
27. Pastor-Pérez, L. and A. Sepúlveda-Escribano, *Low temperature glycerol steam reforming on bimetallic PtSn/C catalysts: On the effect of the Sn content.* Fuel, 2017. **194**: p. 222-228.
28. Wang, K.W. and C.T. Yeh, *Temperature-programmed reduction study on carbon-supported platinum-gold alloy catalysts.* Journal of Colloid and Interface Science, 2008. **325**(1): p. 203-206.
29. Díaz, J.A., et al., *Carbon nanofibers and nanospheres-supported bimetallic (Co and Fe) catalysts for the Fischer–Tropsch synthesis.* Fuel Processing Technology, 2015. **138**: p. 455-462.
30. Perez, J., V.A. Paganin, and E. Antolini, *Particle size effect for ethanol electro-oxidation on Pt/C catalysts in half-cell and in a single direct ethanol fuel cell.* Journal of Electroanalytical Chemistry, 2011. **654**(1–2): p. 108-115.
31. Dabo, P., et al., *Selective electrocatalytic hydrogenation of 2-cyclohexen-1-one to cyclohexanone.* Electrochimica Acta, 1997. **42**(9): p. 1457-1459.
32. Durst, J., et al., *Hydrogen oxidation and evolution reaction kinetics on carbon supported Pt, Ir, Rh, and Pd electrocatalysts in acidic media.* Journal of the Electrochemical Society, 2015. **162**(1): p. F190-F203.
33. Kadakia, K.S., et al., *Nanostructured F doped IrO2 electro-catalyst powders for PEM based water electrolysis.* Journal of Power Sources, 2014. **269**: p. 855-865.
34. Tian, Z., et al., *Nitrogen- and oxygen-functionalized carbon nanotubes supported Pt-based catalyst for the selective hydrogenation of cinnamaldehyde.* Applied Catalysis A: General, 2015. **506**: p. 134-142.
35. Durndell, L.J., et al., *Selectivity control in Pt-catalyzed cinnamaldehyde hydrogenation.* Scientific Reports, 2015. **5**.
36. Leng, F., et al., *Selectivity shifts in hydrogenation of cinnamaldehyde on electron-deficient ruthenium nanoparticles.* Comptes Rendus Chimie, 2018. **21**(3): p. 346-353.

37. Li, Y., et al., *Influence of Preparation Modes on Pt–Ni/CNTs Catalysts Used in the Selective Hydrogenation of Cinnamaldehyde to Hydrocinnamaldehyde.* Catalysis Letters, 2008. **126**(3): p. 280-285.
38. Wang, D. and Y. Zhu, *An Effective Pt-Cu/SiO2 Catalyst for the Selective Hydrogenation of Cinnamaldehyde.* Journal of Chemistry, 2018. **2018**: p. 7.
39. Gallezot, P., A. Giroir-Fendler, and D. Richard, *Chemioselectivity in cinnamaldehyde hydrogenation induced by shape selectivity effects in Pt-Y zeolite catalysts.* Catalysis Letters, 1990. **5**(2): p. 169-174.
40. Prashar, A.K., S. Mayadevi, and R. Nandini Devi, *Effect of particle size on selective hydrogenation of cinnamaldehyde by Pt encapsulated in mesoporous silica.* Catalysis Communications, 2012. **28**: p. 42-46.
41. Oduro, W.O., et al., *Geometric and electronic effects on hydrogenation of cinnamaldehyde over unsupported Pt-based nanocrystals.* Physical Chemistry Chemical Physics, 2011. **13**(7): p. 2590-2602.
42. Wang, Y., et al., *Highly Active Supported Pt Nanocatalysts Synthesized by Alcohol Reduction towards Hydrogenation of Cinnamaldehyde: Synergy of Metal Valence and Hydroxyl Groups.* Chemistry – An Asian Journal, 2015. **10**(7): p. 1561-1570.

Chapter 3: Pt/C catalysts for the electrocatalytic Hydrogenation of Cinnamaldehyde: Influence of the reducing agent

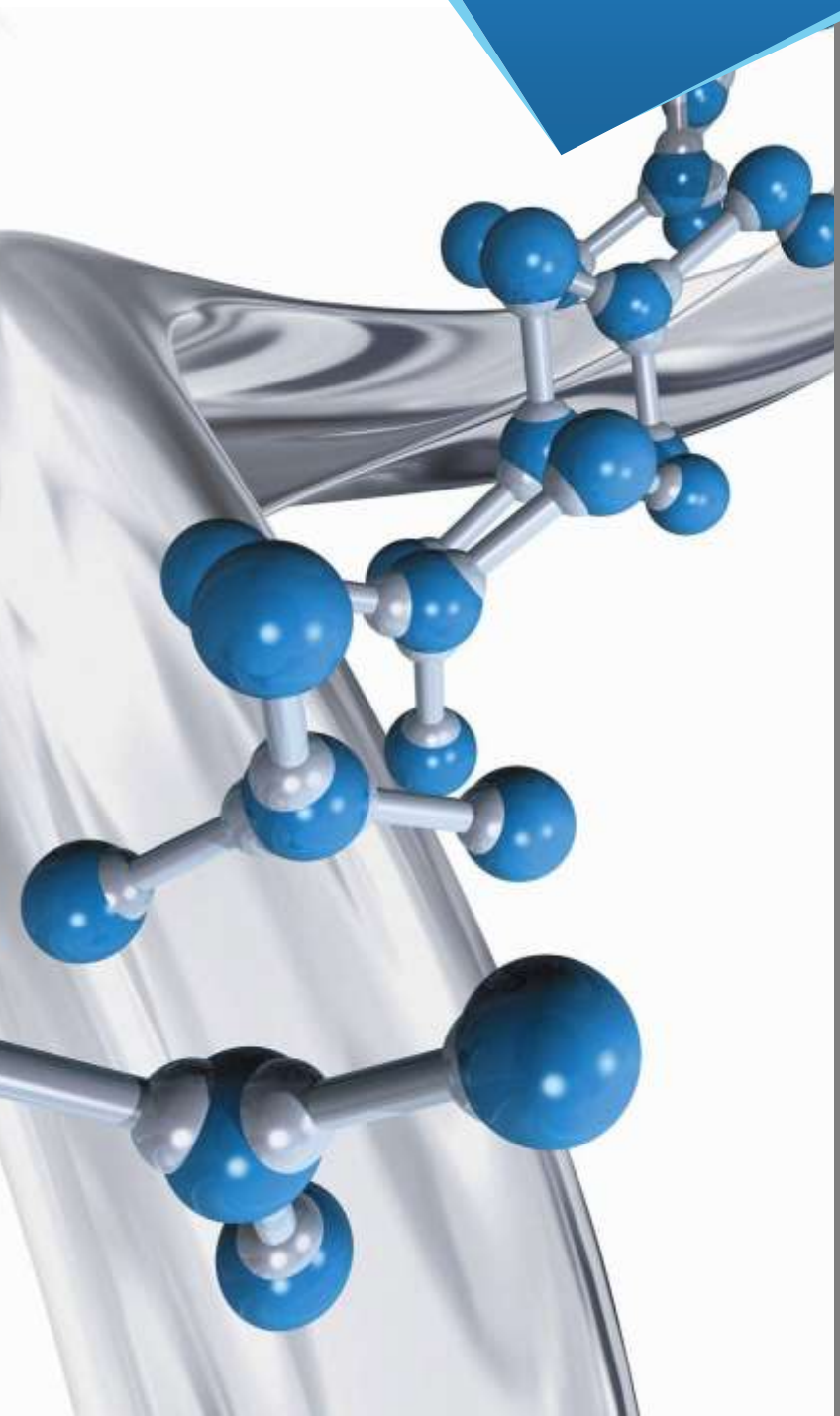

1. INTRODUCTION

2. EXPERIMENTAL
2.1. Synthesis of Pt/C-R cathodic catalysts
2.2. Physicochemical characterization
2.3. Electrochemical characterization
2.4. Membrane electrode assembly (MEA) preparation
2.5. Electrocatalytic hydrogenation tests

3. RESULTS AND DISCUSSION
3.1 Physicochemical characterization
3.2. Electrochemical characterization
3.3. Electrocatalytic hydrogenation of CMA in a PEM cell

4. CONCLUSIONS

Abstract

In this work, carbon-supported platinum catalysts were synthesized using different reducing agents. 20 wt.% Pt loading catalyst were tested in a PEM reactor for the electrocatalytic hydrogenation of cinnamaldehyde (CMA), with the aim to maximize the production of cinnamyl alcohol (CMO). Physicochemical characterization was carried out by N_2 adsorption-desorption, TPR, XRD, H_2 pulse chemisorption and acid-base titrations. Electrochemical characterization was performed by means of cyclic voltammetry and kinetic studies of the hydrogen evolution reaction (HER/HOR). Results revealed that catalyst synthetized by the modified polyol method showed a good compromise in terms of CMA conversion and selectivity due to suitable Pt dispersion, basic character and electrochemical surface area.

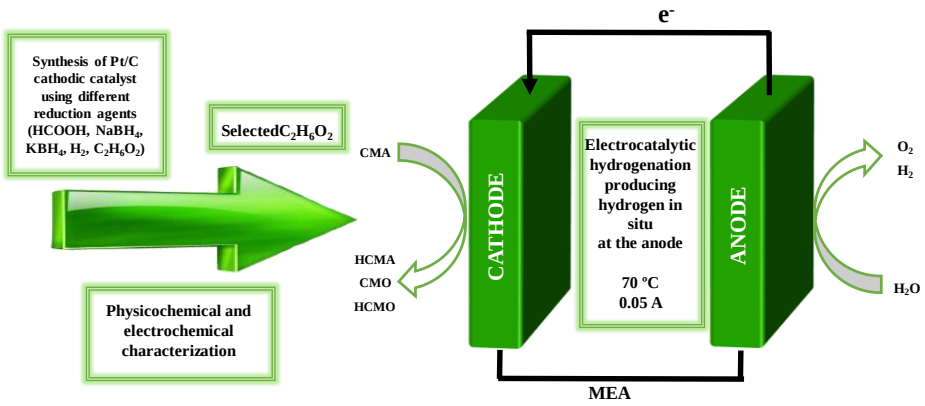

Figure 3.1. *Graphical abstract Chapter 3.*

1. INTRODUCTION

Selective electrocatalytic hydrogenation of organic molecules has gained interest in the recent years as an alternative route to produce added-value chemicals, which are usually employed in food, fragrance and pharmaceutical industries [1]. The electrocatalytic route has several advantages respect to the conventional one, such as the possibility to operate in continuous at mild conditions (atmospheric pressure and low temperature), easy scale-up and *in situ* generation of the hydrogen source (H^+) in the anode *via* H_2O electrolysis [2]. In this regard, electrocatalytic hydrogenation of acetylene [3, 4], acetophenone [5, 6] or more recently cinnamaldehyde have been studied [7].

The selective hydrogenation of cinnamaldehyde (CMA) aims the synthesis of cinnamyl alcohol (CMO), which is attained by the hydrogenation of the C=O bond. However, the hydrogenation of the C=C bond, which lead to hydrocinnamaldehyde (HCMA), is thermodynamically favorable, so that the search of selective catalysts that are prone to hydrogenate the C=O bond is still a challenge [8, 9]. Indeed, the catalytic properties such as the crystallite size of the active phase, the metal-support interaction or the surface acidity have been reported to have a strong influence on both CMA conversion and CMO selectivity [10]. Therefore, special attention should be paid to the catalyst synthesis method.

One-pot impregnation-reduction method has gained a great interest to synthesize supported catalysts. Classical methods, such as impregnation or deposition-precipitation, usually require a further reduction step carried out under high-temperature H_2 atmosphere. However, one-pot impregnation-reduction method is carried out using chemicals such as sodium borohydride [11], formic acid [12] or ethylene

glycol [13], which are applied during the synthesis procedure at relative low temperatures (60-170 °C).

The most popular reducing agent is sodium borohydride ($NaBH_4$), which is a non-toxic, strong reducing agent that perform properly even at room temperature [11]. Among the most recent literature reported the use of NaB, López-Suárez *et al.* [14] synthesized Pt-Sn/C catalysts for alcohol oxidation in fuel cells, whereas Calderón *et al.* [15] using different dendrimers to synthesize Pt-Ru nanoparticles supported on carbon nanofibers, and then applied them in the oxidation of methanol. Potassium borohydride (KBH_4) also exhibits interesting properties as a reducing agent, but it has been demonstrated to be less active than NaB. Hajek *et al.* [16] prepared Ru-Sn catalysts using these reducing agents, and concluded that prepared by KB showed less Ru active surface. This difference affected the activity of these catalysts in the selective hydrogenation of CMA, as the NaB-reduced catalyst show higher CMA conversion and CMO selectivity.

Formic acid (FA) has been demonstrated to be a promising reducing agent as well. It has been reported to disperse Pt nanoparticles better than NaB, which had a strong influence on the catalytic activity in the oxygen reduction reaction [17]. On the other hand, Lobato *et al.* [12] synthesize Ti-SiC-supported Pt catalysts using FA as reducing agent, and tested them in high-temperature proton-exchange membrane (PEM) fuel cells. Finally, the use of ethylene glycol ($C_2H_6O_2$) (EG) as reducing agent of catalyst has increased sharply since Bock *et al.* [18] reported the synthesis of Pt-Ru nanoparticles using this agent for the first time. EG is an alcohol that can be readily oxidized to the corresponding aldehydes and carboxylic acids, being the electrons donated used in the reduction of the corresponding metals. Later, Baranova *et al.* [19] synthesized Pt-Ru nanoparticles of average diameter up to 1.4 nm by EG reduction method,

and developed a computational approach to calculate the average crystallite size by X-ray diffraction. Recently, Barthi *et al.* [11] synthesize Pt/CNT catalysts for PEM fuel cells using a mixture of NaB and EG as reducing agents, which combined the stronger reduction ability of NaB and good dispersion attained when using EG.

In the present work, the species listed above were used to synthesize carbon Vulcan (XC-72)-supported Pt catalysts (Pt/C) by one-pot impregnation-reduction method. Moreover, another Pt/C catalyst was prepared by classical impregnation method for comparison purposes. All samples were characterized and tested in the electrocatalytic hydrogenation of CMA in a PEM cell. The aim is therfore to analyze the influence of the reducing agent on the catalyst properties, and subsequently, CMA conversion and selectivity to the desired compounds.

2. EXPERIMENTAL

2.1. Synthesis of Pt/C-R cathodic catalysts

Five carbon-supported Pt electrocatalysts have been synthesized by different methods in order to study the influence of the nature of the reducing agent and in situ reduction conditions on the physicochemical and electrochemical properties of the cathode used for the electrocatalytic hydrogenation of cinnamaldehyde. IrO_2 (99 wt.%, purchased from Alfa Aesar) served as standard electrocatalyst for the anode in this study.

Equivalent Pt/C-R (where R is the reducing agent) catalysts, with metal loading of 20 wt. % were prepared. In all cases, H_2PtCl_{6-x} H_2O (99.9%, Sigma-Aldrich) and carbon Vulcan XC-72 (FuelCell Store, United States) were used as metal precursor and catalyst support, respectively.

Catalyst Pt/C-NaB was prepared based in the procedure described by Zheng *et al.* [9] (Section B.2.1.)

Pt/C-FA, was prepared using HCOOH (98%, Panreac, Spain) as reducing agent by the procedure of Lobato *et al*. [12] as described in Section B.2.2.

Catalyst Pt/C-EG was synthetized using the modified polyol method described by Baranova et al [13] (Section B.2.3.)

Pt/C-KB was prepared by the same procedure used for Pt/C-NaB, but using KBH_4 (99.9 % Sigma Aldrich, Germany) as reducing agent.

A last catalyst, Pt/C-IM, was prepared by common wetness impregnation [20] as described in Section B.2.4.

2.2. Physicochemical characterization

XRD analyses were performed on a Phillips PW-1700 diffractometer using nickel-filtered Cu Kα radiation. H_2 pulse chemisorption and Temperature Programmed Reduction (TPR) measurements were conducted in a commercial Micromeritics AutoChem 2950 HP unit with TCD detection. Surface area/porosity measurements were analyzed in a Micromeritics ASAP 2010 sorptometer unit, using N_2 at 77 K as the adsorbate. And finally, HCl titrations were performed on a SCHOTT Titroline with automatic dosager. All the physicochemical characterization techniques were described in more detail in Section B.4.

2.3. Electrochemical characterization

Electrochemical characterization was carried out in a computer-controlled potentiostat Autolab PGSTAT128N (Ecochemie, The Netherlands), using a standard three-electrode electrochemical cell. A polished 0.196 cm^2 Glassy Carbon Rotating Disk Electrode (GC-RDE, Metrohm Autolab) was used as the working electrode, a platinum wire (Metrohm) as the counter electrode and Ag/AgCl (Metrohm) as the reference electrode. A solution of $HClO_4$ 0.1 M (Scharlau) was used as electrolyte. Note that prior to each electrochemical measurement, the surface of the working electrode was polished with an aluminum oxide slurry (grain size 0.3 μm).

Activity of the Pt/C-X electrocatalysts was determined through the Cyclic Voltammetry technique (CV) as described in Section B.5.1.

In order to study the kinetics of the Hydrogen Evolution Reaction (HER/HOR), polarization curves were performed as described in Section B.5.2.

2.4. Membrane electrode assembly (MEA) preparation

Membrane electrode assembly (MEA) was prepared by spraying (with a common airbrush (Sogolee)) an ink containing the electrocatalyst and Nafion ionomer in water for the anode and 2-propanol for the cathode directly to the Nafion membrane according to the procedure described in Section B.3. 2 $mg \cdot cm^{-2}$ commercial IrO_2 was used as anode while synthesized Pt/C-R samples were used as cathode in the electrochemical PEM cell with 0.5 $mg \cdot cm^{-2}$ loading.

2.5. Electrocatalytic Hydrogenation Tests

Electrochemical hydrogenation experiments were carried out using a PEM cell as that illustrated in Figure 3.2., described in more detail in Section B.7.2. All experiments were subjected to reproducibility analyses. Electrochemical hydrogenation products were analyzed offline in an Agilent 7820A gas chromatograph, equipped with a FID detector and a capillary column (Agilent DB-624, 30 m x 0.25 mm x 0.5 μm), using helium as a carrier gas. CMA conversion, product selectivity and turnover frequency were calculated as described in Section B.6.

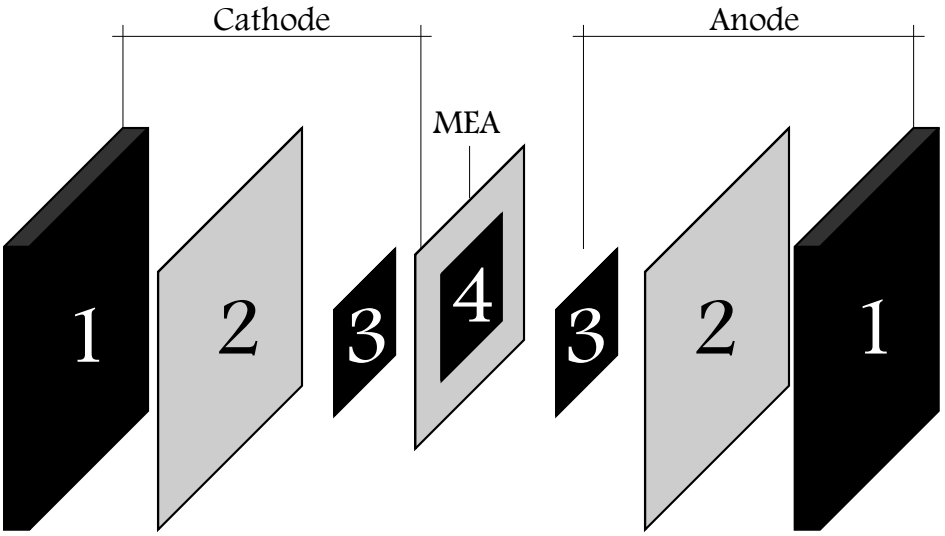

Figure 3.2. Scheme of the PEM cell prepared.
1. Bipolar Plates, 2. Gaskets, 3. Gas Diffusion Layer, 4. MEA

3. RESULTS AND DISCUSSION

3.1. Physicochemical characterization

Figure 3.3. displays the crystalline structures of the carbon Vulcan XC-72 support and those of the as-prepared cathodic catalysts analyzed by X-ray diffraction. Two low-index diffraction peaks around 2θ: 25 and 43° can be observed in the support sample, which correspond to the (002) and (100) planes of carbon, characteristic of graphite, confirming

the intermediate structure between amorphous and slightly graphitic of Vulcan XC-72. Apart from reflections related to the carbonaceous support, electrocatalysts exhibited diffraction peaks at 40, 47, 68, 82 and 87°, which are ascribed to the (111), (200), (220), (311) and (222). These planes are characteristic of the face-centered cubic structure of platinum (JCPDS: 87-0647), indicating the effective reduction of Pt precursor.

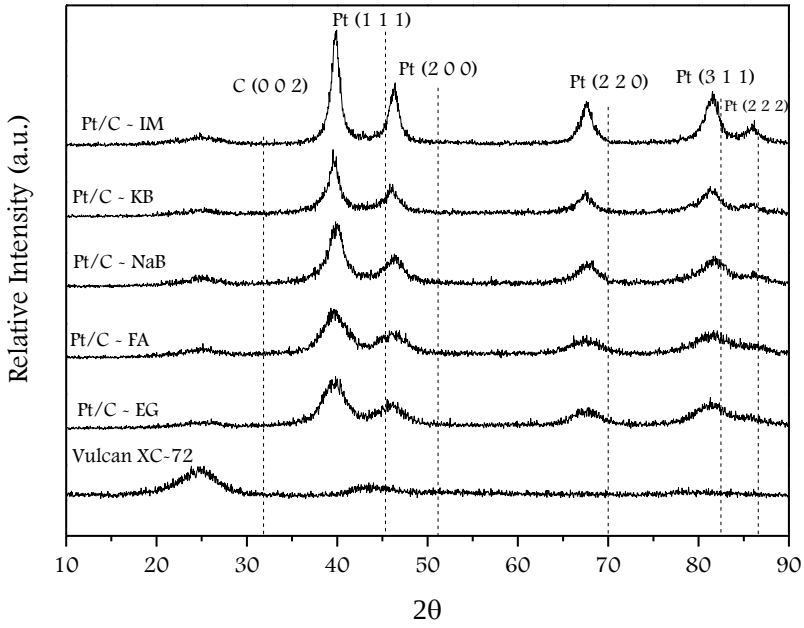

Figure 3.3. *XRD patterns of the synthesized Pt/C catalysts and the support.*

Pt (111) crystal facets exhibited the highest intensity in the diffractogram, suggesting high densities of (1 1 1)-orientated crystals. However, depending on the synthesis procedure differences on the intensity and width of these peaks can be observed, which are associated to changes of the Pt crystallite size: the wider the peak, the smaller the Pt crystallite. The average Pt crystallite size was calculated by the Debye-Scherrer's equation using the (220) peak of the Pt fcc structure since (111) and (200) Pt reflections overlapped with those from carbon

support. Results summarized in Table 3.1. revealed that Pt/C-IM shows the largest Pt crystals, followed by Pt/C-KB, Pt/C-NaB, Pt/C-EG and finally, Pt/C-FA, which presents the smallest Pt crystallite size. According to the literature, the size and morphology of metal particles supported on carbon materials depend on the metal-carbon interaction [21-23]. Therefore, the synthesis method (mainly the reducing agent nature) has an important influence on the Pt crystallite size, which is expected to modify active surface area and, as a consequence, the electrocatalytic conversion.

This technique provided information about the metal dispersion, active metal particle size and chemical surface area (CSA) of the catalysts under study.

Table 3.1. Main physicochemical properties of the catalysts

Sample	XRD Particle size (nm)[1]	BET specific surface area ($m^2 \cdot g^{-1}$)	Total pore volume ($cm^3 \cdot g^{-1}$)	Average pore diameter (nm)[2]
Pt/C-NaB	10	159	0.486	12.4
Pt/C-FA	5	202	0.367	7.8
Pt/C-EG	5	100	0.447	17.7
Pt/C-KB	10	176	0.616	14.3
Pt/C-IM	14	156	0.554	14.9

	Dispersion (%)[3]	Active particle size (nm)[3]	CSA ($m^2 \cdot g^{-1}$)[3]
Pt/C-NaB	35.4	3.2	87
Pt/C-FA	27.5	4.1	68
Pt/C-EG	13.1	8.6	32
Pt/C-KB	57.7	1.96	143
Pt/C-IM	11.9	9.5	29

From data listed in Table 3.1 it can be observed that catalyst Pt/C-IM showed the lowest dispersion value and chemical surface area suggesting that one-pot reduction methods favor the formation of smaller Pt particles and enhance dispersion. Within the catalysts synthetized by one-pot procedure, Pt/C-EG and Pt/C-FA showed lower

dispersion than those of Pt/C-NaB and Pt/C-KB. As reported before, the presence of a certain amount of alkali compounds may result in an enhancement of dispersion values [24]. In agreement, Pt/C-KB catalyst presents the highest dispersion value and CSA.

The textural parameters (surface area and porosity) of Pt/C-R electrocatalysts were evaluated by N_2 adsorption-desorption measurements. Vulcan XC-72 was also analyzed in order to determine the contribution of the support. Table 3.1. shows the main physicochemical properties of the support and Pt/C-R samples while isotherms are presented in Figure 3.4.

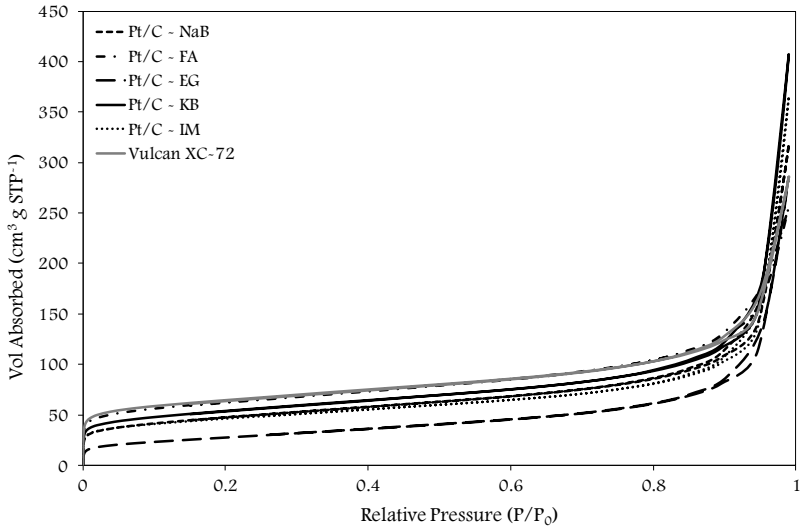

Figure 3.4. *Nitrogen adsorption desorption isotherms of the catalysts studied.*

It can be observed that all isotherms showed a type I-IV adsorption-desorption profile, according to the IUPAC classification. It is associated to the presence of microporous solids having relatively small external surfaces. Firstly, the N_2 adsorption volume increased sharply in the micropore region at very low partial pressures ($P/P_0 < 0.005$). Then, there was a slight increase of N_2 at higher partial pressures, which could

be attributed to the presence of mesopores in the sample. This fact was corroborated with the hysteresis loop observed in the multilayer range of physisorption isotherms, which is ascribed to the capillary condensation that takes place on mesopores and associated with their filling and emptying [25, 26]. From data recorded in Table 3.1., it was observed that once the metal precursor was deposited into the support, the parent BET surface area (231± 1 $m^2 \cdot g^{-1}$) experienced an important decrease. This fact could be attributed to a pore blockage by the metal particles, which prevent from the adsorption of N_2 molecules. In agreement with results from XRD analysis, Pt/C-FA catalyst showed the lowest reduction of specific surface area associated with the deposition of the smallest Pt cristallites. It was also observed that the average pore diameter and pore volume of Pt/C-R catalysts, except for Pt/C-FA, were higher than those of the support (7.7 nm and 0.403 $cm^3 \cdot g^{-1}$, respectively), which suggested that Pt particles were mainly deposited on the micropores.

In order to verify if Pt particles were properly reduced during the catalyst synthesis, TPR analysis were performed. Figure 3.5. showed the TPR profiles of the catalysts used as cathode in this work. Vulcan XC-72 was also analyzed as a background material to discriminate the contribution of the support from the profile. The support profile was observed to present only a H_2 consumption peak at temperatures above 650°C, which can be attributed to the decomposition of the support (CO desorption, CH_4 formation). According to the available literature, for Pt-based catalysts, two distinct phases are usually observed: Pt^{4+} (as PtO_2) as a highly-active phase with reduction to PtO occurring below 0 °C and Pt^{2+} (as PtO) as the dominant phase with reduction to Pt occurring above 100 °C [27]. However, it is interesting to note that no consumption of hydrogen was observed at temperatures lower than 150°C for all the catalysts except for Pt/C-IM, suggesting the proper reduction to the

active phase by the different one-pot synthesis and reduction procedures. Pt-based catalyst synthetized by conventional impregnation showed a dominant peak of hydrogen consumption due to Pt reduction in the range of 130-230 °C [27, 28], which is in consonance with the requirement of an ex-situ reduction step prior to reaction.

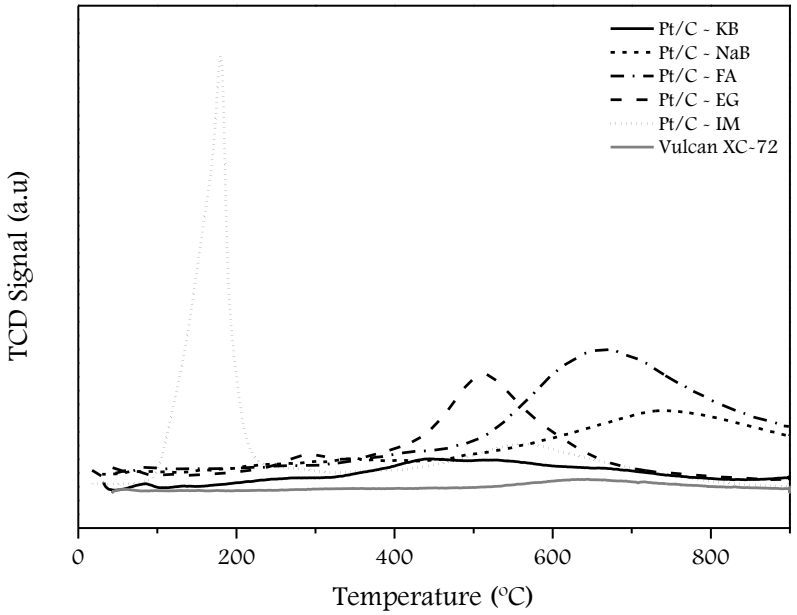

Figure 3.5. Temperature-programmed reduction (TPR) profiles of the synthesized Pt/C catalysts and the support.

Catalysts Pt/C-FA, Pt/C-EG, Pt/C-NaB, Pt/C-KB did not display any appreciable reduction peaks below 350 °C: a shoulder at 360-380 °C (attributed to the reduction of platinum metal complex deposited on the surface of the carbonaceous support and no located near metal particles) and another peak at high temperatures (between 500 and 900 °C). However, all samples showed hydrogen consumption peaks at high temperatures (>500 °C) in the range 600-700 °C, that can be explained by the gasification of the carbonaceous support [29-32], which was catalyzed by the Pt particles and could be possibly displaced to lower temperatures due to the platinum spillover effect [33].

The acid-base character of the support (Vulcan XC-72) and the synthetized Pt/C-R catalysts was evaluated by HCl titrations. It can be observed from curves depicted in Figure 3.6 that all samples exhibited basic character since more volume of HCl than that of blank solution was required to reach the equivalence point.

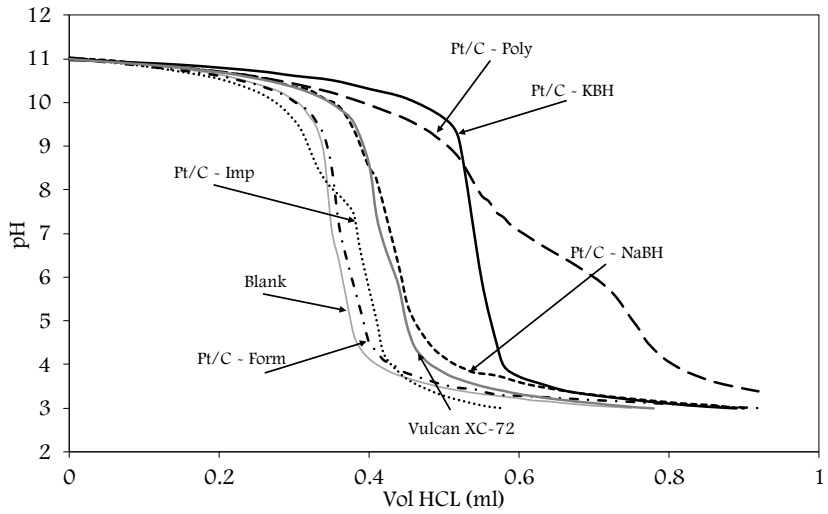

Figure 3.6. HCl titration curves.

However, basic character is found to depend on the reducing agent. Pt/C-IM and Pt/C-FA curves were shifted towards the corresponding blank one, which revealed a partial neutralization of the basicity of the support. The basic character increased in the following order: Pt/C-FA < Pt/C-IM < Pt/C-NaB ≤ Pt/C-KB < Pt/C-EG. Therefore, catalyst reduction with alkali agents seem to prevent the catalyst from losing basic sites, which is even more noticeable in the case of KBH_4. On the other hand, the use of NaOH in the polyol method provided basic character to the Pt/C-EG sample being responsible for the slight difference of this catalyst compared to Pt/C-KB.

3.2. Electrochemical characterization

The effect of the different one-pot synthesis methods (nature of the reducing agent) on the electrochemical activity of Pt/Vulcan catalysts has been explored by cyclic voltammetry (CV) and linear sweep voltammetry (LSV) tests.

Sequential cyclic voltammetry tests in perchloric acid media (0.1 M) were carried out in order to measure the electrochemical surface area and the the degree of deactivation of the as-prepared electrodes. Figure 3.7. shows the cyclic voltammograms of the samples between 0.05 and 1.4 V vs RHE at a scan rate of 50 mV s^{-1}. The cathodic scan exhibits platinum reduction peaks between 0.5 and 1.0 V vs RHE, whereas hydrogen was desorbed at potential below 0.4 V vs RHE. On the other hand, Pt/C-NaB, Pt/C-FA, Pt/C-IM and Pt/C-KB samples showed various peaks in the anodic scan (0-0.25 V vs RHE) that can be ascribed to the electro-oxidation of Pt-H_{ads} to H^+. The different morphology of the peaks revealed differences in the faces of the platinum monocrystals for each catalyst [12, 34].

During consecutive potential cycling, both the anodic and cathodic number of cycles increased, the adsorption/desorption peaks above mentioned (see Figure 3.7.) decreased, which revealed a loss of electrochemical surface area as a result of the dissolution of small amounts of Pt from the electrode surface in the case of smooth and finely divided Pt catalyst, where Pt appears to be trapped in electrode structure pores and is finally redeposited on the metal crystallites at low potentials resulting in crystallite growth of the [35].

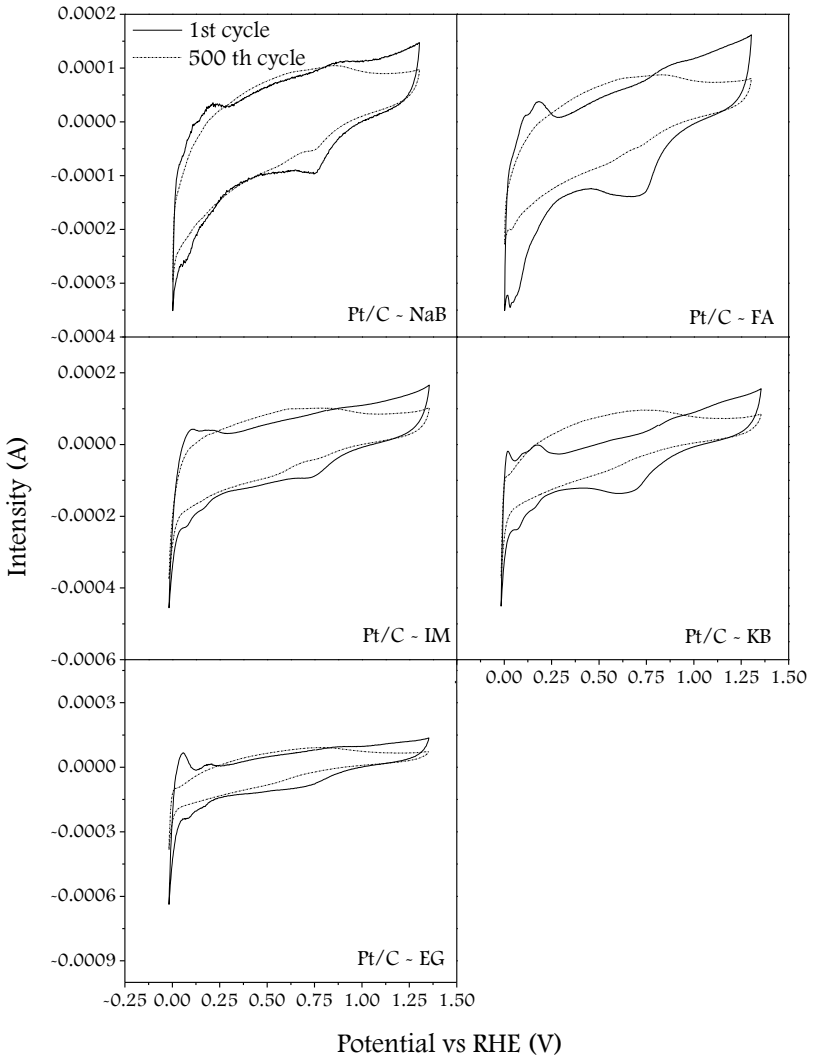

Figure 3.7. Cyclic voltammograms of Pt/C catalysts in 0.1 $HClO_4$, with a scan rate of 50 mV s^{-1} at 25 °C.

This loss was quantified by comparing the electrochemical surface area (ECSA) between the cycles 1 and 500. Table 3.2 lists de ECSA of the samples at cycles 1 and 500, as well as the deactivation percentage of each sample. After 500 cycles, all samples experienced a decrease of ECSA values due to degradation, which causes losses on the fraction of platinum that is available to participate in electrode reactions. The lowest electrochemical active area of the Pt/C-IM is consistent with the poor

dispersion of Pt particles on this catalyst revealed by physicochemical characterization. However, according to deactivation values, Pt/C-IM was the most stable catalyst despite of its low initial ECSA, followed by Pt/C-NaB, Pt/C-EG, Pt/C-FA and finally Pt/C-KB. Taking into account these results, it can be concluded that the reducing agent plays an important role in the electrocatalytic properties. Is important to note that there is a difference between the chemical (measured by H_2 pulse chemisorption) and electrochemical surface area. This difference can be explained considering the fact that part of the Pt atoms were deposited inside the small pores of the support, being no accessible to reactants and therefore not electrochemically active [36].

Table 3.2. ECSA values after 0 and 500 cycles and deactivation percentage of all the catalysts studied

Catalyst	ECSA 0 cycles ($m^2 \cdot g^{-1}$)	ECSA 0 cycles ($m^2 \cdot g^{-1}$)	Deactivation (%)	TOF (h^{-1})
Pt/C - NaB	46	30	35	1.3
Pt/C - FA	41	15	63.4	2.4
Pt/C - EG	30	14	53	4.6
Pt/C - KB	31	10	67.7	1.8
Pt/C - IM	15	11	26.7	5.2

Electrocatalytic hydrogenation of organic molecules and hydrogen evolution reaction (HER) are competitive reactions [5, 37]. So that in order to determine the HER contribution of each Pt/C-R cathode, HER/HOR catalytic reaction were studied by linear sweep voltammetry using a rotating disk electrode. Moreover, kinetics parameters of the HER/HOR reaction (i.e. kinetic rate constant 'k' and the number of electrons transferred 'n') were also obtained from the linearized Koutecky-Levich plot at 0.4 V (Figure 3.8.). It is important to note that HOR and HER occur simultaneously in both branches, although with different rates [37] so measured current was calculated as the sum of the anodic (HOR) and cathodic (HER) currents.

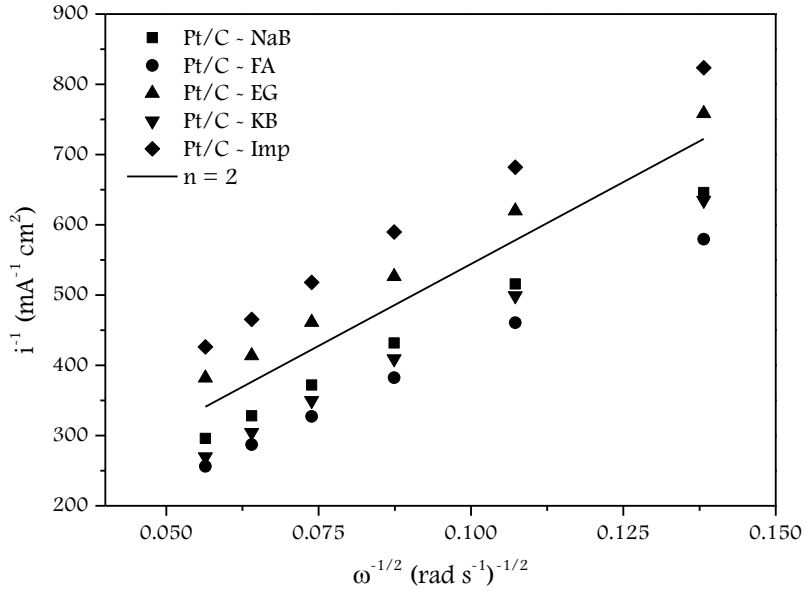

Figure 3.8. Koutecky – Levich plot in RDE at 0.4 V (vs RHE) in $HClO_4$ 0.1 M at 25 °C.

Table 3.3 shows the values of n and k of each catalyst. The catalyst Pt/C-KB and Pt/C-FA showed the highest k values whereas Pt/C-IM showed the lowest value which indicates that this catalyst would have less affinity for the HER reaction and hydrogen would be more available to participate in the hydrogenation reaction. Attending to n results, it is possible to conclude that, in all cases, the HER/HOR reaction follows the two electron mechanism.

Table 3.3. Number of electrons transferred in the HER/HOR reaction and kinetic rate constants determined from the Koutecky – Levich plots.

Catalyst	n	k (cm·s^{-1})
Pt/C - NaB	2.17	0.124
Pt/C- FA	2.36	0.182
Pt/C-EG	2.01	0.067
Pt/C-KB	2.09	0.377
Pt/C-IM	1.92	0.049

3.3. Electrocatalytic hydrogenation of CMA in PEM cell

Cinnamaldehyde has two distinct competing sites of hydrogenation resulting in CMO and HCMA from C=O and the conjugated C=C hydrogenation bonds, respectively. Further hydrogenation of both species produced hydrocinnamyl alcohol (HCMO). Principal reaction pathway is represented (in bold, Figure 3.9) along with undesired products originated from the irreversible acetalisation [38, 39].

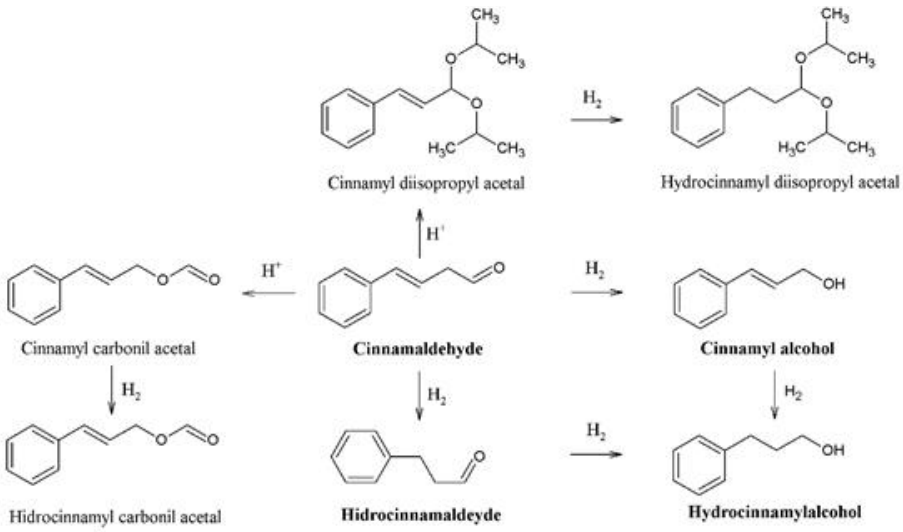

Figure 3.9. Main reaction pathways of the hydrogenation of cinnamaldehyde

Electrocatalytic results are listed in Figure 3.10. Reducing agent is shown to play an important role on the CMA electrochemical hydrogenation performance. Regarding conversion values, Pt/C-KB showed de highest value, following for Pt/C-FA < Pt/C -IM < Pt/C-EG < Pt/C-NaB. According to the dispersion results, Pt/C-KB catalyst, which shows much higher dispersion than the others, shows the higher conversion. On the other hand, the Pt/C-NaB conversion was not as high as expected considering its dispersion [24], probably due to the activity of the catalyst in HER/HOR reaction and to its basicity, which allows

higher selectivity to CMO at the expenses of a lower conversion. However, it should be mentioned that for catalysts with small particles it was difficult to find a clear trend as a function of dispersion [40].

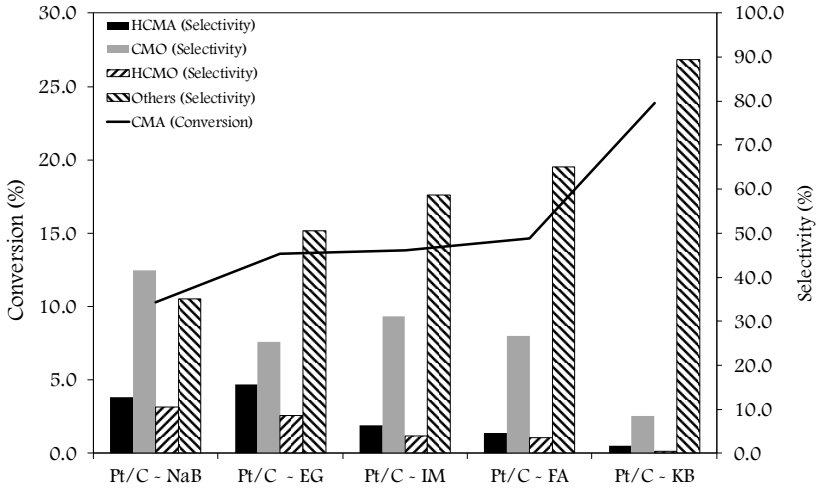

Figure 3.10. Influence of the reducing agent on the CMA conversion and products selectivity. Reaction conditions: Anodic solution: H_2O, Cathodic solution: 100 ppm CMA in 2 – propanol, Inlet flow: 1 ml·min^{-1}, Intensity: 0.05 A, Temperature: 70 ^{o}C

Regarding CMO selectivity, results showed a different sequence: Pt/C-NaB > Pt/C-IM > Pt/C-FA > Pt/C-Pt/C-EG > Pt/C-KB. In this case, there was not a straightforward explanation about the observed differences. According to literature, Pt/C-EG and Pt/C-FA were not expected to be selective to CMO since larger faceted metal particles are more selective to CMO, due to the steric constrains when CMA molecule is absorbed on the catalyst [40, 41]. In agreement, Pt/C-KB, which present the lowest active particle size, resulted in 90% of by-product formation. Therefore, it can be concluded that the Pt/C catalyst prepared by this method was not suitable to carry out the selective hydrogenation of CMA in a PEM cell. However, all the as-prepared catalyst present basic character, could shift selectivity to CMO by favoring the activation of the carbonyl group. Therefore, among the other Pt/C-R cathodes, Pt/C-NaB

shows the best selectivity to CMO despite not showing the best electrocatalytic properties (higher metal dispersion, ECSA or less deactivation). However, it should be noted that catalyst Pt/C-EG, despite of a higher production of undesired compounds, provides the same yield to the value-added products (CMO+HCMA) than that of Pt/C-NaB. It is also important to mention that the modified polyol method allows particle size control, which offers a promising alternative to carry out further studies looking for the reduction of by-products.

4. CONCLUSIONS

Considering the results above explained, the following conclusions were reached:

- Pt/C catalysts were successfully synthesized by one-pot impregnation-reduction method and wet impregnation method and lately used in the electrocatalytic hydrogenation of CMA.
- The reducing agent noticeably affected the Pt particle size, dispersion on the support and basicity.
- The utilization of sodium borohydride as reducing agent improves the selectivity towards CMO. However, the catalyst reduced with polyol present a good compromise between conversion, selectivity and non-desired products production. Therefore, this catalyst was proposed as a good choice for further studies.

REFERENCES

1. Guo, Z., et al., *Carbon nanotube-supported Pt-based bimetallic catalysts prepared by a microwave-assisted polyol reduction method and their catalytic applications in the selective hydrogenation.* Journal of Catalysis, 2010. **276**(2): p. 314-326.
2. Gutiérrez-Guerra, N., et al., *Gas phase electrocatalytic conversion of CO2 to syn-fuels on Cu based catalysts-electrodes.* Applied Catalysis B: Environmental, 2016. **188**: p. 272-282.
3. Huang, B., et al., *Highly selective electrochemical hydrogenation of acetylene to ethylene at Ag and Cu cathodes.* Electrochemistry Communications, 2013. **34**: p. 90-93.
4. Otsuka, K. and T. Yagi, *An Electrochemical Membrane Reactor for Selective Hydrogenation of Acetylene in Abundant Ethylene.* Journal of Catalysis, 1994. **145**(2): p. 289-294.
5. Sáez, A., et al., *Electrocatalytic hydrogenation of acetophenone using a Polymer Electrolyte Membrane Electrochemical Reactor.* Electrochimica Acta, 2013. **91**: p. 69-74.
6. Villalba, M., M. del Pozo, and E.J. Calvo, *Electrocatalytic hydrogenation of acetophenone and benzophenone using palladium electrodes.* Electrochimica Acta, 2015. **164**: p. 125-131.
7. Mahdavi, B., et al., *Electrocatalytic hydrogenation of conjugated enones on nickel boride, nickel, and Raney nickel electrodes*. Vol. 73. 2011. 846-852.
8. He, S., et al., *Chemoselective hydrogenation of α,β-unsaturated aldehydes on hydrogenated MoOx nanorods supported iridium nanoparticles.* Journal of Molecular Catalysis A: Chemical, 2016. **425**: p. 248-254.
9. Zheng, Q., et al., *An Effective Co-promoted Platinum of Co–Pt/SBA-15 Catalyst for Selective Hydrogenation of Cinnamaldehyde to Cinnamyl Alcohol.* Catalysis Letters, 2016. **146**(8): p. 1535-1543.
10. Handjani, S., et al., *Influence of the support composition and acidity on the catalytic properties of mesoporous SBA-15, Al-SBA-15, and Al2O3-supported Pt catalysts for cinnamaldehyde hydrogenation.* Journal of Catalysis, 2011. **282**(1): p. 228-236.
11. Bharti, A., G. Cheruvally, and S. Muliankeezhu, *Microwave assisted, facile synthesis of Pt/CNT catalyst for proton exchange membrane fuel cell application.* International Journal of Hydrogen Energy, 2017. **42**(16): p. 11622-11631.

12. Lobato, J., et al., *Composite Titanium Silicon Carbide as a Promising Catalyst Support for High-Temperature Proton-Exchange Membrane Fuel Cell Electrodes.* ChemCatChem, 2016. **8**(4): p. 848-854.
13. Baranova, E.A., et al., *Single-step polyol synthesis of alloy Pt7Sn3 versus bi-phase Pt/SnOx nano-catalysts of controlled size for ethanol electro-oxidation.* Journal of Applied Electrochemistry, 2010. **40**(10): p. 1767-1777.
14. López-Suárez, F.E., et al., *Pt–Sn/C catalysts prepared by sodium borohydride reduction for alcohol oxidation in fuel cells: Effect of the precursor addition order.* Journal of Power Sources, 2014. **268**: p. 225-232.
15. Calderón, J., et al., *Effect of the Dendrimer Generation Used in the Synthesis of Pt-Ru Nanoparticles Supported on Carbon Nanofibers on the Catalytic Activity towards Methanol Oxidation.* Energies, 2017. **10**(2): p. 159.
16. Hájek, J., et al., *The Effect of Chemical Reducing Agents in the Synthesis of Sol-Gel Ru-Sn Catalysts: Selective Hydrogenation of Cinnamaldehyde.* Journal of Sol-Gel Science and Technology, 2004. **30**(3): p. 187-195.
17. Alegre, C., et al., *Towards an optimal synthesis route for the preparation of highly mesoporous carbon xerogel-supported Pt catalysts for the oxygen reduction reaction.* Applied Catalysis B: Environmental, 2014. **147**: p. 947-957.
18. Bock, C., et al., *Size-Selected Synthesis of PtRu Nano-Catalysts: Reaction and Size Control Mechanism.* Journal of the American Chemical Society, 2004. **126**(25): p. 8028-8037.
19. Baranova, E.A., et al., *Size and composition for 1-5 nm Ø PtRu alloy nano-particles from Cu Kα X-ray patterns.* Journal of Alloys and Compounds, 2009. **471**(1-2): p. 387-394.
20. Díez-Ramírez, J., et al., *Carbon Nanofiber-Based Palladium/Zinc Catalysts for the Hydrogenation of Carbon Dioxide to Methanol at Atmospheric Pressure.* Industrial & Engineering Chemistry Research, 2016. **55**(12): p. 3556-3567.
21. Bessel, C.A., et al., *Graphite Nanofibers as an Electrode for Fuel Cell Applications.* The Journal of Physical Chemistry B, 2001. **105**(6): p. 1115-1118.
22. Serp, P., M. Corrias, and P. Kalck, *Carbon Nanotubes and Nanofibers in Catalysis.* Applied Catalysis A-general - APPL CATAL A-GEN, 2003. **253**: p. 337-358.
23. Ismagilov, Z.R., et al., *Development of active catalysts for low Pt loading cathodes of PEMFC by surface tailoring of nanocarbon materials.* Catalysis Today, 2005. **102-103**: p. 58-66.

24. de la Osa, A.R., et al., *Influence of alkali promoters on synthetic diesel production over Co catalyst.* Catalysis Today, 2011. **167**(1): p. 96-106.
25. Sing, K.S.W., et al., *Reporting Physisorption Data for Gas/Solid Systems*, in *Handbook of Heterogeneous Catalysis*. 2008, Wiley-VCH Verlag GmbH & Co. KGaA.
26. Sing, K., *The use of nitrogen adsorption for the characterisation of porous materials.* Colloids and Surfaces A: Physicochemical and Engineering Aspects, 2001. **187-188**: p. 3-9.
27. Wang, K.W. and C.T. Yeh, *Temperature-programmed reduction study on carbon-supported platinum-gold alloy catalysts.* Journal of Colloid and Interface Science, 2008. **325**(1): p. 203-206.
28. Wang, L., et al., *Highly active Pt/NaxTiO2 catalyst for low temperature formaldehyde decomposition.* Applied Catalysis B: Environmental, 2017. **219**(Supplement C): p. 301-313.
29. Díaz, J.A., et al., *Carbon nanofibers and nanospheres-supported bimetallic (Co and Fe) catalysts for the Fischer–Tropsch synthesis.* Fuel Processing Technology, 2015. **138**: p. 455-462.
30. Nieto-Márquez, A., et al., *Gas phase hydrogenation of nitrobenzene over acid treated structured and amorphous carbon supported Ni catalysts.* Applied Catalysis A: General, 2009. **363**(1): p. 188-198.
31. Contreras-andrade, I., G. Pérez, and T. Viveros-García, *The Influence Of The Support On The Deactivation Behaviour of Pt-Sn Reforming Catalysts.* International Journal of Chemical Reactor Engineering - INT J CHEM REACT ENG, 2005. **3**.
32. Kohki, E. and H. Hideshi, *Combined Temperature-Programmed Reduction (TPR)- Temperature-Programmed Desorption (TPD) Study of Supported Platinum Catalysts.* Bulletin of the Chemical Society of Japan, 1991. **64**(8): p. 2422-2427.
33. Dosso, L.A., C.R. Vera, and J.M. Grau, *Pt-Co and Pt-Ni Catalysts of Low Metal Content for H2 Production by Reforming of Oxygenated Hydrocarbons and Comparison with Reported Pt-Based Catalysts.* International Journal of Chemical Engineering, 2018. **2018**: p. 10.
34. Fang, L., et al., *Preparation, characterization and catalytic performance of a novel Pt/SiC.* Electrochemistry Communications, 2011. **13**(12): p. 1309-1312.

35. Kinoshita, K., J.T. Lundquist, and P. Stonehart, *Potential cycling effects on platinum electrocatalyst surfaces.* Journal of Electroanalytical Chemistry and Interfacial Electrochemistry, 1973. **48**(2): p. 157-166.
36. Perez, J., V.A. Paganin, and E. Antolini, *Particle size effect for ethanol electro-oxidation on Pt/C catalysts in half-cell and in a single direct ethanol fuel cell.* Journal of Electroanalytical Chemistry, 2011. **654**(1): p. 108-115.
37. Dabo, P., et al., *Selective electrocatalytic hydrogenation of 2-cyclohexen-1-one to cyclohexanone.* Electrochimica Acta, 1997. **42**(9): p. 1457-1459.
38. Hájek, J., et al., *Ruthenium-modified MCM-41 mesoporous molecular sieve and Y zeolite catalysts for selective hydrogenation of cinnamaldehyde.* Applied Catalysis A: General, 2003. **251**(2): p. 385-396.
39. Yepez, A., et al., *Mechanistic insights into the hydroconversion of cinnamaldehyde using mechanochemically-synthesized Pd/Al-SBA-15 catalysts.* Green Chemistry, 2015. **17**(1): p. 565-572.
40. Englisch, M., A. Jentys, and J.A. Lercher, *Structure Sensitivity of the Hydrogenation of Crotonaldehyde over Pt/SiO2and Pt/TiO2.* Journal of Catalysis, 1997. **166**(1): p. 25-35.
41. Gallezot, P., A. Giroir-Fendler, and D. Richard, *Chemioselectivity in cinnamaldehyde hydrogenation induced by shape selectivity effects in Pt-Y zeolite catalysts.* Catalysis Letters, 1990. **5**(2): p. 169-174.

Chapter 4: Electrocatalytic hydrogenation of cinnamaldehyde in a PEM cell. The role of sodium hydroxide and Platinum Loading

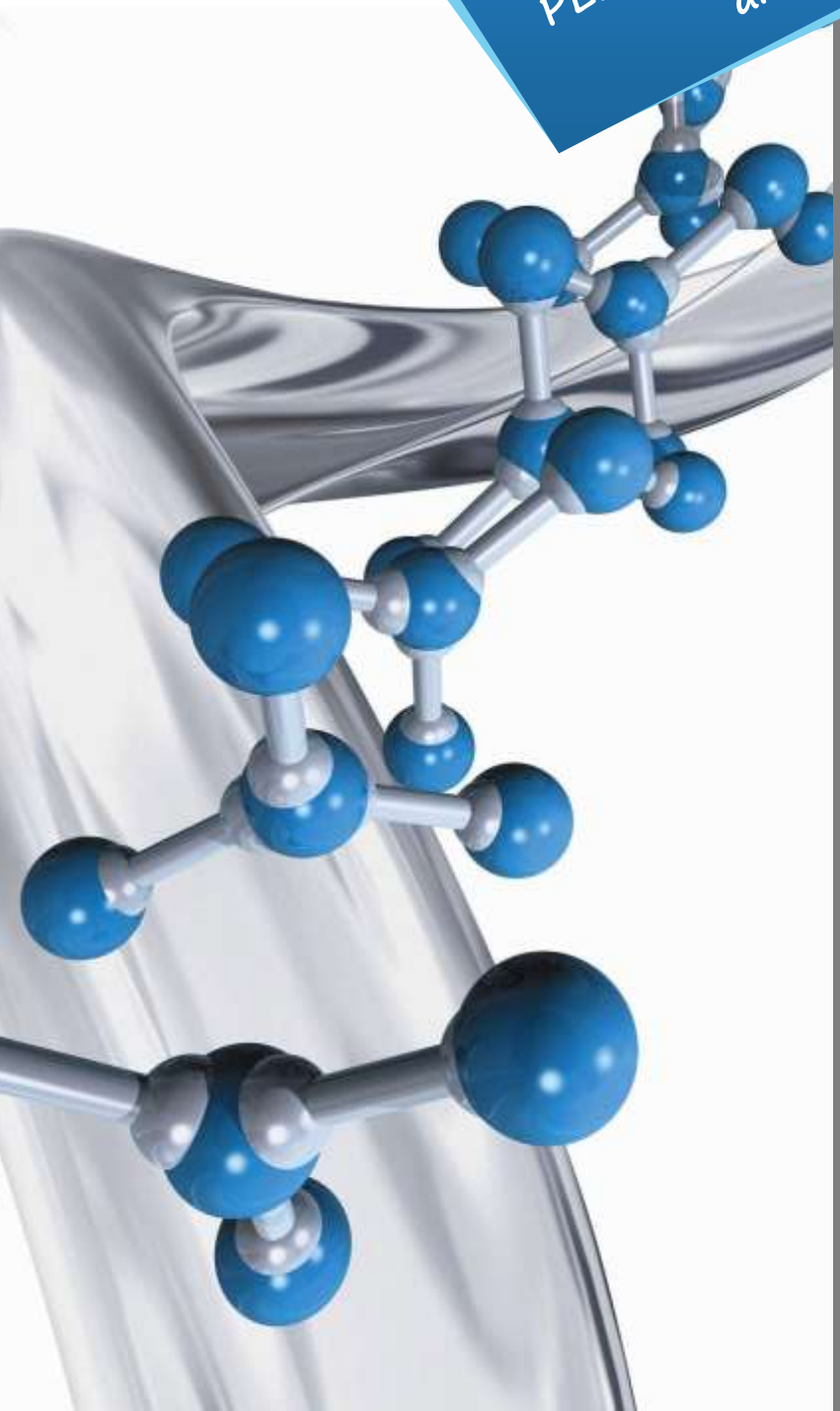

1. INTRODUCTION

2. EXPERIMENTAL
2.1. Catalysts synthesis
2.2. Physicochemical characterization
2.3. Electrochemical characterization
2.4. Membrane electrode assembly (MEA) preparation
2.5. Electrocatalytic hydrogenation of CMA in a proton exchange membrane reactor

3. RESULTS AND DISCUSSION
3.1. Influence of platinum loading
3.1.1. Physicochemical characterization of Pt-m/C-0.2 cathodes
3.1.2. Electrochemical characterization of Pt-m/C-0.2 cathodes
3.1.3. Electrocatalytic hydrogenation of CMA in a PEM cell on Pt-m/C-0.2 cathodes
3.2. Influence of the pH in the synthesis procedure
3.2.1. Physicochemicall characterization of Pt-15/C-X cathodes
3.2.2. Electrochemical characterization of Pt-15/C-X cathodes
3.2.3. Electrochemical hydrogenation of cinnamaldehyde in PEM cell on Pt-15/C-X cathodes

4. CONCLUSIONS

Abstract

In order to improve the electrocatalytic performance of Vulcan XC-72 supported Pt catalyst used as cathode electrode towards the electrocatalytic hydrogenation of cinnamaldehyde in a PEM cell, two different studies were carried out. In a first stage,the influence of the cathode Pt loading was evaluated. In a second study the influence of the pH during the catalyst synthesis procedure (by modifying the required amount of NaOH) was explored. Results from physicochemical and electrochemical characterization and PEM essays showed that both pH and metal loading play a direct role on the obtained active particle size, basicity as well as on the electrochemical surface area and degradation of the samples. As a consequence, the electrochemical hydrogenation activity and selectivity are highly modified by both parameters. Hence, the catalyst prepared with 15 wt.% of Pt using a 0.2 M NaOH solution showed the best electrocatalytic performance due to its relative basicity and suitable metal dispersion, which provide adequate ECSA value, deactivation degree and selectivity to the value-added compounds.

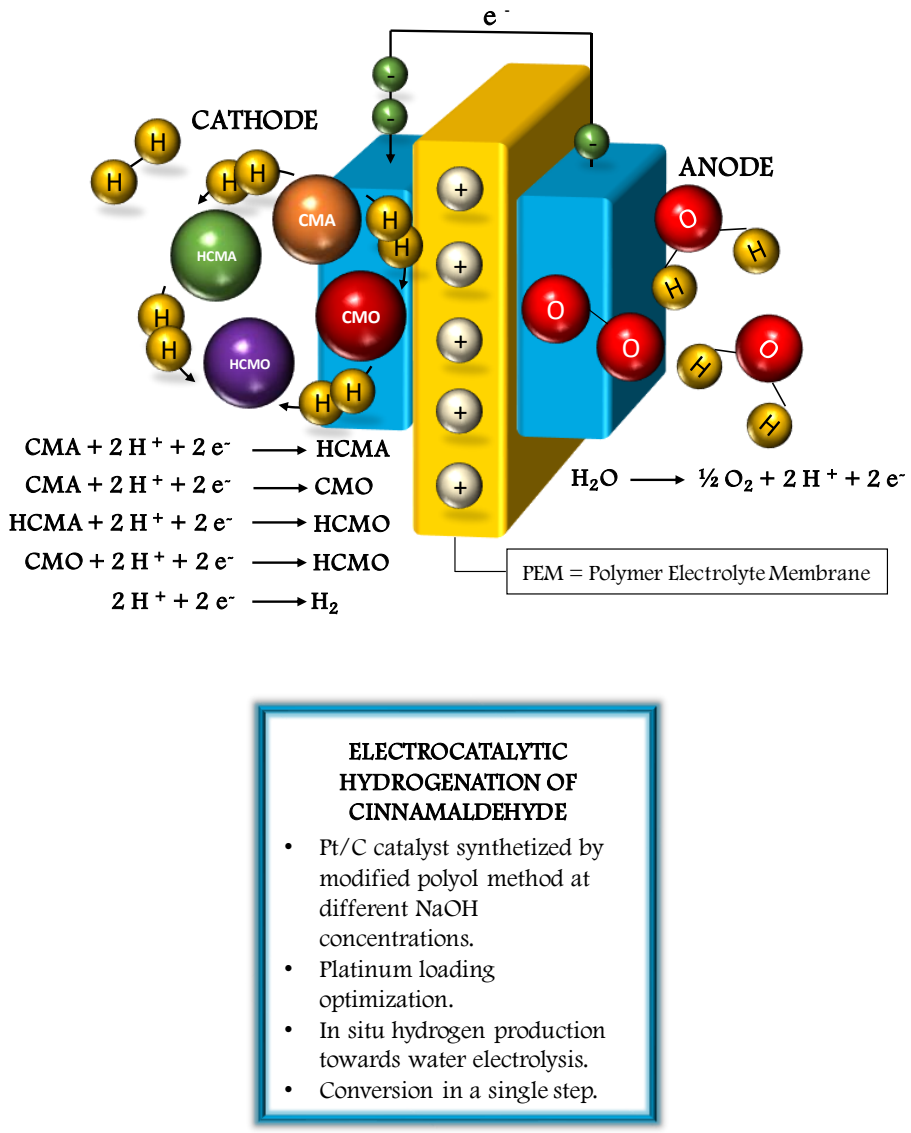

Figure 4.1. *Graphical abstract Chapter 4.*

1. INTRODUCTION

During the last years, the global market of flavors and fragrances has experienced a significant growth, especially in North America, Europe and in the Asia-Pacific region reaching 8 billion of dollars. This growth is produced by the high availability of spices in Asian countries, by the increasing population in developing countries, where the demand for cosmetics and products for personal care, as well as perfumery, medicines or the preference for organic food ingredients has markedly increased due to the associated aging [1, 2].

Among the most demanded compounds of this market is cinnamaldehyde and its derivatives. A natural organic compound present in cinnamon with exclusive properties that make it ideal for improving the taste of food, beverages and medicines, its use in agricultural crops. It is an upward market that supposes more than 40% of the market share as aromatic agent, more than 15% as an antimicrobial agent, and supposes a benefit of more than 650 Million of dollars as flavoring.

Its derivatives, which are obtained from the catalytic hydrogenation of this molecule are no less interesting. From the hydrogenation of the C=C bond, which is thermodynamically favored, hydrocinamaldehyde (HCMA), an important intermediate in the preparation of pharmaceuticals used in the treatment of HIV [3], is obtained. The hydrogenation of the carbonyl group produces cinnamyl alcohol (denoted as CMO), which finds application in the synthesis of a large number of flavors and fragances as a fixative of jasmine, lilac and pink mixtures [4]. It is also used in the pharmaceutical industry in the synthesis of the chloromycetin antibiotic. By successive hydrogenation, hydrocinnamyl alcohol (HCMO) is formed. It finds use as a preservative in cosmetics due to its antimicrobial properties.

Industrially, these processes are carried out under severe conditions of pressure and temperature, operating in batch mode, which results in high operating, separation and safety costs [5]. Electrochemical hydrogenation has been demonstrated to be an alternative route to catalytic hydrogenation since it is performed under more benign conditions (room temperature and atmospheric pressure). In this sense, attention has been paid to the coupling of water electrolysis and electrohydrogenation in a proton exchange membrane (PEM) cell reactor, since this system is advantageous compared with the classical process in terms of energy efficiency, specific production capacity, and a simplicity (pure hydrogen production at a low temperature without any external gaseous source) [6-8]. However, in order to improve both the electrocatalytic performance of the system and stability, and taking into account the cost and availability of the active phase of the catalyst, further studies should be carried out.

Various factors such as the type of metal [9-11], particle size [12], additives [13-16] and supports [17-19] are found to influence the activity and selectivity of the catalysts in CMA hydrogenation. Platinum is widely employed in heterogeneous catalytic hydrogenation, able to reduce diverse functional groups [20], including C=C [21], C≡C [22], C=O [23], C≡N [24] with molecular hydrogen. It is generally observed that the selectivity towards the unsaturated alcohols highly depends on the morphology, size and electronic structure of Pt particles [25]. For instance, it is reported that metal loading has a great influence on hydrogenation reactions, due to the modification of both size and homogeneity of the distribution of active metal particles [26, 27]. On the other hand, Baranova et al. have reported that structure can be easily controlled by pH (i.e. modifying the NaOH concentration) in synthesis processes using the polyol method [28].

Therefore, the present work was focus on: i) the study of the influence of Pt loading of the cathode electrode and ii) the modifications of the electrocatalyst by means of changes of pH (variation of the NaOH concentration) during the preparation through the modified polyol method on the electrocatalytic hydrogenation of cinnamaldehyde conducted in a PEM cell.

2. EXPERIMENTAL

2.1. Catalysts synthesis

For this study Pt-m/C-X catalysts has been prepared with different loadings and amount of NaOH by de modified polyol method described in Section B.2.3.

2.2. Physicochemical characterization

An ICP (inductively coupled plasma spectrometer, Model Liberty Sequential, VARIAN) was used to analyze Pt content.

A Phillips PW-1700 diffractometer (using nickel-filtered Cu Kα radiation) were used in order to carried out the XRD analyses.

A Micromeritics AutoChem 2950 HP unit with TCD detection were used for the Temperature-programmed reduction (TPR) and H_2 pulse chemisorption experiments.

A Micromeritics ASAP 2010 sorptometer unit was used for the surface area/porosity measurements, with N_2 at 77 K as the adsorbate.

A SCHOTT Titroline apparatus, equipped with an automatic dosager were used for the HCl titrations.

All the physicochemical characterization procedures are described in Section B.4.

2.3. Electrochemical characterization

Electrochemical characterization was performed using a single cell of three-electrode system coupled to a computer-controlled potentiostat Autolab PGSTAT128N (Ecochemie, The Netherlands). The half-cell is composed of working electrode (Glassy Carbon, Metrohm Autolab, 5 mm diameter), a counter electrode (Pt wire, Metrohm) and reference electrode (Ag/AgCl, Metrohm). $HClO_4$ 0.1 M (Scharlab) was used as electrolyte (Section B.5.)

2.4. Membrane electrode assembly (MEA) preparation

Anodic and cathodic inks were prepared from commercial IrO_2 (99 wt. %, 2 mg·cm^{-2}, Alfa Aesar) for the anode and as-prepared Pt-m/C-x (m refers to the Pt metal loading varying from 10 to 20 wt.%; x denotes NaOH concentration used in the modified poliol one-pot method, ranging from 0.05 to 0.2 M) (0.5 mg·cm^{-2}) for the cathode, respectively following the procedures described in Section B.3

2.5. Electrocatalytic hydrogenation of CMA in a proton exchange membrane reactor

Electrocatalytic hydrogenation was carried out in a proton exchange membrane cell described in section B.7.2. consisting of the MEA detailed above, two current collectors of 2 mm thickness made of Grade 1 Titanium and two porous titanium gas diffusion layers. The previous composition is sandwiched between two PTFE gaskets in order to seal and avoid short circuiting of the cell.

Product distribution from the electrocatalytic hydrogenation of CMA was analyzed offline in a gas chromatograph (Agilent Technologies

7820A) equipped with a FID detector and capillary column (Agilent DB-624, 30 m x 0.25 mm x 0.5 μm) using He as carried gas.

3. RESULTS AND DISCUSSION

3.1. Influence of the platinum loading

3.1.1. Physicochemical characterization of Pt-m/C-0.2 cathodes

The crystallographic structure and phase purity of the as-prepared Pt-m/C-0.2 catalysts are studied by XRD (Figure 4.2). The diffraction peak seen at 25° (0 0 2) are characteristic of the carbon support. Furthermore, the diffraction peaks seen at 39.5°, 46.1°, 67.5° and 80.9° correspond to the (1 1 1), (2 2 0), (2 0 0) and (3 1 1) crystalline planes of the face-centered cubic (fcc) Pt crystallites, respectively [29, 30]. It should be noted that no characteristic reflexions of Pt oxides can be appreciated, suggesting the correct reduction to the active phase during the synthesis procedure (modified polyol method).

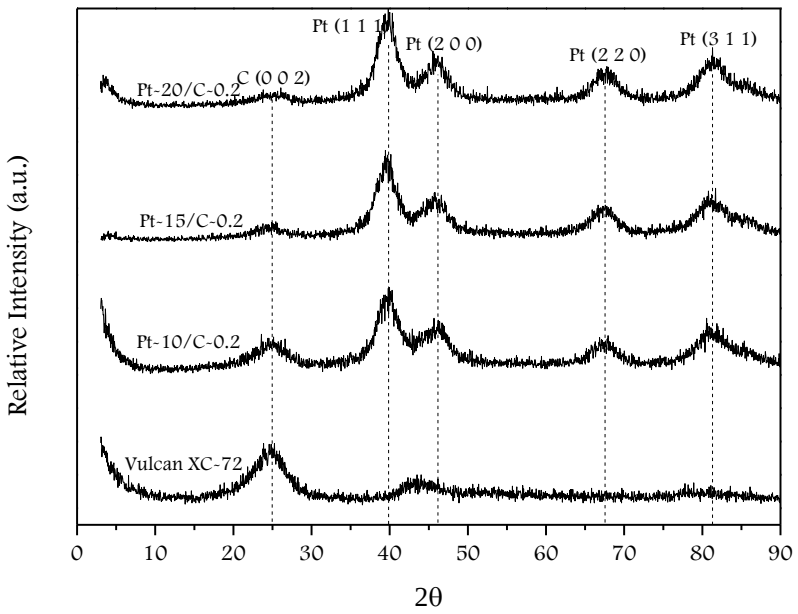

Figure 4.2. XRD patterns of the synthesized Pt-m/C-0.2 catalysts.

Table 4.1 shows the main physicochemical parameters of the platinum-based catalyst synthetized by the modified polyol method. The mean particle size was calculated by Scherrer equation from $2\theta = 68^{o}$, which corresponds to the peak of Pt (2 0 0). Although the average particle size calculated by the Scherrer equation seemed to be barely affected by the platinum loading in the range of study, hydrogen chemisorption measurements allow to observe that the active particle size increased from 3 to 8.6 nm with Pt loading. As a consequence, the chemically active surface decreased to one third.

Table 4.1. Physicochemical properties of Pt-m/C-0.2 catalysts.

Sample	wt. % Pt	XRD Particle size (nm)[1]	BET specific surface area ($m^2 \cdot g^{-1}$)	Total pore volume ($cm^3 \cdot g^{-1}$)
Vulcan XC-72	-	-	231	0.408
Pt-10/C-0.2	10	4	87	0.539
Pt-15/C-0.2	14.5	4	94	0.529
Pt-20/C-0.2	20.3	5	100	0.447
	Average pore diameter (nm)[2]	**Dispersion (%)[3]**	**Active particle size (nm)[3]**	**CSA ($m^2 \cdot g^{-1}$)[3]**
Vulcan XC-72	7.7	-	-	-
Pt-10/C-0.2	24.6	38.4	3.0	95
Pt-15/C-0.2	24.4	26.2	4.0	70
Pt-20/C-0.2	17.7	13.1	8.6	32

1 Calculated from the Pt (2 2 0) peak using the Debye-Scherrer equation.

2 Calculated assuming cylindrical pore geometry.

3 Calculated from H_2 chemisorption using equations 1, 2 and 3.

In order to analyze the oxidation state of the platinum particles which are present in the synthesized catalysts, temperature programmed reduction (TPR) measurements were conducted. As displayed in Figure 4.3. none of the as-synthetized catalysts presents hydrogen consumptions at temperatures below 200 °C, which would indicate that the reducing agent used during the synthesis procedure (ethylene glycol) is capable of reducing a large part of platinum to its metallic state, which is the real active phase in the hydrogenation reaction. Moreover, the

reduction profiles presented similar characteristics with no dependence of the Pt loading, showing two main maxima of hydrogen consumption at 280-300 °C and 500-600 °C, respectively. The first maximum would correspond to the reduction of platinum complex deposited on the surface of the carbonaceous support and no located near metal particles [31, 32] whereas that at high temperature is attributable to the gasification of the carbonaceous support catalyzed by the Pt particles [33-35]. This second peak shifts to lower temperatures when platinum is present due to the platinum spillover effect [36]. However, it can be also observed that as the metal loading increases, and therefore the crystallite size, reduction profiles move to lower temperatures.

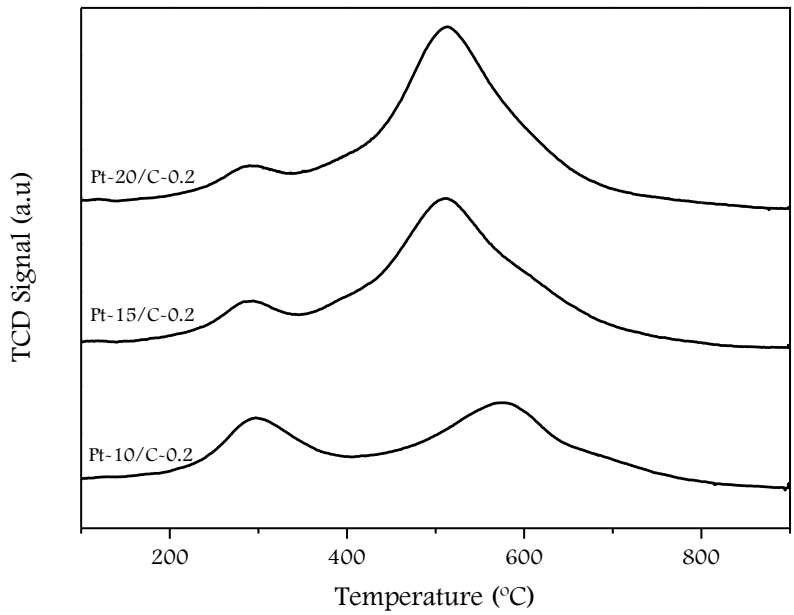

Figure 4.3. Temperature-programmed reduction (TPR) profiles of Pt-m/C-0.2 catalysts.

Table 4.1. summarizes the textural properties corresponding to each of the synthesized catalysts, obtained after analysis of the surface area and pore volume, calculated by means of nitrogen adsorption-desorption isotherms. According to the IUPAC classification, the isotherms observed on Figure 4.4. are a combination of types I and IV.

The hysteresis cycle shown by type IV isotherms is due to capillary condensation at high partial pressures and is associated with the presence of mesopores [37]. The initial of these isotherms is very similar to type I isotherms, which correspond to a monolayer adsorption characteristic of microporous solids (specially at the support) [38]. This type of isotherms occurs at relatively low pressures.

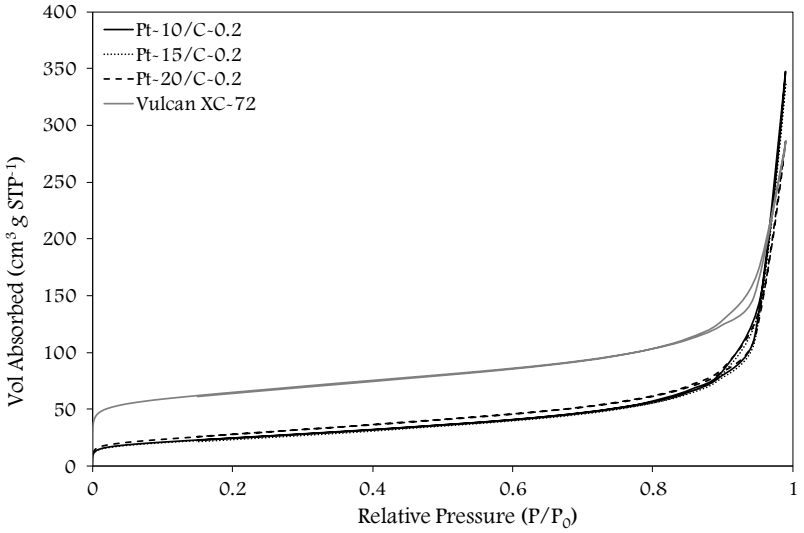

Figure 4.4. Nitrogen adsorption/desorption isotherms of Pt-m/C-0.2 catalysts.

According to the results summarized in Table 4.1., it can be observed that, after incorporation of the active metal in the support, the surface area decreases, which indicates a partial blockage of the pores due to the deposition of the metallic particles on the support surface. According to the pore volume and pore diameter values, it can be observed that, Pt-20/C-0.2 catalyst presents higher surface area as well as lower pore volume and diameter. However, in catalysts Pt-10/C-02 and Pt-15/C-02 with smaller particle size, both the pore volume and the average pore diameter increase. This can be explained by a possible blockage of the micropores present in the catalyst, which shifts the pore size distribution (Figure 4.5.) to higher average values [39, 40].

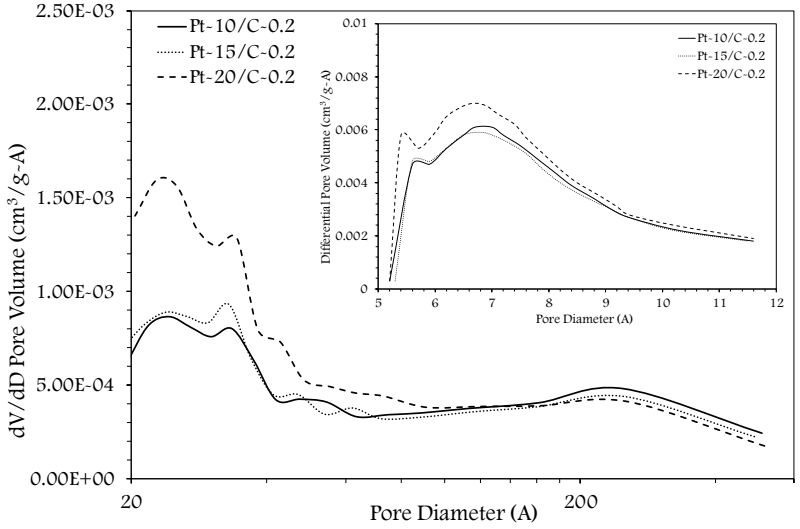

Figure 4.5. Pore distribution of Pt-m/C-0.2 catalysts.

In addition, in order to know the acid-base character of the catalysts, acid-base titration analyses have been carried out. From Figure 4.6. a slight increase in the relative basicity of the sample can be observed by increasing the Pt content, which could modify the selectivity of the reaction towards the formation of CMO.

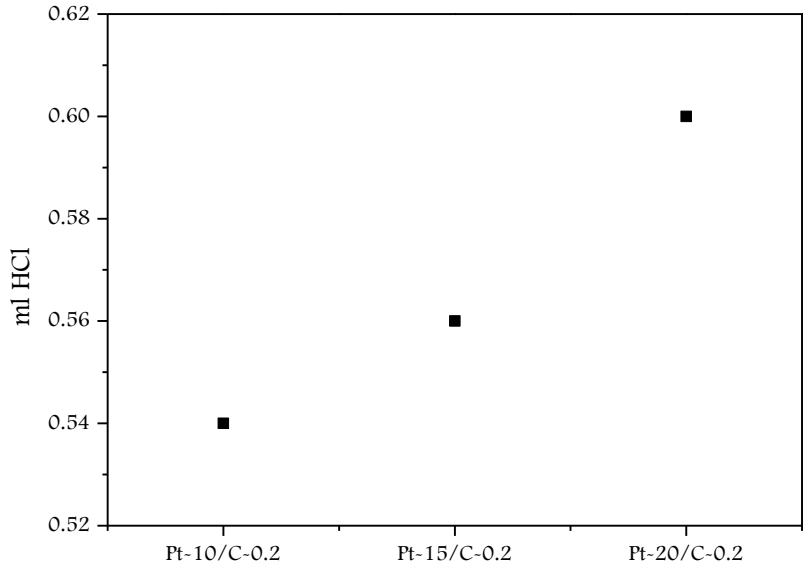

Figure 4.6. Acid-base titration results for Pt-m/C-0.2 catalysts.

3.1.2. Electrochemical characterization of Pt-m/C-0.2 cathodes

Characterization techniques using a rotating disk electrode (RDE) has been extensively used to estimate the activity of electrocatalysts in a lab scale. In this sense, cyclic voltammetry tests were performed in order to estimate the electrochemically active surface (ECSA) corresponding to each of the synthesized catalysts. In addition, in order to analyze the stability of the catalysts used as cathodes, accelerated degradation experiments were carried out (500 cycles, 25 ^{o}C in 0.1 M $HClO_4$ with a scan rate of 50 mV s^{-1}.). Figure 4.7.a., 4.7.b. and 4.7.5.c. show the voltammograms of the as prepared catalysts. All the samples show the corresponding adsorption-desorption of hydrogen, which appears at a potential of 0 and +0.25 V vs RHE, the double layer region, and another two peaks corresponding to the oxidation and reduction of platinum, at a potential of approximately 1.25 and 0.75 V vs RHE, respectively. Pt-15/C-0.2, and Pt-20/C-0.2 presents two peaks in de hydrogen adsorption region, which are related to the (1 0 0) and (1 1 1) crystal face planes of the platinum. For Pt-10/C-0.2 both peaks overlap generating a single one corresponding to the (1 0 0) [41, 42], it is possible that this catalysts showed lower peaks due to the amount of Nafion used to prepare de ink, which interaction with Pt may affect the H_2 adsorption-desorption and influence negatively on the peak size.

From these figures and data collected in Table 4.2., it can be also observed that as the number of cycles increases, the area of the H_2 adsorption/desorption peak decreases, indicating certain degradation of the sample.

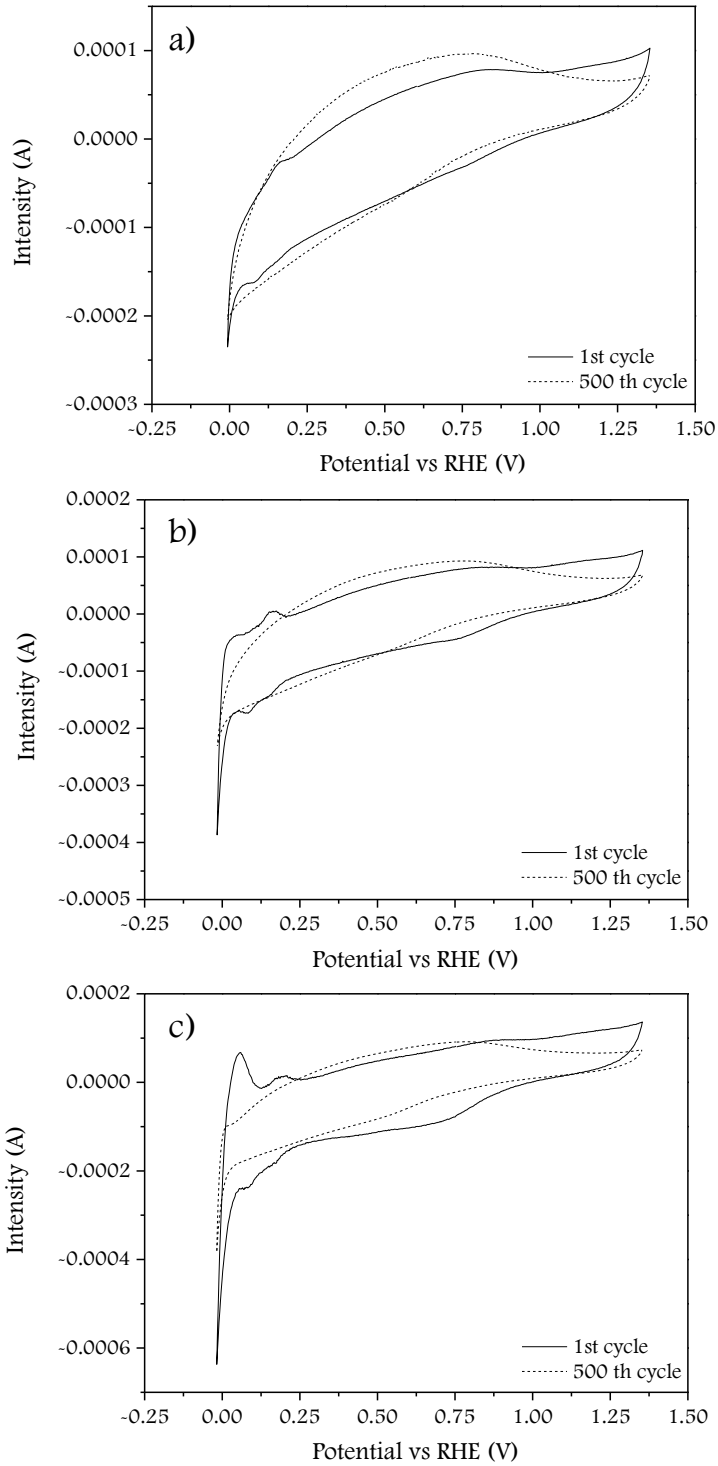

Figure 4.7. Cyclic voltammograms of a) Pt-10/C-0.2, b) Pt-15/C-0.2 and c) Pt-20/C-0.2 catalysts at 25 °C in 0.1 M $HClO_4$ with a scan rate of 50 mV s^{-1}.

Table 4.2. ECSA and deactivation degree of Pt-m/C-0.2 catalysts.

Catalyst	ECSA 0 cycles ($m^2 \cdot g^{-1}$)	ECSA 500 cycles ($m^2 \cdot g^{-1}$)	Deactivation (%)
Pt-10/C-0.2	29	21	28
Pt-15/C-0.2	35	15	57
Pt-20/C-0.2	30	14	53

The loss of active electrochemical area can be caused as a result of the dissolution of small amounts of Pt from the electrode surface. In this context, although the catalyst with a higher Pt loading (20 wt.%) presents a suitable ECSA value, consistent with that of literature [43], it also shows the highest deactivation degree. However, despite of a lower ECSA, below 15 wt.% of Pt, deactivation is similar to that of commercial Pt-based catalyst. In this sense, Pt-15/C-0.2 shows the best compromise between electrochemical surface area and degradation value.

3.1.3. Electrochemical hydrogenation of cinnamaldehyde in PEM cell on Pt-m/C-0.2 cathodes

According to Fuente-Hernandez et al., the use of a higher percentage of Pt in the catalyst does not favor an increased conversion of cinnamaldehyde compared to lower loading catalyst [27]. These authors explain this fact in terms of the reduced homogeneity of Pt distribution, which is a consequence of the higher loading impregnation. Selectivity for CMO and HCMA are reduced and the production of secondary by-products is higher. On the other hand, Manikandan et al. claim that higher metal loadings favor the selectivity to CMO instead of secondary by-products [4]. Figure 4.8. shows the comparison between the conversion and selectivity related to each Pt-m/C-0.2 cathode. Results from PEM cell tests indicate that the electrochemical hydrogenation reaction is sensitive to the Pt crystallite size so that a maximum of 23% conversion per pass was obtained with the catalyst synthesized with 15

wt. % of Pt. CMA conversion increases with Pt loading up to 15 wt. % due to the availability of more catalytic sites. From this load on conversion decreases due to the loss of homogeneity of the particle distribution on the catalyst. In terms of product distribution, as reported by Reyes et al, the catalyst loading does not have a great influence on the selectivity to the desired compounds [44].

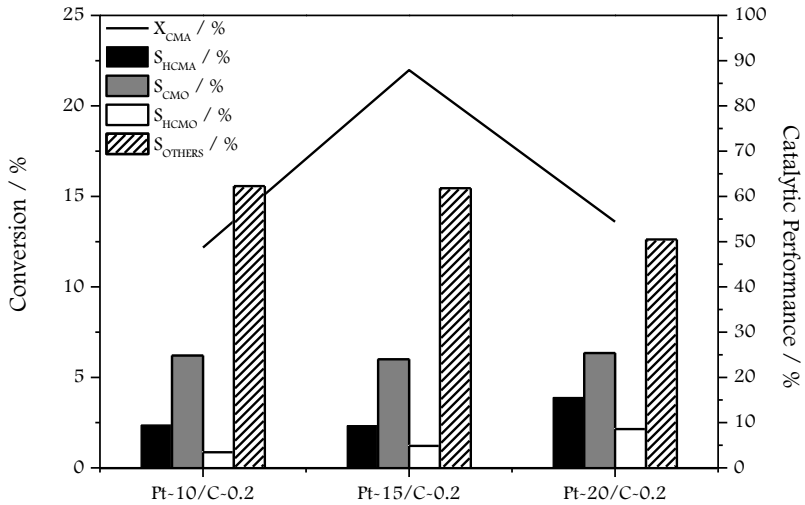

Figure 4.8. Influence of the platinum loading on the electrocatalytic hydrogenation of CMA in a PEM cell. Reaction conditions: Anodic solution: H_2O, Cathodic solution: 100 ppm CMA in 2-propanol, Inlet flow: 1 ml·min^{-1}, Intensity: 0.05 A, Temperature: 70 °C.

It can be observed that the total selectivity to HCMA, CMO and HCMO was 40-50%, which is in good agreement to that reported under more severe conditions on conventional catalysis [45-47]. It is also important to say that although 50-62% of undesired-by-product were formed, it is consistent and even lower than that reported on conventional catalysis using polar solvents, such as 2-propanol [48, 49]. On the basis of the above affirmations, it can be said that Pt-15/C-0.2 catalyst presents a suitable crystallite size and relative basicity to establish a compromise between conversion and selectivity, comparable to certain conventional catalytic systems carried out under analogous conditions.

3.2. Influence of the pH in the synthesis procedure

3.2.1. Physicochemical characterization of Pt-15/C-X cathodes

Table 4.3 shows the physicochemical parameters of synthetized Pt/C catalysts. From data collected in this table, it can be noted that the choice of a suitable pH for the synthesis procedure (by means of modifying the NaOH concentration of the media) plays a key role on the resulting crystallite size, active area and basic character of the catalyst.

Table 4.3. Physicochemical properties of Pt-15/C-X catalysts.

Sample	wt. % Pt	XRD Particle size (nm)[1]	BET specific surface area ($m^2 \cdot g^{-1}$)	Total pore volume ($cm^3 \cdot g^{-1}$)
Vulcan XC-72	-	-	231	0.408
Pt-15/C-0.05	14.5	11	173	0.498
Pt-15/C-0.125		9	119	0.419
Pt-15/C-0.2		4	94	0.525
	Average pore diameter (nm)[2]	**Dispersion (%)[3]**	**Active particle size (nm)[3]**	**CSA ($m^2 \cdot g^{-1}$)[3]**
Vulcan XC-72	7.7	-	-	-
Pt-15/C-0.05	12.0	13.1	8.6	32
Pt-15/C-0.125	13.9	28.4	4.3	65
Pt-15/C-0.2	24.4	26.2	4.0	70

1 Calculated from the Pt (2 2 0) peak using the Debye-Scherrer equation.

2 Calculated assuming cylindrical pore geometry.

3 Calculated from H_2 chemisorption using equations 1, 2 and 3.

The XRD patterns of the platinum-based catalyst prepared under pH control (by using different NaOH concentration) display the characteristic diffraction peaks of the carbon support at 25° (0 0 2) and the Pt diffraction peaks (1 1 1), (2 0 0), (2 2 0) and (3 1 1) (vertical based lines) at $2\theta = 39.5°$, 46.1°, 67.5° and 80.9° respectively, characteristic of metallic Pt with face-centered cubic structure (Figure 4.9.). From data summarized in Table 4.3. it can be observed that the higher concentration of sodium hydroxide in the preparation of the catalyst, the smaller Pt crystallite size, which was in agreement with the research

carried out by Baranova et al. [28]. By reducing NaOH concentration to the half, Pt crystallite calculated from XRD (by means of Scherrer equation) was found to double its size. The increase was however less intense when varying NaOH concentration to 0.05 M. On the other hand, chemisorption analyses show that the active particle size remains almost constant despite lowering NaOH concentration to the half. From that point on, a decrease in NaOH concentration to 0.05M causes an increase of the active particle size to the double and, as a consequence, the corresponding chemical active surface is reduced to the half.

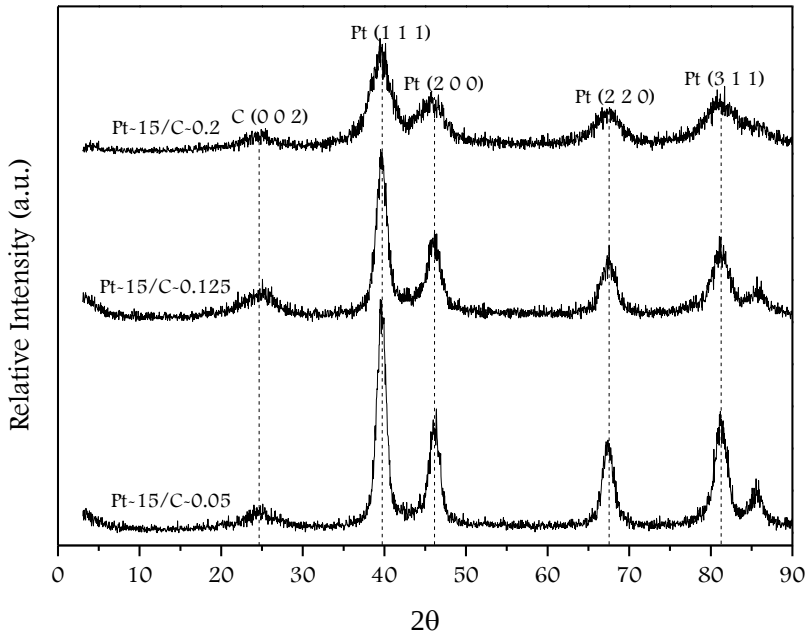

Figure 4.9. XRD patterns of the synthesized Pt-15/C-X catalysts.

Figure 4.10. shows the adsorption/desorption isotherms of the as-prepared catalysts. It can be observed that pH variation does not modify the kind of N_2 adsorption/desorption isotherm, which according to the IUPAC is a combination of types I and IV, presenting the same characteristics described above. However, it should be noted that the higher the concentration of the NaOH, the lower particle size causing a higher decrease of the specific surface area.

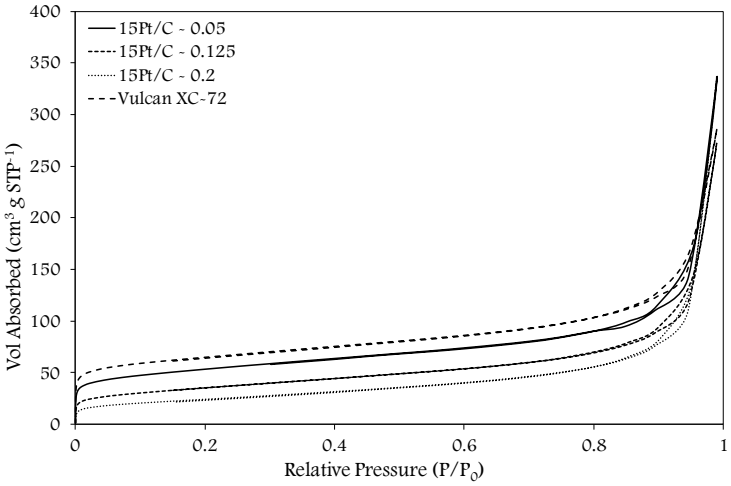

Figure 4.10. Nitrogen adsorption/desorption isotherms of Pt-15/C-X catalysts.

Attending to the pore size distribution (Figure 4.11.), it can be observed that in the case of the Pt-15/C-0.2 catalyst, its pore diameter is noticeably larger compared with Pt-15/C-0.125 and Pt-15/C-0.05. The variation of pore volume also shows the same trend, which is in agreement to the possible blockage of the micropores as explained above for Pt-m/C-X catalysts.

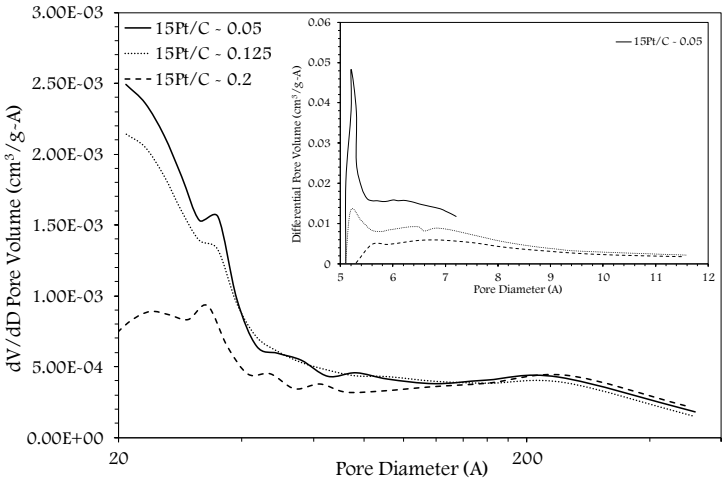

Figure 4.11. Pore distribution of Pt-15/C-X catalysts.

The TPR-H_2 profiles of these samples also fit that commented above. As an example, Pt-15/C-0.2 and Pt-15/C-0.125 catalysts are shown in Figure 4.12. Results show that, similar to the catalyst prepared in the previous study, no peaks are found at temperatures below 200 ºC, suggesting a proper reduction of Pt particles to its metallic state. Only in the case of the catalyst prepared with the highest NaOH concentration a peak between 200-300 ºC can be observed, characteristic of weak interactions between PtOx and the support [31]. However, the peak in a temperature range of 500-600 ºC is common to all the catalysts, corresponding to the gasification of the carbonaceous support and the reduction of platinum complex deposited on the surface of the carbonaceous support as described previously [33-35]. It should be noted that since the control of the pH modifies the active particle size, as expected, those catalysts with smaller particles displace the maxima towards higher reduction temperatures, so it would be more difficult to reduce than those with bigger particles, resulting in a lower concentration of available active species.

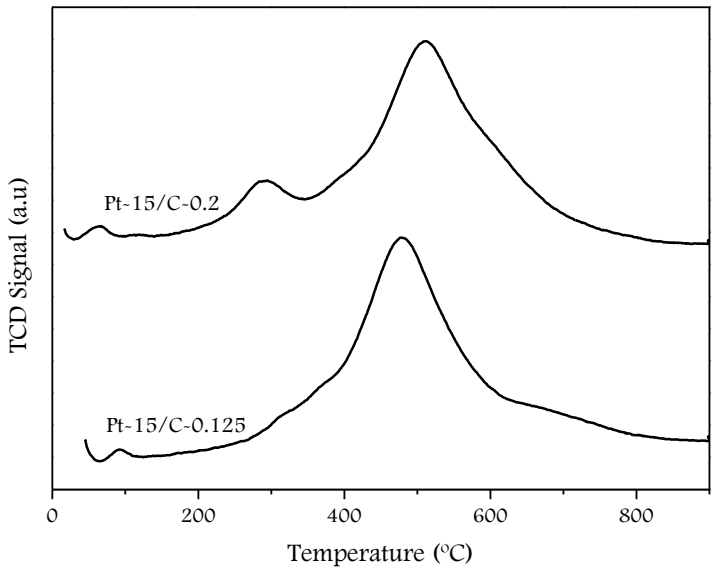

Figure 4.12. Temperature-programmed reduction (TPR) profiles of some of the synthesized Pt-15/C-X catalysts.

Finally, titration tests confirmed the increase of the basic character of the catalysts as a function of the pH used during the synthesis procedure (Figure 4.13).

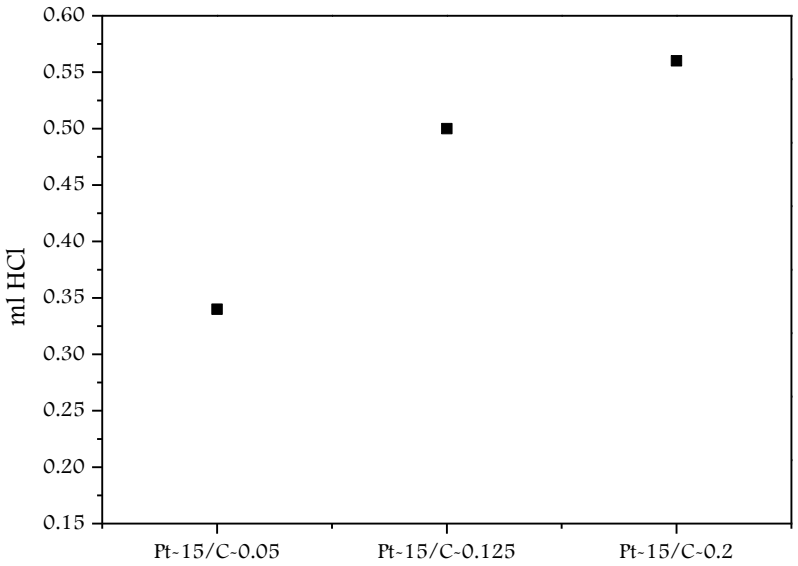

Figure 4.13. Acid-base titration results for Pt-15/C-X catalysts.

3.2.2. Electrochemical characterization of Pt-15/C-X cathodes

Cyclic voltammograms (CV) were recorded for each of the prepared catalysts (condiciones) and the corresponding results are show in Figures 4.14.a, b. and c. The CV profile confirms the presence of polycrystalline Pt for all samples. Taking into account the ECSA values summarized in Table 4.4, it can be seen that, as occurs for the chemical surface, the electrochemical surface area strongly depends on particle size. As reported by Perez et al. [50] the ECSA linearly decreases with increasing Pt particle size. Accordingly, the decrease in the pH of the synthesis procedure, by varying NaOH concentration from 0.2 M to 0.05 M, is found to reduce the ECSA value to the half due to the increase in the particle size.

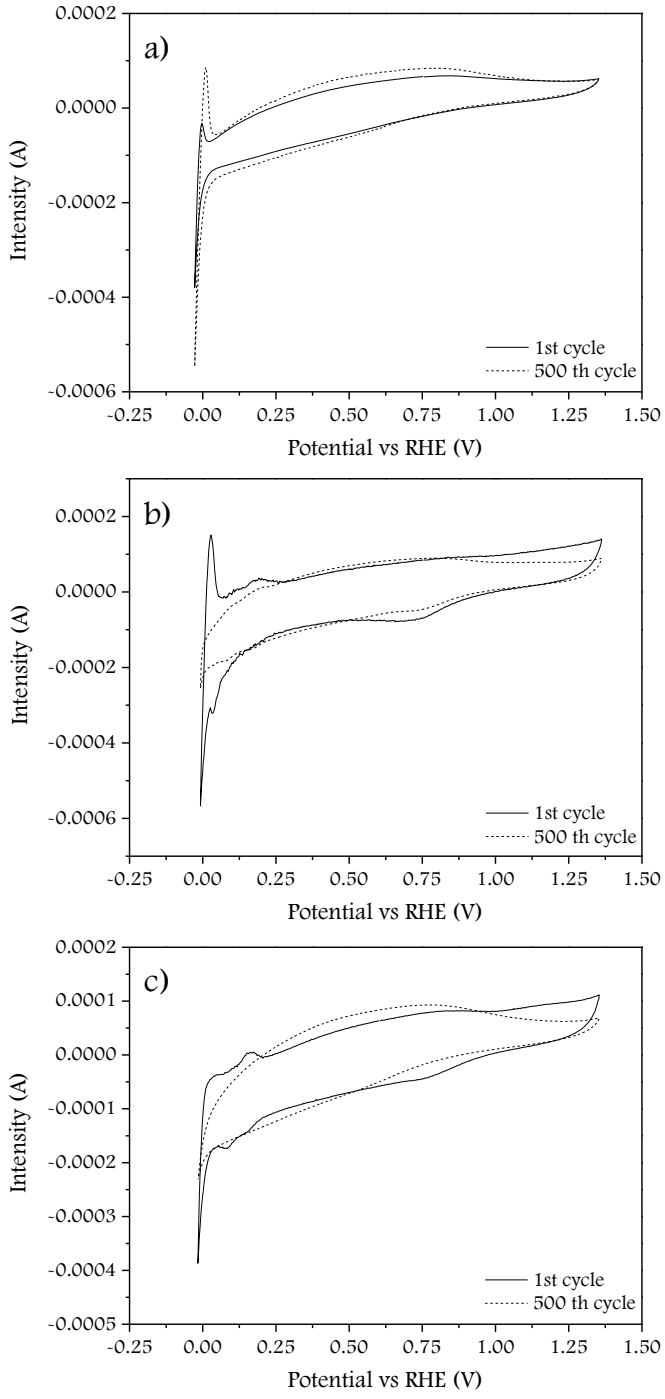

Figure 4.14. Cyclic voltammograms of a) Pt-15/C-0.05 and b) Pt-15/C-0.2 catalysts at 25 °C in 0.1 M $HClO_4$, with a scan rate of 50 mV s^{-1}.

It should be mentioned that the difference between the chemical and electrochemical surface active area can be explained considering that a not negligible part of Pt atoms present on the catalyst surface are not electrochemically active, being not accessible to reactants since they are localized inside the small pores. However, despite of the difference in ECSA values, pH seemed not to affect to the degradation of the catalysts, which was kept almost constant at 56%.

Table 4.4. ECSA and deactivation degree of Pt-15/C-X catalysts.

Catalyst	ECSA 0 cycles ($m^2 \cdot g^{-1}$)	ECSA 500 cycles ($m^2 \cdot g^{-1}$)	Deactivation (%)
Pt-15/C-0.05	18	8	56
Pt-15/C-0.2	35	15	57

3.2.3. Electrochemical hydrogenation of cinnamaldehyde in PEM cell on Pt-15/C-X cathodes

Particle size plays a fundamental role in the electrochemical hydrogenation reaction as an increase in crystallite size would lead to a decrease in the dispersion, thus reducing electrocatalytic activity. This variation in the catalytic activity with the change in size is due to variations at molecular scale including changes in surface structure, electronic state and metal-support interaction. Since the nature of the crystalline planes on the surface of the nanoparticles changes with particle size is imperative that active nanoparticles are as widely dispersed as possible, and with less tendency to the agglomeration during the reactions on the hydrogenation [12, 20, 51, 52].

On the other hand, according to Durndell et al, the variation in the particle size modifies the selectivity, so that an increase in the size of the Pt crystallite would favor the formation of CMO due to the increase of (1 1 1) faces that could block the hydrogenation of the C=C bond, thus

favoring the hydrogenation of carbonyl group [51, 53, 54]. For this reason, it is necessary to find a suitable size that involves a compromise between conversion and selectivity to CMO.

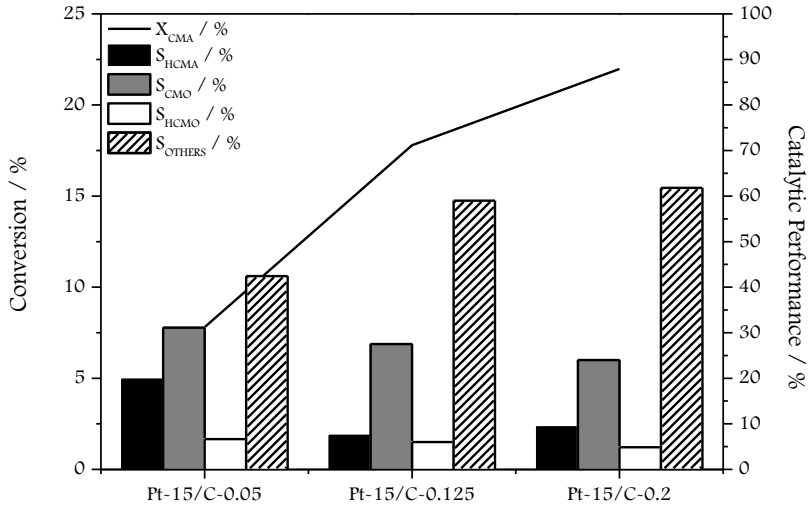

Figure 4.15. Influence of the pH (NaOH concentration) on the electrocatalytic hydrogenation of CMA in a PEM cell. Reaction conditions: Anodic solution: H_2O, Cathodic solution: 100 ppm CMA in 2-propanol, Inlet flow: 1 ml·min^{-1}, Intensity: 0.05 A, Temperature: 70 °C.

Figure 4.15. shows the electrocatalytic results (CMA conversion and selectivity variation) as a function of the NaOH concentration. Due to the presence of the C=C and C=O groups conjugated in the cinnamaldehyde molecule, electrocatalytic hydrogenation results in a mixture of cinnamyl alcohol (C=O bond hydrogenation) and hydrocinnamaldehyde (C=C hydrogenation). Consecutive hydrogenation of both forms hydrocinnamyl alcohol although in a lesser extent. It can be observed that although the selective production of CMO is difficult because the hydrogenation of the C=C bond is thermodynamically favored over that of the C=O bond, in all cases, the proportion of CMO is higher than the proportion of HCMA. This could be due to the use of Pt as active phase and to the catalyst synthesis method

(modified polyol method), which favors a suitable particle size dispersion, geometry and basicity for this purpose. In addition, significant amounts of unwanted by-products are generated by aldolic condensation in the presence of polar solvents, such as 2-propanol, forming acetals. It should be pointed out that these results are consistent with those included in the available bibliography on conventional hydrogenation of cinnamaldehyde, where between 70 and 90 % acetals are obtained under similar conditions (polar solvents and certain acidity) despite working at high pressure [48].

From PEM cell tests and acording to the characterization results, it could be verified that the Pt-15/C-0.05 catalyst provided the lowest conversion but the highest selectivity to CMO, which could be associated to its bigger particle size and lower ECSA value. On the other side, those catalysts synthetized using a NaOH concentration ranging from 0.125 to 0.2 M, whose active particle size were found to be similar, despite of a different basicity, resulted in a similar product distribution. However, the increase in the pH highly modified the electrochemical active surface. As a consequence, conversion was tripled after increasing NaOH concentration from 0.05 M to 0.2 M. Therefore, the catalyst synthesized with a NaOH concentration of 0.2 M and 15 wt. % Pt loading, which presents a suitable particle size and basicity (key parameters to establish a compromise between conversion and selectivity), in addition to a better ECSA value, resulted in the highest CMO yield, despite producing a higher proportion of acetals. It should be also mentioned that, in addition to the reduction in cost resulting from a diminishing of a 5 wt. % in the metallic load, this promising catalyst shows a deactivation degree quite similar to that obtained with the catalyst synthetized with the lowest platinum load.

4. CONCLUSIONS

In this work, the electrocatalytic hydrogenation performance of Pt-based catalysts, synthetized by the modified polyol method, is shown to be strongly influenced by both Pt loading and pH of the synthesis media (controlled by the NaOH concentration). We have investigated the influence of these modifications in physicochemical and electrochemical parameters and finally in the electrochemical hydrogenation of cinnamaldehyde in a PEM cell.

Results have shown Pt loading mainly affects active particle size ad basicity. In this sense, although product distribution resulted to be similar, CMA conversion was strongly influenced by particle size displaying a maximum value at 15 wt. % Pt loading. The choice of a suitable pH to carry out the synthesis of the catalysts seemed to have also a direct influence on the particle size and basicity but, what is more important on the electrochemical active surface. The increase of pH by augmenting NaOH concentration up to 0.2 M reduces particle size to the half, which results in double electrochemical surface area and triple CMA conversion. However, degradation does not vary with NaOH concentration. Therefore, it can be concluded that Pt-15/C-0.2 (5 wt. % Pt lower than the commercial one) is the catalyst that offers a better compromise between conversion and selectivity to the desired products per cell pass in PEM cell.

REFERENCES

1. *Cinnamaldehyde Market Overview*. Available from: https://www.psmarketresearch.com/.
2. *Cinnamic Aldehyde Market to exceed $2 bn by 2024*. Available from: https://www.gminsights.com/.
3. Lashdaf, M., et al., *Behaviour of palladium and ruthenium catalysts on alumina and silica prepared by gas and liquid phase deposition in cinnamaldehyde hydrogenation.* Applied Catalysis A: General, 2003. **241**(1): p. 65-75.
4. Manikandan, D., D. Divakar, and T. Sivakumar, *Utilization of clay minerals for developing Pt nanoparticles and their catalytic activity in the selective hydrogenation of cinnamaldehyde.* Catalysis Communications, 2007. **8**(11): p. 1781-1786.
5. Nagpure, A., et al., *Hydrogenation of cinnamaldehyde to hydrocinnamaldehyde over Pd nanoparticles deposited on nitrogen-doped mesoporous carbon.* RSC Adv., 2016. **6**.
6. Ye, F., et al., *Electrocatalytic properties of Ti/Pt–IrO2 anode for oxygen evolution in PEM water electrolysis.* International Journal of Hydrogen Energy, 2010. **35**(15): p. 8049-8055.
7. Millet, P., F. Andolfatto, and R. Durand, *Design and performance of a solid polymer electrolyte water electrolyzer.* International Journal of Hydrogen Energy, 1996. **21**(2): p. 87-93.
8. Grigoriev, S., V. Porembsky, and V. Fateev, *Pure hydrogen production by PEM electrolysis for hydrogen energy.* International Journal of Hydrogen Energy, 2006. **31**(2): p. 171-175.
9. Bai, Y., et al., *Highly Selective Continuous Flow Hydrogenation of Cinnamaldehyde to Cinnamyl Alcohol in a Pt/SiO2 Coated Tube Reactor.* Catalysts, 2018. **8**(2): p. 58.
10. Malobela, L.J., et al., *Nickel–Cobalt on Carbonaceous Supports for the Selective Catalytic Hydrogenation of Cinnamaldehyde.* Industrial & Engineering Chemistry Research, 2014. **53**(36): p. 13910-13919.
11. Han, X., et al., *Selective Hydrogenation of Cinnamaldehyde over Pt/ZrO2 Catalyst Modified by Cr, Mn, Fe, Co and Ni.* Catalysis Letters, 2006. **109**(3): p. 157-161.
12. Plomp, A.J., et al., *Particle size effects for carbon nanofiber supported platinum and ruthenium catalysts for the selective hydrogenation of cinnamaldehyde.* Applied Catalysis A: General, 2008. **351**(1): p. 9-15.

13. Szatmári, I., et al., *Promoter effect of bicarbonate in hydrogenation of cinnamaldehyde catalyzed by a water-soluble Ru(II)-phosphine complex.* Inorganica Chimica Acta, 2018. **472**: p. 302-306.
14. Li, Y., et al., *Influence of Preparation Modes on Pt–Ni/CNTs Catalysts Used in the Selective Hydrogenation of Cinnamaldehyde to Hydrocinnamaldehyde.* Catalysis Letters, 2008. **126**(3): p. 280-285.
15. Koo-amornpattana, W. and J.M. Winterbottom, *Pt and Pt-alloy catalysts and their properties for the liquid-phase hydrogenation of cinnamaldehyde.* Catalysis Today, 2001. **66**(2): p. 277-287.
16. Li, Y., Z.-G. Li, and R.-X. Zhou, *Bimetallic Pt-Co catalysis on carbon nanotubes for the selective hydrogenation of cinnamaldehyde to cinnamyl alcohol: Preparation and characterization.* Journal of Molecular Catalysis A: Chemical, 2008. **279**(1): p. 140-146.
17. Zhang, Y., et al., *Selective hydrogenation of cinnamaldehyde to cinnamyl alcohol over Au catalysts: influence of the oxide-supports.* Catalysis Letters, 2017. **147**(1): p. 102-109.
18. Song, S., et al., *Confining the Nucleation of Pt to In Situ Form (Pt-Enriched Cage)@ CeO2 Core@ Shell Nanostructure as Excellent Catalysts for Hydrogenation Reactions.* Advanced Materials, 2017. **29**(28): p. 1700495.
19. Coq, B., et al., *Liquid phase hydrogenation of cinnamaldehyde over supported ruthenium catalysts: influence of particle size, bimetallics and nature of support.* Journal of molecular catalysis, 1993. **85**(2): p. 215-228.
20. Durndell, L.J., et al., *Selectivity control in Pt-catalyzed cinnamaldehyde hydrogenation.* Scientific Reports, 2015. **5**: p. 9425.
21. Lee, I., et al., *Tuning selectivity in catalysis by controlling particle shape.* Nature materials, 2009. **8**(2): p. 132.
22. Attard, G.A., et al., *Semi-hydrogenation of alkynes at single crystal, nanoparticle and biogenic nanoparticle surfaces: the role of defects in Lindlar-type catalysts and the origin of their selectivity.* Faraday discussions, 2013. **162**: p. 57-75.
23. An, K., et al., *Preparation of mesoporous oxides and their support effects on Pt nanoparticle catalysts in catalytic hydrogenation of furfural.* Journal of colloid and interface science, 2013. **392**: p. 122-128.
24. Poupin, C., et al., *Effect of Al2O3/MgO molar ratio on catalytic performance of Pt/MgO–Al2O3 catalyst in acetonitrile hydrogenation followed by Fourier transform infrared spectroscopy.* Applied Catalysis A: General, 2014. **475**: p. 363-370.

25. Cao, Z., et al., *Selective hydrogenation of cinnamaldehyde to cinnamyl alcohol over BN-supported Pt catalysts at room temperature.* Applied Catalysis A: General, 2019. **578**: p. 105-115.
26. Dhanagopal, M., et al., *Nanosized Noble Metals Intercalated in Clay as Catalysts for Selective Hydrogenation.* Chinese Journal of Catalysis, 2010. **31**(9): p. 1200-1208.
27. Fuente-Hernández, A., et al., *Reduction of Furfural to Furfuryl Alcohol in Liquid Phase over a Biochar-Supported Platinum Catalyst.* Energies, 2017. **10**(3): p. 286.
28. Baranova, E., et al., *Single-step polyol synthesis of alloy Pt 7 Sn 3 versus bi-phase Pt/SnO x nano-catalysts of controlled size for ethanol electro-oxidation.* Vol. 40. 2010. 1767-1777.
29. Avcioglu, G.S., et al., *High performance PEM fuel cell catalyst layers with hydrophobic channels.* International Journal of Hydrogen Energy, 2015. **40**(24): p. 7720-7731.
30. Li, W., et al., *Preparation and Characterization of Multiwalled Carbon Nanotube-Supported Platinum for Cathode Catalysts of Direct Methanol Fuel Cells.* The Journal of Physical Chemistry B, 2003. **107**(26): p. 6292-6299.
31. Contreras-andrade, I., G. Pérez, and T. Viveros-García, *The Influence Of The Support On The Deactivation Behaviour of Pt-Sn Reforming Catalysts*. Vol. 3. 2005.
32. Kohki, E. and H. Hideshi, *Combined Temperature-Programmed Reduction (TPR)- Temperature-Programmed Desorption (TPD) Study of Supported Platinum Catalysts.* Bulletin of the Chemical Society of Japan, 1991. **64**(8): p. 2422-2427.
33. Pastor-Pérez, L. and A. Sepúlveda-Escribano, *Low temperature glycerol steam reforming on bimetallic PtSn/C catalysts: On the effect of the Sn content.* Fuel, 2017. **194**: p. 222-228.
34. Wang, K.-W. and C.-T. Yeh, *Temperature-programmed reduction study on carbon-supported platinum–gold alloy catalysts.* Journal of Colloid and Interface Science, 2008. **325**(1): p. 203-206.
35. Díaz, J.A., et al., *Carbon nanofibers and nanospheres-supported bimetallic (Co and Fe) catalysts for the Fischer–Tropsch synthesis.* Fuel Processing Technology, 2015. **138**: p. 455-462.
36. Dosso, L.A., C.R. Vera, and J.M. Grau, *Pt-Co and Pt-Ni Catalysts of Low Metal Content for H2 Production by Reforming of Oxygenated Hydrocarbons and*

Comparison with Reported Pt-Based Catalysts. International Journal of Chemical Engineering, 2018. **2018**: p. 10.

37. Leofanti, G., et al., *Surface area and pore texture of catalysts.* Catalysis Today, 1998. **41**(1): p. 207-219.
38. Sing, K.S.W., et al., *Reporting Physisorption Data for Gas/Solid Systems With Special Reference to the Determination of Surface Area and Porosity.*
39. Tan, Y.H., et al., *Surface area and pore size characteristics of nanoporous gold subjected to thermal, mechanical, or surface modification studied using gas adsorption isotherms, cyclic voltammetry, thermogravimetric analysis, and scanning electron microscopy.* Journal of materials chemistry, 2012. **22**(14): p. 6733-6745.
40. Nematollahzadeh, A., M.J. Abdekhodaie, and A. Shojaei, *Submicron nanoporous polyacrylamide beads with tunable size for verapamil imprinting.* Journal of Applied Polymer Science, 2012. **125**(1): p. 189-199.
41. Millán, M., et al., *Enhancement of Electrode Stability Using Platinum–Cobalt Nanocrystals on a Novel Composite SiCTiC Support.* ACS Applied Materials & Interfaces, 2017. **9**(7): p. 5927-5936.
42. Lobato, J., et al., *Composite Titanium Silicon Carbide as a Promising Catalyst Support for High-Temperature Proton-Exchange Membrane Fuel Cell Electrodes.* ChemCatChem, 2016. **8**(4): p. 848-854.
43. Devivaraprasad, R., et al., *Oxygen Reduction Reaction and Peroxide Generation on Shape-Controlled and Polycrystalline Platinum Nanoparticles in Acidic and Alkaline Electrolytes.* Langmuir, 2014. **30**(29): p. 8995-9006.
44. Reyes, P., Rojas, and Hugo, *Hydrogenation of citral over pt and pt-fe/sio2 catalysts.* Reaction Kinetics and Catalysis Letters, 2006. **88**(2): p. 363-369.
45. Toebes, M.L., et al., *Support effects in the hydrogenation of cinnamaldehyde over carbon nanofiber-supported platinum catalysts: characterization and catalysis.* Journal of Catalysis, 2004. **226**(1): p. 215-225.
46. Serrano-Ruiz, J.C., et al., *Hydrogenation of α, β unsaturated aldehydes over polycrystalline, (111) and (100) preferentially oriented Pt nanoparticles supported on carbon.* Journal of Catalysis, 2008. **253**(1): p. 159-166.
47. Ide, M.S., et al., *Mechanistic Insights on the Hydrogenation of α,β-Unsaturated Ketones and Aldehydes to Unsaturated Alcohols over Metal Catalysts.* ACS Catalysis, 2012. **2**(4): p. 671-683.
48. Leng, F., et al., *Selectivity shifts in hydrogenation of cinnamaldehyde on electron-deficient ruthenium nanoparticles.* Comptes Rendus Chimie, 2018. **21**(3): p. 346-353.

49. Wang, D. and Y. Zhu, *An Effective Pt-Cu/SiO2 Catalyst for the Selective Hydrogenation of Cinnamaldehyde.* Journal of Chemistry, 2018. **2018**: p. 7.

50. Perez, J., V.A. Paganin, and E. Antolini, *Particle size effect for ethanol electro-oxidation on Pt/C catalysts in half-cell and in a single direct ethanol fuel cell.* Journal of Electroanalytical Chemistry, 2011. **654**(1): p. 108-115.

51. Oduro, W., et al., *Geometric and electronic effects on hydrogenation of cinnamaldehyde over unsupported Pt-based nanocrystals.* Vol. 13. 2011. 2590-602.

52. Prashar, A.K., S. Mayadevi, and R. Nandini Devi, *Effect of particle size on selective hydrogenation of cinnamaldehyde by Pt encapsulated in mesoporous silica.* Catalysis Communications, 2012. **28**: p. 42-46.

53. Tsang, S.C., et al., *Engineering Preformed Cobalt-Doped Platinum Nanocatalysts For Ultraselective Hydrogenation.* ACS Nano, 2008. **2**(12): p. 2547-2553.

54. Gallezot, P., A. Giroir-Fendler, and D. Richard, *Chemioselectivity in cinnamaldehyde hydrogenation induced by shape selectivity effects in Pt-Y zeolite catalysts.* Catalysis Letters, 1990. **5**(2): p. 169-174.

Section III: Electrocatalytic hydrogenation of cinnamaldehyde: influence of active metals and additives

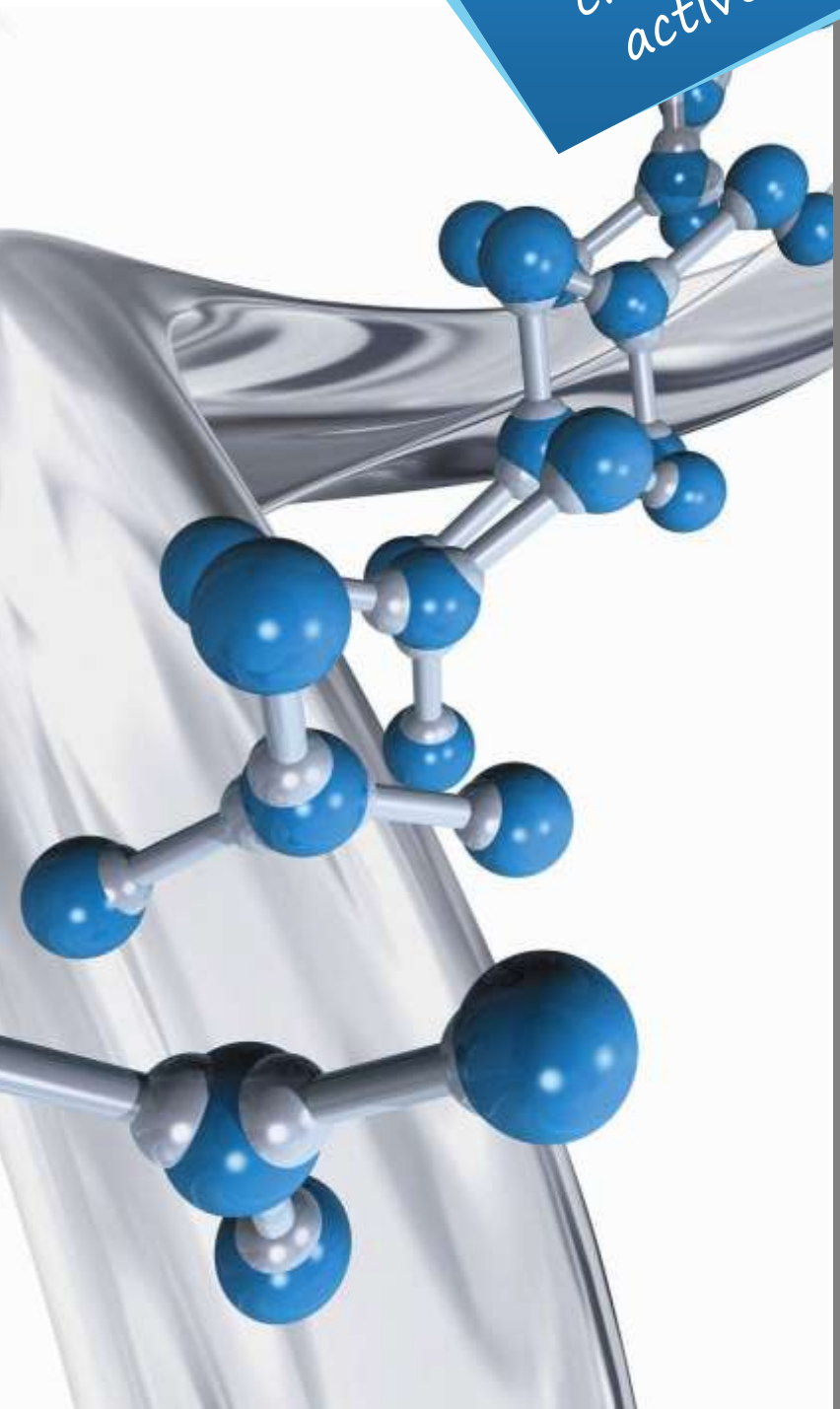

Chapter 5: Bimetallic cathodes for the electrocatalytic hydrogenation of cinnamaldehyde in a PEM cell.

Chapter 6: Bimetallic PtNi/C and PtCo/C cathodes for the selective hydrogenation of cinnamaldehyde in a PEM cell: Influence of the Pt/M ratio and cathodic media additives.

Chapter 5: Bimetallic catalyst for the electrocatalytic hydrogenation of cinnamaldehyde in a PEM cell

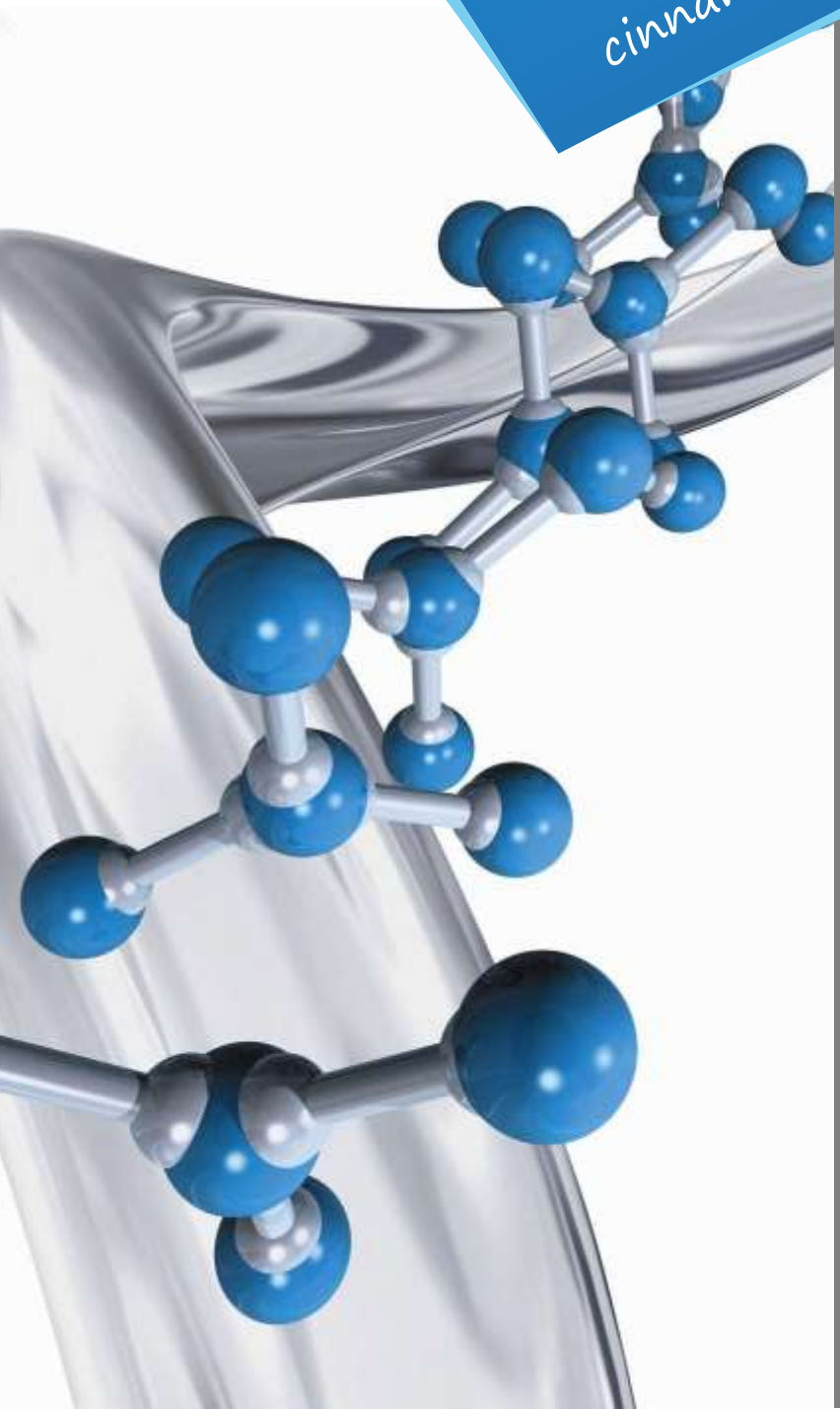

1. INTRODUCTION

2. EXPERIMENTAL
2.1. Catalysts
2.2. Physicochemical characterization
2.3. Electrochemical characterization
2.4. Membrane electrode assembly (MEA) preparation
2.5. Electrocatalytic hydrogenation tests

3. RESULTS AND DISCUSSION
3.1 Physicochemical characterization
3.2. Electrochemical characterization
3.3. Electrocatalytic hydrogenation tests in PEM cell

4. CONCLUSIONS

Abstract

Alloying a second metal in a monometallic catalyst is an efficient way to improve the catalytic performance of hydrogenation reactions. In this sense, Vulcan XC-72-suported PtM (M = Sn, Cu, Ni, Co, Fe) cathodic catalysts were prepared by the modified polyol method in order to explore the effect of the incorporation of a second non-noble metal on the selective electrocatalytic hydrogenation of cinnamaldehyde (CMA) to the corresponding cinnamyl alcohol (CMO). Electrochemical hydrogenation was carried out at mild reaction conditions (1 atm and room temperature, continuous mode) in a PEM cell where H_2 was produced in-situ by water electrolysis. The selectivity of PtM/C catalysts to CMO can be significantly improved by incorporating Co to the catalyst structure due to the presence of cobalt electropositive oxides that may absorb and activate C=O bond. On the other hand, the combination of Ni and Pt minimizes the production of by-products, probably due to the presence of small amounts of Ni^{2+} that favour the CMA hydrogenation to the products of interest.

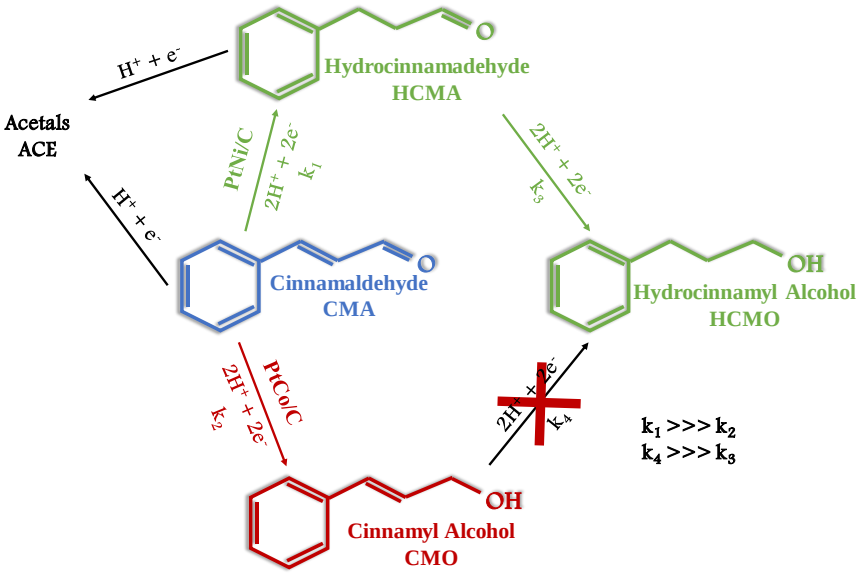

Figure 5.1. *Graphical abstract Chapter 5.*

1. INTRODUCCIÓN

Electrochemical hydrogenation of unsaturated organic molecules in aqueous or mixed aqueous-organic phase is an alternative route to catalytic hydrogenation carried out since the beginning of the last century that present several advantages. Firstly, it is performed under more benign conditions (low temperature and atmospheric pressure) and the chemisorbed hydrogen is produced in situ, at the surface of the catalyst. Furthermore, its generation can be controlled by adjusting the current density, which makes the reaction easier to handle and may also increase the reaction selectivity Secondly, there is no mass transport of poorly soluble molecular hydrogen, the kinetic barrier for its dissociation is bypassed and, in some cases, the adsorption of poisons can be diminished or even prevented by cathodic polarization of the catalyst.

From the point of view of green chemistry, the development of industrial processes for direct production of organic intermediates operating in continuous mode and using heterogeneous catalysts is an industrially meaningful target. Selective hydrogenation of α,β-unsaturated aldehydes to unsaturated alcohols is of great importance for the preparation of various fine chemicals [1-4]. In this sense, selective hydrogenation of cinnamaldehyde (CMA) to cinnamyl alcohol (CMO) is a representative example of such reactions, which is known to be influenced by different factors such as pressure, temperature, solvent nature and promoters as well as others related to the process conditions. Compared to the traditional method (where reductants such as aluminum benzylcoxide are used to reduce CMA), the electrocatalytic hydrogenation method is superior in saving resources, reducing waste disposal and protecting the environment [5, 6]. Nevertheless, besides the competing hydrogenation pathways of α,β-unsaturated aldehydes through the C=C bond (to produce the saturated aldehydes) and the

carbonyl group (to produce unsaturated alcohols), CMA may form other by-products such as hydrocinnamaldehyde (HCMA) and hydrocinnamyl alcohol (HCMO). In many cases, by-products such as acetals and other unidentified high molecular weight compounds may also be produced in large quantity [3, 7-9]. Hydrogenation of the C=C bond is thermodynamically more favorable, and hence research efforts have been directed at improving the selectivity to the more desirable unsaturated alcohols [10]. In this sense, many methods have been developed to improve the catalytic performance, such as screening several transition metals [11], supports [12, 13] and promoters [8, 14].

Generally, suitable materials such as carbon have been widely used as support for Pt based catalysts in the hydrogenation of α,β-aldehydes. However, carbon Vulcan XC-72, which is a conventional electrode support is not such conventional for hydrogenation reactions. Pt catalysts has been long considered in the production of adsorbed atomic hydrogen to be added to unsaturated bonds. Hence, it is well known as a typical catalyst for the selective hydrogenation of cinnamaldehyde [11-13] and has still been widely used as the first option for the catalyst compared to other candidates. However, besides high overpotential, the Pt catalyst has other inconvenient like expensive cost, decrease in catalytic activity by CO poisoning and short catalytic stability [15-18] and it is necessary to modify its characteristics either by addition of a second metal, by support effects, or by modifications in the crystallite size to shift the selectivity toward C=O hydrogenation. Therefore, one promising approach to enhance the catalytic properties of Pt nanoparticles which has show growing attention is to introduce a second metal (or metal oxides) to form bimetallic catalysts.

Many attempts has been made to promote the selective hydrogenation of α,β- unsaturated aldehydes by taking advantage of the synergistic effects of bimetallic catalysts using metals as Fe, Co, Cu or Ni [15-23]. The 3D-Pt bimetallic catalysts often show properties that differ clearly from those of their parent metals, offering the opportunity to obtain novel catalysts with enhanced activity and/or selectivity [15, 24-26]. Specially, noble metal-based bimetallic catalysts with promoters like Co or Ni exhibit high activity and selectivity for CMO and HCMA in the conventional catalytic route, respectively [27, 28]. In a bid to synthesize the bimetallic alloying, several methods such as impregnation, polyol, solvothermal, sputtering and nanoencapsulation have been tried [16, 23, 29, 30]. However, determining proper bimetallic catalyst structure and synthetic route has not been completed yet. Therefore, the aim of the present work is to explore the properties of PtM/C cathodes (C: carbon Vulcan XC-72 and M: Fe, Co, Ni, Cu and Sn, respectively) on the electrohydrogenation of cinnamaldehyde, conducted in a PEM reactor, especially in terms of C=O hydrogenation. In addition to the physicochemical characterization techniques such as X-Ray diffraction, H_2-temperature-programmed reduction (TPR), N_2 adsorption /desorption or acid base titration, electrochemistry measurements including cyclic voltammetry (CV) and HER/HOR linear sweep voltammetry are also applied to understand the catalytic behavior and bimetallic effects.

2. EXPERIMENTAL

2.1. Catalysts

The carbon supported PtM (M = Sn, Cu, Co, Ni, Fe) catalyst (PtM/C) were prepared by modified polyol method, using ethylene glycol (Sigma-Aldrich, Germany) as described in Section B.2.3. In an initial step, proper amounts of hexachloroplatinic acid (H_2PtCl_6) and M metal precursors

(tin (II) chloride dihydrate for Sn, copper (II) chloride for Cu, cobalt (II) chloride hexahydrate for Co, nickel (II) chloride hexahydrate for Ni, and Iron (III) chloride for Fe) were dissolved in 50 ml of ethylene glycol (99 % Sigma Aldrich) containing 0.2 M of NaOH (99.8 %, Panreac, Spain) with pH = 11. The solution was stirred for 1 hour at room temperature and heat to 190 °C for 2 h. Then, the solution was cooled to room temperature. After that, the support was added to the solution under stirring up to 24 hours. After finishing the stirring, the solution was filtered and was washed several times with deonized water, and the remaining powders were dried at 80 °C oven for 12h. The resulting catalyst were denoted as PtSn/C (55%wt Pt), PtCu/C (55%wt Pt), PtCo/C (55%wt Pt), PtNi/C (65%wt Pt) and PtFe/C (60%wt Pt), it has been verified by ICP that these metals conform to the above-mentioned proportion.

2.2. Physicochemical characterization

In order to analize Pt content, an inductively coupled plasma spectrometer (ICP, Model Liberty Sequential, VARIAN) was used. Surface area/porosity measurements were collected in a Micromeritics ASAP 2010 sorptometer unit, with N_2 at 77 K as the adsorbate. Acid-base titrations were carried out in order to know the properties of the catalyst and support performed on a SCHOTT Titroline apparatus. XRD analyses were performed on a Phillips PW-1700 diffractometer using nickel-filtered Cu Kα radiation in order to check species present in the catalyst, and also to calculate particle size. In addition, temperature-programmed reduction (TPR) experiments were conducted in a Micromeritics AutoChem 2950 HP unit.

2.3. Electrochemical characterization

Electrochemical characterization was performed by means of cyclic voltammetry experiments carried out in a computer-controlled potentiostat Autolab PGSTAT128N (Ecochemie, The Netherlands), using a single cell of three-electrode system (see Section B.5.) in order to measure the electrochemical surface area (ECSA) and deactivation degree of the catalysts [31]. Additionally, polarization curves were also conducted from 500 to 3000 rpm, by applying a potential range between 0.2 and 0.7 V (vs RHE) (5 $mV \cdot s^{-1}$ scan rate) in order to study the kinetics of the Hydrogen Evolution Reaction (HER/HOR).

2.4. Membrane Electrode assembly (MEA) preparation

For the preparation of the Membrane Electrode Assembly (MEA) inks containing catalysts solutions and Nafion ionomer were sprayed directly to the pretreated Nafion ®115 membrane. For the anodic ink, a commercial IrO_2 solution (diluted in water) was used with a fixed loading of 2 $mg \cdot cm^{-2}$ while the synthesized cathodic PtM/C catalysts (diluted in 2-propanol) were used in the electrochemical PEM cell with 0.5 $mg \cdot cm^{-2}$ loading.

2.5. Electrocatalytic hydrogenation tests

Electrocatalytic hydrogenation experiments (100 ppm of CMA in 2-propanol, 1 $mL \cdot min^{-1}$ feeding rate) were carried out at ambient pressure, 70^{o}C, using a Polymer Electrolyte Membrane (PEM) described in detail in Section B.7. [32].

3. RESULTS AND DISCUSSION

3.1. Physicochemical characterization

First, Pt and M (Co, Ni, Cu, Fe and Sn) proportion was determined to fit to the setting value by means of ICP. Then, the synthesized cathodes were characterized in terms of composition and morphology. X-ray diffraction patterns of PtM/C electrocatalysts are shown in Figure 5.2.

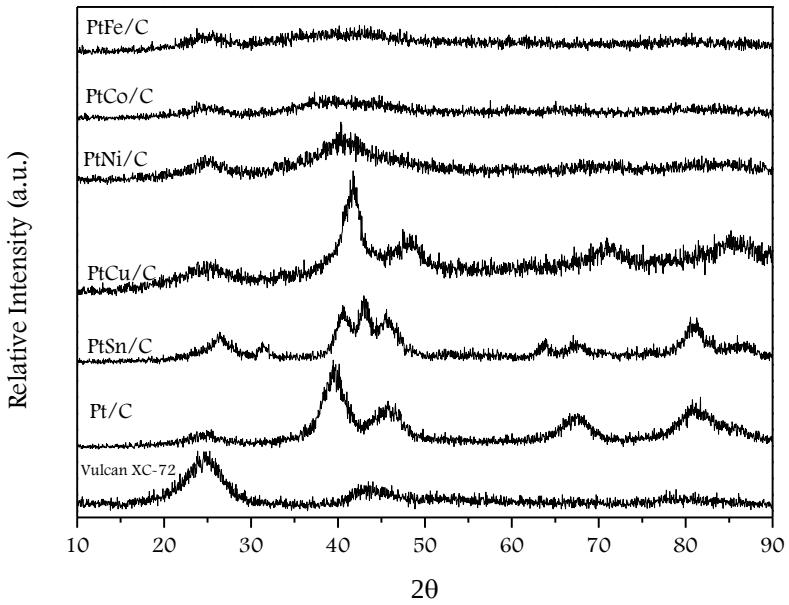

Figure 5.2. XRD patterns of the synthesized PtM/C catalysts and the support.

Diffraction peaks at 2θ: 25-30° and 43° observed in all patterns of the carbon supported catalysts are attributed to the (0 0 2) and (1 0 0) planes of hexagonal structure of amorphous Vulcan XC-72 support. In the diffractograms corresponding to Pt/C and PtM/C the first reflection, attributable to the nature of the support, is also observed. However, that corresponding to the (1 0 0) plane cannot be appreciated due to overlapping with the characteristic reflections of metal species. After impregnation and reduction following the modified polyol method,

peaks located at 39°, 46°, 67° and 82° correspond to the face-centered cubic (fcc) (1 1 1), (2 0 0), (2 2 0) and (3 1 1) Pt crystalline planes, respectively [15].

As evidence from Figure 5.2, the addition of Sn to Pt shifts Pt peaks from 39°, 67° and 82° to lower diffraction angles (38°, 66° and 79°) due to the extent of the fcc lattice parameter. Beside Pt reflections, peaks at 30.5°, 41.5°, 44° and 62.2° can be indexed to crystalline Sn (JCPDS card no.86-2264) (2 0 0) plane and Pt-Sn (1 0 2), Pt-Sn (1 1 0) and Pt-Sn (2 0 2), respectively (JCPDF-250614), which may confirm the formation of pure crystalline Sn metal and Pt-Sn alloy to some extent [33-35]. Note that no peaks belonging to SnO or SnO_2 can be observed. Compared to Pt/C, it can be seen that the incorporation of Ni results in the shift and widening of Pt plane (1 1 1) to a higher angle while Pt planes (2 0 0), (2 2 0) and (3 1 1) disappear, which suggests a decrease in particle size and a narrow size distribution in a disordered form. In case of the bimetallic catalysts PtFe/C and PtCo/C, this effect was even more evident, making any characteristic reflex indistinguishable, which hinders the estimation of particle size using this technique. In addition, no obvious peaks that correspond to the presence of free M or platinum and M oxides species were observed in the XRD patterns, which suggests Fe and Co were involved in the formation of PtM alloy after polyol-reducing treatment. The diffraction peaks of the PtCu/C and PtNi/C alloyed catalysts shift to higher angles as compared to that of Pt/C, indicating a lattice contraction arising from the substitution of the larger Pt atoms for the smaller Cu or Ni atoms. All the XRD peaks can be indexed as face-centered cubic (fcc) structure. However, it is assumed that PtNi/C has a disordered phase of face-centered cubic structure, where Ni and Pt atoms are randomly located at the corner and face-centered positions, since the shoulder at $2\theta = 70^{o}$ is not present in the XRD pattern [36]. In case of PtCu/C

typical fcc metallic crystalline planes were observed at 2θ: 43.5°, 50.3° and 74.1°, respectively. Interestingly, besides the broadened peaks (indicating the smaller particle size of the Cu nanoparticles) the high purity of the sample was verified through the absence of oxide, hydroxide, and precursor reflections within the detection limit of the XRD measurements.

The above observations are consistent with those of literature where it is reported that, taking into account the different atomic sizes (R_{Co}= 0.125 nm, R_{Ni}: 0.124 nm; R_{Fe}: 0.126 nm and R_{Cu}: 0.128 nm), the incorporation of smaller atoms results in the contraction of the Pt crystallite net (by contraction of Pt-Pt bond distance; R_{Pt} = 0.139 nm) unlike Sn (R_{Sn}: 0.141 nm), which expands the unit cell due to the larger atomic radius. Therefore, due to the solubility of M in the face-centered cubic Pt lattice the alloy lattice parameter is modified compared to that of pure Pt (Pt = 0.392 nm) [37-39].

Pt (2 2 0) was selected to calculate the particle size and the crystalline lattice parameters of Pt in order to avoid the disturbance of C and M, which have no peaks at around this angle. The degree of alloying related to each catalyst was calculated by means of Vegard´s law [15, 25, 26]. According to the law, in the XRD pattern of PtM/C, the Pt (220) peak was selected for the determination of lattice parameter that was one of requisite factors to calculate alloying degree of the PtM/Cs because the peak was far from the background signal of carbon support [15, 26, 40]. The lattice parameter ($a_{(220)}$) of PtM/C was initially obtained by a combination of the Pt (220) peak position (θ_{max}) and the wavelength of Cu K_α radiation ($\lambda_{k\alpha}$).

$$a_{(220)} = \frac{2^{0.5} \cdot \lambda_{K\alpha}}{\sin \theta_{max}} \qquad \text{[Ec. 5.1]}$$

In turn, the alloying degree of each PtM/C catalyst was expressed as a function of (i) Pt atomic fraction (X_{Pt}) in PtM/C and (ii) nominal Pt/M atomic ratio ($(Pt/M)_{nom}$) that were attained by the lattice parameter with the following equations.

$$a(220) = 3.8013 + 0.124 \cdot X_{Pt} \qquad \text{[Ec. 5.2]}$$

$$\text{Alloying degree} = \frac{X_{Pt}}{(1 - X_{Pt}) \cdot (Pt/M)_{nom}} \qquad \text{[Ec. 5.3]}$$

Table 5.1. summarizes the Pt (2 2 0) peak position, average particle size, alloying degree and lattice parameter of the PtM/Cs catalyst used in this work. From data collected in Table 5.1. the average particle size of catalysts synthetized using the modified polyol method was found to be 6 nm for Pt/C and slightly higher for PtSn/C and PtCu/C, being close to 10 nm. Note that in case of the catalysts PtNi/C, PtCo/C and PtFe/C, particle size could not be calculated due to the small size of the crystallites.

Table 5.1. Physicochemical properties of PtM/C bimetallic catalysts.

Catalyst	2θ (degree)	Alloying Degree (%)	$a_{(220)}$ (nm)	XRD Particle size (nm)[1]	BET surface area ($m^2 \cdot g^{-1}$)	Pore volume ($cm^3 \cdot g^{-1}$)	Average pore diameter (nm)[2]
Pt/C	67.6	-	0.392[3]	6	85	0.548	24.4
PtSn/C	65.6	6	0.394	9	84	0.367	16.2
PtCu/C	70.9	9	0.376	8	114	0.559	18.3
PtNi/C	68.9	42	0.385	-	115	0.485	15.5
PtCo/C	68.5	54	0.388	-	156	0.555	13.3
PtFe/C	68.8	49	0.386	-	97	0.439	16.9

[1] Calculated from the Pt (220) peak (67°) using the Debye-Scherrer equation.
[2] Calculated assuming cylindrical pore geometry.
[3] [38]

Regarding the lattice parameter, compared to of bulk Pt (3.92 A), Pt lattice parameter was extended with the addition of Sn to the Pt net and reduced after the replacement of Pt by smaller-sized Cu, Co, Ni or Fe, which indicates a moderate degree of alloying being slightly shorter for PtCu/C and PtSn/C.

Table 5.1. also shows the main physicochemical properties of the catalyst used in this work. The textural parameters (BET surface area, pore volume and diameter) were evaluated by N_2 adsorption-desorption measurements.

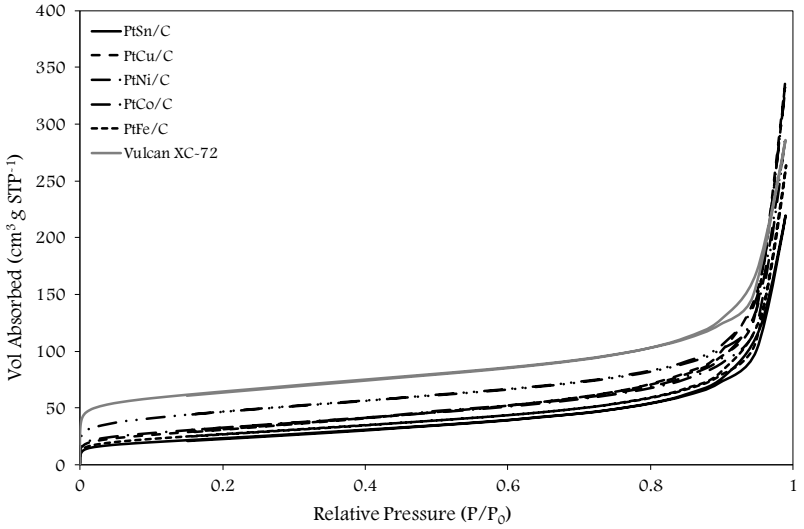

Figure 5.3. Nitrogen adsorption desorption isotherms of the PtM/C catalysts studied.

Isotherms of the support and PtM/C catalysts can be seen in Figure 5.3. All isotherms showed a type I-IV adsorption-desorption profile, according to the IUPAC classification, associated to a mesoporous structure with microporous. Firstly, especially in case of the support sample, the N_2 adsorption volume increased sharply in the micropore region at very low partial pressures ($P/P_0 < 0.005$) because of the strong interaction between the pore walls and adsorbate. Then, at high relative

pressures the adsorption in mesopores leads to multilayer adsorption and give a sharp adsorption volume increase. This fact was corroborated with the hysteresis loop observed in the multilayer range of physisorption isotherms, which is ascribed to the capillary condensation that takes place on mesopores and associated with their different filling and emptying, and characteristic of pores with uniform size and shape [41-43]. In all cases, it was observed that, once the metal precursor was deposited in the support (231 $m^2 \cdot g^{-1}$, 0.408 $cm^3 \cdot g^{-1}$ total pore volume and 7.7 nm average pore diameter), the specific BET surface area experienced an important decrease in contrast with pore volume and diameter. This fact could be attributed to the pore blockage by the metal particles, which prevent N_2 molecules to be adsorbed on them, and with the deposition of the metal particles on the micropores.

TPR analysis was performed in order to determine the oxidation state of platinum and M nanoparticles present on the surface of the catalyst. Figure 5.4. shows the TPR analyses for the synthesized Pt/C, PtM/C catalysts and carbonaceous support. It can be observed that in all the catalysts samples consumption peaks have been displaced to lower temperatures compared to those of carbon Vulcan XC-72 as a result of the catalyzed decomposition of functional groups of the support in presence of metals (e.a. the formation of CH_4 or derivatives of volatile organic compounds adsorbed on the support). The support profile also revealed the presence of basic or weakly sites that would interact with hydrogen at high temperatures but in the range were CO desorption would not occur. On the monometallic Pt/C catalyst two reduction peaks centered at 290°C and 530°C were observed which were found to correspond to the reduction of deposited platinum complex and oxygenated groups on the surface of the carbonaceous support that are not located near metallic particles [44]. On the bimetallic catalysts,

especially those of PtCu/C and PtSn/C, similar patterns were obtained although shifted to higher reduction temperatures. As can be seen in Figure 5.4., PtSn/C and PtCu/C, which present the biggest particle size, need lower H_2 consumption to be reduced. Note that no reduction of ionic Sn species, which would occur at higher temperature, was observed. However, a small fraction of metallic Sn species could be also present and less retained over the support surface as postulated by Stassi et al. [45], allowing the possible alloy formation (as evidenced by XRD). On the other hand, profiles related to carbon supported PtFe, PtCo and PtNi catalysts show a displacement of the hydrogen consumption peaks (referred to the parent Pt/C) due to the interference of Ni, Fe and Co ions and exhibit larger H_2 consumptions, especially at temperatures lower than 400°C, which is indicative of alloy particles formation, the correduction of part of Pt and M species and to the hydrogen spillover from reduced Pt^0 onto the support [46, 47].

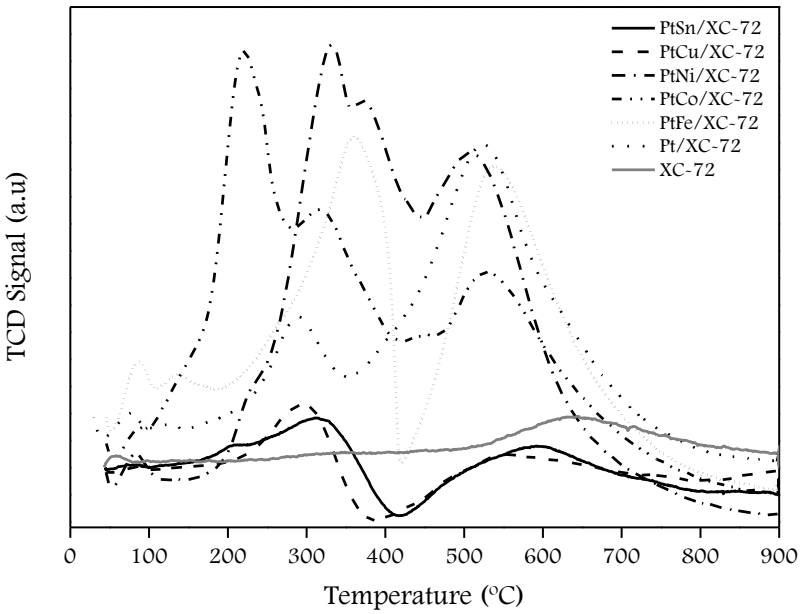

Figure 5.4. Temperature-programmed reduction (TPR) profiles of the synthesized PtM/C catalysts and the support.

It is known that due to the interaction between Pt and Co, Pt used to form a shell and the peak for Pt reduction shifts towards higher temperature. As seen from TPR profile, for PtCo/C, the maximum H_2 consumption observed at 200-400 °C may be the result of the reduction of a PtCo alloy or the correduction of Pt particles, capable of providing dissociated hydrogen to reduce nearby CoO phases [48-51]. It is noteworthy that despite no characteristic diffraction peaks of the cobalt oxide species or even metallic cobalt were indicated in Figure 5.2., their presence could not be dismissed. Such phases (low amount) would be either amorphous or small crystals (nanosize scale), which precludes their detection from XRD. In case of PtNi- and PtFe/C, first hydrogen consumption maximum was also shifted to higher reduction temperatures after M incorporation. For PtNi/C, the presence of Ni^{3+} can be excluded since the characteristic reduction peak at 260 °C does not appear [7]. The peak at 300-400°C can be attributed to the reduction of PtNi or PtFe alloy or NiO particles catalysed by the presence of Pt in the vicinity with no interaction with the support [52, 53]. The increase of the first maximum area after M incorporation suggests a strong interaction between Pt and M, which would increase the activated hydrogen number and improve the selectivity of CMA to HCMA.

The acid-base character of the support and the corresponding PtM-based cathodic catalysts were evaluated by acid-base titration (Figure 5.5.). As expected from characterization results commented above, all samples exhibited basic character since they required more volume of HCl than that of the blank solution to reach the equivalence point. However, the addition of a second metal has a great influence on the acid-basic catalyst character. PtM/C samples were more basic than the carbonaceous support unlike PtCu/C, which was shifted towards the corresponding blank one revealing a partial neutralization of the basicity of the support. Then, the basic character increased in the following order

attending to the consumed HCl (mL) per gram of metal in the catalyst sample to achieve a pH ≤7: PtCu/C < PtCo/C < PtSn/C < PtNi/C < PtFe/C < Pt/C.

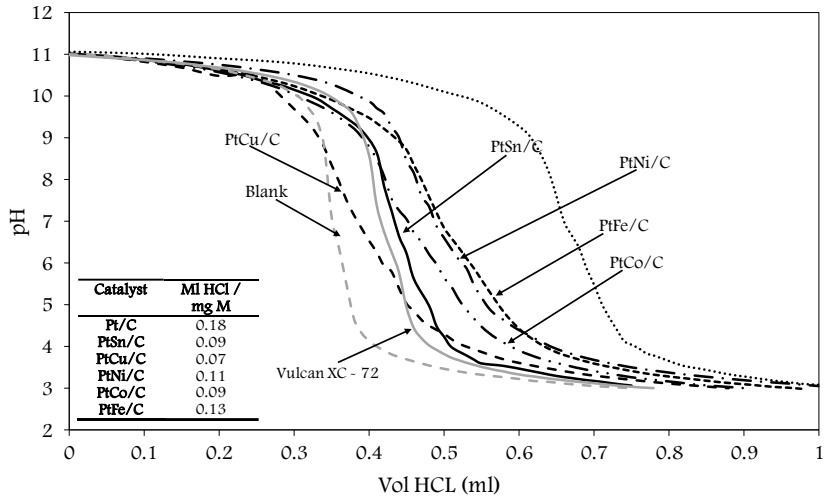

Figure 5.5. Acid-base titration curves.

Taking into account characterization results commented above, it is interesting to mention that the modified polyol method allowed to obtain alloy PtM-based catalysts with the same metal loading, nearly the same structure and small particle size and a good dispersion. Hence, under these conditions, it is suitable to compare their catalytic activity for the direct electrohydrogenation of CMA in a PEM reactor.

3.2. Electrochemical characterization

To achieve complete characterization ex situ RDE (Rotating Disk Electrode) evaluation of each cathodic electrode was carried out. The activity of Pt/C and the effect of the incorporation of a second metal (M: Sn, Cu, Ni, Co and Fe) were determined by cyclic and linear sweep voltammetry (CV and LSV, respectively). Figures 5.6. and 5.8. report the detailed cyclic voltammetry and linear sweep voltammetries at different rotation rates measurements for Pt/C and PtM/C, respectively.

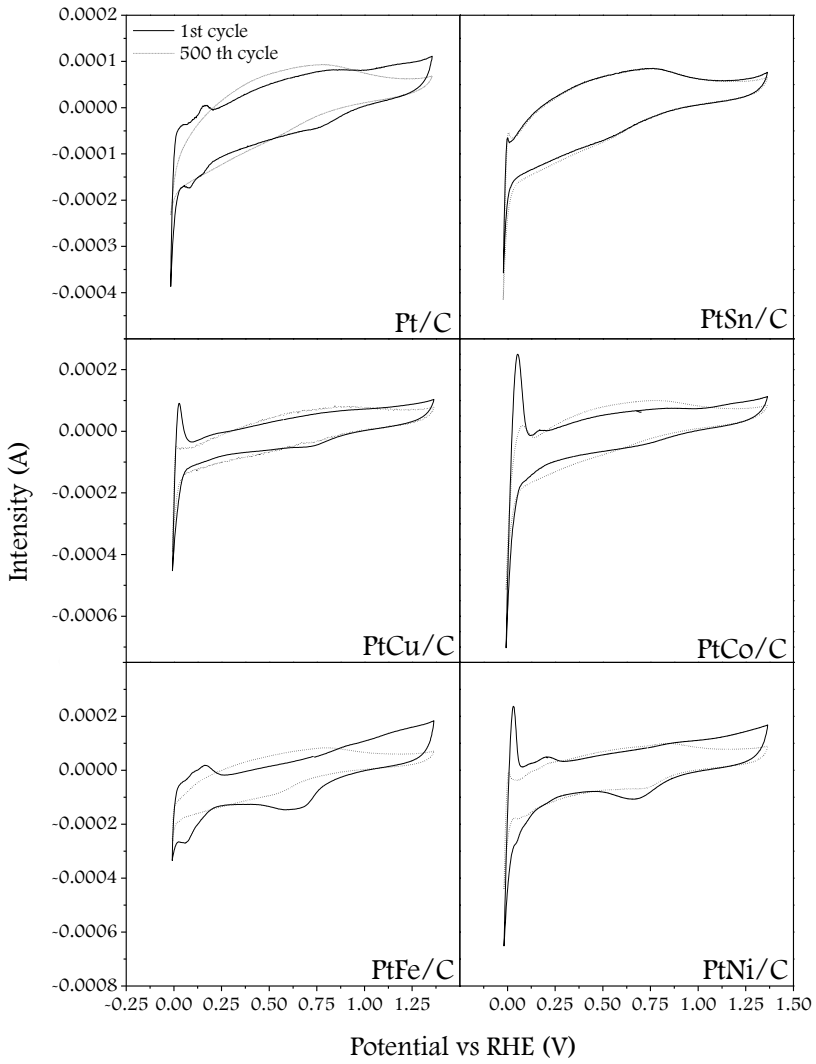

Figure 5.6. Cyclic voltammograms of PtM/C catalysts in 0.1 M $HClO_4$, with a scan rate of 50 mV s^{-1} at 25 °C

First, the electrochemical active surface area (ECSA) for each cathode was compared and its loss was evaluated in acidic media through an accelerated degradation test to simulate the stability of the electrocatalyst (Figure 5.6.). Figure 5.6. shows the cyclic voltammograms related to reference Pt/C and each PtM/C sample between 0.05 and 1.3 V vs RHE (50 mV s^{-1} scan rate). Sequential cyclic voltammetry (500 voltage cycles) in deaerated $HClO_4$ (0.1 M) electrolyte was carried out at

room temperature in order to measure the long-term behavior of the synthetized cathodic Pt-and PtM-based electrodes. From CV profiles, the hydrogen adsorption/desorption peaks and oxidation/reduction peaks of the Pt surface on Pt can be observed. The cathodic scan exhibits platinum reduction peaks between 0.5 and 1.0 vs RHE, whereas hydrogen was desorbed at a potential below 0.4 vs RHE.

CV curves display (1 1 0) and (1 0 0)/(1 1 1) Pt crystal face planes. However, (1 0 0) and (1 1 1) peaks may overlap generating a single peak that corresponds to (1 0 0) facet due to its higher activity. A more intense (1 1 0) peak can be seen in case of PtCu/C, PtNi/C and PtCo/C which, as reported by Delbecq et al. can disfavour the hydrogenation selectivity towards the compounds of interest by leading hydrogenation towards undesirable compounds [54]. It can be also observed that the oxidation of PtM/C slightly shifts to higher potentials than Pt/C, which may suggest that their surface is oxidized easily than that of M-free cathode.

On the other hand, the oxidation of the carbon surface on carbon Vulcan XC-72 (in aqueous acid electrolytes) occurs at a potential close to 0.6 V (vs. RHE). However, that fact was not observed after 500 cycles indicating that no surface oxidation occured. Moreover, Pt/C and PtM-alloy-based catalysts present a similar double layer, suggesting that all samples have the same resistances to charge transfer. Note that the shape of the double layer does not significantly varied after 500 cycles suggesting that the catalysts should be stable unlike for PtFe/C. However, the higher double layer contribution for PtSn/C and PtCo/C catalysts could mask part of the H_2 adsorption/desorption peak diminishing the experimentally observed active area.

During consecutive potential cycling, both the anodic and cathodic number of cycles increased, the area of adsorption/desorption

peaks above mentioned (see Figure 5.6.) decreased, which revealed a loss of electrochemical surface area as a result of polarization of the catalysts in acid media or the dissolution of small amounts of Pt and or M (e.g. Co and Ni) from the electrode surface under the experimental conditions. From CV characterization results, PtNi/C was found to have the largest electrochemical surface area this may be due because the PtNi/C catalyst has the highest platinum percentage compared to the other catalysts (65% Pt, 35% Ni) [55]. Regarding to the deactivation of the catalysts, PtCu/C, which presents a higher crystallite size combined with alloy formation may be beneficial for achieving higher stability than PtNi-, PtFe or PtCo-based cathodes. However, after incorporation of the transition metal, the surface area becomes smaller since part of platinum in the surface is replaced by M, despite the crystal size reduction (due to alloy formation) may increase the availability of active centers for oxygen adsorption, which would derive in a suitable ECSA value [56].

Figure 5.7. shows the loss of electrochemical surface (EAS) for the Pt/C and PtM/C cathodes. According to the CVs, loss in EAS of the catalysts consecutively occurred with run of CV and after 500 cycles unlike for PtCo/C sample, which presented an increase of EAS from the first and after 100 cycles. This gain in ECSA can be linked to a temporary enhancement in platinum dispersion by surface atoms or Pt particle rearrangement. In any case, relative EAS (present EAS/ initial EAS) of PtM/Cs descends in the following order: PtCu/C > PtCo/C > PtC/C > PtNi/C > PtSn/C > PtFe/C, which means that PtCu/C have better long-term stability (lifetime) than the rest of bimetallic catalyst. However, the normalized ECSA loss and curve trend is very similar for Pt/C and PtCu/C and PtCo/C based catalysts and indicate a similar behavior of degradation of both catalysts. In the other hand, the observed ECSA decrease in the PtNi/C catalyst may be due to the particle dealloying and the consequent nickel leaching and agglomeration of the nanoparticles

during electrochemical cycling [57]. For PtSn/C, despite of its higher crystallite size, the observed ECSA decrease after Sn incorporation may be caused by the amount of Nafion used to prepare the ink, which may negatively influence on the observed ECSA due to its interaction with Pt that affects to the H_2 adsorption-desorption.

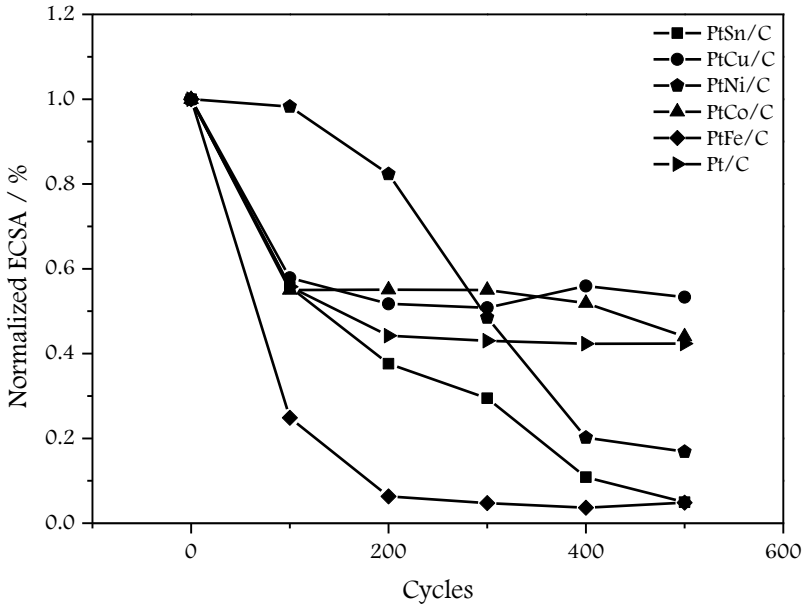

Figure 5.7. Normalized ECSA as a function on the number of cycles.

Hydrogen evolution/oxidation reactions (HER/HOR) were also studied. Electrocatalytic hydrogenation of organic molecules and hydrogen evolution reaction (HER) are competitive reactions [58, 59]. Therefore, HER/HOR catalytic reaction were studied by LSV in order to determine the HER contribution for each PtM-based cathode. As oxidation and evolution hydrogen reaction cannot be studied separately, measured current was calculated as the sum of the anodic (HOR) and cathodic (HER) currents, according to the equation:

$$i = i_{HOR} + i_{HER} \qquad \text{[Ec. 5.3]}$$

For the Koutecky-Levich plot the rotation speed on linear sweep voltammetries was varied in a range between 500 and 3000 rpm. LSV were conducted at room temperature in dilute perchloric acid saturated with H_2 gas in order to obtain RDE hydrodynamic parameters.

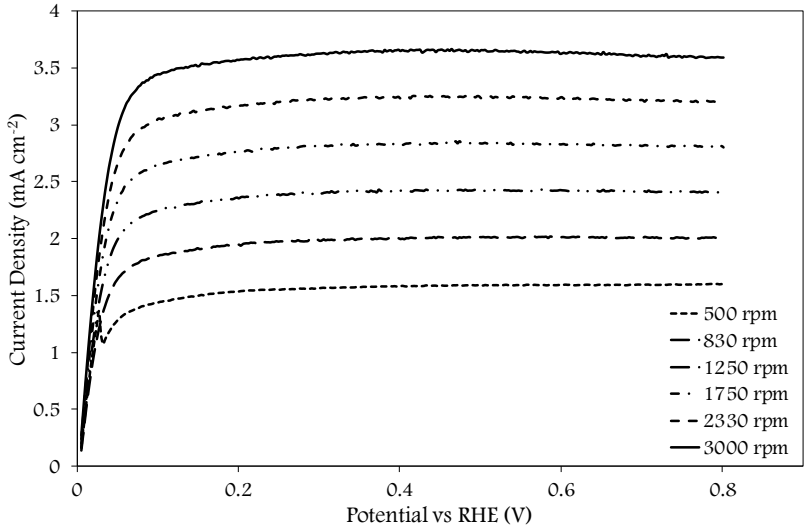

Figure 5.8. Polarization curves for PtFe/C catalyst (5 mV·s^{-1} scan rate) in H_2 saturated.

The plot of 1/j vs. $\omega^{-1/2}$ (not shown here) was linear and the fits run parallel, which suggests a similar slope for various electrode potentials. Assuming laminar flow, the mass transport rate and, consequently, the limiting diffusional current density can be described mathematically by the Levich equation, as a function of the rotational frequency of the RDE, ω (rpm) [60].

$$i_d = 0.62 \cdot F \cdot n \cdot \nu^{-1/6} \cdot D^{2/3} \cdot C_0 \cdot \omega^{1/2} = B \cdot C_0 \cdot \omega^{1/2} \qquad \text{[Ec. 5.4]}$$

where 0.62 is a constant, ω is the angular frequency of rotation (rpm), F stands for the Faraday constant (96,485 C · mol^{-1}), C_O is the

concentration of reactive species ($7\cdot 10^{-7}$ mol · cm^3), D is the diffusion coefficient ($4\cdot 10^{-5}$ $cm^2 \cdot s^{-1}$) and ν is the viscosity (0.01 $cm^2 \cdot s^{-1}$).

The total current density, in a process controlled equally by activation (charge transfer) and diffusion (mass transport), can be expressed in terms of the kinetic (i_k) and diffusional (i_d) current densities, as follows [60].

$$\frac{1}{i} = \frac{1}{i_k} + \frac{1}{i_d} = \frac{1}{i_k} + \frac{1}{B \cdot C_0 \cdot \omega^{-1/2}} \qquad \text{[Ec. 5.5]}$$

The different linear sweep voltammetries obtained for each catalyst at different rotation rates (Figure 5.8. shown PtFe/C catalyst as an example) were used to represent the Koutecky-Levich plot, and the slope of the linear fitting of these data (i^{-1} vs $\omega^{-1/2}$) were used to estimate i_k from their intercepts with the i^{-1} axis and BC_0 from their slopes. All electrode potentials and reported activities were established at 0.4 V vs. RHE and compared to each other.

Table 5.2. *Kinetic parameters for PtM/C bimetallic catalysts.*

Catalyst	$B\cdot C_0$ ($mA\cdot cm^{-2}\cdot rpm^{-1/2}$)	i_k ($mA\cdot cm^{-2}$)	i_{dmax} ($mA\cdot cm^{-2}$)
Pt/C	0.0556	7.315	0.985
PtSn/C	0.0255	2.348	0.451
PtCu/C	0.0544	11.329	0.963
PtNi/C	0.0421	5.674	0.745
PtCo/C	0.0579	17.732	1.026
PtFe/C	0.0693	36.822	1.227

Table 5.2. shows kinetic and maximum limiting diffusional currents for Pt/C and bimetallic PtM-based catalyst. The experimentally extracted BC_0 values are in reasonable agreement with those previously reported [61, 62] except for PtSn/C catalyst, which suggest that

HER/HOR reaction are poorly controlled by H_2 diffusion. In this sense, in all catalysts with the only exception of PtSn, iK value is much higher than id value (especially in the catalyst PtCo/C, PtCu/C and PtFe/C), this difference suggest that the process is controlled by mass transport, i.e. by diffusion. This trend may affect the catalytic results in the sense that catalysts whose constants are closer to the theoretical values will have a more adequate disposition to the hydrogen evolution reaction and, consequently, the hydrogenation reaction could be disadvantaged.

3.3. Electrocatalytic hydrogenation tests in PEM cell

Pt-based catalysts supported on carbon have been widely used to carry out the hydrogenation reaction of cinnamaldehyde but they have the inconvenient of their high cost. In this sense, interest in bimetallic catalysts has grown since the addition of a second metal can drastically modify the activity and/or selectivity towards the desired products through the modification of the structure of the Pt particles by the second metal. In this context, different effects may occur (formation of alloys, blocking or dilution) depending on the selected support and promoter. Results in the current work are referred to Cu, Ni, Co, Fe and Sn promoted Pt-based catalyst using carbon Vulcan XC-72 as characteristic electrode support and explored differences in terms of electrocatalytic performance.

As expected, the combination of a second metal such as those presented in this work with Pt as active phase results in all cases in a decrease in the reaction rate and consequently in the conversion of CMA (X_{CMA} = [20-10 %) since ECSA values are lower (related to a lower amount of available active centers). This can be explained by the change of the electronic environment on the surface of Pt through metal-to-metal interaction [1] and dilution or blocking effects of M on Pt particles

that could be associated with the alloy form. However, the incorporation of a second metal such as Sn, Cu, Ni, Co or Fe into the Pt net has a direct influence on the product selectivity.

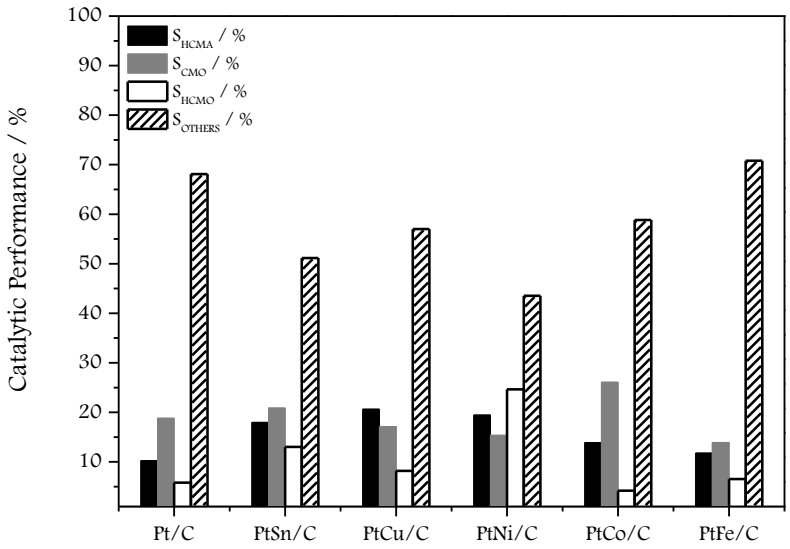

Figure 5.9. *Influence of the second metal on the ECH of CMA performance. Reaction conditions: Anodic solution: H_2O, Cathodic solution: 100 ppm CMA in 2- propanol, Inlet flow: 1 mL·min^{-1}, Intensity: 0.05 A, Temperature: 70 ºC.*

The hydrogenation of CMA typically produces a mixture of the unsaturated alcohol CMO, the saturated aldehyde HCMA and the saturated alcohol HCMO. Acetals (from aldol condensation) and other unidentified high molecular weight products are also produced when polar solvents are used [63]. It is well known that the use of 2-propanol as solvent favors the formation of by-products, especially acetals but to a lesser extent that other alcoholic solvents. From results displayed in Figure 5.9. it can be seen that selectivity leads to 45-70% by-products, which is in agreement and even lower than that reported working at high pressure conditions and using polar solvents [64-67]. In this sense, it can be observed that monometallic cathode is not selective to the desired compounds (HCMA, CMO and HCMO in a lesser extent). Pt/C catalyst

was found to be prone to form side products, whose selectivity was close to 70%, instead of favoring the hydrogenation of the double bonds present in CMA molecule. It can be also seen that the second metal (M), which is in the vicinity of Pt atoms, plays a critical role in the ECH selectivity by promoting certain hydrogenation reactions and hindering the formation of undesirable side compounds. Nevertheless, promotional effects depend on the promoter loading and the possible formation of different species configuration, the reducibility of Pt and promoter and the interaction degree, among others. Except for PtFe/C, PtM/C catalysts displayed a higher selectivity to the target compounds by reducing the formation of unwanted compounds compared with the reference Pt/C cathode. PtSn/C generates 20 % less of secondary products, maintaining CMO production and generating more quantity of HCMA and HCMO, as suggested by Lin et al. [68, 69], and similarly to PtCu/C catalyst, that favors the formation of HCMA over CMO [10, 70, 71]. Beside alloyed PtSn, which apart from the presence of oxidized species are reported to be responsible for the activation of the carbonyl group [45], metallic Sn present in the catalyst sample are not known to favor polarization of C=O but to produce a dilution/blocking effect of Pt atoms [72]. However, from characterization results, the combination of PtSn alloyed species with a certain fraction of metallic Sn (in the vicinity of Pt) are postulated to contribute to not only to the polarization of C=O but to the hydrogenation of C=C bond. In agreement with characterization results, PtNi/C presents a great selectivity towards HCMA (20%) [47, 71, 73-75] and HCMO (26%) reducing the formation of by-products more than any other cathode (from 70% to 44%). It is known that conversion from HCMA to HCMO occurs at a slower rate compared to CMO conversion to HCMO. In this sense, the steric impediment due to the adsorption of CMO and the presence of small amounts of Ni^{2+} favor the adsorption of CMA through the group C=O, which leads to a higher production of HCMO derived from the consecutive hydrogenation of CMO enhanced

by the use of a protic solvent like 2-propanol [76]. In the case of PtCo/C, this cathode presents the highest activation of the carbonyl group and therefore it provided the highest CMO selectivity (27%) [77] by inhibiting HCMO derivation (HCMO formation close to 3%). According to Guo et al., it may be due to the presence of cobalt oxidized species attached on Pt surface (in agreement with TPR characterization results) as electrophilic or Lewis sites [3, 7]. With lower electronegativity, Co oxide atoms may adsorb (increasing electron density of Pt) and activate C=O bond via the unoccupied electron pair of oxygen (weaken the strength of the metal-oxygen bond) [78]. It can be also observed that the shorter Pt-Pt nearest-neighbor distance in the alloys results in easier C=O activation (reduction) enhancing the electrocatalytic performance. Therefore, electrochemical hydrogenation tests on bimetallic catalyst PtCo/C amd PtNi/C showed the best results in terms of CMO selectivity and by-products production, respectively. Nevertheless, further studies must be performed to optimize the composition of the PtCo- and PtNi-based cathodic electrode to improve the electrocatalytic hydrogenation performance.

4. CONCLUSIONS

The current work extends the direct hydrogenation of cinnamaldehyde in an electrocatalytic PEM cell using bimetallic PtM (M: Sn, Fe, Ni, Cu, Co) catalysts supported on carbon Vulcan XC-72. Synthetized using chemical reduction with ethylene glycol and characterized by physicochemical techniques and cyclic and linear sweep voltammetry essays, these materials have been tested as cathodes in order to identify the most appropriate electrocatalyst for the production of value-added compounds such as CMO. From characterization results, the addition of Ni, Co, Fe, Cu or Sn to Pt has an important role in the catalyst synthesis, whose structure for the selective

electrohydrogenation of CMA is modified according to the promoter. Results from physico-chemical characterization showed evidence of a mesoporous structure with certain microporous character as well as the formation of alloys in all cases. However, the presence of metal oxides in case of using Co as second metal or metallic Sn could not be discarded. Electrochemical characterization showed that PtCo/C and PtCu/C catalysts present lower deactivation compared with other bimetallic catalysts, and linear sweep voltammetries suggest diffusional control. From electrochemical hydrogenation tests, PtCo nanocatalyst exhibited a promising performance compared with monometallic Pt cathode under the same operation conditions, providing the best results in terms of CMO selectivity (close to 30%). On the other hand, bimetallic PtNi/C catalyst showed the lowest formation of by-products (<45%), keeping a reasonable HCMA and CMO production but enhanced further hydrogenation to HCMO (>25%).

REFERENCES

1. Rong, Z., et al., *Selective hydrogenation of cinnamaldehyde to cinnamyl alcohol over graphene supported Pt-Co bimetallic catalysts.* Catalysis Letters, 2014. **144**(6): p. 980-986.
2. Ide, M.S., et al., *Mechanistic insights on the hydrogenation of α,β-unsaturated ketones and aldehydes to unsaturated alcohols over metal catalysts.* ACS Catalysis, 2012. **2**(4): p. 671-683.
3. Gallezot, P. and D. Richard, *Selective Hydrogenation of α,β-Unsaturated Aldehydes.* Catalysis Reviews, 1998. **40**(1-2): p. 81-126.
4. Yan, W., et al., *Model-aided optimization and analysis of multi-component catalysts: Application to selective hydrogenation of cinnamaldehyde.* Chemical Engineering Science, 2012. **76**: p. 26-36.
5. Li, H., et al., *Selective hydrogenation of cinnamaldehyde to cinnamyl alcohol over an ultrafine Co-B amorphous alloy catalyst.* Applied Catalysis A: General, 2002. **225**(1-2): p. 117-130.
6. Young, W.G., W.H. Hartung, and F.S. Crossley, *Reduction of Aldehydes with Aluminum Isopropoxide.* Journal of the American Chemical Society, 1936. **58**(1): p. 100-102.
7. Guo, Z., et al., *Carbon nanotube-supported Pt-based bimetallic catalysts prepared by a microwave-assisted polyol reduction method and their catalytic applications in the selective hydrogenation.* Journal of Catalysis, 2010. **276**(2): p. 314-326.
8. Han, X., et al., *Selective hydrogenation of cinnamaldehyde over Pt/ZrO2 catalyst modified by Cr, Mn, Fe, Co and Ni.* Catalysis Letters, 2006. **109**(3-4): p. 157-161.
9. Li, Y., et al., *Influence of preparation modes on Pt-Ni/CNTs catalysts used in the selective hydrogenation of cinnamaldehyde to hydrocinnamaldehyde.* Catalysis Letters, 2008. **126**(3-4): p. 280-285.
10. Zheng, R., et al., *Controlling hydrogenation of C=O and C=C bonds in cinnamaldehyde using silica supported Co-Pt and Cu-Pt bimetallic catalysts.* Applied Catalysis A: General, 2012. **419-420**: p. 126-132.
11. Teddy, J., et al., *Influence of particles alloying on the performances of Pt-Ru/CNT catalysts for selective hydrogenation.* Journal of Catalysis, 2011. **278**(1): p. 59-70.

12. Ramos-Fernández, E.V., et al., *Selective hydrogenation of cinnamaldehyde over (111) preferentially oriented Pt particles supported on expanded graphite.* Catalysis Letters, 2009. **133**(3-4): p. 267-272.
13. Handjani, S., et al., *Influence of the support composition and acidity on the catalytic properties of mesoporous SBA-15, Al-SBA-15, and Al2O 3-supported Pt catalysts for cinnamaldehyde hydrogenation.* Journal of Catalysis, 2011. **282**(1): p. 228-236.
14. Plomp, A.J., et al., *Catalysts based on platinum-tin and platinum-gallium in close contact for the selective hydrogenation of cinnamaldehyde.* Journal of Catalysis, 2009. **263**(1): p. 146-154.
15. Hyun, K., et al., *The effect of platinum based bimetallic electrocatalysts on oxygen reduction reaction of proton exchange membrane fuel cells.* International Journal of Electrochemical Science, 2013. **8**(10): p. 11752-11767.
16. Jeon, T.Y., et al., *Enhanced activity of Pt-based electrocatalysts for oxygen reduction via a selective Pt deposition process.* Journal of Electroanalytical Chemistry, 2011. **662**(1): p. 70-79.
17. Oh, H.S., et al., *Development of highly active and stable non-precious oxygen reduction catalysts for PEM fuel cells using polypyrrole and a chelating agent.* Electrochemistry Communications, 2011. **13**(8): p. 879-881.
18. He, D., S. Mu, and M. Pan, *Perfluorosulfonic acid-functionalized Pt/carbon nanotube catalysts with enhanced stability and performance for use in proton exchange membrane fuel cells.* Carbon, 2011. **49**(1): p. 82-88.
19. Rao, C.V. and B. Viswanathan, *ORR activity and direct ethanol fuel cell performance of carbon-supported Pt-M (M) Fe, Co, and Cr) alloys prepared by polyol reduction method.* Journal of Physical Chemistry C, 2009. **113**(43): p. 18907-18913.
20. Mukerjee, S. and S. Srinivasan, *Enhanced electrocatalysis of oxygen reduction on platinum alloys in proton exchange membrane fuel cells.* Journal of Electroanalytical Chemistry, 1993. **357**(1-2): p. 201-224.
21. Xiong, L., A.M. Kannan, and A. Manthiram, *Pt-M (M = Fe, Co, Ni and Cu) electrocatalysts synthesized by an aqueous route for proton exchange membrane fuel cells.* Electrochemistry Communications, 2002. **4**(11): p. 898-903.
22. Duong, H.T., et al., *Oxygen reduction catalysis of the Pt3Co alloy in alkaline and acidic media studied by X-ray photoelectron spectroscopy and*

electrochemical methods. Journal of Physical Chemistry C, 2007. **111**(36): p. 13460-13465.

23. Yano, H., et al., *Oxygen reduction activity of carbon-supported Pt-M (M = V, Ni, Cr, Co, and Fe) alloys prepared by nanocapsule method.* Langmuir, 2007. **23**(11): p. 6438-6445.
24. Maass, S., et al., *Carbon support oxidation in PEM fuel cell cathodes.* Journal of Power Sources, 2008. **176**(2): p. 444-451.
25. Wang, D., L. Zhuang, and J. Lu, *An alloying-degree-controlling step in the impregnation synthesis of PtRu/C catalysts.* Journal of Physical Chemistry C, 2007. **111**(44): p. 16416-16422.
26. Antolini, E. and F. Cardellini, *Formation of carbon supported PtRu alloys: An XRD analysis.* Journal of Alloys and Compounds, 2001. **315**(1-2): p. 118-122.
27. Ashokkumar, S., et al., *Bimetallic Co–Ni/TiO2 catalysts for selective hydrogenation of cinnamaldehyde.* Research on Chemical Intermediates, 2018. **44**(11): p. 6703-6720.
28. Malobela, L.J., et al., *Nickel–Cobalt on Carbonaceous Supports for the Selective Catalytic Hydrogenation of Cinnamaldehyde.* Industrial & Engineering Chemistry Research, 2014. **53**(36): p. 13910-13919.
29. Toda, T., et al., *Enhancement of the electroreduction of oxygen on Pt alloys with Fe, Ni, and Co.* Journal of the Electrochemical Society, 1999. **146**(10): p. 3750-3756.
30. Jong Yoo, S., et al., *Enhanced stability and activity of Pt-Y alloy catalysts for electrocatalytic oxygen reduction.* Chemical Communications, 2011. **47**(41): p. 11414-11416.
31. Lobato, J., et al., *Composite Titanium Silicon Carbide as a Promising Catalyst Support for High-Temperature Proton-Exchange Membrane Fuel Cell Electrodes.* ChemCatChem, 2016. **8**(4): p. 848-854.
32. Corrales-Sánchez, T., J. Ampurdanés, and A. Urakawa, *MoS2-based materials as alternative cathode catalyst for PEM electrolysis.* International Journal of Hydrogen Energy, 2014. **39**(35): p. 20837-20843.
33. Goel, J., B. Rawat, and S. Basu, *Bi-metallic and tri-metallic PteSn/C, PteIr/C, PteIreSn/C catalysts for electro-oxidation of ethanol in direct ethanol fuel cell.* 2011.
34. Zhou, W.J., et al., *Direct ethanol fuel cells based on PtSn anodes: the effect of Sn content on the fuel cell performance.* Journal of Power Sources, 2005. **140**(1): p. 50-58.

35. Agubra, V., et al., *Forcespinning: A new method for the mass production of Sn/C composite nanofiber anodes for lithium ion batteries.* Solid State Ionics, 2016. **286**: p. 72-82.
36. Rusnaeni, N., et al., *The Influence of Pt atomic ratio in the activity PtNi/C nanocatalysts for the PEMFC.* ITB Journal of Engineering Science, 2011. **43**.
37. Borbath, I., et al., *Controlled Synthesis of Pt3Sn/C Electrocatalysts with Exclusive Sn–Pt Interaction Designed for Use in Direct Methanol Fuel Cells.* Topics in Catalysis, 2013. **56**: p. 1033-1046.
38. Rao, C.V., et al., *High temperature polymer electrolyte membrane fuel cell performance of PtxCoy/C cathodes.* Journal of Power Sources, 2010. **195**(11): p. 3425-3430.
39. Lobato, J., et al., *Study of different bimetallic anodic catalysts supported on carbon for a high temperature polybenzimidazole-based direct ethanol fuel cell.* Applied Catalysis B: Environmental, 2009. **91**(1): p. 269-274.
40. Rao, C.V., et al., *Synthesis and electrocatalytic oxygen reduction activity of graphene-supported Pt3Co and Pt3Cr alloy nanoparticles.* Carbon, 2011. **49**(3): p. 931-936.
41. Sing, K., et al., *Reporting physisorption data for gas/solid systems. Handbook of heterogeneous catalysis*, in *Wiley Online Library*. 2008.
42. Sing, K., *The use of nitrogen adsorption for the characterisation of porous materials.* Colloids and Surfaces A: Physicochemical and Engineering Aspects, 2001. **187-188**: p. 3-9.
43. Leofanti, G., et al., *Surface area and pore texture of catalysts.* Catalysis Today, 1998. **41**(1): p. 207-219.
44. Pastor-Pérez, L. and A. Sepúlveda-Escribano, *Low temperature glycerol steam reforming on bimetallic PtSn/C catalysts: On the effect of the Sn content.* Fuel, 2017. **194**: p. 222-228.
45. Stassi, J.P., et al., *Formation of different promoted metallic phases in PtFe and PtSn catalysts supported on carbonaceous materials used for selective hydrogenation.* Journal of Catalysis, 2013. **306**: p. 11-29.
46. Dosso, L.A., C.R. Vera, and J.M. Grau, *Pt-Co and Pt-Ni Catalysts of Low Metal Content for H2 Production by Reforming of Oxygenated Hydrocarbons and Comparison with Reported Pt-Based Catalysts.* International Journal of Chemical Engineering, 2018. **2018**: p. 10.
47. Li, Y., G.-H. Lai, and R.-X. Zhou, *Carbon nanotubes supported Pt–Ni catalysts and their properties for the liquid phase hydrogenation of cinnamaldehyde to*

hydrocinnamaldehyde. Applied Surface Science, 2007. **253**(11): p. 4978-4984.

48. Luu, C.L., et al., *The role of carriers in properties and performance of Pt-CuO nanocatalysts in low temperature oxidation of CO and p-xylene.* Advances in Natural Sciences: Nanoscience and Nanotechnology, 2014. **6**(1): p. 015011.
49. Dosso, L.A., C.R. Vera, and J.M. Grau, *Aqueous phase reforming of polyols from glucose degradation by reaction over Pt/alumina catalysts modified by Ni or Co.* International Journal of Hydrogen Energy, 2017. **42**(30): p. 18853-18864.
50. Kim, M.-C., et al., *Aqueous phase reforming of polyols for hydrogen production using supported PtFe bimetallic catalysts.* Renewable Energy, 2016. **95**: p. 396-403.
51. Venuto, P.B. and E.L. Wu, *Sorption and exchange patterns of benzene-phenolic mixtures over faujasite catalyst: Relevance to phenol ethylation.* Journal of Catalysis, 1969. **15**(2): p. 205-208.
52. Tanksale, A., et al., *Effect of Pt and Pd promoter on Ni supported catalysts—A TPR/TPO/TPD and microcalorimetry study.* Journal of Catalysis, 2008. **258**(2): p. 366-377.
53. Yang, R., et al., *Hydrotreating of crude 2-ethylhexanol over Ni/Al2O3 catalysts: Surface Ni species-catalytic activity correlation.* Applied Catalysis A: General, 2009. **368**(1): p. 105-112.
54. Delbecq, F. and P. Sautet, *Competitive C□C and C□O Adsorption of α-β-Unsaturated Aldehydes on Pt and Pd Surfaces in Relation with the Selectivity of Hydrogenation Reactions: A Theoretical Approach.* Journal of Catalysis, 1995. **152**(2): p. 217-236.
55. Do Chi, L., et al., *Synthesis and characterization of alloy catalyst nanoparticles PtNi/C for oxygen reduction reaction in proton exchange membrane fuel cell.* Advances in Natural Sciences: Nanoscience and Nanotechnology, 2015. **6**: p. 025009.
56. Devivaraprasad, R., et al., *Oxygen Reduction Reaction and Peroxide Generation on Shape-Controlled and Polycrystalline Platinum Nanoparticles in Acidic and Alkaline Electrolytes.* Langmuir, 2014. **30**(29): p. 8995-9006.
57. Huang, J.-F. and P.-K. Tseng, *High performance layer-by-layer Pt(3)Ni(Pt-skin)-modified Pd/C for the oxygen reduction reaction.* Chemical science, 2018. **9**(28): p. 6134-6142.

58. Sáez, A., et al., *Electrocatalytic hydrogenation of acetophenone using a Polymer Electrolyte Membrane Electrochemical Reactor.* Electrochimica Acta, 2013. **91**: p. 69-74.
59. Dabo, P., et al., *Selective electrocatalytic hydrogenation of 2-cyclohexen-1-one to cyclohexanone.* Electrochimica Acta, 1997. **42**(9): p. 1457-1459.
60. Innocente, A.F. and A.C.D. Ângelo, *Electrocatalysis of oxidation of hydrogen on platinum ordered intermetallic phases: Kinetic and mechanistic studies.* Journal of Power Sources, 2006. **162**(1): p. 151-159.
61. Zheng, J., et al., *Correlating Hydrogen Oxidation/Evolution Reaction Activity with the Minority Weak Hydrogen-Binding Sites on Ir/C Catalysts.* ACS Catalysis, 2015. **5**(7): p. 4449-4455.
62. Zheng, J., Y. Yan, and B. Xu, *Correcting the Hydrogen Diffusion Limitation in Rotating Disk Electrode Measurements of Hydrogen Evolution Reaction Kinetics.* Journal of The Electrochemical Society, 2015. **162**: p. F1470-F1481.
63. Kennes, C. and F. Thalasso, *Review: Waste gas biotreatment technology.* Journal of Chemical Technology & Biotechnology, 1998. **72**(4): p. 303-319.
64. Li, Y., et al., *Influence of Preparation Modes on Pt–Ni/CNTs Catalysts Used in the Selective Hydrogenation of Cinnamaldehyde to Hydrocinnamaldehyde.* Catalysis Letters, 2008. **126**(3): p. 280-285.
65. Wang, D. and Y. Zhu, *An Effective Pt-Cu/SiO2 Catalyst for the Selective Hydrogenation of Cinnamaldehyde.* Journal of Chemistry, 2018. **2018**: p. 7.
66. Zhang, L., *Selective hydrogenation of α,β[alpha,beta]-unsaturated aldehydes towards clean synthesis over noble metal catalysts in mass transfer efficient three phase reactors*, in *School of Chemical Engineering*. 1998, University of Birmingham. p. 409.
67. Leng, F., et al., *Selectivity shifts in hydrogenation of cinnamaldehyde on electron-deficient ruthenium nanoparticles.* Comptes Rendus Chimie, 2018. **21**(3): p. 346-353.
68. Dai, L.-X., et al., *Self-supported composites of thin Pt–Sn crosslinked nanowires for the highly chemoselective hydrogenation of cinnamaldehyde under ambient conditions.* Inorganic Chemistry Frontiers, 2015. **2**(10): p. 949-956.
69. Merlo, A.B., *Hidrogenación selectiva de furfuraldehído en fase líquida empleando catalizadores metálicos y multimetálicos soportados*. 2010, Facultad de Ciencias Exactas.

70. Prakash, M.G., et al., *Selective hydrogenation of cinnamaldehyde on nickel nanoparticles supported on titania: role of catalyst preparation methods.* Catalysis Science & Technology, 2015. **5**(6): p. 3313-3321.
71. Ungureanu, A., et al., *Composition-Dependent Morphostructural Properties of Ni–Cu Oxide Nanoparticles Confined within the Channels of Ordered Mesoporous SBA-15 Silica.* ACS Applied Materials & Interfaces, 2013. **5**(8): p. 3010-3025.
72. Vilella, I.M.J., et al., *Catalytic performance in citral hydrogenation and characterization of PtSn catalysts supported on activated carbon felt and powder.* Applied Catalysis A: General, 2005. **281**(1): p. 247-258.
73. Zhao, Z.-F., et al., *Synthesis of a nano-nickel catalyst modified by ruthenium for hydrogenation and hydrodechlorination.* Catalysis Communications, 2008. **9**(13): p. 2191-2194.
74. Chen, X., et al., *Nickel–Silicon Intermetallics with Enhanced Selectivity in Hydrogenation Reactions of Cinnamaldehyde and Phenylacetylene.* Industrial & Engineering Chemistry Research, 2012. **51**(9): p. 3604-3611.
75. Gryglewicz, S., et al., *Performance of Carbon Nanofiber and Activated Carbon Supported Nickel Catalysts for Liquid-Phase Hydrogenation of Cinnamaldehyde into Hydrocinnamaldehyde.* Catalysis Letters, 2014. **144**(1): p. 62-69.
76. Newland, S.H., et al., *Highly effective design strategy for the heterogenisation of chemo- and enantioselective organocatalysts.* Catalysis Science & Technology, 2015. **5**(2): p. 660-665.
77. Zheng, R., et al., *Controlling hydrogenation of CO and CC bonds in cinnamaldehyde using silica supported Co-Pt and Cu-Pt bimetallic catalysts.* Applied Catalysis A: General, 2012. **419-420**: p. 126-132.
78. Li, Y., P.-F. Zhu, and R.-X. Zhou, *Selective hydrogenation of cinnamaldehyde to cinnamyl alcohol with carbon nanotubes supported Pt-Co catalysts.* Applied Surface Science, 2008. **254**(9): p. 2609-2614.

Chapter 6: Bimetallic PtNi/C and PtCo/C cathodes for the selective Hydrogenation of Cinnamaldehyde in a PEM cell: Influence of the Pt/M ratio and Cathodic Media Additives

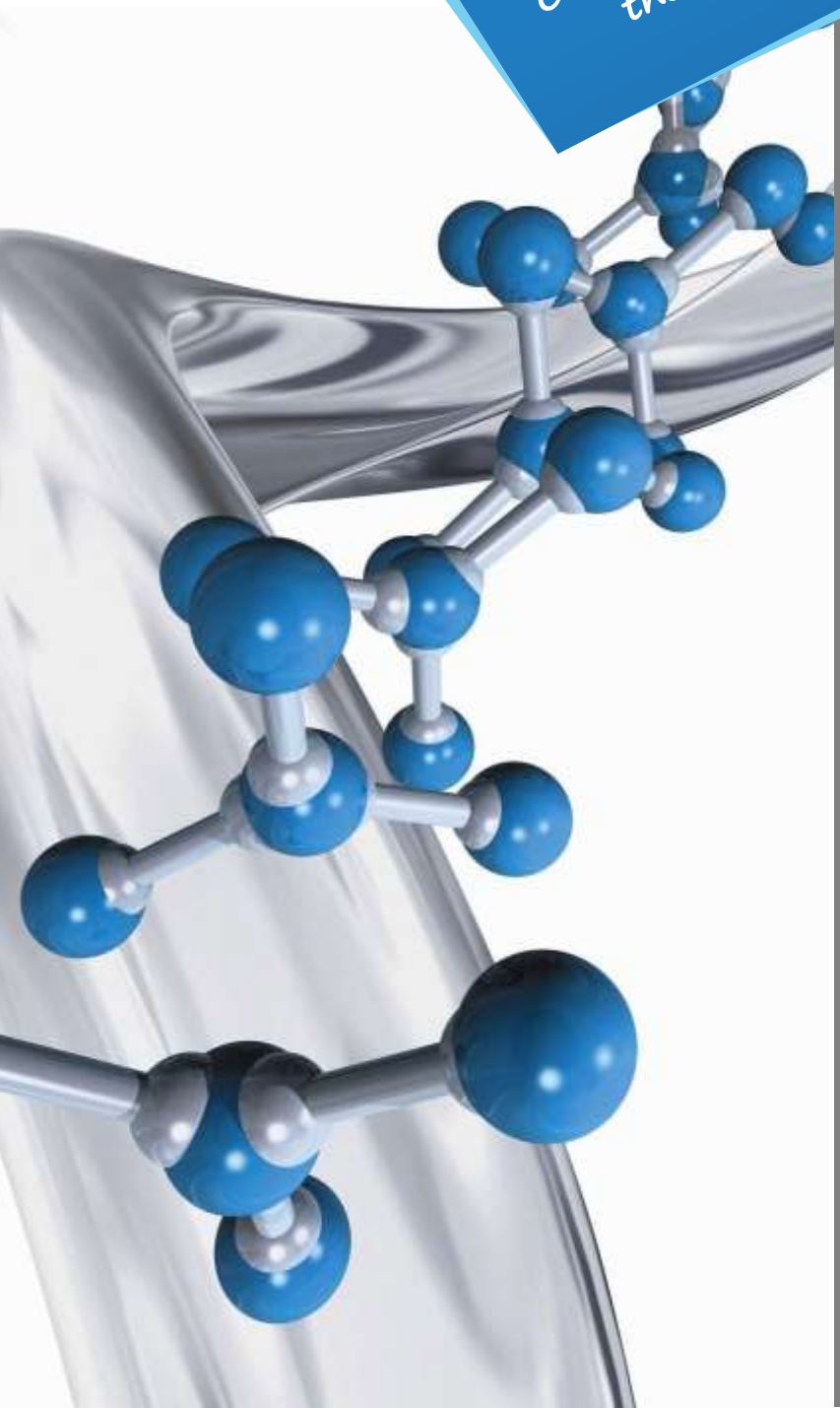

1. INTRODUCTION

2. EXPERIMENTAL
2.1. Cathode catalyts synthesis
2.2. Physicochemical characterization
2.3. Electrochemical characterization
2.4. Membrane electrode assembly (MEA) preparation
2.5. Electrocatalytic hydrogenation tests

3. RESULTS AND DISCUSSION
3.1 Physicochemical characterization Pt_yM_{1-y}/C cathodic catalysts
3.2. Electrochemical characterization Pt_yM_{1-y}/C cathodic catalysts
3.3. Electrochemical hydrogenation of CMA in PEM cell

4. CONCLUSIONS

Abstract

In this work, two series of PtCo- and PtNi-based catalysts supported on Vulcan XC-72 with different Pt/M (M: Ni or Co) ratios have been tested on the electrocatalytic hydrogenation of cinnamaldehyde in a PEM cell. Catalysts were prepared by the modified polyol impregnation-reduction method using chlorides as precursors. Supported catalysts were physicochemically (XRD, temperature programmed reduction, N_2 adsorption/desorption and HCl titrations) and electrochemically (deactivation cyclic voltammetries and HER/HOR reaction) characterized. From hydrogenation and characterization results, the incorporation a Ni or Co to the catalyst structure in a proper Pt/M ratio is found to strongly modify the production of HCMA, CMO or HCMO. The use of higher amounts of cobalt and nickel do not enhance the product selectivity, which is related to the basicity of the catalysts. In addition, the incorporation of NH4OH and $NaHCO_3$ into the reaction media was also evaluated. Results showed that small quantities of NH_4OH (0.75 equivalents) could shift selectivity to the almost complete elimination of by-products generation, increasing the selectivity to CMO up to 55 % per cell pass on $Pt_{55}Co_{45}$/C cathode.

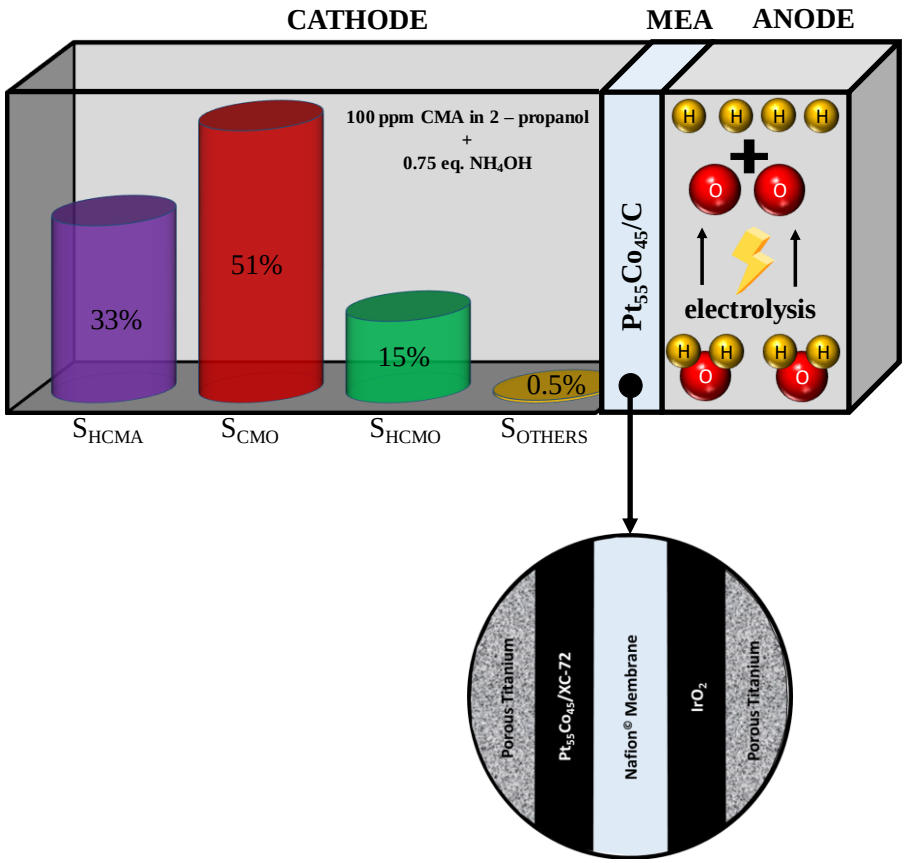

Figure 6.1. *Graphical abstract Chapter 6.*

1. INTRODUCTION

Nowadays, cinnamaldehyde, which represents a 5 % of the industry of aromas and flavors, is experiencing a growth due to its growing application in industries such as cosmetics, home care and factors such as the growth of emerging economies such as India and China, where the demand of such products has been increased. Its sales are expected to increase by 50 % in 2024. In addition to its applications as flavoring agent and aroma, this compound has antifungal, antibacterial properties with very interesting applications in the agricultural sector. For instance, α, β-unsaturated aldehyde cinnamaldehyde (CMA) is principally used as a test molecule in the catalytic production of cinnamyl alcohol (CMO) and hydrocinnamaldehyde (HCMA), which are important intermediates for the syntheses of fine chemicals, particularly flavors, perfumes, and pharmaceuticals [1-3]. As shown in Figure 2.9., the hydrogenation of CMA mainly results in the formation of i) CMO (via C=O bond hydrogenation), an important source for cinnamates, which are widely used in the production of perfumes [4, 5], HCMA (by C=C bond hydrogenation), which is an important intermediate in the preparation of pharmaceuticals used for the treatment of HIV [2] and iii) hydrocinnamyl alcohol (HCMO). Moreover, acetals and other high molecular weight compounds can be also produced in significant quantities.

CMO is commercially manufactured from CMA by a Meerwein-Ponndorf-Verley reduction process, where aluminum triisopropoxide is used as a reagent. Although CMO is obtained in high yields by this process, disposal of aluminum salts is a major drawback of this method [6]. Hence, it is necessary to develop an alternative process, which will avoid the use of stoichiometric reagents [7]. In this sense, proton exchange membrane (PEM) cells are proposed as a promising alternative

for conventional reactors for the selective hydrogenation of unsaturated organic compounds due to their versatile characteristics and dynamic response [8, 9]. Moreover, the coupling of water electrolysis [10-12] with hydrogenation reactions in a PEM cell have been reported to be an attractive process which avoids the necessity for the external supply of hydrogen gas and allows the selective operation under mild conditions. Previous works have shown that low hydrogen overpotential catalysts such as, platinum, rhodium and palladium can be used to electrocatalytically hydrogenate a variety of organic compounds such as alcohols [13-15], acetophenone and benzophenone [16, 17], glucose [18, 19], benzene [20] or aldehydes [21, 22]. However, selectivities to hydrocinnamaldehyde and cinnamyl alcohol considerably are known to vary with the method for catalyst preparation, the solvent, the incorporation of additives to the reaction media, the choice of a suitable active metal, the support nature, active particle size, the presence of impurities in the reactant as well as the process conditions [2, 3, 23-32]. Platinum and palladium are the most active metals that can be used in CMA selective hydrogenation reactions, being Pt more prone to reduce the C=O bond than Pd. However, under mild reaction conditions, although the hydrogenation of the C=C double bond is readily achieved by most platinum-based catalysts [33], the selective reduction to the unsaturated alcohol is a difficult task since the hydrogenation of C=O bond is thermodynamically unfavored. In this sense, a way to enhance the catalytic properties of Pt nanoparticles while reducing Pt loading in the cathode, which is a key factor to implement the electrocatalytic technology, is to introduce a second metal to form bimetallic catalysts [19]. For instance, it is well known that, in conventional hydrogenation of cinnamaldehyde molecule, metals such as Co and Ni could shift the selectivity to CMO and HCMA, respectively [34, 35]. In addition, it has been suggested that supported platinum-based catalysts with Lewis acid sites [20] or weak basicity in presence of aqueous base [21-23] [2, 11,

13, 14] can provide good selectivity to the products of interest, such as CMO. On the other hand, regarding the improvement of the electrode, the development of Pt-alloys with different transition metals is currently under study. In this context, the choice of a suitable metal to be alloyed and a proper Pt/promoter proportion is found to be key in the variation of the Pt–Pt distance and available active sites and, as a consequence, in the performance of the electrocatalyst. In a previous work carried out by our group, PtNi and PtCo-based catalysts have been postulated as promising cathodes for the electrochemical hydrogenation of cinnamaldehyde in a PEM cell. Therefore, in the aim to going one step further, as an alternative to high-pressure and temperature processing, the proposal of this work deals with the continuous electrocatalytic hydrogenation of cinnamaldehyde carried out at low temperature and ambient pressure in a PEM cell. In particular, a study on the electrocatalytic behavior of two series of PtNi and PtCo-based cathodes, synthetized by the modified polyol method with different Pt/Ni and Pt/Co ratios and supported on carbon Vulcan XC-72, is conducted. In addition, the effect of the incorporation of basic additives to the reaction medium (catholyte) on the selective electrochemical hydrogenation of cinnamaldehyde is reported.

2. EXPERIMENTAL

2.1. Cathode - Catalysts synthesis

Pt_yCo_{y-1}/C and Pt_yNi_{y-1}/C (C = Vulcan XC-72) catalyst were prepared by modified polyol method, using ethylene glycol (Sigma-Aldrich, Germany) as reducing agent as described in Section B.3. using pproper amounts of hexachloroplatinic acid (H_2PtCl_6) and cobalt (II) chloride hexahydrate or nickel (II) chloride hexahidrate for PtCo and PtNi bimetallic catalysts respectively.

2.2. Physicochemical characterization

As described in Section B.4., a Phillips PW-1700 diffractometer using nickel-filtered Cu Kα radiation (λ = 1.5418 Å) was used in order to measure the XRD profiles of the samples. Pt content was measured by an inductively coupled plasma spectrometer (ICP, Model Liberty Sequential, Varian). Temperature-programmed reduction (TPR) experiments were conducted in a commercial Micromeritics AutoChem 2950 HP unit with TCD detection. A Micromeritics ASAP 2010 sorptometer unit were used in order to measure the surface area/porosity of the samples, using N_2 at -196 ^{o}C as the adsorbate. And finally, HCl titrations were performed on a SCHOTT Titroline apparatus, equipped with an automatic dosager. 25 mg of the sample were immersed in 25 ml of 0.1 M NaCl and basified to pH = 11 with NaOH (0.1 M) with constant stirring. A 0.1 M HCl solution was used as titrant agent, which was added dropwise (0.01 mL·drop^{-1}). The starting NaCl solution served as a blank.

2.3. Electrochemical characterization

Electrochemical essays were carried out using a computer connected potentiostat Autolab PGSTAT128N (Ecochemie, The Netherlands) following the procedures described in Section B.5. A glassy carbon rotating disk electrode (GC-RDE, Metrohm Autolab) of 5 mm diameter was used as the working electrode, a platinum wire (Metrohm) as the counter electrode and a Ag/AgCl (Metrohm 3 M KI) reference electrode were used for the three-electrode cell measurements like cyclic voltammetry and linear sweep voltammetry.

2.4. Membrane electrode assembly (MEA) preparation

For the preparation of the membrane Electrode Assembly (MEA) inks containing a solution of the anodic and cathodic electrocatalysts and Nafion ionomer were directly spraying on the Nafion membrane (2 x 2 cm^2 active area, 3.5 x 3.5 cm^2 total area), using a common airbrush (Sogolee). Previously, Nafion® 115 membrane (180 μm, Hidrogena) was pretreated at described in Section B.3.

2.5. Electrocatalytic hydrogenation Tests

Electrocatalytic experiments were performed in a polymer electrolyte membrane (PEM) electrode cell described in Section B.7.2. In the case of the experiments using NH_4OH and $NaHCO_3$, proper amounts of the bases were added into the cathodic solutions before the experiments.

3. RESULTS AND DISCUSSION

3.1. Physicochemical characterization of Pt_yM_{1-y}/C cathodic catalysts

In order to know the atomic ratios of Pt_yM_{1-y}/C cathodic catalysts (where M is Co or Ni and y/y-1 refers to the Pt/M proportion, respectively), ICP analyses were carried out. Results are summarized in Table 6.1.

Table 6.1 Physicochemical properties of Pt_yM_{y-1}/C catalysts.

Catalyst	Pt atomic ratio (%)	BET surface area ($m^2 \cdot g^{-1}$)	Pore volume ($cm^3 \cdot g^{-1}$)	Average pore diameter $(nm)^2$
Vulcan XC-72	-	231	0.403	7.7
$Pt_{65}Co_{35}/C$	65	179	0.485	11.3
$Pt_{55}Co_{55}/C$	55	156	0.504	13.3
$Pt_{40}Co_{60}/C$	40	113	0.401	14.0
$Pt_{75}Ni_{25}/C$	75	103	0.415	15.8
$Pt_{65}Ni_{35}/C$	65	115	0.450	15.5
$Pt_{40}Ni_{60}/C$	40	95	0.386	16.1

XRD patterns of two series of Pt_yM_{1-y}/C catalysts are shown in Figure 6.2. The broad diffraction peak observed around $2\theta = 25^o$ is due to the hexagonal structure of Vulcan XC-72 carbon black support. Diffraction peaks at 39^o, 46^o, and 67^o corresponding to the (1 1 1), (2 0 0) and (2 2 0) crystal planes of the typical character of Pt face-centered cubic crystalline structure were also observed although broadly diffused.

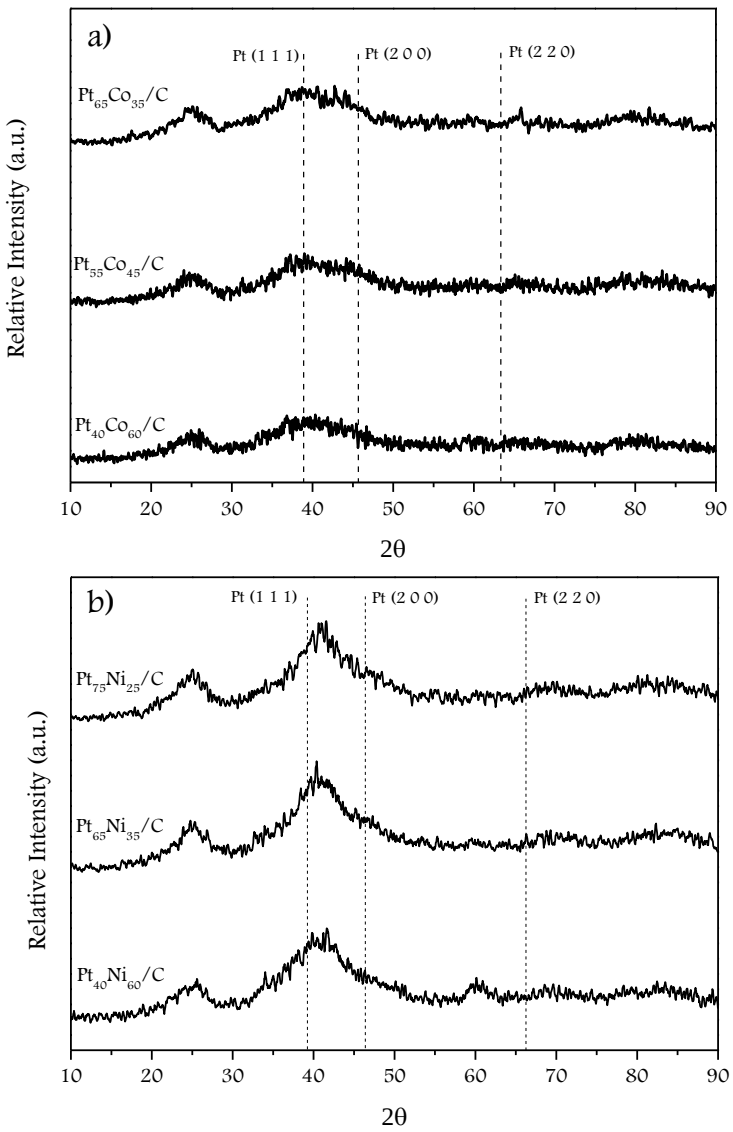

Figure 6.2. XRD patterns of the synthesized **a**. Pt_yCo_{y-1}/C catalysts, **b.** Pt_yNi_{y-1}/C catalysts.

Compared with the pattern of monometallic Pt, diffraction peaks of Pt_yM_{1-y}/C catalysts slightly shift to higher 2θ values, which suggests that Co and Ni atoms have entered into the Pt lattice and alloys can be formed [36] causing the contraction of the crystallite structure. Results from XRD also show the appearance of NiO for the highest Ni loading since the characteristic peak at 2θ = 63°, corresponding to the plane (2 2 0) of cubic NiO species, is visible [37]. However, peaks associated with PtO phase, free Co or cobalt oxides were not observed in any sample, which may indicate the proper reduction to the active phase during the synthesis procedure. On the other side, diffraction peaks of PtCo-based samples did not show any appreciable variation or displacement despite of an increased Co content along the interval of study. It should be noted that no particle size was calculated from this technique since it is well know that, for clusters smaller than 5 nm, which corresponds to the interval of study, Scherrer´s formula is not adequate for the simultaneous interpretation of the size and composition from diffraction patterns [38, 39]. However, the inclusion of smaller atoms of Ni and Co (R_{Ni}= 0.124 nm and R_{Co}: 0.125 nm vs R_{Pt} = 0.139 nm) would result in the narrowing of the Pt crystallite net (alloy lattice parameter) [40-42]. Moreover, smaller lattice parameters are usually associated with moderate alloying degrees, which is consistent with the obtained result [41] ($a_{Pt(2\,2\,0)}$ = 0.392, $a_{Co(2\,2\,0)}$ = 0.388, $a_{Ni(2\,2\,0)}$ = 0.388, Alloying degree (Co) = 42 %, (Ni) = 54 % for the Pt55Co65/C and Pt65Ni35/C catalysts, respectively).

Table 6.1. shows the main physicochemical properties of the support and Pt_yM_{1-y}/C catalyst synthetized in this work (BET surface area, pore volume and average pore diameter) evaluated by N_2 adsorption-desorption measurements. Isotherms of Pt_yM_{1-y}/C catalysts are displayed in Figure 6.3.

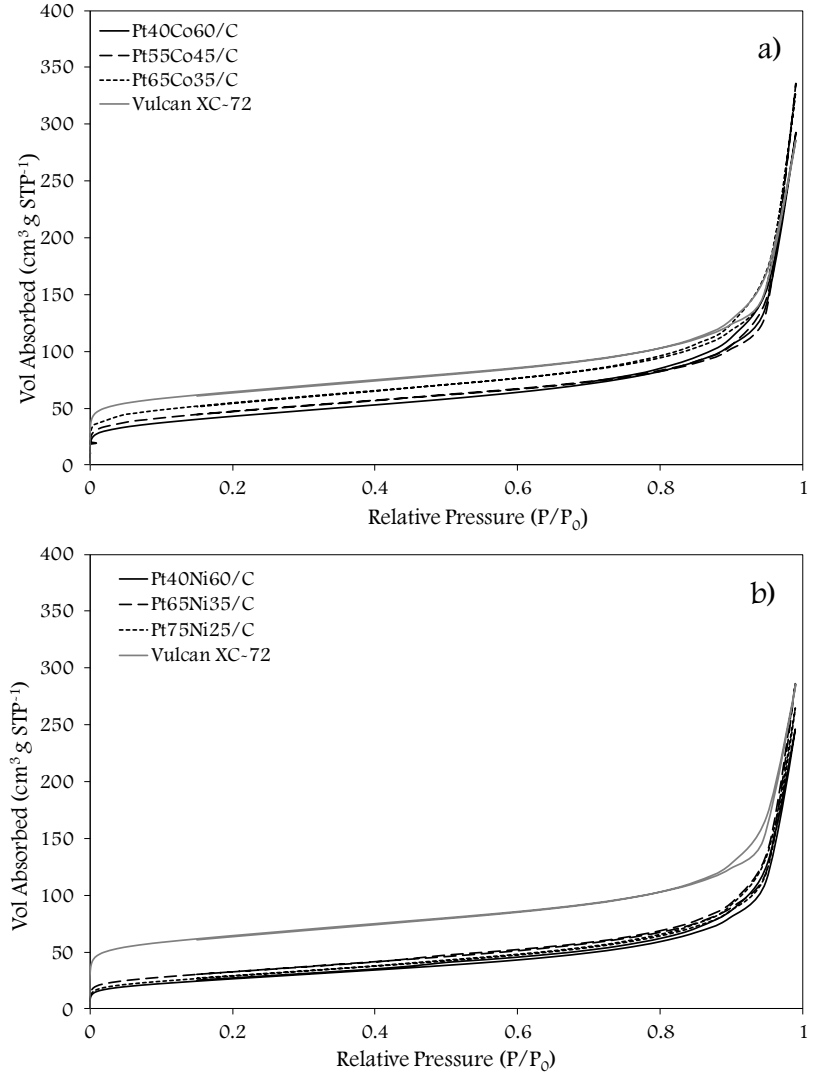

Figure 6.3. *Nitrogen adsorption desorption isotherms of a.* Pt_yCo_{y-1}/C *catalysts* ***b.*** Pt_yNi_{y-1}/C *catalysts.*

All isotherms showed a type I-IV adsorption-desorption profile, according to the IUPAC classification, which is associated to microporous solids having relatively small external surfaces. Firstly, especially in the case of the support, the N_2 adsorption volume increased sharply in the micropore (size < 2 nm) region at very low partial pressures (P/P_0 < 0.005) due to the strong interaction between pore walls and adsorbate. Then, there was an increase at high relative pressures when the

adsorption in mesopores (2 nm < size < 50 nm) leads to multilayer adsorption. This fact was corroborated with the H3 hysteresis loop observed in the multilayer range of physisorption isotherms. This is related to the capillary condensation associated with their different filling and emptying that takes place on mesopores. In this sense, this condensation is characteristic of solid pores of aggregates or agglomerates of particles forming slit shaped pores, with nonuniform size or shape [43-45]. It can be also observed that, after metal precursor deposition, BET surface area experienced an important decrease in contrast with the pore volume and pore diameter, being most pronounced in the case of bimetallic Pt/Ni catalysts. This fact could be attributed to the pore blockage by the metal particles, which prevent N_2 molecules to be adsorbed on them. It seems that metal nanoparticles localized in the micropores and mesopores of Pt_yM_{1-y}/C Vulcan XC-72 are trapped in the internal small pores, as can be demonstrated by changes in the average pore size before (7.7 nm) and after metal deposition (> 11 nm for Pt_yCo_{1-y} and >15 nm in case of Pt_yNi_{1-y}).

Temperature programmed reduction (TPR) analyses were performed in order to verify the proper reduction of PtM during the catalysts synthesis. Figure 6.4. showed the TPR profiles of Pt_yM_{1-y}/C catalysts used in this work. In the case of Pt_yNi_{1-y}/C catalysts, two main hydrogen consumption peaks can be observed (Figure 6.4.a.). It should be noted that the maxima shift to lower reduction temperatures when increasing the nickel loading. In addition, hydrogen consumption signal is enlarged, especially that related to the first peak up to produce overlapping of both maxima for the lowest Pt/Ni ratio (i.e. $Pt_{40}Ni_{60}$/C). This is indicative of a strong Pt-Ni interaction, which is expected to shift selectivity to HCMA formation. The first consumption peak from 330 to 400°C corresponds to Ni species catalyzed by Pt with different interaction with the support [46-48]and to the reduction of PtNi alloy. Hydrogen consumption peaks

in a temperature range between 500-650 ºC can be attributed to the decomposition of the carbonaceous support [49].

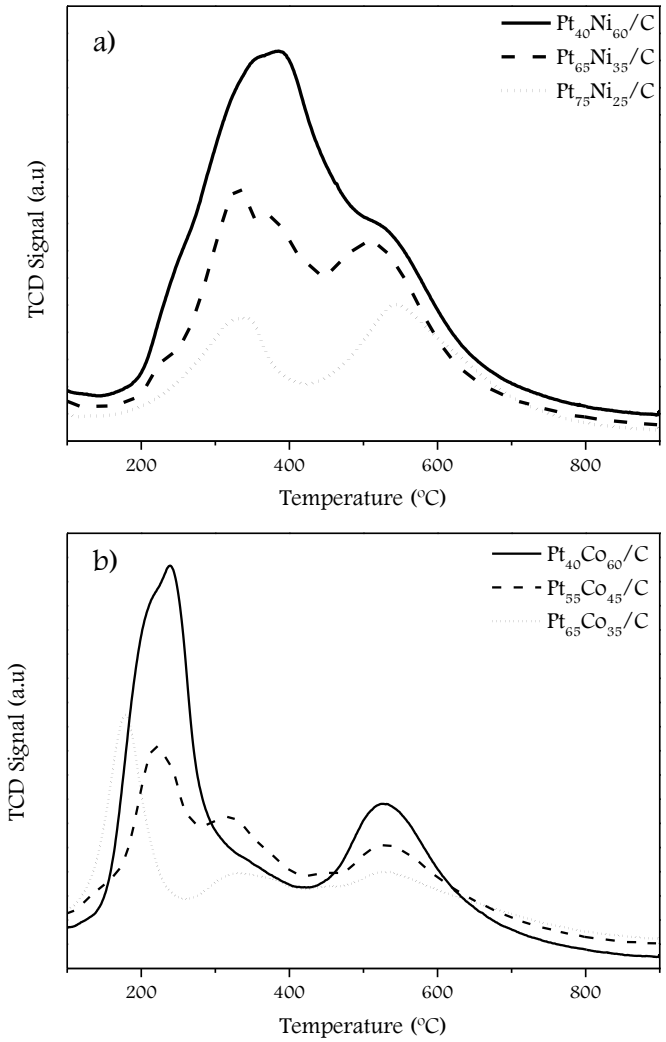

Figure 6.4. Temperature-programmed reduction (TPR) profiles of the synthesized **a.** Pt_yNi_{y-1}/C catalysts. **b.** Pt_yCo_{y-1}/C catalysts

From Figure 6.4.b. it can be observed that, as occurs with PtNi-based cathodic catalysts, H_2 consumption also increases with Co loading due to the co-reduction of Co and Pt species. For Pt_yCo_{1-y}/C catalysts three maxima of hydrogen consumption appear. The first peak in the region

from 180 to 230ºC could be related to the reduction of Pt species of easy access or low interaction with the support [50, 51]. The intermediate region at 240 - 400 ºC could be due to the reduction of Pt and Co, which would be present in the vicinity of the Pt and to the reduction of cobalt oxide [50, 52, 53] along with the beginning of the gasification of the support, which mainly takes place at 500ºC. The shift to lower temperatures associated with H_2 spillover over Pt it is also observed.

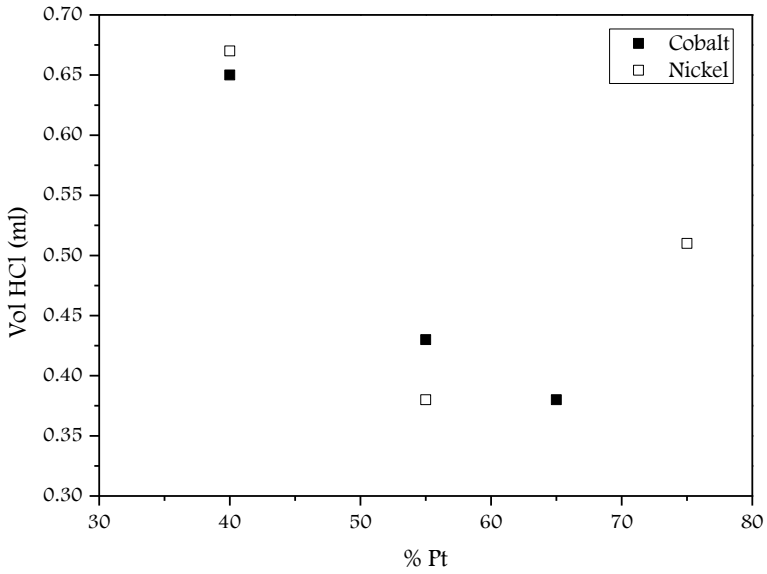

Figure 6.5. Acid/Basic behavior/character of the Pt_yM_{y-1}/C catalysts studied.

Acid-base titration was also conducted to evaluate the acid-base character of the support and the synthetized Pt_yM_{1-y}/C catalysts (Figure 6.5.). Although all samples exhibited basic character, Pt/M atomic ratio has a great influence on the acid-basic character of each sample. For comparison purposes, the same Pt/M ratio (40/60) was firstly analyzed. As can be observed from Figure 6.5., regardless the M nature, the amount of HCl required to neutralize the basic sites is practically the same, which suggests that platinum content is key on the basic-acid character of the catalyst. Therefore, an increase of Pt content would lead to a decrease of the basicity of the catalyst sample. For Pt_yCo_{1-y}/C catalysts a variation of

Pt/M from 40/60 to 55/45 lead to a large diminishing of the basic character, being much lower from 55/45 to 65/35 In case of Pt_yNi_{1-y}/C catalysts, the same trend was followed unlike for $Pt_{75}Ni_{25}/C$ sample, in which basicity increases with platinum content. Is well known that basicity can have an impact on hydrogenation results. In this sense, Handjani et al. reported that particles whose surface was enriched in electrons achieve greater selectivity to CMO [54].

3.2. Electrochemical characterization of Pt_yM_{1-y}/C cathodic catalysts

In order to explore the influence of cathodic Pt/M ratio on the electrochemical performance of the as-prepared Pt_yM_{1-y}/C electrodes cyclic voltammetry (CV) essays were carried out at room temperature in nitrogen saturated 0.1 M $HClO_4$. The electrochemical active surface area (ECSA) of each catalyst was calculated CV curves. Prior to that, electrodes were cycled at 50 $mV \cdot s^{-1}$ until cyclic voltammograms were reproducible. In addition, accelerated durability tests were performed under the same conditions by applying cyclic potential sweeps between 0.05 and 1.4 V versus RHE at a sweep rate of 50 mV s^{-1} for 500 cycles.

Figure 6.6. displays cyclic voltammograms of the six as-obtained electrocatalysts between 0.05 and 1.4 V vs RHE. It can be seen that all catalysts exhibit the typical CV curves, consisting of hydrogen adsorption-desorption, oxidation-reduction of metallic surface and double-layer regions [55]. However, the electrochemical performance is found to depend on the Pt/M ratio. When cycling between 0.05 and 1.3 vs RHE, some changes in the shape and size of the CV curves are found under Pt/M variation, suggesting that possible changes in Pt surface area and/or composition may occur. It is clearly illustrated that the hydrogen adsorption-desorption region shrinks with increasing cycle numbers.

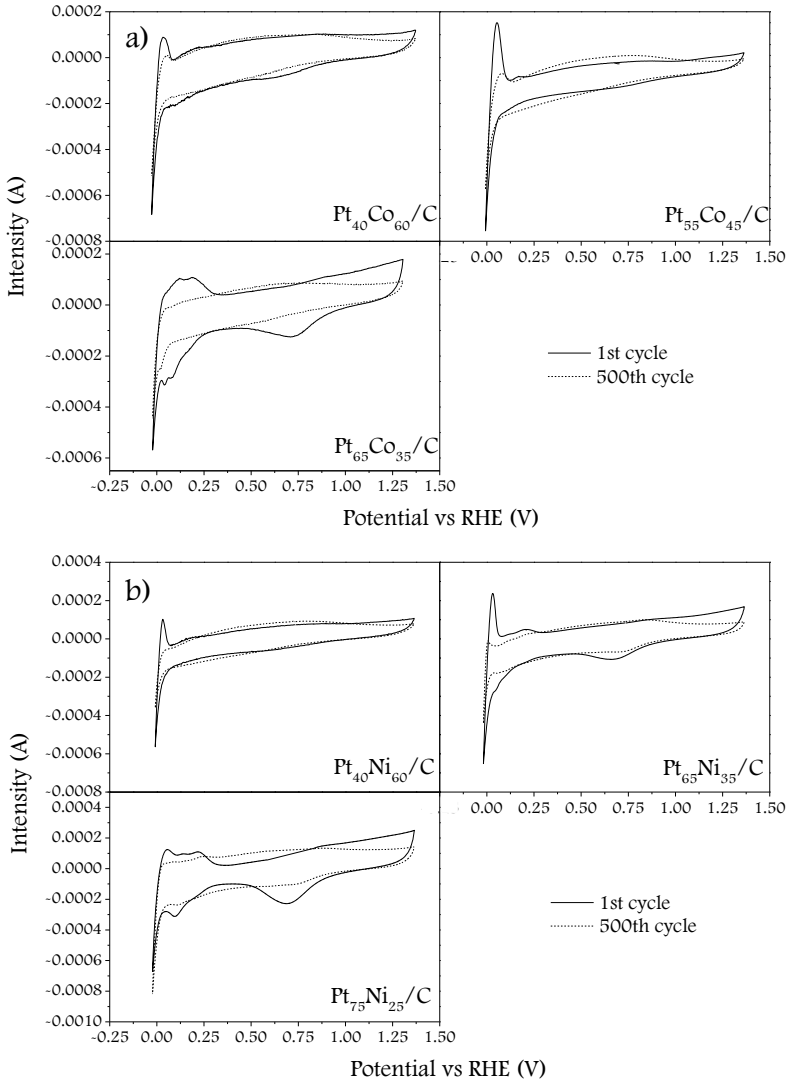

Figure 6.6. Cyclic voltammograms (at 25 °C in 0.1 M $HClO_4$, with a scan rate of 50 mV s^{-1}) of **a.** Pt_yCo_{y-1}/C catalysts.**b.** Pt_yNi_{y-1}/C catalysts

These variations are closely related to the surface structures of the catalysts. The diminishment in the number of active sites in the catalysts is responsible for the shrink of the hydrogen adsoption-desorption regions [55]. CV curves present (1 1 0) and (1 0 0)/(1 1 1) Pt crystal planes, which are related to weak and strong hydrogen adsorption, respectively [56, 57], being clearly distinguished for those cathodes with

the lowest M loading. However, a preferential orientation for Pt in a (1 1 0) facet (+0.13 V vs RHE) is shown when increasing M loading at the expense of (1 0 0) Pt orientation (at a potential of +0.25 vs RHE), which may decrease the selectivity towards compounds of interest. It can be also observed that onset potentials of the oxide formation/oxide reduction of Pt_yM_{y-1}/C shifts to less positive potentials when increasing Ni or Co content, which reveals that the alloying of Pt with Co or Ni does not hinder OH chemisorption on Pt at > 0.8 V [58-60]. This may be helpful for the enhancement of kinetics of the reaction of interest.

Table 6.2. Deactivation parameters of Pt_yM_{y-1}/C catalysts.

Catalyst	ECSA 1st cycle	ECSA After 500 cycles	Deactivation (%)
	($m^2 \cdot g^{-1}$)		
$Pt_{65}Co_{35}/C$	52	6	88
$Pt_{55}Co_{45}/C$	37	16	57
$Pt_{40}Co_{60}/C$	22	8	64
$Pt_{75}Ni_{25}/C$	63	24	62
$Pt_{65}Ni_{35}/C$	40	7	83
$Pt_{40}Ni_{60}/C$	14	7	50

Table 6.2. summarizes the electrochemical surface area (ECSA) of each catalyst. Deactivation degree is also included and calculated based on the difference of areas after 500 cycles. Although all samples experienced certain degradation degree as denoted by the decrease of the electrochemical surface area shown this table, in agreement to that reported by [61](ref. bimetálicos) Pt-Co and Pt-Ni alloying does not enhance ECSA value, being Pt/M a critical factor for the electrochemical performance. Attending to the initial value of ECSA, catalyst with a higher amount of platinum show the highest value of electrochemical surface area, according to Chakkrapong et al [62, 63]. The replacement of Pt by Ni or Co causes a strong interaction between Pt and the transition metal and the loss of a fraction of the exposed Pt atoms available to

participate in electrode reaction, which diminishes the ECSA value [64]. As a consequence, the electrocatalytic activity can be reduced. On the other hand, the incorporation of a higher proportion of Co to the Pt structure seems to prevent from deactivation as shown in Table 6.2. The as-synthetized Pt_yNi_{y-1}/C catalysts does not follow the same trend although present a deactivation degree of 50% for the highest Ni loading.

According to Saéz et al and Dabo et al, electrocatalytic hydrogenation of organic molecules and hydrogen evolution reaction (HER) are competitive reactions [17, 65]. It is important to note that HOR (hydrogen oxidation reaction) and HER occur simultaneously in both branches, although with different rates [65]. According to this, HER/HOR catalytic reaction were studied by potential step voltammetry using a rotating disk electrode in order to evaluate the kinetics of HER/HOR reaction for each synthesized catalyst to stablish the corresponding HER contribution.

HER/HOR kinetic rate constant (k) as well as the number of electrons transferred (n) have been obtained from the slope and intercept of the representation of the linearized Koutecky-Levich (KL) plot at 0.4 V (Figure 6.7.). Kinetic constant is known to depend on the applied potential, temperature, electrode surface structure, composition of the catalysts, surface adsorption and reaction intermediates [66, 67]. Attached tables in Figure 6.7. shows the values of n and k for each electrode. Attending to n results, it is possible to conclude that as-synthetized catalysts followed a two electron mechanism in HER/HOR reaction. Taking into account both the number of electrons and kinetic constant parameters, $Pt_{55}Co_{45}/C$ and $Pt_{65}Ni_{35}/C$ seem to be more suitable for the hydrogenation reaction to the desired compounds, since they are less prone for hydrogen evolution reaction.

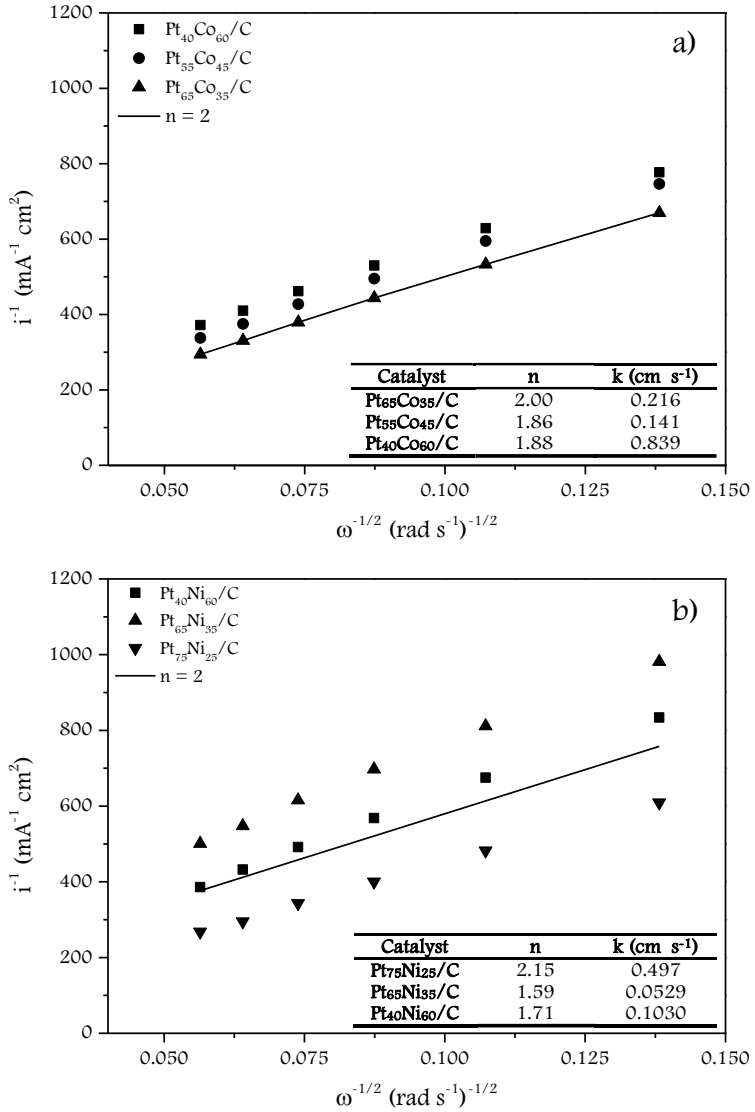

Figure 6.7. *Koutecky-Levich plot in RDE at 0.4 V (vs RHE) in $HClO_4$ 0.1 M at 25 ºC of* ***a.*** *Pt_yCo_{y-1}/C catalysts.* ***b.*** *Pt_yNi_{y-1}/C catalysts.*

3.3. Electrochemical hydrogenation of CMA in PEM cell

The catalytic performance of the as-prepared Pt_yM_{1-y}/C cathodes, exploring three different atomic ratios (Pt/Co: 65/35, 55/45 and 40/60 and Pt/Ni: 75/25, 65/35 and 40/60, respectively), was evaluated towards CMA electrocatalytic hydrogenation.

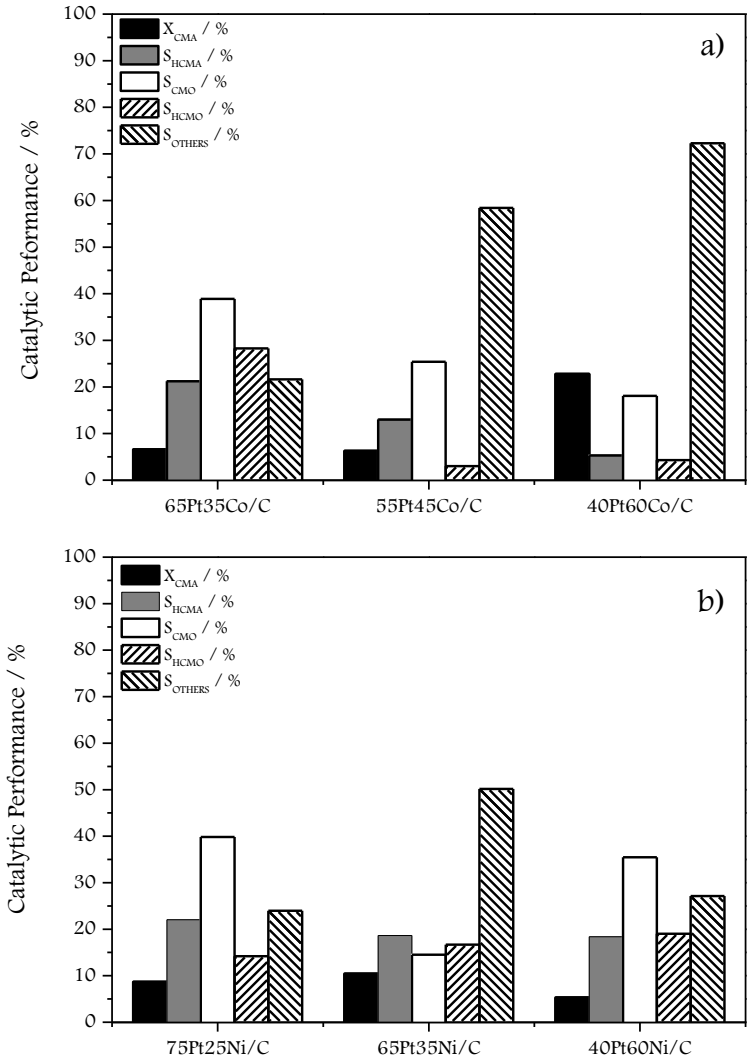

Figure 6.8. Influence of the Pt_yM_{y-1}/C on the CMA conversion and products selectivity. Reaction conditions: Anodic solution: H_2O, Cathodic solution: 100 ppm CMA in 2-propanol, Inlet flow: 1 mL·min^{-1}, Intensity: 0.05 A, Temperature: 70 ^{o}C. **a.** Pt_yCo_{y-1}/C. **b.** Pt_yNi_{y-1}/C.

As can be seen in Figure 6.8.a. the increase of cobalt in the catalyst structure seems not to favor the selectivity to CMO, neither the reduction of secondary by-products formation although it has great influence on the conversion. On the contrary, the replacement of Pt by smaller amounts of cobalt enhanced the formation of CMO [68]. According to Guo et al. [69], an excess of Co oxides (confirmed by TPR analysis) would

cover the surface of Pt. Hence, a suitable Pt/Co ratio is required to obtain the highest electrocatalytic performance. It can be observed that, in agreement with KL characterization results, cathodes with Pt/Co ratios below 55/45 are likely to favor hydrogenation. However, due to the lowest basicity of these samples, further hydrogenation to form acetal-based compounds is catalyzed. It should be mentioned that the proportion of by-products formed from the reaction over any of the Pt_yCo_{y-1}/C catalysts is consistent and even lower than that reported for those system operating under conventional catalyzed conditions [7, 70]. From figure 6.8.b. it is suggested PtNi-based catalysts showed the same trend toward HCMA and CMO formation, decreasing with Ni loading [71] although slight differences can be observed between $Pt_{75}Ni_{25}/C$ and $Pt_{40}Ni_{60}/C$. In this sense, as mentioned above, the basicity of the catalysts seems to have a great influence on the hydrogenation results. In this context, as shown in Figures 6.5. and 6.8.b. PtNi/C catalysts with 40/60 and 75/25 ratios, which have a higher basicity, have very similar selectivity values. However, catalyst with 65/35 Pt/Ni ratio presents an exceptional selectivity towards the formation of by-products, which was much higher than expected and arose from the lower basicity of the sample that results to be key on the selective performance.

One step further, in order to reduce the amount of undesired by-product, two bases were added into the reaction medium [70, 72, 73]. The roles of different organic and inorganic bases as promoters for improving the activity and selectivity to CMO and HCMA are also investigated. Based on the available literature published to date, two weak bases were chosen to perform this study. First, NH_4OH was selected since, according to Wanida Koo et al. [72] OH^- ions may combine with the C=C bond, inhibiting its hydrogenation by following a mechanism as the one showed in Figure 6.9.

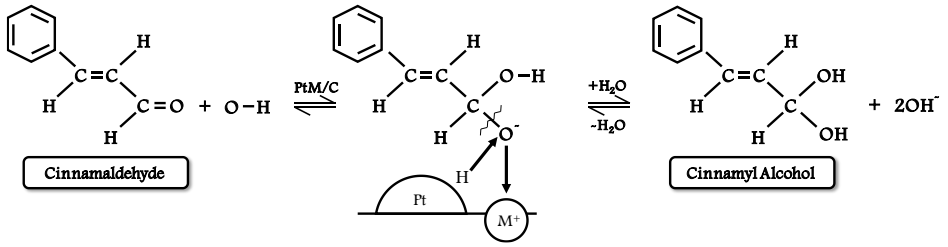

Figure 6.9. Cinnamaldehyde reaction pathway with bimetallic catalysts adapted from proposed by Wanida-Koo for citral.

In the second place, sodium bicarbonate was chosen considering the hydrogenation of bicarbonate to formiate, a good H-donor that might facilitate the aldehyde hydrogenation, according to Szatmári et al. [73]. Different equivalents of each base (0.75-18 equivalents for NH_4OH and 0.75-3 equivalent for $NaHCO_3$) were added into the cathodic reaction medium in order to explore the effect of this variable on the electrocatalytic performance of $Pt_{55}Co_{45}/C$ and $Pt_{65}Ni_{35}/C$ cathodes, which are more sensitive for hydrogenation according to KL characterization. As can be seen from data collected in Table 6.3, only the addition of NH_4OH in the range of 0.75-3 equivalents (specially 0.75 equivalents) is interesting in order to minimize the production of undesired products, which drops to 0.5% in the case of Pt_yCo_{1-y}/C catalyst, following the mechanism proposed by Koo-Amornpattana et al [72]. Due to the steric effect of the benzene ring, in addition to its greater electron density, there is a possibility that the OH^- ion combines in some way with the C=C bond, inhibiting its hydrogenation and favoring the CMA electrochemical hydrogenation to CMO, instead of HCMA and secondary by-products. On the other hand, the addition of the lowest amount of $NaHCO_3$ to the catholyte did not modify the electrocatalytic performance. However, above 0.75 equivalents it resulted in a drop of the selectivity to the value-added compounds, especially CMO. The beneficious effect of the introduction of bicarbonate into the catholyte has been demonstrated in mostly aqueous media in the presence of

ruthenium catalysts but according to the observed data from this work, this effect cannot be extrapolable to other electrocatalytic systems operating in organic media [73]. Therefore, with the aim of exploring the combination of both the Pt/M ratio and the selected equivalents (0.75) of NH_4OH, a last series of experiments was carried out.

Table 6.3. Influence of the addition of NH_4OH or $NaHCO_3$ to the catholyte on the electrocatalytic hydrogenation of CMA over/on $Pt_{55}Co_{45}/C$ (conversion and products selectivity). Reaction conditions: Anodic solution: H_2O, Cathodic solution: 100 ppm CMA in 2-propanol, Inlet flow: 1 mL·min^{-1}, Intensity: 0.05 A, Temperature: 70 °C.

Additive	Eq. Additive	Conversion (%) CMA	Selectivity (%)			
			HCMA	CMO	HCMO	Others
$Pt_{55}Co_{45}/C$						
-	0	6.3	13.0	25.4	3.2	58.41
NH_4OH	0.75	5.9	33.2	51.0	15.3	0.5
	1.5	6.9	26.1	38.1	18.0	21.9
	3	7.2	17.4	31.8	3.5	47.3
	9	18.0	5.8	5.4	0.5	88.3
	18	18.9	3.2	1.3	0.1	95.4
$HNaCO_3$	0.75	7.9	15.2	17.8	9.7	57.3
	1.5	6.3	23.6	0.0	10.6	65.8
	3	6.0	25.1	0.9	5.1	69.0
$Pt_{65}Ni_{35}/C$						
-	0	10.5	18.6	14.5	16.7	50.2
NH_4OH	0.75	8.3	13.6	55.6	9.2	21.6

Figure 6.10. shows the electrocatalytic hydrogenation results obtained for all the atomic ratios. It can be observed from Figure 6.10.a. that the addition of NH_4OH improved the ECH results, especially in the case of $Pt_{55}Co_{45}/C$, which was found to be the less selective toward HER, resulting in the almost complete elimination of undesired by-products (<0.5%). From Figure 6.10.b. it can be concluded that the incorporation of a low amount of NH_4OH clearly shifts selectivity toward CMO formation over PtNi-based cathodes except for that with a Pt/Ni ratio of 40/60. In this case, the production of unwanted products is very high,

perhaps because the addition of NH_4OH is not beneficial to an already very basic sample, according to the titration results.

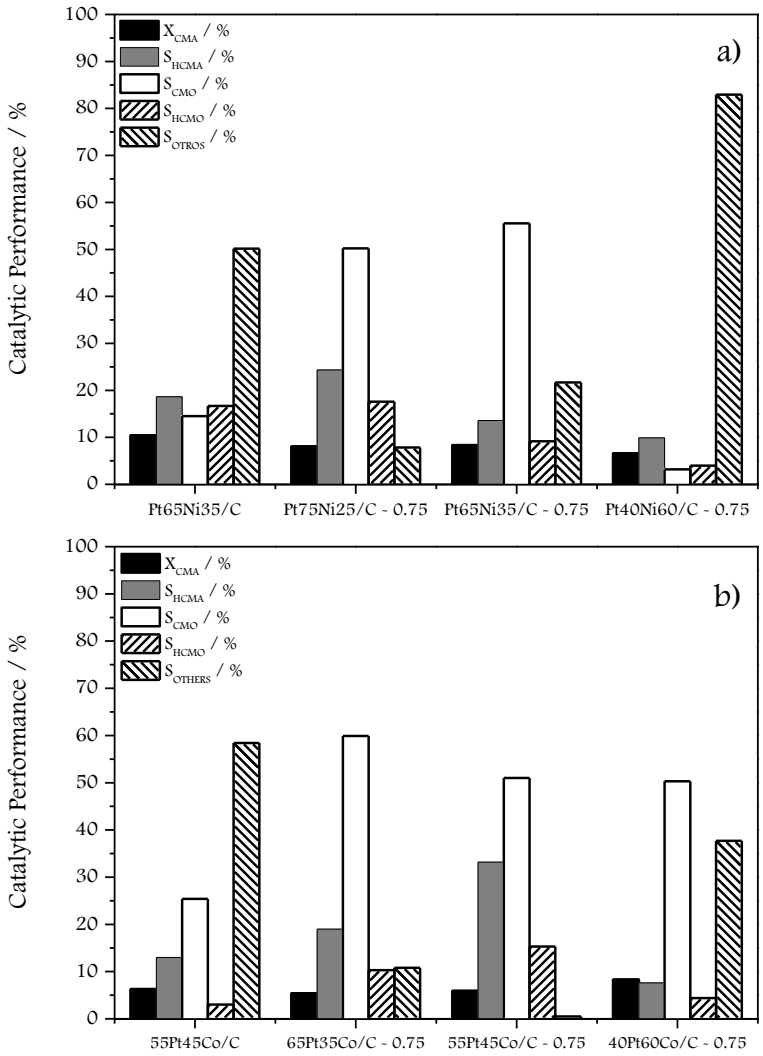

Figure 6.10. Influence of NH_4OH addition to the catholyte on the electrocatalytic hydrogenation of CMA. Over Pt_xM_y/C catalysts. Reaction conditions: Anodic solution: H_2O, Cathodic solution: 100 ppm CMA in 2-propanol, Inlet flow: 1 ml·min^{-1}, Intensity: 0.05 A, Temperature: 70 °C. **a.** Pt_yCo_{y-1}/C. **b.** Pt_yNi_{y-1}/C.

In any case, the minimum production of acetals achieved by this series of catalysts was 7.8 %. Accordingly, this PtCo-based cathode resulted to be the best option in order to maximize the electrochemical selectivity to valuable products, mainly CMO (close to 55%). It is important to note that these promising results were obtained under mild reaction conditions, per cell pass, operating the PEM cathodic chamber in continuous mode.

4. CONCLUSIONS

The incorporation a Ni or Co to a Pt_yM_{1-y}/C (where M stands for Co or Ni) cathode in a suitable Pt/M ratio is found to be key in the synthesis of value added products such as HCMA, CMO or HCMO by means of the electrocatalytic hydrogenation of cinnamaldehyde in a PEM cell. ECH and characterization results showed that the incorporation of certain percentages of cobalt and nickel modifies the catalysts structure and promotes the selectivity to the products of interest. Higher Ni or Co loadings seem to negatively influence on the basicity of the sample enhancing side reactions. In addition, the combination of a suitable Pt/M ratio with the addition of NH_4OH (<3 equivalents) improves CMO production by inhibiting undesirable side reactions (acetal formation). The best electrocatalytic results (33% of selectivity to HCMA, 51 % to CMO and 0.5 % of by-products selectivity) were obtained over $Pt_{55}Co_{45}/C$ cathode when 0.75 equivalents of NH_4OH were used.

REFERENCES

1. Zhao, B.-H., et al., *Selective Hydrogenation of Cinnamaldehyde over Pt and Pd Supported on Multiwalled Carbon Nanotubes in a CO2-Expanded Alcoholic Medium.* Industrial & Engineering Chemistry Research, 2012. **51**(34): p. 11112-11121.
2. Gallezot, P. and D. Richard, *Selective Hydrogenation of α,β-Unsaturated Aldehydes.* Catalysis Reviews, 1998. **40**(1-2): p. 81-126.
3. Chen, X., et al., *Selective hydrogenation of cinnamaldehyde to cinnamyl alcohol over the Co-La-B/SiO2 amorphous catalyst and the promoting effect of La-dopant.* Applied Catalysis A: General, 2003. **253**(2): p. 359-369.
4. Lashdaf, M., et al., *Behaviour of palladium and ruthenium catalysts on alumina and silica prepared by gas and liquid phase deposition in cinnamaldehyde hydrogenation.* Applied Catalysis A: General, 2003. **241**(1): p. 65-75.
5. Li, G.J., et al., *Selective hydrogenation of cinnamaldehyde to cinnamyl alcohol on L-zeolite supported catalysts*, in *Studies in Surface Science and Catalysis*, H. Chon, S.-K. Ihm, and Y.S. Uh, Editors. 1997, Elsevier. p. 1203-1210.
6. Eilerman, R.G. and U.b. Staff, *Cinnamic acid, cinnamaldehyde, and cinnamyl alcohol.* Kirk-Othmer Encyclopedia of Chemical Technology, 2000: p. 1-11.
7. Leng, F., et al., *Selectivity shifts in hydrogenation of cinnamaldehyde on electron-deficient ruthenium nanoparticles.* Comptes Rendus Chimie, 2018. **21**(3): p. 346-353.
8. Jayakumar, A., et al., *Manufacturing the Gas Diffusion Layer for PEM Fuel Cell Using a Novel 3D Printing Technique and Critical Assessment of the Challenges Encountered.* Materials, 2017. **10**(7): p. 796.
9. Kumar, J.A., P. Kalyani, and R. Saravanan, *Studies on PEM fuel cells using various alcohols for low power applications.* 2008.
10. Grigoriev, S.A., et al., *Platinum and palladium nano-particles supported by graphitic nano-fibers as catalysts for PEM water electrolysis.* International Journal of Hydrogen Energy, 2011. **36**(6): p. 4143-4147.
11. Grigoriev, S.A., V.I. Porembsky, and V.N. Fateev, *Pure hydrogen production by PEM electrolysis for hydrogen energy.* International Journal of Hydrogen Energy, 2006. **31**(2): p. 171-175.
12. Millet, P., et al., *PEM water electrolyzers: From electrocatalysis to stack development.* International Journal of Hydrogen Energy, 2010. **35**(10): p. 5043-5052.

13. Ramesh Raju, R., J. Damodar, and S. Jayarama Reddy, *The electrocatalytic hydrogenation of α-aryl acrylic acids.* Electrochemistry Communications, 2002. **4**(2): p. 115-117.
14. Song, Y., et al., *Aqueous phase electrocatalysis and thermal catalysis for the hydrogenation of phenol at mild conditions.* Applied Catalysis B: Environmental, 2016. **182**: p. 236-246.
15. Huang, S., et al., *A bilateral electrochemical hydrogen pump reactor for 2-propanol dehydrogenation and phenol hydrogenation.* Green Chemistry, 2016. **18**(8): p. 2353-2362.
16. Villalba, M., M. del Pozo, and E.J. Calvo, *Electrocatalytic hydrogenation of acetophenone and benzophenone using palladium electrodes.* Electrochimica Acta, 2015. **164**: p. 125-131.
17. Sáez, A., et al., *Electrocatalytic hydrogenation of acetophenone using a Polymer Electrolyte Membrane Electrochemical Reactor.* Electrochimica Acta, 2013. **91**: p. 69-74.
18. Park, K., et al., *Flow reactor studies of the paired electro-oxidation and electroreduction of glucose.* Journal of the Electrochemical Society, 1985. **132**(8): p. 1850-1855.
19. Zhao, D. and C. Xu, *A nanoporous palladium-nickel alloy with high sensing performance towards hydrogen peroxide and glucose.* Journal of Colloid and Interface Science, 2015. **447**: p. 50-57.
20. Pintauro, P.N. and J.R. Bontha, *The role of supporting electrolyte during the electrocatalytic hydrogenation of aromatic compounds.* Journal of Applied Electrochemistry, 1991. **21**(9): p. 799-804.
21. Cirtiu, C.M. and H. Ménard, *Electrocatalytic hydrogenation of octyl aldehyde over Pd catalysts*. Vol. 85. 2011. 475-478.
22. Mahdavi, B., et al., *Electrocatalytic hydrogenation of conjugated enones on nickel boride, nickel, and Raney nickel electrodes*. Vol. 73. 2011. 846-852.
23. Han, X., et al., *Selective Hydrogenation of Cinnamaldehyde over Pt/ZrO2 Catalyst Modified by Cr, Mn, Fe, Co and Ni.* Catalysis Letters, 2006. **109**(3): p. 157-161.
24. Szöllösi, G., et al., *Chemoselective Hydrogenation of Cinnamaldehyde to Cinnamyl Alcohol over Pt/K-10 Catalyst.* Journal of Catalysis, 1998. **179**(2): p. 619-623.
25. Solymosi, F. and A. Szo˝ke, *Conversion of ethane into benzene on Mo2C/ZSM-5 catalyst.* Applied Catalysis A: General, 1998. **166**(1): p. 225-235.

26. Zhu, J., et al., *Thermo-responsive polymer grafted carbon nanotubes as the catalyst support for selective hydrogenation of cinnamaldehyde: Effects of surface chemistry on catalytic performance.* Applied Catalysis A: General, 2019. **575**: p. 11-19.
27. Jiang, F., et al., *Particle size effects in the selective hydrogenation of cinnamaldehyde over supported palladium catalysts.* RSC Advances, 2016. **6**(79): p. 75541-75551.
28. Plomp, A.J., et al., *Particle size effects for carbon nanofiber supported platinum and ruthenium catalysts for the selective hydrogenation of cinnamaldehyde.* Applied Catalysis A: General, 2008. **351**(1): p. 9-15.
29. Li, Y., et al., *Solvent effects on heterogeneous catalysis in the selective hydrogenation of cinnamaldehyde over a conventional Pd/C catalyst.* Catalysis Science and Technology, 2018. **8**(14): p. 3580-3589.
30. Zhang, L., et al., *Studies on the hydrogenation of cinnamaldehyde over Pd/C catalysts.* Journal of Chemical Technology & Biotechnology, 1998. **72**(3): p. 264-272.
31. Sun, Z., et al., *Selective hydrogenation of cinnamaldehyde over Pt nanoparticles deposited on reduced graphene oxide.* RSC Advances, 2014. **4**(4): p. 1874-1878.
32. Bhogeswararao, S. and D. Srinivas, *Intramolecular selective hydrogenation of cinnamaldehyde over CeO2–ZrO2-supported Pt catalysts.* Journal of Catalysis, 2012. **285**(1): p. 31-40.
33. Galvagno, S., et al., *Hydrogenation of cinnamaldehyde over Ru/C catalysts: effect of Ru particle size.* Journal of Molecular Catalysis, 1991. **64**(2): p. 237-246.
34. Ungureanu, A., et al., *Composition-Dependent Morphostructural Properties of Ni–Cu Oxide Nanoparticles Confined within the Channels of Ordered Mesoporous SBA-15 Silica.* ACS Applied Materials & Interfaces, 2013. **5**(8): p. 3010-3025.
35. Zheng, R., et al., *Controlling hydrogenation of CO and CC bonds in cinnamaldehyde using silica supported Co-Pt and Cu-Pt bimetallic catalysts.* Applied Catalysis A: General, 2012. **419-420**: p. 126-132.
36. Luo, B., et al., *PtNi alloy nanoparticles supported on polyelectrolyte functionalized graphene as effective electrocatalysts for methanol oxidation.* Journal of the Electrochemical Society, 2013. **160**(3): p. F262-F268.

37. Kirumakki, S.R., et al., *Hydrogenation of Naphthalene over NiO/SiO2–Al2O3 catalysts: Structure–activity correlation.* Journal of Catalysis, 2006. **242**(2): p. 319-331.
38. Baranova, E.A., et al., *Size and composition for 1–5nm Ø PtRu alloy nano-particles from Cu Kα X-ray patterns.* Journal of Alloys and Compounds, 2009. **471**(1): p. 387-394.
39. West, A.R., *Basic solid state chemistry*. 1999: John Wiley & Sons Inc.
40. Borbath, I., et al., *Controlled Synthesis of Pt3Sn/C Electrocatalysts with Exclusive Sn–Pt Interaction Designed for Use in Direct Methanol Fuel Cells.* Topics in Catalysis, 2013. **56**: p. 1033-1046.
41. Rao, C., et al., *High temperature polymer electrolyte membrane fuel cell performance of PtxCoy/C cathodes.* Journal of Power Sources - J POWER SOURCES, 2010. **195**: p. 3425-3430.
42. Lobato, J., et al., *Study of different bimetallic anodic catalysts supported on carbon for a high temperature polybenzimidazole-based direct ethanol fuel cell.* Applied Catalysis B: Environmental, 2009. **91**(1): p. 269-274.
43. Cantu, D.C., et al., *A Combined Experimental and Theoretical Study on the Activity and Selectivity of the Electrocatalytic Hydrogenation of Aldehydes.* ACS Catalysis, 2018. **8**(8): p. 7645-7658.
44. Sing, K., *The use of nitrogen adsorption for the characterisation of porous materials.* Colloids and Surfaces A: Physicochemical and Engineering Aspects, 2001. **187-188**: p. 3-9.
45. Leofanti, G., et al., *Surface area and pore texture of catalysts.* Catalysis Today, 1998. **41**(1): p. 207-219.
46. Navarro, R.M., et al., *Bimetallic MNi/Al2O3-La catalysts (M=Pt, Cu) for acetone steam reforming: Role of M on catalyst structure and activity.* Applied Catalysis A: General, 2014. **474**: p. 168-177.
47. Venuto, P.B. and E.L. Wu, *Sorption and exchange patterns of benzene-phenolic mixtures over faujasite catalyst: Relevance to phenol ethylation.* Journal of Catalysis, 1969. **15**(2): p. 205-208.
48. Tanksale, A., et al., *Effect of Pt and Pd promoter on Ni supported catalysts—A TPR/TPO/TPD and microcalorimetry study.* Journal of Catalysis, 2008. **258**(2): p. 366-377.
49. Pastor-Pérez, L. and A. Sepúlveda-Escribano, *Low temperature glycerol steam reforming on bimetallic PtSn/C catalysts: On the effect of the Sn content.* Fuel, 2017. **194**: p. 222-228.

50. Dosso, L.A., C.R. Vera, and J.M. Grau, *Aqueous phase reforming of polyols from glucose degradation by reaction over Pt/alumina catalysts modified by Ni or Co.* International Journal of Hydrogen Energy, 2017. **42**(30): p. 18853-18864.

51. Jia, J., et al., *A study on reduction behaviors of the supported platinum–iron catalysts.* Journal of Molecular Catalysis A: Chemical, 1999. **138**(2): p. 177-184.

52. Liotta, L.F., et al., *CoOx catalysts supported on alumina and alumina-baria: influence of the support on the cobalt species and their activity in NO reduction by C3H6 in lean conditions.* Applied Catalysis A: General, 2003. **245**(1): p. 167-177.

53. Dosso, L.A., C.R. Vera, and J.M. Grau, *Pt-Co and Pt-Ni Catalysts of Low Metal Content for H2 Production by Reforming of Oxygenated Hydrocarbons and Comparison with Reported Pt-Based Catalysts.* International Journal of Chemical Engineering, 2018. **2018**: p. 10.

54. Handjani, S., et al., *Influence of the support composition and acidity on the catalytic properties of mesoporous SBA-15, Al-SBA-15, and Al2O3-supported Pt catalysts for cinnamaldehyde hydrogenation.* Journal of Catalysis, 2011. **282**(1): p. 228-236.

55. Shen, Y., et al., *In Situ Assembly of Ultrathin PtRh Nanowires to Graphene Nanosheets as Highly Efficient Electrocatalysts for the Oxidation of Ethanol.* ACS Applied Materials & Interfaces, 2017. **9**(4): p. 3535-3543.

56. Lobato, J., et al., *Composite Titanium Silicon Carbide as a Promising Catalyst Support for High-Temperature Proton-Exchange Membrane Fuel Cell Electrodes.* ChemCatChem, 2016. **8**(4): p. 848-854.

57. Fang, L., et al., *Preparation, characterization and catalytic performance of a novel Pt/SiC.* Electrochemistry Communications, 2011. **13**(12): p. 1309-1312.

58. Yang, H., et al., *Structure and Electrocatalytic Activity of Carbon-Supported Pt−Ni Alloy Nanoparticles Toward the Oxygen Reduction Reaction.* Journal of Physical Chemistry B - J PHYS CHEM B, 2004. **108**.

59. Anderson, A.B., *O2 reduction and CO oxidation at the Pt-electrolyte interface. The role of H2O and OH adsorption bond strengths.* Electrochimica acta, 2002. **47**(22-23): p. 3759-3763.

60. Hernández-Fernández, P., et al., *An opening route to the design of cathode materials for fuel cells based on PtCo nanoparticles.* Applied Catalysis B Environmental, 2007. **77**: p. 19-28.

61. Devivaraprasad, R., et al., *Oxygen Reduction Reaction and Peroxide Generation on Shape-Controlled and Polycrystalline Platinum Nanoparticles in Acidic and Alkaline Electrolytes.* Langmuir, 2014. **30**(29): p. 8995-9006.
62. Chaiburi, C. and V. Hacker, *Catalytic activity of various platinum loading in acid electrolyte at 303 K.* Energy Procedia, 2017. **138**: p. 229-234.
63. Tengco, J.M.M., et al., *Synthesis and Electrochemical Evaluation of Carbon Supported Pt-Co Bimetallic Catalysts Prepared by Electroless Deposition and Modified Charge Enhanced Dry Impregnation.* Catalysts, 2016. **6**(6): p. 83.
64. Rusnaeni, N., et al., *The Influence of Pt Atomic Ratio in the Activity PtNi/C Nanocatalysts for the PEMFC*. Vol. 43. 2013.
65. Dabo, P., et al., *Selective electrocatalytic hydrogenation of 2-cyclohexen-1-one to cyclohexanone.* Electrochimica Acta, 1997. **42**(9): p. 1457-1459.
66. Kadakia, K.S., et al., *Nanostructured F doped IrO2 electro-catalyst powders for PEM based water electrolysis.* Journal of Power Sources, 2014. **269**: p. 855-865.
67. Lust, E., et al., *Pt and Pt–Ru catalysts for polymer electrolyte fuel cells deposited onto carbide derived carbon supports.* Electrochimica Acta, 2013. **101**: p. 130-141.
68. Stassi, J.P., et al., *Formation of different promoted metallic phases in PtFe and PtSn catalysts supported on carbonaceous materials used for selective hydrogenation.* Journal of Catalysis, 2013. **306**: p. 11-29.
69. Guo, Z., et al., *Carbon nanotube-supported Pt-based bimetallic catalysts prepared by a microwave-assisted polyol reduction method and their catalytic applications in the selective hydrogenation.* Journal of Catalysis, 2010. **276**(2): p. 314-326.
70. Li, Y., et al., *Influence of Preparation Modes on Pt–Ni/CNTs Catalysts Used in the Selective Hydrogenation of Cinnamaldehyde to Hydrocinnamaldehyde.* Catalysis Letters, 2008. **126**(3): p. 280-285.
71. Gryglewicz, S., et al., *Performance of Carbon Nanofiber and Activated Carbon Supported Nickel Catalysts for Liquid-Phase Hydrogenation of Cinnamaldehyde into Hydrocinnamaldehyde.* Catalysis Letters, 2014. **144**(1): p. 62-69.
72. Koo-amornpattana, W. and J.M. Winterbottom, *Pt and Pt-alloy catalysts and their properties for the liquid-phase hydrogenation of cinnamaldehyde.* Catalysis Today, 2001. **66**(2): p. 277-287.

73. Szatmári, I., et al., *Promoter effect of bicarbonate in hydrogenation of cinnamaldehyde catalyzed by a water-soluble Ru(II)-phosphine complex.* Inorganica Chimica Acta, 2018. **472**: p. 302-306.

Section IV: Supports and GDL materials for the electrocatalytic hydrogenation of cinnamaldehyde

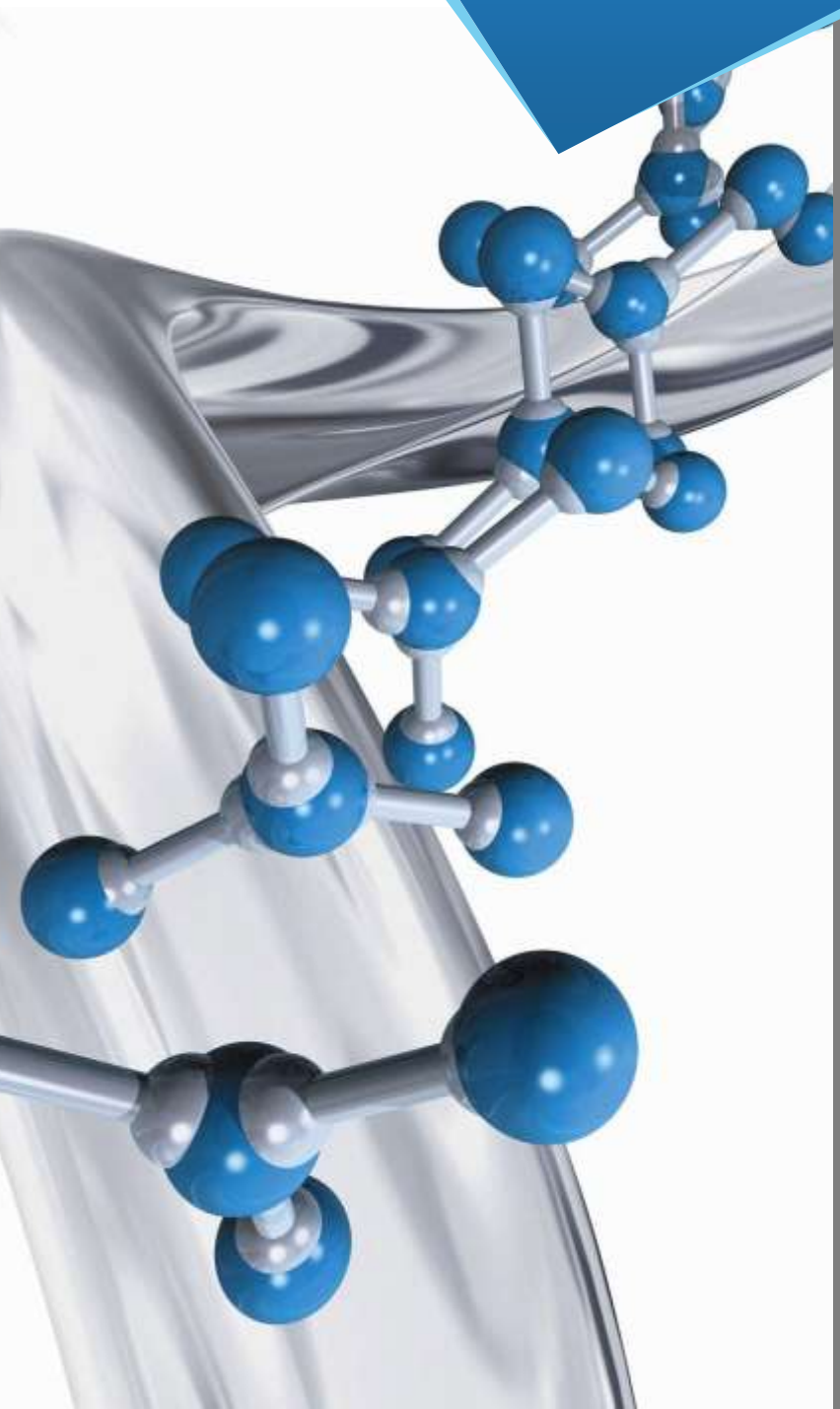

Chapter 7: Electrocatalytic hydrogenation of cinnamaldehyde in a polymeric electrolyte membrane reactor: Influence of the cathodic support and GDL

Chapter 7: Electrocatalytic Hydrogenation of Cinnamaldehyde in a Polimeric Electrolyte Membrane Reactor: Influence of the Cathodic Support and GDL.

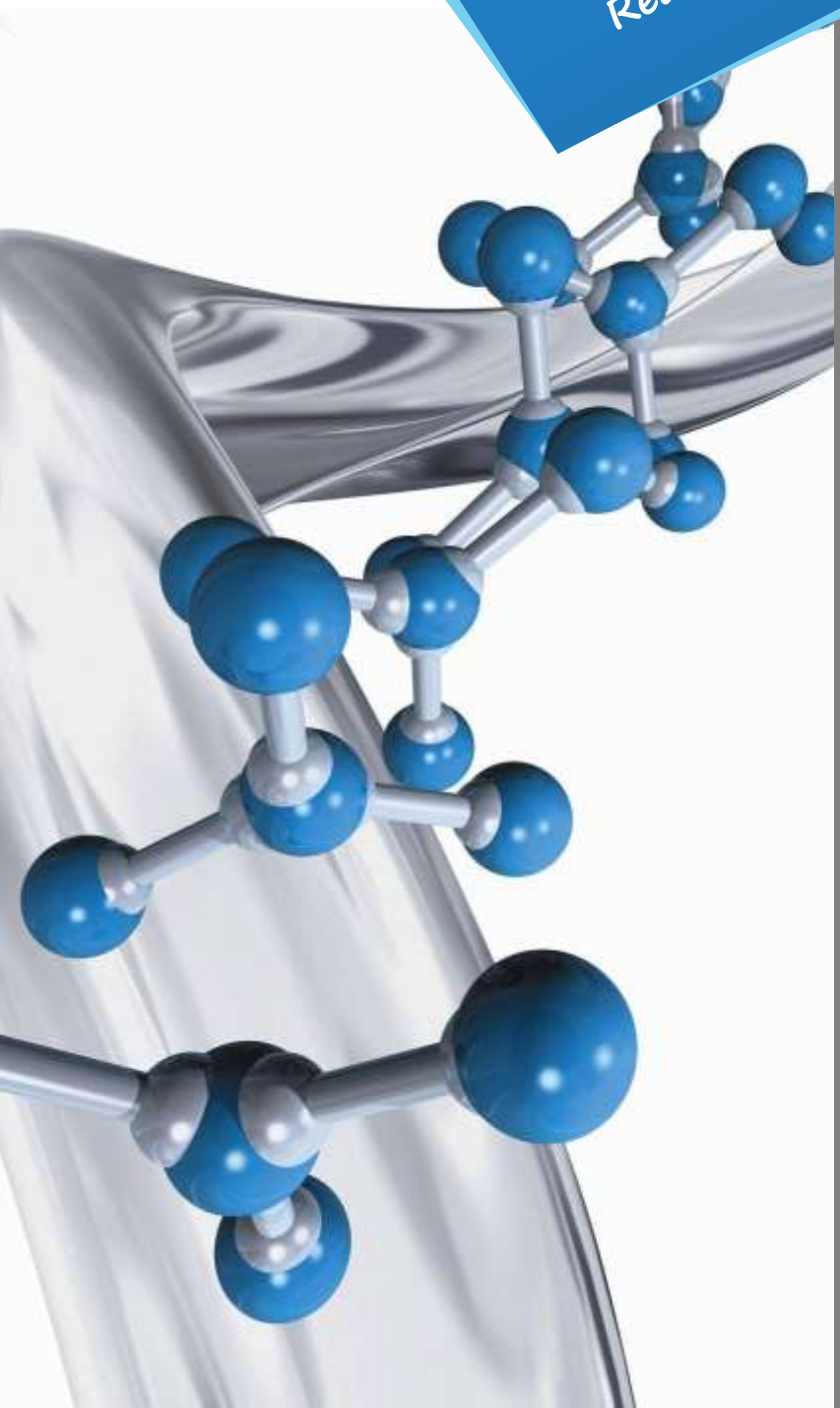

1. INTRODUCTION

2. EXPERIMENTAL
2.1. Catalysts synthesis
2.2. Physicochemical characterization
2.3. Electrochemical characterization
2.4. Membrane electrode assembly (MEA) preparation
2.5. Electrocatalytic hydrogenation tests

3. RESULTS AND DISCUSSION
3.1. Characterization of PtCo-based electrocatalysts
3.1.1. Physicochemical characterization
3.1.2. Electrochemical characterization
3.1.3. Influence of the support on the electrochemical hydrogenation of cinnamaldehyde
3.2. Influence of the gas diffusion layer on the electrocatalytic hydrogenation of cinnamaldehyde

4. CONCLUSIONS

Abstract

This work has been carried out through two studies: i) influence of gas diffusion layer (porous titanium and carbon paper) and, ii) influence of support (Vulcan XC-72, functionalized carbon nanofibers and functionalized carbon nanofibers with a demineralization treatment), using PtCo as cathode in the electrocatalytic hydrogenation of cinnamaldehyde in a PEM cell. From the results of characterization and reaction, from the first study it is extracted as conclusion that porous titanium shows better characteristics to carry out the reaction in terms of mechanical and electrical resistance. On the other hand, the second study shows that the support based on carbon Vulcan XC-72, which presents better crystalline orientation and physicochemical properties offers better hydrogenation results in terms of conversion and selectivity eliminating undesired compounds almost completely.

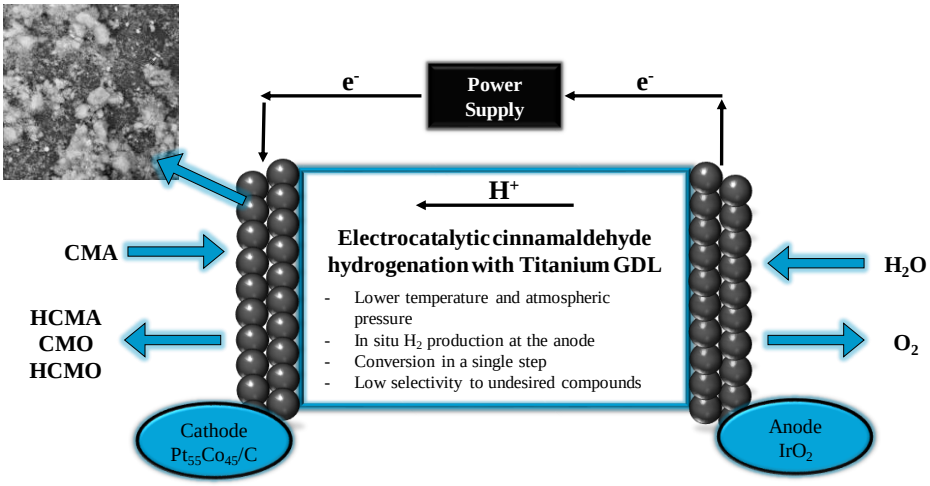

Figure 7.1. *Graphical abstract Chapter 7.*

1. INTRODUCTION

Electrochemical hydrogenation is an alternative route to catalytic hydrogenation. It is performed under more benign conditions (room temperature and atmospheric pressure) and has been carried out since the beginning of the last century [1]. However, at industrial scale, this process has never been as successful as catalytic hydrogenation [2]. In this sense, polymer electrolyte membrane cells have provided an alternative to heterogeneous catalytic hydrogenation due to its ability to produce dissociated hydrogen in-situ on a catalyst surface with high efficiency [3, 4]. In a PEM cell, under an applied electrical current, water is oxidized to generate protons in the anode [5], which pass through the polymeric membrane to the cathode where take part in the hydrogenation reaction on the catalyst surface. Researchers have investigated related topics in furfural [6], acetophenone [2], phenol [7], and cinnamaldehyde [8] hydrogenation.

The membrane electrode assembly (MEA) is the prime component/heart of a PEM cell, it consists of an electrolyte (proton - exchange membrane), sandwiched between two gas diffusion electrodes (GDEs), Figure 7.2. provide a 2D view of all the key functional components of a GDE. One of the most important components of a GDE is the gas diffusion layer (GDL). This component is responsible for the transportation of electrons, heat and reactants or products to and from the catalyst layer with minimal voltage, current, thermal, interfacial and fluidic losses. Graphite bipolar plates, carbon cloth and carbon paper are widely used for GDL materials [9, 10] but the contact with reaction media and consumption of carbon result in the degradation of the GDL decreasing the efficiency and performance of the system. Therefore, materials with high- corrosion resistance and high positive overpotential

such as porous titanium can be used as an alternative to carbon based ones [11].

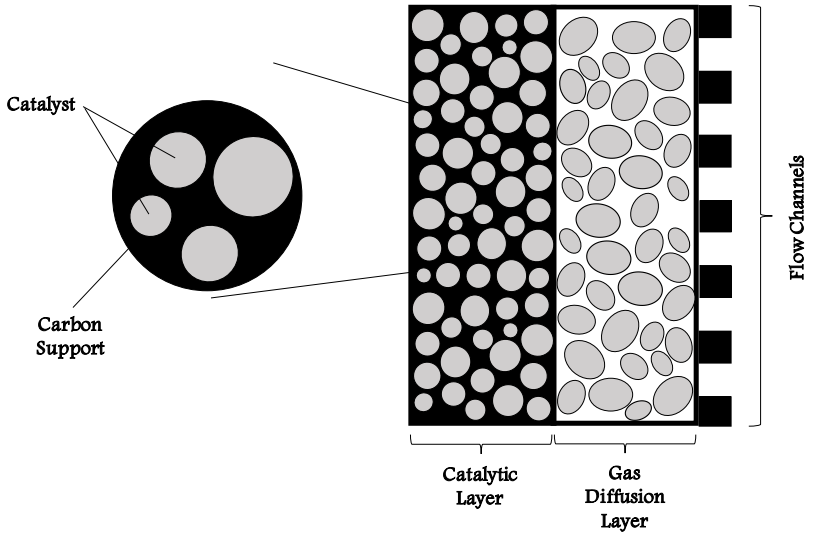

Figure 7.2. *Microscopic scheme of a gas diffusion electrode.*

On the other hand, chemioselective hydrogenation of α,β-unsaturated aldehydes to their semihydrogenated products, that is, saturated aldehydes from hydrogenation of the C=C bond conjugated with the carbonyl group or unsaturated alcohols from hydrogenation at the C=O bond, is particularly challenging [12] in the synthesis of many important chemicals, such as fragrances, pharmaceuticals, and others [13]. An example of this compound is the cinnamaldehyde (CMA). This compound is a vinylogue of benzaldehyde, and the behavior of this aldehyde group is the same as if it was an aromatic aldehyde [14], it is a biologically active compound found in the essential oils of the genus cinnamomum, which is responsible for the distinctive aroma and flavor of cinnamon [15-17]. The carbonyl group present in cinnamaldehyde competes with saturation of the carbon-carbon double bond [18-20]. The hydrogenation of CMA leads usually to a mixture of hydrocinnamaldehyde (HCMA), cinnamyl alcohol (CMO) and phenylpropanol (HCMO) [21]. Moreover, acetals and other unidentified

high molecular weight compounds can also be produced in significant quantities (60 – 90 %) when polar solvents are used [12, 20, 22]. However, this side reaction can be controlled by the addition of basic compounds to the reaction media. Figure 7.3. shows the schematically pathway of cinnamaldehyde hydrogenation. HCMA is found to be an important intermediate in the preparation of pharmaceuticals used in the treatment of HIV [23], and CMO is a source material for cinnamates, which are widely used in the production of perfumes [24]. Because of the competitive reduction of the aldehyde carbonyl and olefin groups, the selectivity of CMA to HCMA or CMO varies considerably with the catalyst composition and structure. This catalytic properties are influenced by many factors as the addition of a second metal, the size and orientation of the metal particles would favor the adsorption of cinnamaldehyde for the production of HCMA or CMO, the nature of the support, the metal precursor of the catalyst, presence of promoters, the solvent, additives, the process conditions applied and even trace impurities in the reactant [14, 25-29].

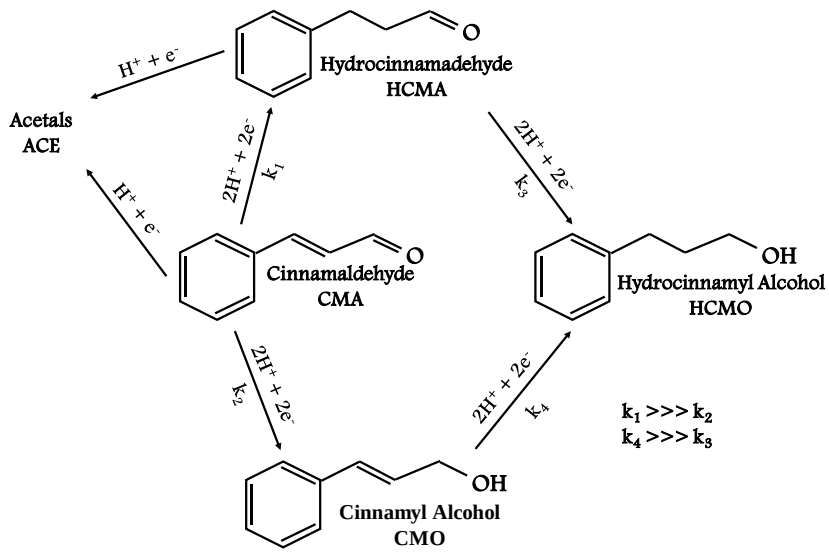

Figure 7.3. Main reaction pathways of the hydrogenation of cinnamaldehyde

Much interest has been focused on the use of homogeneous catalyst, despite the critical drawbacks associated with such catalysts. However, from the point of view of green chemistry, the development of industrial processes for the direct production of organic intermediates using heterogeneous catalysts is a meaningful target, since the catalyst could be easily removed from the reaction mixtures and wastes could be largely diminished. Monometallic-supported catalysts are widely used for this purpose, but bimetallic catalysts show growing attention. The strategy of introducing second metals such as Fe, Co, Cu, Ni, Co, Fe and Sn into Pt is widely used to increase hydrogenation selectivity to unsaturated alcohols [14, 30-33]. In particular, the addition of cobalt to platinum is found to increase the selectivity to CMO. However, although the selectivity patterns of these metals and their positive effects on the catalytic performance are known in conventional catalysis, their effects in electrocatalysis medium have not been studied in any detail.

Furthermore, support plays an important role in the selectivity of cinnamaldehyde hydrogenation. Porous carbon-based materials such as activated carbons (ACs), carbon black, carbon nanotubes (CNTs) and carbon nanofibers (CNFs) have been mainly used as support of mono and bimetallic catalyst for the selective hydrogenation of CMA [34-37]. In this sense, carbon blacks, especially Vulcan XC-72, are one of the most widely used as electrocatalytic supports in PEM cells, due to their high electrical conductivity, corrosion resistance and advantageous textural characteristic, among them extended mesoporous structure and hydrophobous character [38]. This support has been used successfully in CMA hydrogenation reactions with very satisfactory results in terms of conversion and selectivity to interest products [39]. In the other hand, carbon nanofibers have attracted interest because of their unique textural and mechanical properties and the absence of micropores or impurities in the structure, which provide a rare set of properties: high

electrical conductivity, combined with a large fraction of active sites corresponding to the exposed edges of the graphite platelets, which are available for chemical and physical interactions with various species [40]. In this sense, platinum supported on carbon nanofibers (CNFs) turned out to be one of the most active catalysts for the hydrogenation of cinnamaldehyde [36, 41]. In general, the activity for hydrogenation was high, while the selectivity towards the desired cinnamyl alcohol was low [12, 36]. Therefore, the challenge is to increase the selectivity of these Pt/CNF catalysts while maintaining high activity [41]. Recently, Toebes et al. reported an influence between the oxygen-containing surface groups and the selectivity to C=O bond when Pt/CNF catalyst were used [35, 36].

Among some of the most robust methods for the preparation of one-pot reduced catalysts are polyol method. This method entails several key parameters such as metal precursor concentration, pH, temperature, etc. However, the precise control of these parameters allowed for the preparation well defined monodispersed, energy-efficient, environmental friendly and not susceptible of impurities catalysts [42, 43]. In previous studies carried out by this research group the effectiveness of this method has been demonstrated in the preparation of selective catalysts towards CMO and HCMA with a low production of unwanted products.

In this paper, the major objective is to report the the influence of different supports for PtCo-based bimetallic catalysts on the selective electrocatalytic hydrogenation of CMA carried out in a PEM cell, producing hydrogen in-situ by water electrolysis. Then, after selection of the best cathodic support, the influence of the gas diffusion layer has been also explored. The chemical, physical and electrochemical characteristics of the catalysts were also studied.

2. EXPERIMENTAL

2.1. Catalysts Synthesis

For this study PtCo (ratio) has been deposited on three different carbonaceous supports. Firstly, Commercial Vulcan XC-72 (PtCo/XC-72), functionalized low density carbon nanofibers prepared in our laboratory (PtCo/CNF LS) [44], and functionalized low density carbon nanofibers washed with fluorhydric acid in order to eliminate the possible traces of Si and Ni present in the support (PtCo/CNF LS D).
The carbon supported PtCo/C (C: Vulcan XC-72, CNF-LS, CNF-LS D) catalysts were prepared by the modified polyol method as described in Section B.2.3., using ethylene glycol as reducing agent (Sigma-Aldrich, Germany) as described by Baranova et al [42].

2.2. Physicochemical characterization

Pt content was measured by using an inductively coupled plasma spectrometer (ICP, Model Liberty Sequential, Varian). XRD analyses were performed on a Phillips PW-1700 diffractometer using Nickel-filtered Cu Kα radiation. The morphology of the PtCo supported samples was observed with Scanning Electron Microscopy (SEM) (Phenom ProX) with a field emission gun with a resolution of 15 kV and a magnification of 2000 x. Temperature-programmed reduction (TPR) experiments were conducted in a commercial Micromeritics AutoChem 2950 HP unit with TCD detection. Surface area/porosity measurements were analyzed in a Micromeritics ASAP 2010 sorptometer unit, with N_2 at 77 K as the adsorbate. The total specific surface area was determined by the multipoint BET method and the distributions of mesopore and micropore diameters were determined by the methods proposed by Barret, Joyner and Halenda (BJH) and Horvath-Kawazoe, respectively. HCl titrations were performed on a SCHOTT Titroline with automatic dosager. Using a starting NaCl solution served as a blank.

2.3. Electrochemical characterization

Electrochemical characterization was carried out by means of voltammetric experiments (CV), using a computer connected potentiostat Autolab PGSTAT128N (Ecochemie, The Netherlands) and a three-electrode cell. Measurements like CV and HER/HOR reaction were performed using a glassy carbon rotating disk electrode (GC-RDE, Metrohm Autolab) of 5 mm diameter using as working electrode, a platinum wire (Metrohm) as the counter electrode and a Ag/AgCl (Metrohm, KI 3 M) reference electrode. Impedance spectroscopy measurement were also carried out. All the procedures of the electrochemical characterization tecniques described above are found in Section B.5., as well as the ink preparation procedure.

2.4. Membrane electrode assembly (MEA) preparation

Membrane Electrode Assembly (MEA) was prepared using commercial IrO_2 (99 wt. %) purchased from Alfa Aesar and PtCo/C (using CNF LS, CNF LS D and Vulcan XC-72 as supports) with a catalyst loading of 2 and 0.5 mg/cm^2, respectively. Electrodes were prepared by spraying inks contained proper amounts of each electrocatalyst dispersed in a solution of Nafion ionomer (5 wt.%, Sigma-Aldrich) and water (anode) or 2-propanol (cathode) directly on the Nafion membrane as described in Section B.3.

2.5. Electrocatalytic Hydrogenation Tests

Electrocatalytic experiments were performed with an Autolab PGSTAT128N potentiostat – galvanostat in a polymer electrolyte membrane (PEM) electrode cell.

Electrochemical hydrogenation products were analyzed by means of gas chromatography, using an Agilent 7820A apparatus equipped with

a FID detector and a capillary column (Agilent DB-624, 30 m x 0.25 mm x 0.5 μm). The CMA conversion and products selectivity/yield were calculated as described in Section B.6.

3. RESULTS AND DISCUSSION

3.1. Characterization of PtCo-based electrocatalyst

3.1.1. Physicochemical characterization

Physicochemical characterization of the synthesized electrocatalysts was performed by means of X-Ray diffraction (XRD), Inductively Coupled Plasma-Atomic Emission Spectroscopy (ICP-AES) and N_2 physisorption measurements, as summarized in Table 1.

Fig 7.4. shows the XRD patterns for the different supported platinum-cobalt-based cathodic electrocatalysts. The clear diffraction peak at 25º is associated with the (0 0 2) graphitic planes of carbon (hexagonal structure). However, the intensity of this reflection related to carbon Vulcan XC-72 is quite lower than those of low surface carbon nanofibers supports, which could be assigned to the graphitization degree of the latter ones and the higher specific surface area of carbon Vulcan. Regarding the electrocatalysts, all of them display the characteristic patterns of Pt fcc diffraction peaks, although the 2θ values related to (1 1 1), (1 0 0) and (1 1 0) diffractions, which appear at around 40º, 46º and 68º, are slightly displaced towards higher values due to the incorporation of cobalt into the Pt lattice and the formation of alloys [45]. Furthermore, the broader peaks corresponding to (1 0 0) and (1 1 0) and overlapping with Co-species reflections make difficult the calculation of the average particle size by the Scherrer equation [46]. Hence, no particle size could be determined by this technique although modified polyol method is expected to lead small crystallites (<5 nm).

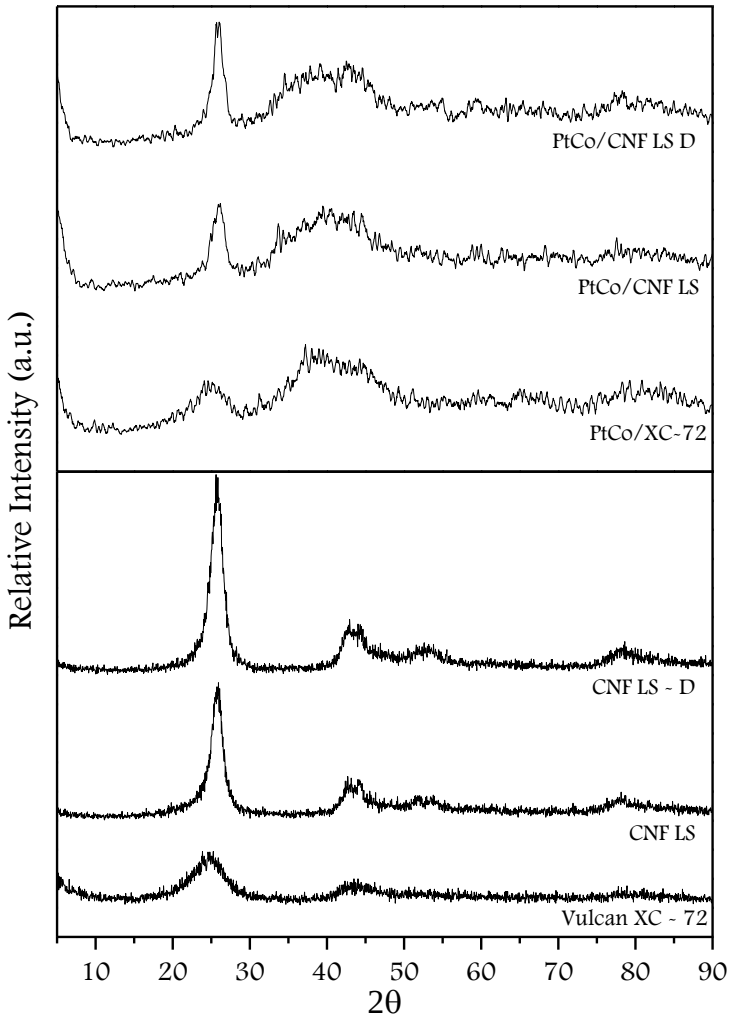

Figure 7.4. XRD patterns of the synthesized PtCo/C catalyst and the supports.

Figure 7.5. shows the possible morphological changes of the different as-prepared catalysts evaluated by Scanning Electron Microscopy (SEM). It can be observed that the catalyst particles are less aggregated when XC-72 is used as support. However, not important differences can be seen between both CNF-based catalysts, which suggests similar properties after the purification process compared to the parent CNF support.

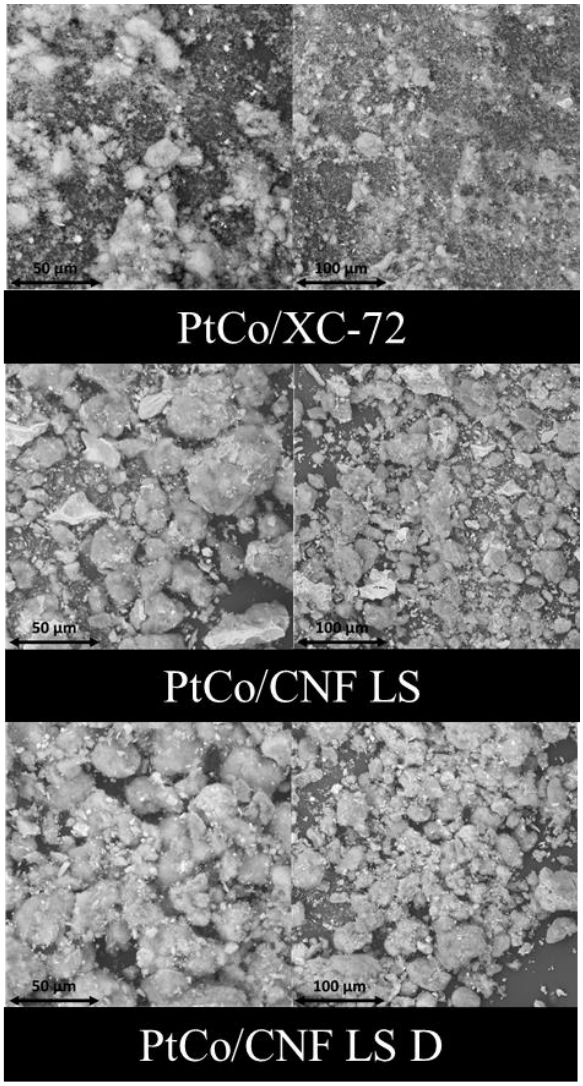

Figure 7.5. SEM images of the catalyst studied.

The reducibility of supported bimetallic catalysts is an important factor influencing the catalytic behavior. Figure 7.6. illustrates the TPR profiles of each PtCo/C catalyst studied. Supported PtCo cathodic catalyst show hydrogen consumption peaks in the region between 280 - 325 °C, attributed to the reduction of the cobalt oxide CoO to Co [47, 48]. Additionally, PtCo/XC-72 catalyst showed an additional consumption peak at 220 °C, corresponding to the reduction of cobalt oxide spinel

(Co_3O_4) to CoO, throughout the reduction of Co^{3+} surface ions [49, 50], the shift to lower temperatures could be related to H_2 spillover over Pt. Finally, the peaks observed above 500 °C can be ascribed to gasification of the carbon support producing methane [51, 52].

It can be observed that this peak is shifted to lower reduction temperatures in case of CNF-based supports, which might be due to the large crystallites formed due to a higher number of oxygen surface groups.

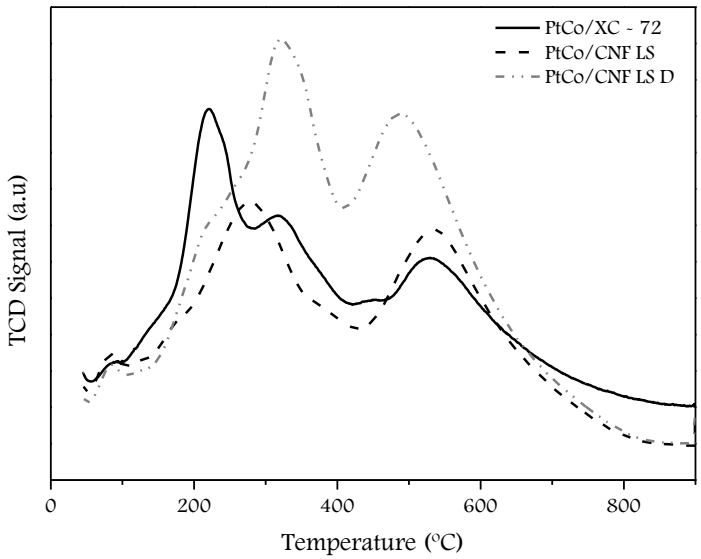

Figure 7.6. Temperature-programmed reduction (TPR) profiles of the synthesized PtCo/C catalysts.

According to the nitrogen adsorption/desorption analysis, Table 7.1. shows the main physicochemical characteristics of both the supports and PtCo catalysts synthetized in this work (BET surface area, pore volume and diameter).

Tabla 7.1. Textural parameters of the bimetallic catalysts.

Catalyst	Pt atomic ratio (%)	BET Surface Area ($m^2 \cdot g^{-1}$)	Pore Volume ($cm^3 \cdot g^{-1}$)	Average Pore Diameter (nm)
Vulcan XC-72	-	231	0.403	7.7
CNF LS	-	115	0.485	16.7
CNF LS – D	-	110	0.476	17.4
PtCo/XC-72	55	156	0.504	13.3
PtCo/CNF LS	55	81	0.301	15.1
PtCo/CNF LS-D	55	80	0.265	13.6

Isotherms of PtCo/C catalysts and those related to each support can be seen in Figure 7.7. According to the IUPAC classification, all isotherms are adjusted to a type I-IV adsorption-desorption profile, which is relative to microporous solids that have an adsorption profile at very low relative pressures. This fact is due to the strong interaction between the pore walls and the adsorbate, but also at higher relative pressures.

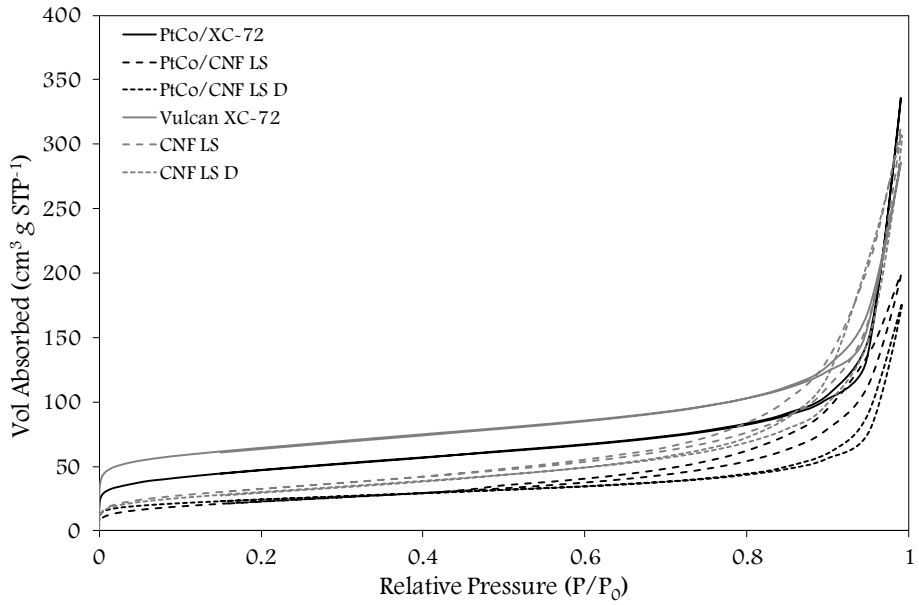

Figure 7.7. Nitrogen adsorption/desorption isotherms

The mesoporous adsorption leads to multilayer formation until, at a certain temperature condensation takes place, giving a sharp adsorption volume increase [53]. All profiles have an H3 hysteresis type related to the mesoporous capillary condensation associated with their different filling and emptying characteristic of solids pores formed from aggregates or agglomerates of particles forming slit shaped pores, with non-uniform size or shape. The changes in surface area of these catalysts can be seen clearly from the surface area and pore size. Carbon Vulcan XC-72 combines double specific surface area and much larger number of micropores (Figure 7.8.) than CNF LS and CNF LS-D supports. After metal deposition, PtCo supported on CNFs LS and CNF LS-D catalysts displayed lower BET areas and average pore diameter than those corresponding to the parent supports, which can be attributed to the pore blockage by the metal particles that prevent from the adsorption of N_2 molecules on their surface. In case of PtCo/XC-72 catalyst, a lower BET area was also observed but pore volume and average pore diameter was increased, probably due to the blockage of micropores located in its structure.

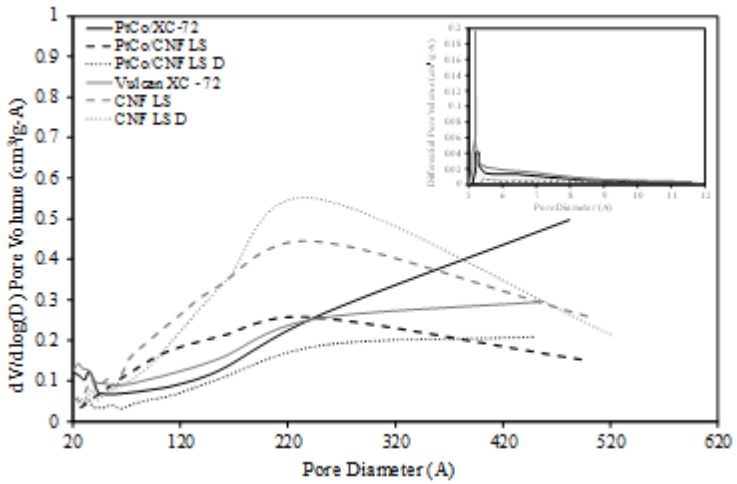

Figure 7.8. Pore distribution of the PtCo/C catalysts and parent supports.

In order to evaluate the acid-base character of the supports and the as-prepared PtCo catalysts HCl titrations were carried out (Figure 7.9.). Prior to the metal incorporation, all samples presented a basic character since HCl consumption is higher than of the blank especially in case of the carbon nanofibers. However, after metal incorporation, the basic character of the resulting catalysts increases, suggesting that the actives metals provide the catalysts of more basic sites. According to previous studies, basicity may influence selectivity towards the products of interest.

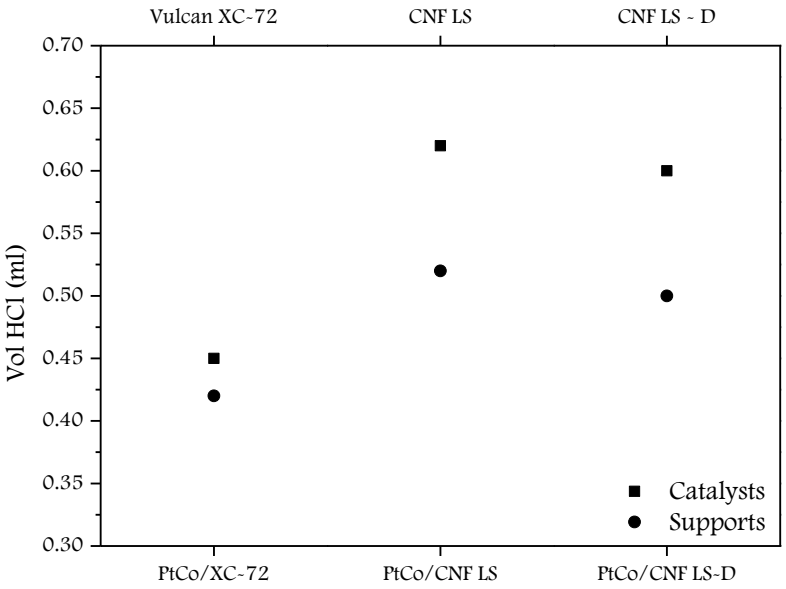

Figure 7.9. HCl titration results of the catalyst and the supports studied.

3.1.2. Electrochemical characterization

In order to evaluate the influence of the cathodic support on the electrochemical performance of the as-prepared PtCo/C catalysts cyclic voltammetry essays were carried out by ranging potential from 0.05 to 1.4 V vs RHE at a scan rate of 50 $mV \cdot s^{-1}$. Figure 7.10. shows the cyclic voltammograms related to each of the synthetized catalysts conducted for 500 cycles in order to calculate the ECSA and to simulate the degradation

of each sample. Degradation of these materials/catalysts is clearly noticeable since, as the number of cycles increases, the areas of the peaks associated to the adsorption and desorption of H_2 decreased. Electrodes based on PtCo/XC-72 and PtCo/CNF LS only showed hydrogen desorption peaks at a potential of 0.13 V vs RHE, which were characteristic of platinum orientation in a (1 1 0) plane. However, electrode based on Pt/GNF LS D presented two platinum preferential orientations, one higher peak at 0.13 V vs RHE (characteristic to (1 1 0) plane) and a second lower peak at 0.25 V vs RHE, that shows a (1 0 0) orientation, characteristic of strong hydrogen adsorption [54]. According to Durndell et al. an increase of (1 0 0) facets density favors the hydrogenation of C=C bond [55].

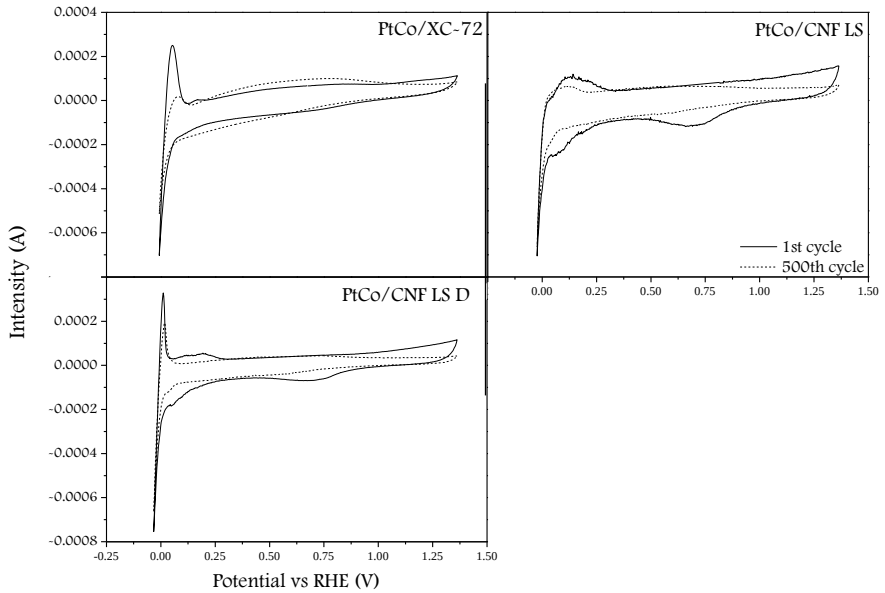

Figure 7.10. Cyclic voltammograms in 0.1 M $HClO_4$, at 25 °C (50 mV s^{-1} scan rate).

Moreover, Figure 7.11 shows the normalized ECSA along the cycles. As can be seen, the ECSA values decreases with the increasing number of cycles, which implies degradation of the catalyst and suggests that the fraction of the bimetallic catalyst that is available to participate

in electrode reactions decreases during the operation of the electrode. Attending to the initial values of ECSA, active sites on PtCo/CNF LS D catalyst seemed to be less accessible to the electrolyte [56]. According to the deactivation values, both are very similar, despite the PtCo/CNF LS D catalyst show values half lower than the other catalysts, being the less electrochemical active catalyst. This decrease in ECSA value may be related with the treatment received by the support, that could favors the formation of cobalt oxides (visible with higher intensity in the TPR profile of Figure 7.6.) and as reported by Millán et al., the presence of cobalt oxides could block the active centers of Pt [57].

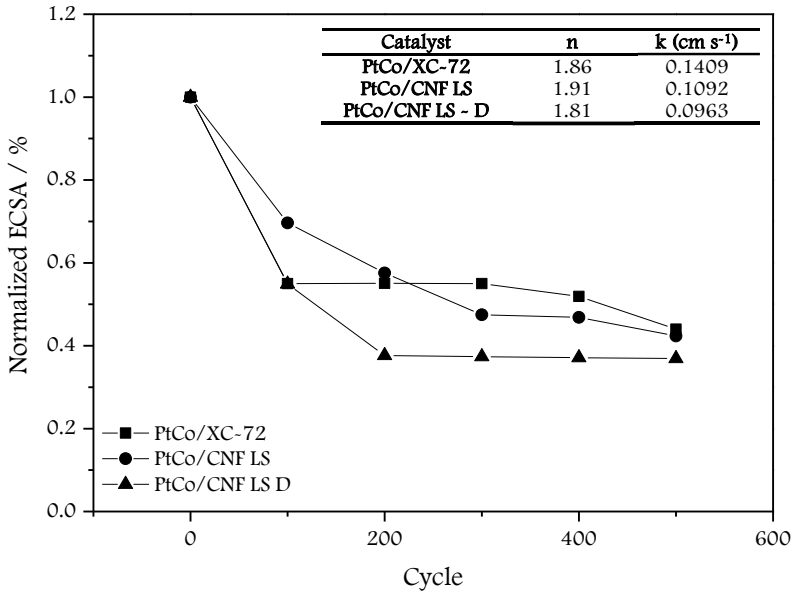

Figure 7.11. Normalized ECSA of the catalysts studied.

On the other hand, HER/HOR catalytic reactions were studied by potential step voltammetry in a half cell (three electrodes) using a rotating disk electrode in order to evaluate the kinetics for all the catalysts synthesized with the aim to determine the HER contribution related to each synthetized cathode. It is well known that electrocatalytic hydrogenation of organic compounds and hydrogen evolution reaction

(HER) are competitive reactions [2, 58]. However, it is important to note that HER and hydrogen oxidation reaction (HOR) occur simultaneously in both branches, although with different rates [58]. In this sense, LSVs were carried out in order to study HER/HOR catalytic reactions and determine the HER contribution for each catalyst.

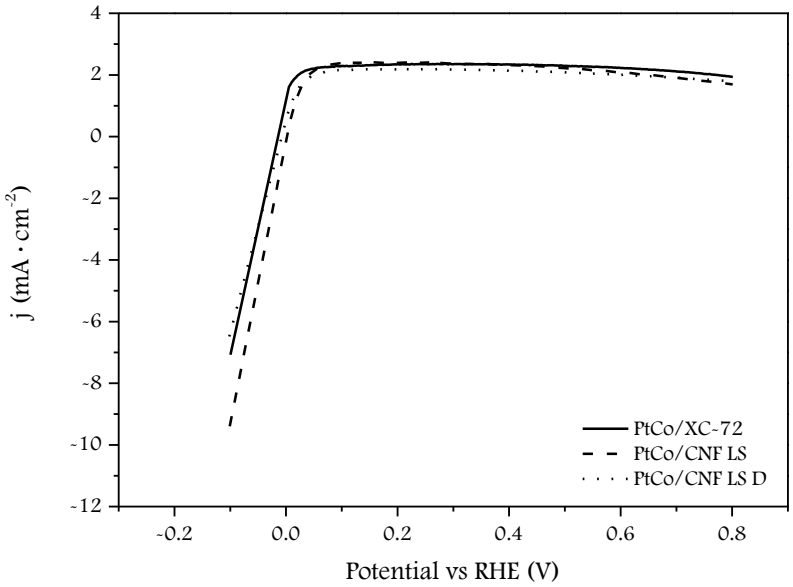

Figure **7.12.** Linear sweep voltammetry scans (5 mV·s^{-1} scan rate)

Figure 7.12. shows linear sweep voltammograms performed for the as-prepared catalysts studied. PtCo/CNF LS exhibits better HER activity, showing that this catalyst has better properties for the hydrogen evolution reaction. In addition, linear sweep voltammetries had been carried out at different rotation rates for each catalyst in order to know the HER/HOR kinetic rate constant (k) and the number of electrons transferred (n), which were obtained from the slope and intercept of the linearized Koutecky-Levich plot at 0.4 V (included as an attached table in Figure 7.13). Attending to the number of electrons transferred, as expected, n values are close to 2 suggesting a two electron mechanism in HER/HOR reactions. Taking into account the kinetic constants,

PtCo/CNF LS D shows the lowest value, which suggests that this catalyst shows the least predisposition to the reduction of protons into H_2.

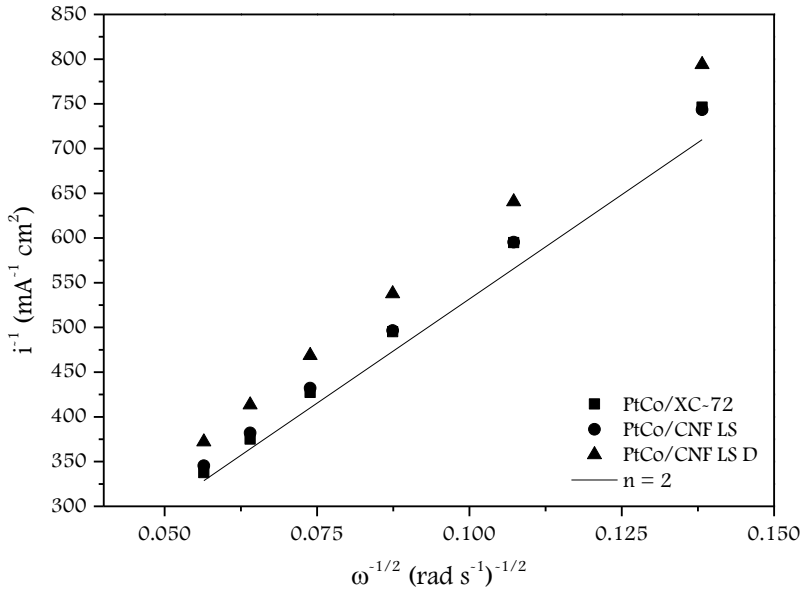

Figure 7.13. Koutecky-Levich plot (RDE at 0.4 V (vs RHE)) in $HClO_4$ 0.1 M at 25 ºC for PtCo/C catalysts.

3.1.3. Influence of the support on the electrochemical hydrogenation of cinnamaldehyde

Figure 7.14. represents the electrochemical hydrogenation results obtained using different carbon-based materials as PtCo cathodic supports. Regarding products selectivity, along with the value-added hydrogenation compounds (HCMA, CMO and HCMO), acetals were also obtained by an acid-catalyzed reaction of CMA and HCMA with 2-propanol solvent [59]. When acetals are formed, the C=O group becomes protected and its hydrogenation is not possible, which results in a decreased selectivity towards CMO [60]. It should be mentioned that PtCo/XC-72 catalyst shows the best electrochemical hydrogenation results since it is able to decrease the production of undesired products below 0.5 %. As reported by Ramli et al. carbon black (and specially one

of its derivates, Vulcan XC-72) is one of the most useful supports for increasing the electrochemical surface area and performance of the cathode catalysts [61]. In contrast, PtCo/CNF LS and PtCo/CNF LS D electrodes show lower catalytic performance. Despite of the slight enhancement in the catalytic activity of the CNF-supported catalysts, probably as a result of the interactions between the support and metal particles, which might modify the geometric characteristic of these electrodes, selectivity towards CMO is highly reduced due to a notable increase in the production of unwanted products, especially in the case of PtCo/CNF LS D catalyst.

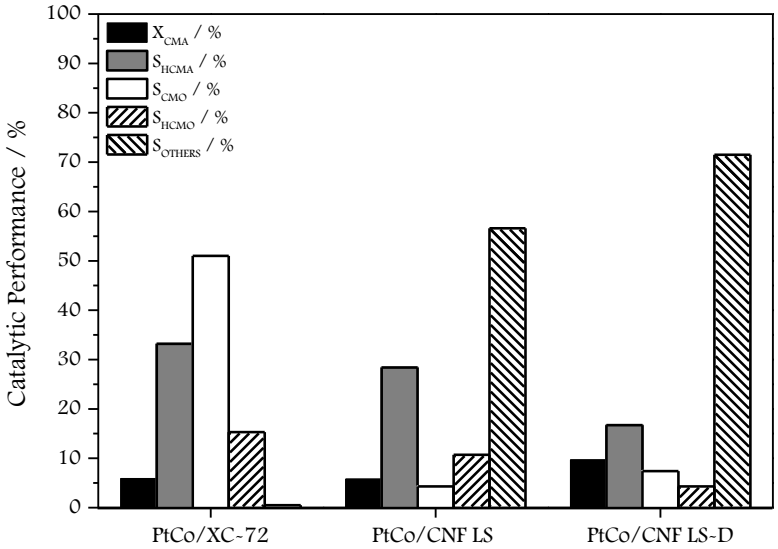

Figure 7.14. Influence of the support on the CMA electrohydrogenation. Reaction conditions: Anodic solution: H_2O, Cathodic solution: 100 ppm CMA in 2-propanol + 0.75 equivalents of NH_4OH, Inlet flow: 1 ml·min^{-1}, Intensity: 0.05 A, Temperature: 70 ^{o}C.

As occurs in conventional catalysis, chemoselective hydrogenation demands a careful control of support polarity and metal particle size-oxidation state in order to obtain a high selectivity to the corresponding unsaturated alcohol. Another factor that can have a great

influence on the hydrogenation results is the amount of oxygenated groups present in the support. Contradictory reports are available in literature with respect to the influence of the surface oxygen groups on the performance of carbon supported catalysts towards the hydrogenation of α, β-unsaturated aldehydes. Some studies point to an increased selectivity towards the unsaturated alcohol with an increased concentration of surface oxygen groups [62], while others observed an opposite trend. In this sense, Mahata et al. emphasized the importance of oxygen-containing surface groups on carbon supports. They found an increased selectivity to the unsaturated alcohol with a lower amount of oxygen-containing groups on the carbon surface, instead of a decrease of conversion [52].

Therefore, additionally, EDX tests have been carried out in order to establish the amount of oxygenated groups comprised on each of the supports used for the preparation of the proposed cathodes. Vulcan XC-72, CNF LS and CNF LS D supports have been determined to have an oxygen concentration of 2.5, 14.7 and 15 %, respectively, which shows that, indeed, a low concentration of oxygenated groups causes an increase in the selectivity towards cinnamyl alcohol. The PtCo/XC-72 catalyst, which has the lowest concentration of oxygenated groups provides the highest selectivity towards CMO (>50%). The lower concentration of electronegative oxygen of this support would facilitate a higher electron transfer from the carbon support to the metal active species. This could result in an increase in the Pt fraction and a rise in the electron density in the Pt sites, which intensify the effect of the addition of the promoters. However, PtCo supported on CNF LS and CNF LS D led to 55-70% by-products, respectively, which suggests that different surface oxygenated groups present on these supports could help to catalyze side reactions. Moreover, due to differences on the structure

of these supports, accessibility to the active sites could occur in a different manner.

On the other hand, the treatment under fluoride acid to eliminate the traces of Si and Ni seemed to negatively affect the selectivity to the desired products. This loss of selectivity of carbon nanofiber supported catalysts could be explained by the lack of surface area regards to the catalyst supported over Vulcan XC-72 [56, 63] and ECSA value, which is half smaller than those of PtCo over non-treated CNFs or XC-72. It is known that the purifying treatment (by inorganic acids) could modify the surface of the carbonaceous material leading to the development of surface oxygenated groups (by oxidation and functionalization). Hence, differences in the textural properties collected in Table 7.1. can be related to a compromise between the partial destruction of micropores (decrease of the surface area) and the elimination of metal particles blocking pore walls, which would increase the specific surface area [64, 65].

In this context, it must be noted that this work presents the best selectivity to CMO (>50%) along with almost nule formation of by-products, which was achieved working in continuous mode and mild reaction conditions in a PEM cell reactor, using water as a source of hydrogen and PtCo/XC-72 as cathode. Synthetized by the modified polyol method, this catalyst presents a suitable particle size, basicity, PtCo ratio/proportion and interaction with the support as well as ECSA value.

3.2. Influence of the gas diffusion layer on the eletrocatalytic hydrogenation of cinnamaldehyde

In order to explore the influence of the gas diffusion layer material on the catalytic performance for the electrochemical hydrogenation of cinnamaldehyde, electrochemical impedance and

electrohydrogenation experiments were carried out using carbon paper and porous titanium (porosity = 10 μm) as GDLs.

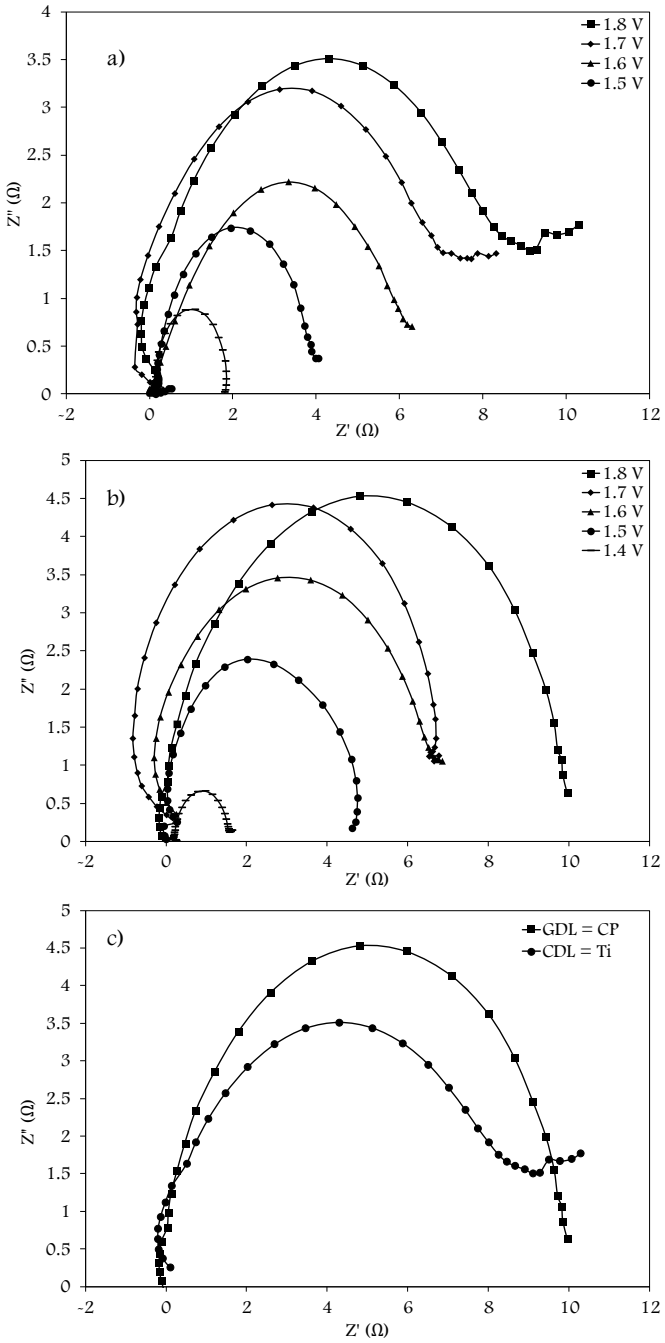

Figure 7.15. Nyquist plots of **a.** porous titanium and **b.** carbon paper gas diffusion layer in the range 1.8-1.4 V. **c.** Comparison of the Nyquist plots of both gas diffusion layers at 1.8 V.

Electrochemical impedance spectroscopy (EIS) essays were conducted in order to quantify the resistances related to the hydrogenation process in the PEM cell. Figures 7.15.a. and 7.15.b. show the Nyquist plots, representing the real component of the resistance (Z') vs the imaginary component (Z") of the cell, using carbon paper and porous titanium GDLs, respectively. It can be seen that in both cases at high cell voltages the spectrum consists of a single depressed semicircle, with the high-frequency (HF) intercept, R_Ω and a diameter R_p. With decreasing voltage, Rp also decreases showing the same behavior as that observed by other authors [66]. Figure 7.15.c. shows a comparison between the two gas diffusion layers at a fixed potential of 1.7 V. Titanium-based gas diffusion layer seems to offer less resistance than carbon paper, which may be due to the easy deformation of the carbon-based material hindering the circulation along the channels of the cell.

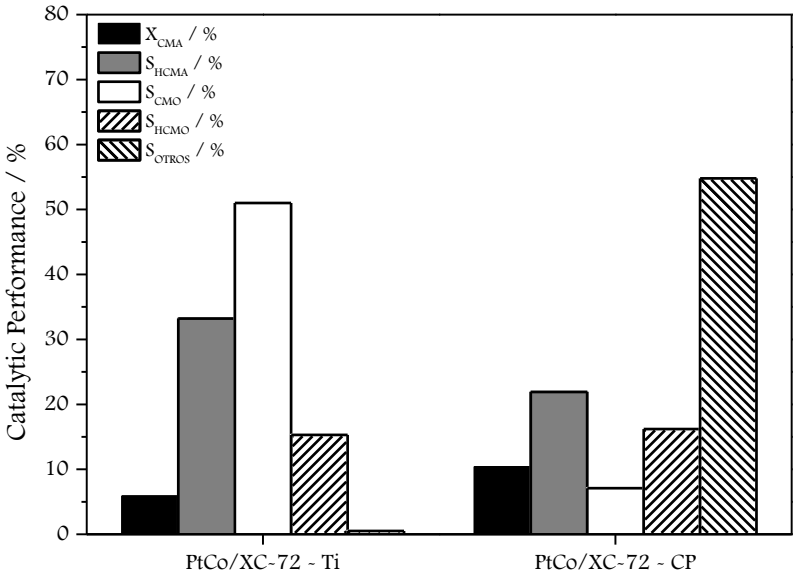

Figure 7.16. Influence of the gas diffusion layer with PtCo/XC-72 catalyst on the CMA conversion and products selectivity. Reaction conditions: Anodic solution: H_2O, Cathodic solution: 100 ppm CMA in 2-propanol+0.75 equivalents of NH_4OH, Inlet flow: 1 ml·min^{-1}, Intensity: 0.05 A, Temperature: 70 ^oC.

Attending to the electrocatalytic hydrogenation results (Figure 7.16) the gas diffusion layer composed of porous titanium shows better results than carbon paper in terms of selectivity. Under selected operating conditions, the carbon paper-based diffusion layers suffer a deformation that hinders the proper circulation of fluids throughout the cell, which increases the residence time of reactants per pass and consequently the conversion. However, it also causes a further hydrogenation of cinnamaldehyde to the undesired by-products. For instance, the carbon paper was observed to be much deteriorated after disassembling of the cell. Even more, some of the channels were invaded with pieces of carbon paper that come off the MEA due to deterioration. However, in the experiments conducted using titanium, no deformation neither deterioration of the GDL were observed.

4. CONCLUSIONS

PtCo catalysts supported on Vulcan XC-72, low surface non-functionalized CNF, and CNF treated with hydrofluoric acid were prepared by the modified polyol method and tested in the electrohydrogenation of CMA in an electrochemical PEM cell, where hydrogen is produced in-situ by water electrolysis.

The influence of the type of carbonaceous material as support on the synthesis of PtCo bimetallic cathodes plays a key role on the selective electrochemical hydrogenation performance of CMA to CMO. Compared with non-functionalized low-density nanofibers (CNF LS) and demineralized non-functionalized low-density nanofibers (CNF LS D), carbon Vulcan XC-72 seems to be the best cathodic catalyst support for the electrochemical hydrogenation of cinnamaldehyde in acidic media. PtCo supported on XC-72 showed the highest CMA electro-reduction to the desired compounds (CMO, HCMA and HCMO), probably related to the physicochemical properties of this material, such as a larger surface

area, a good dispersion of the Pt particles, lower particle size and quite lower content of oxygenated groups in the support. Therefore, this catalyst presents lower electrochemical deactivation and a suitable orientation of the crystalline planes that favors the production of the compounds of interest.

The Influence of the gas diffusion layer on the electrocatalytic hydrogenation of CMA in a PEM cell over PtCo/C cathode and IrO_2-based anode has been also studied using two common materials (porous titanium and carbon paper), whose influence in PEM cells is already reported but unknown for an electrochemical hydrogenation reaction of an α,β-unsaturated aldehyde.

The MEA system based on the porous Ti GDL showed a higher electrochemical hydrogenation performance than that based on the carbon paper gas diffusion layer. This fact could be attributed to the lower ohmic resistance of the Ti-based system, showed by the EIS experiments and a very low deterioration of the GDL. Therefore, the combination of PtCo/XC-72 cathodic electrode and the use of a porous titanium gas diffusion layer has a clear effect on the selectivity of the reaction, resulting in an almost null production of undesired compounds (0.5 %), and reaching, therefore, HCMA and CMO selectivity values of 33 and 51 %, respectively. These results, obtained per single-pass under in continuous mode and using protons generated in situ in the PEM cell, are very competitive compared to those from conventional hydrogenation carried out at atmospheric pressure.

REFERENCES

1. Moutet, J.-C., *Electrocatalytic hydrogenation on hydrogen - active electrodes. A review.* Organic Preparations and Procedures International, 1992. **24**(3): p. 309-325.
2. Sáez, A., et al., *Electrocatalytic hydrogenation of acetophenone using a Polymer Electrolyte Membrane Electrochemical Reactor.* Electrochimica Acta, 2013. **91**: p. 69-74.
3. Wu, X., J. Benziger, and G. He, *Comparison of Pt and Pd catalysts for hydrogen pump separation from reformate.* Journal of Power Sources, 2012. **218**: p. 424-434.
4. Wu, X., et al., *Electrochemical Hydrogen Pump with SPEEK/CrPSSA Semi-Interpenetrating Polymer Network Proton Exchange Membrane for H2/CO2 Separation.* ACS Sustainable Chemistry & Engineering, 2014. **2**(1): p. 75-79.
5. Green, S.K., et al., *Electrocatalytic Reduction of Acetone in a Proton-Exchange-Membrane Reactor: A Model Reaction for the Electrocatalytic Reduction of Biomass.* ChemSusChem, 2012. **5**(12): p. 2410-2420.
6. Green, S.K., et al., *The electrocatalytic hydrogenation of furanic compounds in a continuous electrocatalytic membrane reactor.* Green Chemistry, 2013. **15**(7): p. 1869-1879.
7. Huang, S., et al., *A bilateral electrochemical hydrogen pump reactor for 2-propanol dehydrogenation and phenol hydrogenation.* Green Chemistry, 2016. **18**(8): p. 2353-2362.
8. Mahdavi, B., et al., *Electrocatalytic hydrogenation of conjugated enones on nickel boride, nickel, and Raney nickel electrodes*. Vol. 73. 2011. 846-852.
9. Borup, R., et al., *Scientific Aspects of Polymer Electrolyte Fuel Cell Durability and Degradation.* Chemical Reviews, 2007. **107**(10): p. 3904-3951.
10. Jayakumar, A., et al., *Manufacturing the Gas Diffusion Layer for PEM Fuel Cell Using a Novel 3D Printing Technique and Critical Assessment of the Challenges Encountered.* Materials, 2017. **10**(7): p. 796.
11. Steen, S.M., et al., *Investigation of titanium liquid/gas diffusion layers in proton exchange membrane electrolyzer cells.* International Journal of Green Energy, 2017. **14**(2): p. 162-170.
12. Plomp, A.J., et al., *Particle size effects for carbon nanofiber supported platinum and ruthenium catalysts for the selective hydrogenation of cinnamaldehyde.* Applied Catalysis A: General, 2008. **351**(1): p. 9-15.

13. Jung, A., et al., *Performance of carbon nanomaterial (nanotubes and nanofibres) supported platinum and palladium catalysts for the hydrogenation of cinnamaldehyde and of 1-octyne.* Applied Catalysis A: General, 2009. **362**(1): p. 95-105.
14. Li, Y., et al., *Influence of Preparation Modes on Pt–Ni/CNTs Catalysts Used in the Selective Hydrogenation of Cinnamaldehyde to Hydrocinnamaldehyde.* Catalysis Letters, 2008. **126**(3): p. 280-285.
15. Cocchiara, J., Letizia, C.S., Lalko, J., Lapczynski, A., Api, A.M.,, *Fragrance material review on cinnamaldehyde.* Food and Chemical Toxicology, 2005. **43**(6): p. 867-923.
16. Gruenwald, J., J. Freder, and N. Armbruester, *Cinnamon and Health.* Critical Reviews in Food Science and Nutrition, 2010. **50**(9): p. 822-834.
17. Peter, K., *Handbook of herbs and spices*. Vol. 3. 2006: Woodhead publishing.
18. Lashdaf, M., et al., *Behaviour of palladium and ruthenium catalysts on alumina and silica prepared by gas and liquid phase deposition in cinnamaldehyde hydrogenation.* Applied Catalysis A: General, 2003. **241**(1): p. 65-75.
19. Wang, D. and Y. Zhu, *An Effective Pt-Cu/SiO2 Catalyst for the Selective Hydrogenation of Cinnamaldehyde.* Journal of Chemistry, 2018. **2018**: p. 7.
20. Leng, F., et al., *Selectivity shifts in hydrogenation of cinnamaldehyde on electron-deficient ruthenium nanoparticles.* Comptes Rendus Chimie, 2018. **21**(3): p. 346-353.
21. Hu, D., et al., *Three-Dimensionally Hierarchical Pt/C Nanocomposite with Ultra-High Dispersion of Pt Nanoparticles as a Highly Efficient Catalyst for Chemoselective Cinnamaldehyde Hydrogenation.* ChemCatChem, 2018. **10**(4): p. 779-788.
22. Zhang, L., et al., *Studies on the hydrogenation of cinnamaldehyde over Pd/C catalysts.* Journal of Chemical Technology and Biotechnology, 1998. **72**(3): p. 264-272.
23. Nagpure, A.S., et al., *Hydrogenation of cinnamaldehyde to hydrocinnamaldehyde over Pd nanoparticles deposited on nitrogen-doped mesoporous carbon.* RSC Advances, 2016. **6**(50): p. 44333-44340.
24. Li, Y., Z.-G. Li, and R.-X. Zhou, *Bimetallic Pt-Co catalysis on carbon nanotubes for the selective hydrogenation of cinnamaldehyde to cinnamyl alcohol: Preparation and characterization.* Journal of Molecular Catalysis A: Chemical, 2008. **279**(1): p. 140-146.

25. Merlo, A.B., et al., *PtSn/SiO2 catalysts prepared by surface controlled reactions for the selective hydrogenation of cinnamaldehyde.* Applied Catalysis A: General, 2010. **383**(1): p. 43-49.

26. Yamada, H. and S. Goto, *The Effect of Solvents Polarity on Selective Hydrogenation of Unsaturated Aldehyde in Gas-Liquid-Solid Three Phase Reactor.* JOURNAL OF CHEMICAL ENGINEERING OF JAPAN, 2003. **36**(5): p. 586-589.

27. Tauster, S.J., *Strong metal-support interactions.* Accounts of Chemical Research, 1987. **20**(11): p. 389-394.

28. Gallezot, P. and D. Richard, *Selective Hydrogenation of α,β-Unsaturated Aldehydes.* Catalysis Reviews, 1998. **40**(1-2): p. 81-126.

29. Handjani, S., et al., *Influence of the support composition and acidity on the catalytic properties of mesoporous SBA-15, Al-SBA-15, and Al2O3-supported Pt catalysts for cinnamaldehyde hydrogenation.* Journal of Catalysis, 2011. **282**(1): p. 228-236.

30. Zang, W., et al., *Catalytic hydrogenation by noble-metal nanocrystals with well-defined facets: a review.* Catalysis Science & Technology, 2015. **5**(5): p. 2532-2553.

31. Rong, Z., et al., *Selective hydrogenation of cinnamaldehyde to cinnamyl alcohol over graphene supported Pt-Co bimetallic catalysts.* Vol. 144. 2014. 980-986.

32. Marinelli, T.B.L.W., S. Nabuurs, and V. Ponec, *Activity and Selectivity in the Reactions of Substituted α,β-Unsaturated Aldehydes.* Journal of Catalysis, 1995. **151**(2): p. 431-438.

33. Dai, L.-X., et al., *Self-supported composites of thin Pt–Sn crosslinked nanowires for the highly chemoselective hydrogenation of cinnamaldehyde under ambient conditions.* Inorganic Chemistry Frontiers, 2015. **2**(10): p. 949-956.

34. Planeix, J.M., et al., *Application of Carbon Nanotubes as Supports in Heterogeneous Catalysis.* Journal of the American Chemical Society, 1994. **116**(17): p. 7935-7936.

35. Toebes, M.L., et al., *Support effects in the hydrogenation of cinnamaldehyde over carbon nanofiber-supported platinum catalysts: characterization and catalysis.* Journal of Catalysis, 2004. **226**(1): p. 215-225.

36. Toebes, M.L., et al., *Support effects in hydrogenation of cinnamaldehyde over carbon nanofiber-supported platinum catalysts: Kinetic modeling.* Chemical Engineering Science, 2005. **60**(21): p. 5682-5695.

37. Vu, H., et al., *Bimetallic catalysis on carbon nanotubes for the selective hydrogenation of cinnamaldehyde.* Journal of Catalysis, 2006. **240**(1): p. 18-22.

38. Lázaro, M.J., et al., *Study and application of carbon black vulcan XC-72R in polymeric electrolyte fuel cells.* Carbon Black: Production, Properties and Uses, 2011: p. 41-68.

39. Szumełda, T., et al., *Hydrogenation of cinnamaldehyde in the presence of PdAu/C catalysts prepared by the reverse "water-in-oil" microemulsion method.* Applied Catalysis A: General, 2014. **487**: p. 1-15.

40. Toebes, M.L., et al., *The influence of oxidation on the texture and the number of oxygen-containing surface groups of carbon nanofibers.* Carbon, 2004. **42**(2): p. 307-315.

41. Plomp, A.J., et al., *Catalysts based on platinum–tin and platinum–gallium in close contact for the selective hydrogenation of cinnamaldehyde.* Journal of Catalysis, 2009. **263**(1): p. 146-154.

42. Baranova, E.A., et al., *Single-step polyol synthesis of alloy Pt7Sn3 versus bi-phase Pt/SnOx nano-catalysts of controlled size for ethanol electro-oxidation.* Journal of Applied Electrochemistry, 2010. **40**(10): p. 1767-1777.

43. Nik roseley, N.r., et al., *The Role of Hydroxide Ions in the Synthesis of Ni Nanoparticles Using High Temperature Polyol Method.* Applied Mechanics and Materials, 2013. **391**: p. 18-22.

44. Jiménez, V., et al., *Improving hydrogen storage in modified carbon materials.* International Journal of Hydrogen Energy, 2012. **37**(5): p. 4144-4160.

45. Luo, B., et al., *PtNi alloy nanoparticles supported on polyelectrolyte functionalized graphene as effective electrocatalysts for methanol oxidation.* Journal of the Electrochemical Society, 2013. **160**(3): p. F262-F268.

46. Baranova, E.A., et al., *Size and composition for 1–5nm Ø PtRu alloy nano-particles from Cu Kα X-ray patterns.* Journal of Alloys and Compounds, 2009. **471**(1): p. 387-394.

47. Palma, V., et al., *Hydrogen production through catalytic low-temperature bio-ethanol steam reforming.* Clean Technologies and Environmental Policy, 2012. **14**.

48. Paryjczak, T., J. Rynkowski, and S. Karski, *Thermoprogrammed reduction of cobalt oxide catalysts.* Journal of Chromatography A, 1980. **188**(1): p. 254-256.

49. Liotta, L.F., et al., *CoOx catalysts supported on alumina and alumina-baria: influence of the support on the cobalt species and their activity in NO*

reduction by C3H6 in lean conditions. Applied Catalysis A: General, 2003. **245**(1): p. 167-177.

50. Dosso, L.A., C.R. Vera, and J.M. Grau, *Pt-Co and Pt-Ni Catalysts of Low Metal Content for H2 Production by Reforming of Oxygenated Hydrocarbons and Comparison with Reported Pt-Based Catalysts.* International Journal of Chemical Engineering, 2018. **2018**: p. 10.
51. Crisafulli, R., et al., *On the promotional effect of Cu on Pt for hydrazine electrooxidation in alkaline medium.* Applied Catalysis B: Environmental, 2018. **236**: p. 36-44.
52. Mahata, N., et al., *Selective hydrogenation of cinnamaldehyde to cinnamyl alcohol over mesoporous carbon supported Fe and Zn promoted Pt catalyst.* Applied Catalysis A: General, 2008. **339**(2): p. 159-168.
53. Leofanti, G., et al., *Surface area and pore texture of catalysts.* Catalysis Today, 1998. **41**(1): p. 207-219.
54. Lobato, J., et al., *Composite Titanium Silicon Carbide as a Promising Catalyst Support for High-Temperature Proton-Exchange Membrane Fuel Cell Electrodes.* ChemCatChem, 2016. **8**(4): p. 848-854.
55. Durndell, L.J., et al., *Selectivity control in Pt-catalyzed cinnamaldehyde hydrogenation.* Scientific Reports, 2015. **5**: p. 9425.
56. Andersen, S.M., et al., *Durability of carbon nanofiber (CNF) & carbon nanotube (CNT) as catalyst support for Proton Exchange Membrane Fuel Cells.* Solid State Ionics, 2013. **231**: p. 94-101.
57. Millán, M., et al., *Enhancement of Electrode Stability Using Platinum–Cobalt Nanocrystals on a Novel Composite SiCTiC Support.* ACS Applied Materials & Interfaces, 2017. **9**(7): p. 5927-5936.
58. Dabo, P., et al., *Selective electrocatalytic hydrogenation of 2-cyclohexen-1-one to cyclohexanone.* Electrochimica Acta, 1997. **42**(9): p. 1457-1459.
59. Lashdaf, M., et al., *Role of acidity in hydrogenation of cinnamaldehyde on platinum beta zeolite.* Microporous and Mesoporous Materials, 2004. **75**(1): p. 149-158.
60. Bai, Y., et al., *Highly Selective Continuous Flow Hydrogenation of Cinnamaldehyde to Cinnamyl Alcohol in a Pt/SiO2 Coated Tube Reactor.* Catalysts, 2018. **8**: p. 58.
61. Ramli, Z.A.C. and S.K. Kamarudin, *Platinum-Based Catalysts on Various Carbon Supports and Conducting Polymers for Direct Methanol Fuel Cell Applications: a Review.* Nanoscale Research Letters, 2018. **13**(1): p. 410.

62. Toebes, M.L., et al., *Influence of oxygen-containing surface groups on the activity and selectivity of carbon nanofiber-supported ruthenium catalysts in the hydrogenation of cinnamaldehyde.* Journal of Catalysis, 2003. **214**(1): p. 78-87.

63. Kaluža, L., et al., *Highly loaded carbon black supported Pt catalysts for fuel cells.* Catalysis Today, 2015. **256**: p. 375-383.

64. Solhy, A., et al., *MWCNT activation and its influence on the catalytic performance of Pt/MWCNT catalysts for selective hydrogenation.* Carbon, 2008. **46**(9): p. 1194-1207.

65. Zgolicz, P.D., et al., *Influence of the support and the preparation methods on the performance in citral hydrogenation of Pt-based catalysts supported on carbon nanotubes.* Journal of Catalysis, 2012. **290**: p. 37-54.

66. Ciureanu, M. and R. Roberge, *Electrochemical impedance study of PEM fuel cells. Experimental diagnostics and modeling of air cathodes.* The Journal of Physical Chemistry B, 2001. **105**(17): p. 3531-3539.

Producción científica

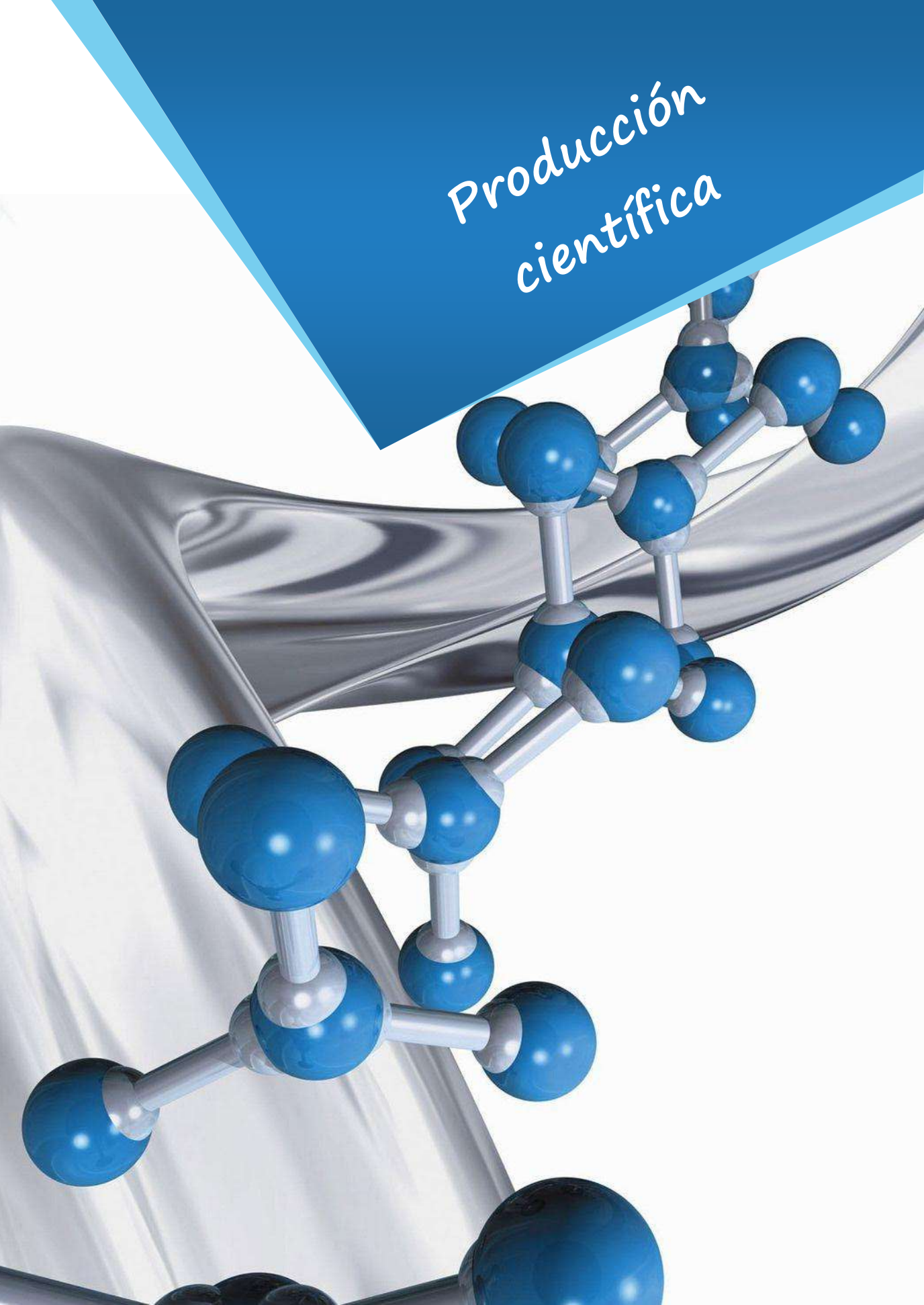

De la presente tesis doctoral han derivado las siguientes publicaciones y contribuciones a congresos tanto nacionales como internacionales:

- Artículos en revisión:

  - Electrocatalytic Hydrogenation of Cinnamaldehyde in a Polymeric Electrolyte Membrane Reactor. Influence of reaction conditions. A.R. de la Osa, M.J. Torres, A. de Lucas-Consuegra, J.A. Díaz, J.L. Valverde, P. Sánchez. Submitted.

  - Electrocatalytic Hydrogenation of Cinnamaldehyde by Pt/C Catalysts Prepared by One-Pot Impregnation-Reduction Method. M.J. Torres, A.R. de la Osa, J.A. Díaz, A. de Lucas- Consuegra, P. Sánchez. Submitted.

  - Pt/C Catalysts for the Electrocatalytic Hydrogenation of Cinnamaldehyde: Influence of the Cathode Reducing Agent. M.J. Torres, A.R. de la Osa, J.A. Díaz, A. de Lucas-Consuegra, P. Sánchez. Submitted.

  - Electrocatalytic Hydrogenation of Cinnamaldehyde in a PEM cell. The role of Sodium Hydroxide and Platinum Loading. M.J. Torres, A.R. de la Osa, A. de Lucas-Consuegra, P. Sánchez. Submitted.

  - Bimetallic cathodes for the Electrocatalytic Hydrogenation of Cinnamaldehyde in a PEM cell. M.J. Torres, A.R. de la Osa, A. de Lucas-Consuegra, P. Sánchez. Submitted.

  - Bimetallic PtNi/C and PtCo/C cathodes for the selective Hydrogenation of Cinnamaldehyde in a PEM cell: Influence of the

Pt/M ratio and Cathodic Media Additives. M.J. Torres, A.R. de la Osa, A. de Lucas-Consuegra, P. Sánchez. Submitted.

- Electrocatalytic Hydrogenation of Cinnamaldehyde in a Polimeric Electrolyte Membrane Reactor: Influence of the Cathodic Support and GDL. M.J. Torres, A.R. de la Osa, A. Romero, A. de Lucas-Consuegra, P. Sánchez. Submitted.

- Comunicaciones orales a congresos nacionales:

  - Catalysts synthesis for the electrochemical hydrogenation of cinnamaldehyde. M.J. Torres, A.R. de la Osa, J. A. Díaz, A. de Lucas-Consuegra, J.L. Valverde, P. Sánchez. **XI Simposio de Ciencia Joven.** Ciudad Real (España), Junio 2017.

  - Hidrogenación de cinamaldehído en celda electroquímica tipo PEM: Optimización de la carga de metal activo y el pH durante la síntesis. M.J. Torres, P. Sánchez, A. de Lucas-Consuegra, J.L. Valverde, A.R. de la Osa. **Reunión de la Sociedad Española de Catálisis**. Córdoba (España), Junio 2019.

- Presentaciones póster en congresos internacionales:

  - Electrochemical hydrogenation for the synthesis of high – added value compounds. M.J. Torres, A.R. de la Osa, P. Sánchez, J.L. Valverde. **European Summer School Electrochemical Engineering (ESSEE) 2015**. Leeuwarden (Países Bajos), Junio 2015.

  - PEM electrocatalytic hydrogenation of cinnamaldehyde. M.J. Torres, A.R. de la Osa, A. de Lucas-Consuegra, J.L. Valverde, P.

Sánchez. **11th European Symposium of Electrochemical Engineering**. Praga (República Checa), Junio 2017.

- Influence of the reducing agent on the performance of Pt/C based cathode for electrochemical hydrogenation of cinnamaldehyde. M.J. Torres, A.R. de la Osa, José A. Díaz, A. de Lucas-Consuegra, J.L. Valverde, P. Sánchez. **69th Annual Meeting of the Intenational Society of Electrochemistry**. Bolonia (Italia), Septiembre 2018.

➢ Presentaciones póster en congresos nacionales:

- Hidrogenación electroquímica para la síntesis de compuestos de alto valor añadido. M.J. Torres, A.R. de la Osa, J.L. Valverde, P. Sánchez. **V Jornadas Doctorales de la Universidad de Castilla La Mancha.** Ciudad Real (España), Octubre 2015.

- Hidrogenación selectiva de aldehídos α,β – insaturados para la síntesis de compuestos de alto valor añadido vía procesos electroquímicos de membrana. M.J. Torres, A.R. de la Osa, A. de Lucas-Consuegra, J.L. Valverde, P. Sánchez. **II Encuentro de Jóvenes Investigadores de la SECAT**. Ciudad Real (España) Junio 2016.

- Procesos electroquímicos para la hidrogenación de aldehídos α,β – insaturados en condiciones suaves. M.J. Torres, A.R. de la Osa, A. de Lucas-Consuegra, J.L. Valverde, P. Sánchez. **VI Jornadas Doctorales de la Universidad de Castilla La Mancha**. Toledo (España), Octubre 2016.

- Hidrogenación electroquímica de cinamaldehído: Influencia de las condiciones de operación. M.J. Torres, A.R. de la Osa, J. A. Díaz, A.

de Lucas-Consuegra, J.L. Valverde, P. Sánchez. **Reunión de la Sociedad Española de Catálisis**. Oviedo (España), Junio 2017.

- Hidrogenación electroquímica de cinamaldehído: Influencia de la carga metálica en el cátodo. M.J. Torres, A.R. de la Osa, A. de Lucas-Consuegra, J.L. Valverde, P. Sánchez. **VII Jornadas Doctorales de la Universidad de Castilla La Mancha.** Albacete (España), Noviembre 2017.

- Cathodic catalyst for the electrochemical hydrogenation of cinnamaldehyde. M.J. Torres, A.R. de la Osa, A. de Lucas-Consuegra, J.L. Valverde, P. Sánchez. **XII Simposio de Ciencia Joven**. Ciudad Real (España), Junio 2018.

- Catalizadores bimetálicos para la hidrogenación de cinamaldehído en celda electroquímica tipo PEM. M.J. Torres, A.R. de la Osa, A. de Lucas-Consuegra, J.L. Valverde, P. Sánchez. **III Encuentro de Jóvenes Investigadores de la SECAT**. Valencia (España), Junio 2018.

- Influencia en el medio catódico en una reacción de hidrogenación de cinamaldehído en una celda de intercambio protónico tipo PEM. M.J. Torres, A.R. de la Osa, A. de Lucas-Consuegra, J.L. Valverde, P. Sánchez. **VIII Jornadas Doctorales de la Universidad de Castilla La Mancha.** Cuenca (España), Octubre 2018.